Neonatal Hyperbilirubinemia: *in vivo* Characterization of Mechanisms of Bilirubin Neurotoxicity and Pharmacological Treatments

Thesis

Neonatal hyperbilirubinemia: *in vivo* characterization of the mechanisms of bilirubin neurotoxicity and pharmacological treatments

Simone Vodret

A Thesis submitted in fulfilment of the requirements of the Open University (UK) for the degree of Doctor of Philosophy

The Open University (UK)

International Centre for Genetic Engineering and Biotechnology (ICGEB), Trieste, Italy

Director of the studies:	Dr. Andrés Fernando Muro
External supervisor:	Dr. Libor Vitek

29th November 2016

ACKNOWLEDGEMENTS

I would like to thank Dr. Andrés Fernando Muro, the director of the study, for the opportunity to work in his lab. The shared knowledge and the constructive discussions over the last four years make me grow not only from the scientific point of view, but also as a person. I would also like to thank Dr. Giulia Bortolussi, for her patience in teaching and the assistance in performing experiments. Also without her, this work would not have been possible. I would like to thank the ICGEB for the financial support.

My gratitude goes to Dr. Libor Vitek, my external supervisor, for the support and the discussions during our meeting and the preparation of the manuscript. I would like to thank Prof. Henkjan Verkade, for the successful collaboration. My acknowledgements also go to Jana Jašprová and Andrea Schreuder, for the determination of tissue UCB and free bilirubin, respectively.

I would also like to thank all the past and present colleagues of the Mouse Molecular Genetics lab, Fabiola Porro, Luka Bockor, Alessia De Caneva, Alessandra Iaconcig, Vipin Singh Rawat, Riccardo 'Seppia' Sola, for the help and the laughs at the end of each Internal Internal Seminar session. My gratitude goes to the staff of the ICGEB animal facility, Willy De Mattia and Stefano Artico (also the captain of the ICGEB football team), for their help.

I would like to thank Lucìa, for all the time and the books we shared, Zain, who provided me half of the lunches of the last year, Chiara, for her carelessness we all need in our life, and Andrea, who shared with me any given Sunday supporting Roma.

I would like to thank my sisters, Cecilia and Caterina, for being together despite the distance, and Lucia and Carlo, for their support in the darkest moments. Thanks to my friends, Dino, Frinky, Miglio, Bob, Giorgio and Gino, you guys are my family.

My gratitude goes also to Giulia, I am lucky to share my life with her.

Finally, I would like to thank Arturo, without you there would not have been me.

TABLE OF CONTENTS

LIST OF FIGURES

LIST OF TABLES

ABBREVIATIONS

ABR	auditory brainstem response
AD	Alzheimer's disease
ALS	amyotrophic lateral sclerosis
ALT	alanine aminotransferase
ARE	antioxidant response elements
Arg1	arginase 1
AST	aspartate aminotransferase
ATF	activating transcription factor
B/A	bilirubin/albumin
BAEP	brainstem auditory evoked potential
BBB	blood-brain barrier
BCG	bromocresolgreen
Bf	UCB free fraction
BIND	bilirubin-induced neurological dysfunction
BMEC	brain microvascular endothelial cell
bp	base pair
CAR	constitutive androstane receptor
CB	cerebellum
CCl_4	carbon tetrachloride
CD	cluster of differentiation
cDNA	complementary DNA
CHOP	C/EBP-Homologous Protein
CGN	cerebellar granule neuron
CNS	central nervous system
CNSI	Crigler-Najjar syndrome type I
CNSII	Crigler-Najjar syndrome type II
DCs	dendritic cells
DR5	death receptor 5
EGL	external germinal layer
ER	endoplasmic reticulum
ERO1L	endoplasmic reticulum oxidoreductase 1-like
ET	exchange transfusion
Et-OH	ethanol
FB	forebrain
g/kg	grams/kilograms
G6PD	glucose 6-phosphate dehydrogenase
GCs	granule cells
gDNA	genomic DNA
GFAP	glial fibrillary acidic protein
GRP	glucose-regulated protein
GS	Gilbert's syndrome
HD	Huntington's disease
HO	heme oxygenase
HSA	human serum albumin
hUGT1	humanized Ugt1
Iba1	ionized calcium-binding adapter molecule 1
IF	immunofluorescence
IGL	internal granular layer
IL	interleukin
INFγ	interferon γ

iNOS	inducible nitric oxide synthase
i.p.	intraperitoneal
i.v.	intravenous
IRE1	inositol requiring 1
kD	kilodalton
LC3	microtubule-associated protein 1A/1B-light chain 3
LIV	liver
MAPK	mitogen-activated protein kinase
Met-OH	methanol
ML	molecular layer
MMP	matrix metalloproteinase
MNC	minocycline
Mps	metalloporphyrins
MRC	mannose receptor complex
MS	multiple sclerosis
NFKβ	nuclear factor kappa-light-chain-enhancer of activated B cells
NO	nitric oxide
Nrf2	nuclear factor (erythroid-derived 2)-like 2
OF	open field
ORF	open reading frame
P	postnatal day
PCR	polymerase chain reaction
PCs	Purkinje cells
PCL	Purkinje cells layer
PD	Parkinson’s disease
PERK	protein kinase RNA-like endoplasmic reticulum kinase
PHZ	phenylhydrazine
PXR	pregnane X receptor
qRT-PCR	quantitative real-time RT-PCR
ROS	reactive oxygen species
RT	reverse transcription
SM	skeletal muscle
SOD	superoxide dismutase
Sulpha	sulphadimethoxine
TB	total bilirubin
TBI	traumatic brain injury
TLR2	toll-like receptor 2
TNFα	tumor necrosis factor α
UCB	unconjugated bilirubin
UDCA	ursodeoxycholic acid
UGT1A1	UDP-glucuronosyl transferase 1A1
UPR	unfolded protein response
WB	western blot
WT	wild type

ABSTRACT

Neonatal jaundice or hyperbilirubinemia is the result of alterations in the bilirubin metabolism. Prolonged and uncontrolled high levels of unconjugated bilirubin lead to bilirubin-induced neurological dysfunction and, if untreated, eventually death by kernicterus. Severe hyperbilirubinemia results in the saturation of the bilirubin binding capacity of plasma albumin, with the consequent increase in the fraction of unconjugated bilirubin (UCB) not bound to albumin (free bilirubin, Bf) that, due to its lipophilicity, crosses the blood brain barrier accumulating in the brain and triggering the neuronal injury. In the developing central nervous system, a wide range of cellular functions are affected and the concerted disruption of their regulation results in cellular damage. Patients experiencing prolonged toxic bilirubin levels are characterized by a number of neurological deficits, such as abnormalities in motor, sensitive and cognitive functions. Despite intensive studies, several aspects of the mechanisms operating at the onset of the disease are still partially understood.

To study severe neonatal hyperbilirubinemia and possible therapies, I took advantage of the *Ugt1*$^{-/-}$ mouse model previously generated in my laboratory. Homozygous mutant mice develop jaundice and accumulate bilirubin in the brain due to the lack of the Ugt1a1 enzyme. If untreated, mutant mice show neurological deficits leading to early neonatal lethality.

The work performed in this Thesis explores three different aspects of bilirubin neurotoxicity:

1. The role of Bf *in vivo* by the administration of human serum albumin;
2. The events preceding death by a time-course analysis of mutant pups;
3. The investigation of the role of neuroinflammation by the administration of a neuroprotective and anti-inflammatory drug.

The obtained results showed that increasing plasma bilirubin-binding capacity by albumin supplementation decreases bilirubin neurotoxicity. In fact, daily albumin administration avoided the accumulation of Bf in the brain by its mobilization from tissues to plasma, resulting in the complete rescue of bilirubin-induced brain impairment and lethality. Moreover, this study highlighted the reliability of Bf as the best marker to predict neurotoxicity risk.

The time-course investigation of the events occurring in the cerebellum of *Ugt1*$^{-/-}$ pups leading to bilirubin-brain damage showed the prevalence of ER stress, oxidative stress and neuroinflammation at the onset of neonatal hyperbilirubinemia

that, in turn, affected brain integrity by their concerted effect resulting in neurodegeneration.

Finally, the administration of minocycline (MNC), an antibiotic with neuroprotective and anti-inflammatory properties, partially prevented lethality by hyperbilirubinemia and rescued animals by significantly reducing neurodegenerative and neuroinflammatory features that characterized the untreated *Ugt1*$^{-/-}$ mouse model.

This study demonstrates the contribution of ER stress and inflammation in the onset of the disease, the relevance of these mechanisms during the attenuation of neurodegeneration by MNC administration, and that albumin supplementation is a potential therapeutic alternative to treat bilirubin neurotoxicity in acute cases in which prompt exchange transfusion is required.

INTRODUCTION

1.1 Bilirubin metabolism

Bilirubin is the end product of heme catabolism in the intravascular compartment. About 80% of bilirubin results from the degradation of erythrocyte haemoglobin in the reticulo-endothelial system; the remaining 20% derives from degradation of myoglobin and other heme-containing proteins, such as cytochromes, and inefficient erythropoiesis in bone marrow (London et al., 1950). Heme oxygenase degrades heme into biliverdin, which is then reduced to UCB by the enzyme biliverdin reductase (Figure 1).

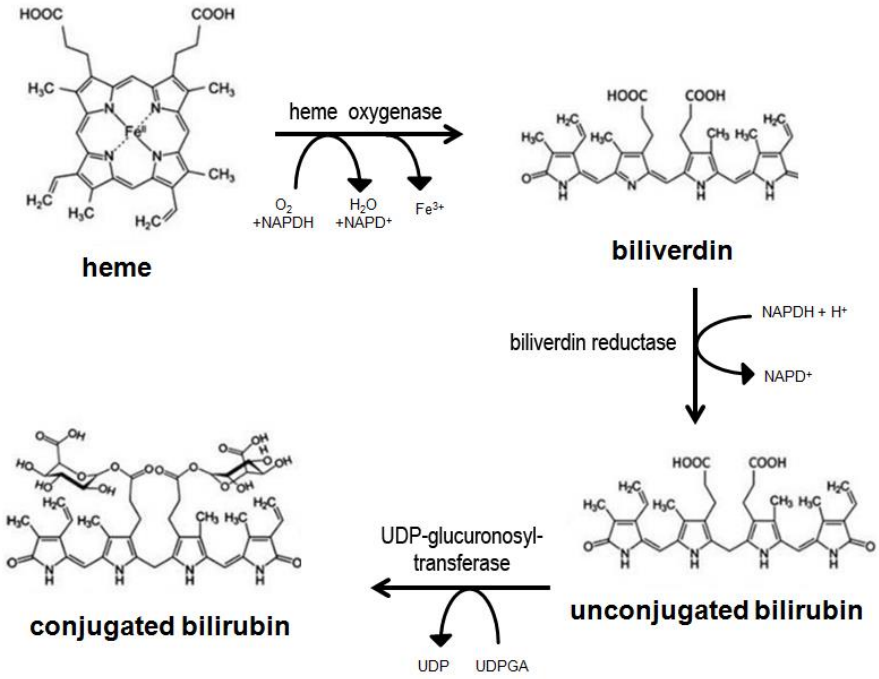

Figure 1. Metabolic reactions of bilirubin pathway. Heme, biliverdin, bilirubin and conjugated bilirubin structures are indicated, as well as the relative by-products and enzymes of each reaction. Adapted from (Jangi et al., 2013).

UCB is water-insoluble and travels in plasma bound to albumin to reach the liver. In the endoplasmic reticulum of hepatocytes, bilirubin is conjugated to glucuronic acid by the enzyme UDP-glucuronosyl transferase 1A1 (UGT1A1) (Figure 2) (Bosma, 2003).

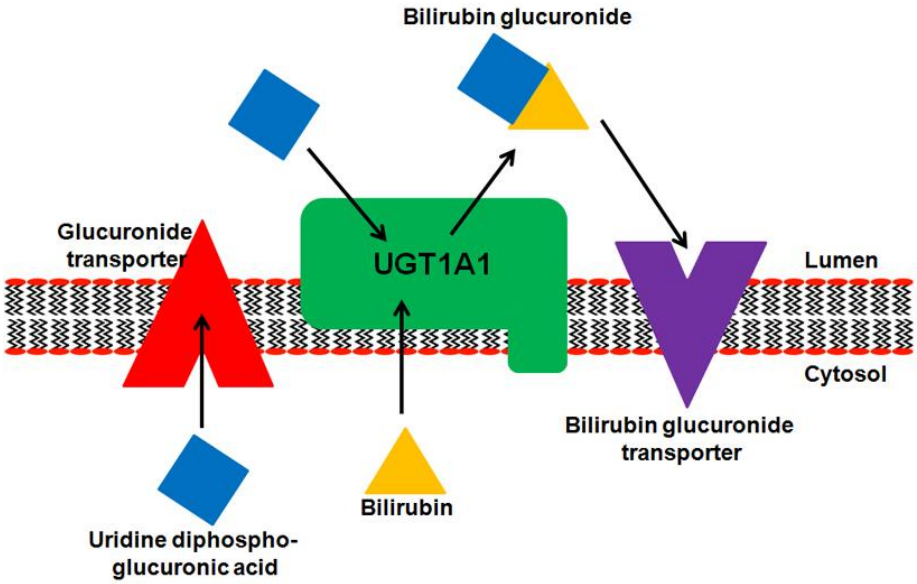

Figure 2. Schematic representation of bilirubin conjugation within the hepatocytes. Bilirubin is conjugated to glucuronic acid in the lumen of the endoplasmic reticulum, and then released to the cytosol through the bilirubin glucuronide transporter. Adapted from Erlinger and colleagues (Erlinger et al., 2014).

Glucuronosylation increases the solubility of bilirubin and is essential for its disposal in the bile fluid, avoiding the toxic accumulation of UCB in tissues. Once conjugated, bilirubin is transported out from hepatocytes to the bile fluid by active transporters, such as the multidrug-associated resistance protein 2 (Mrp2) (Erlinger et al., 2014). In the small intestine, bacterial flora deconjugate bilirubin by β-glucuronidase and degrade it to urobilinoids (urobilinogen and stecobilogen, and their respective oxidation products, urobilin and stercobilin being the major urobilinoid species) (Jangi et al., 2013). Part of the formed UCB is also absorbed by enterocytes and transported back to the liver (Vítek and Carey, 2003). A consistent part of bilirubin glucuronide is also secreted back to the plasma after hydrolyzation, being able to be re-uptaken by hepatocytes (Van De Steeg et al., 2012).

UGT1A1 is expressed also in extra-hepatic tissue at much lower levels, such as intestine, kidney and skin (Fisher et al., 2001; Sumida et al., 2013) and, although in a less extent compared to the liver, UGT1A1 expression in these tissues is important in the bilirubin metabolism.

1.2 *UGT1* gene locus

The human *UGT1* gene locus length is ~200 kb, located on chromosome 2-q37 (Ritter et al., 1992). The different variants result from the translation of the mRNA composed of one of the 13 unique exons encoding the amino-terminal part and the 4 common exons encoding for the active site of the enzyme and the C-terminal transmembrane domain (exons 2, 3, 4 and 5) (Gong et al., 2001). Among the 13 variable exons, 9 of them (exons 1, 3, 4, 5, 6, 7, 8, 9 and 10) form alternative enzymes, while 4 of them are pseudoexons (12p, 11p, 13p and 2p) carrying premature stop codons. Together with the *UGT2* paralog locus, the combination of common and unique exons forms 17 different catalytically active UGT isoforms in humans, which have different substrate preference. Nine isoforms are encoded by the *UGT1* locus (1A1, 1A3, 1A4, 1A5, 1A6, 1A7, 1A8, 1A9 and 1A10) and eight by the *UGT2* locus (2A1, 2B4, 2B7, 2B10, 2B11, 2B15, 2B17 and 2B28) (Mackenzie et al., 2005).

Compared to human, the rat and mouse *UGT1* loci differ in the number of unique exons, but the 4 common exons are very conserved (Figure 3) (Buckley and Klaassen, 2007).

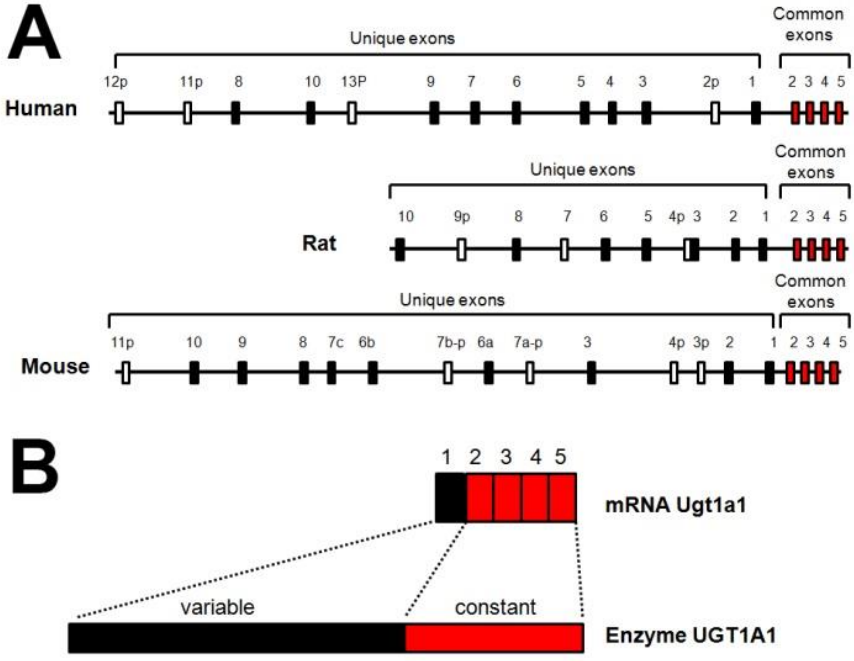

Figure 3. The *Ugt1* locus. Schematic representation of the *Ugt1* locus in human, rat and mouse genomes, the *Ugt1a1* mRNA and the relative enzyme. **A)** Red boxes indicate the common exons, black boxes indicate the unique coding exons and white boxes indicate pseudogenes. **B)** The *Ugt1a1* mRNA and the relative enzyme are indicated. Adapted from (Zhang et al., 2004).

Despite the identified overlapping in enzyme activity of the different UGT variants, UGT1A1 is the only enzyme responsible for bilirubin glucuronosylation (Bosma et al., 1994).

1.3 Bilirubin toxicity and disease

The alteration in bilirubin metabolism results in the accumulation of UCB. Hyperbilirubinemia can be triggered by genetic and non-genetic causes, or by their combination (Table 1 and 2).

1.3.1 Hereditary causes of unconjugated hyperbilirubinemia

High levels of UCB can be the result of genetic disorders (Table 1).

The Crigler-Najjar syndrome is an extremely rare recessive genetic disease, owing a prevalence of 1 in 1,000,000 births. It is characterized by the deficiency of hepatic UGT1A1 activity due to mutations in the *UGT1A1* gene, resulting in hyperbilirubinemia, severe neurological damage and death, if untreated (Crigler and Najjar, 1952). Depending on the severity of the symptoms, the syndrome is classified in two different forms, although there is a continuum of phenotypes: Crigler-Najjar syndrome type I (CNSI) (OMIM 218800) and type II (CNSII) (OMIM 606785).

In CNSI, hyperbilirubinemia is caused by the complete absence of the UGT1A1 activity and bilirubin glucuronides in bile, which result in bilirubin neurotoxicity and death if untreated.

CNSII is a milder form of the disease, distinguished from CNSI by the presence of residual activity of UGT1A1 enzyme due to missense mutations in the gene that reduce the expression or the enzyme affinity for the substrate (Arias, 1962). CNSII patients present low levels of bilirubin glucuronosides in bile, as bilirubin levels are decreased upon phenobarbital administration that induces *UGT1A1* gene expression (see Chapter 1.5.1).

Gilbert's syndrome (GS) is the milder genetic form of unconjugated hyperbilirubinemia. In GS, a mutation in the promoter of the *UGT1A1* gene can cause the decreased expression of the enzyme. Although milder, bilirubin levels in the GS condition may rise by different stress factors, placing GS patient at risk of high UCB levels.

Other genetic causes are those that implicate blood-related disorders, such as ABO and/or Rh incompatibility, or glucose 6-phosphate dehydrogenase (G6PD) deficiency. These conditions affect red blood cells metabolism, generating increased haemolysis and, consequentially, exacerbate hyperbilirubinemia.

Table 1. Genetic causes of hyperbilirubinemia. Syndromes and related causes are listed.

Genetic hyperbilirubinemia	
Syndrome	**Causes**
Crigler-Najjar Syndrome type I (CNSI)	Complete lack of UGT1A1 activity
Crigler-Najjar Syndrome type II (CNSII)	Important reduction of UGT1A1 activity
Gilbert's Syndrome (GS)	*UGT1* promoter polymorphism
ABO incompatibility	Maternal IgG antibodies with specificity for the ABO blood group system pass through the placenta to the fetal circulation where they can cause haemolysis
Glucose 6-phosphate dehydrogenase (G6PD) deficiency	Low levels of G6PD, an enzyme involved in the metabolism of red blood cells, lead to haemolytic anaemia
Rh incompatibility	During birth, the mother may be exposed to the infant's blood, and this causes the development of antibodies, which may affect the health of subsequent Rh+ pregnancies

1.3.2 Non-genetic causes of unconjugated hyperbilirubinemia

Besides hereditary causes, several non-genetic factors can affect the bilirubin metabolism (Table 2). Pathological conditions such as hypoxia, infection, sepsis or hepatic disorder may result in liver dysfunction, impairing the glucuronosylation system and increasing systemic bilirubin levels. Breastfeeding is also a possible cause of hyperbilirubinemia. In fact, breast milk reduces the expression of the intestinal UGT1A1 (see also Chapter 1.4.3), thus contributing to the increase of UCB during the very early postnatal phases, in which expression of the liver enzyme is still very low (Arias et al., 1964). Breast milk contains β-glucoronidase that further

increases bilirubin deconjugation and its reabsorption in the gut lumen. In addition, the inadequate intake of breast milk leads to dehydration, exacerbating the condition.

Neonatal jaundice is one of the most common conditions of the neonatal life (see Chapter 1.3.2), resulting from the delayed induction of *UGT1A1* gene expression that limits the conjugation capacity of newborns. The concomitance of delayed UGT1A1 activity with other causes, such as increased breakdown of fetal erythrocytes and/or inefficient serum albumin transport to the liver, may lead to acute hyperbilirubinemia (Bhutani and Wong, 2013; Greco et al., 2016).

Table 2. Non-genetic hyperbilirubinemia causes. Conditions and related causes are listed.

Non-genetic hyperbilirubinemia	
Conditions	**Causes**
Breast Milk jaundice	Breast milk reduces expression of intestinal UGT1A1.
Hypoxia	
Infections	
Hepatic disorders	Liver dysfunction
Neonatal jaundice	Delay in the UGT1A1 enzyme induction

1.3.3 Neonatal jaundice

Neonatal unconjugated hyperbilirubinemia is a common condition occurring in more than 60% of term newborns and almost all pre-term babies (American Academy of Pediatrics, 2004; Reichman et al., 2015). It is characterized by the typical yellowish skin coloration resulting from UCB accumulation. Neonatal jaundice is the most frequent cause of hospital readmission in the first week of life (75%) (Escobar et al., 2005), since prolonged high bilirubin levels are life-threatening and often lead to permanent brain damage and death by kernicterus (see Chapter 1.3.7) (Watchko, 2006). The expression of the hepatic *UGT1A1* gene in human newborns reaches levels comparable to the adults at 14 weeks of postnatal life, while only 1% of the activity is observed in early developmental stages, such as from the 30th to 40th

week of gestation (Coughtrie et al., 1988). Thus, pre-term delivery and delays in enzyme induction result in neonatal jaundice.

1.3.4 Management of hyperbilirubinemia

Transient neonatal hyperbilirubinemia occurs in the first week of life, and plasma total bilirubin (TB) usually peaks up to 10 mg/dL (170 µmol/L) (American Academy of Pediatrics, 2004). Since high levels of bilirubin may produce encephalopathy, the evaluation of at risk babies is performed by TB measurement. TB measurement related to the infants' age in hours gives the indication for the application of the therapy to reduce the hyperbilirubinemia, such as intensive phototherapy or exchange transfusion, depending on the severity of the condition (see Chapter 1.5) (Muchowski, 2014).

It is generally recognized that newborns with less than 35 weeks of gestation are at greater risk of bilirubin neurotoxicity susceptibility compared to term newborns (Maisels et al., 2012). In fact, the developing brain of premature babies is particularly vulnerable to bilirubin neurotoxicity due to neurodevelopmental maturity differences (Okumura et al., 2009). In particular, the cerebellum is very susceptible to potentially toxic effects of bilirubin, as its development occurs also in peri- and post-natal period (Biran et al., 2012; Fonnum and Lock, 2000), thus, providing an optimal target for bilirubin neurotoxicity. In 2004, the American Academy of Pediatrics indicated the guidelines for the management of hyperbilirubinemic infants (American Academy of Pediatrics, 2004), delineating a general approach to tackle neonatal jaundice in infants with more than 35 weeks of gestation. However, the threshold to predict bilirubin-induced brain damage is not clear. For instance, a study revealed that TB values higher than 31 mg/dL (539 µmol/L) in non-haemolytic jaundice babies resulted in bilirubin encephalopathy (Gamaleldin et al., 2011). On the contrary, another study presenting babies with values ≥ 30 mg/dL (≥ 513 µmol/L) did not show evidences of brain injury or neurodevelopmental sequelae (Newman et al., 2003).

Bilirubin/albumin (B/A) ratio can be used as an alternative to TB. The employment of the B/A ratio in conjunction with TB can improve the accuracy of brain damage prediction and prevent unnecessary invasive therapies, such as exchange transfusion in jaundice neonates (Ardakani et al., 2011). In fact, B/A ratio can be employed as a surrogate parameter to estimate the free fraction of bilirubin (Bf, Chapter 1.3.5), which, in some conditions, is a more precise marker to evaluate the potential brain damage. Several protocols have been proposed to trace guidelines

for free bilirubin threshold (Yokota et al., 2013). Unfortunately, reliable and readily accessible assays for evaluating serum free bilirubin are not yet available. Thus, further investigations are needed to set a valid and reliable parameter to discriminate the at-risk babies.

1.3.5 Bf

The biochemical determination of bilirubin in plasma is divided into direct and indirect measurement. The direct fraction (conjugated bilirubin) is composed by bilirubin mono- and di-glucuronosides, while the indirect fraction is the subtraction of direct bilirubin from the total bilirubin value, also referred as UCB.

Bilirubin is poorly water-soluble at physiological pH and it needs to be up-taken in the liver to be metabolized by hepatocytes. Normally, the majority of UCB travels in the bloodstream bound to albumin, due to the high affinity of binding (Ostrow et al., 1994). As TB levels increase, the UCB amount may rise above the binding capacity supplied by the plasma protein, leading to the increase of UCB free fraction (Bf) (Wennberg et al., 1979). Bf is normally present at levels lower than 0.1% of total bilirubin in plasma. Due to its chemical lipophilic nature, the small fraction of UCB (or Bf) crosses cellular membranes and diffuses into tissues, especially those having high lipid content, being the cause of the neurological damage in the brain. In particular, when the albumin binding capacity is saturated by UCB, Bf is capable of crossing the blood-brain-barrier (BBB), and disrupting several essential neuronal functions, resulting in neuronal cell death (Ostrow et al., 2004). Bilirubin alters the composition, permeability and functions of the cellular membrane, leading to cellular energy failure (Keshavan et al., 2004), oxidative stress (Qaisiya et al., 2014; Vaz et al., 2010) and glutamate excitotoxicity (Brito et al., 2010). All these defects might, in turn, lead to several cell responses such as inflammation, abnormal intracellular calcium levels and effects on others possible cellular necrosis/apoptosis signalling pathways (Watchko, 2006). In premature newborns Bf, but not TB, has been shown to correlate with the development of kernicterus (Amin et al., 2001), which is the characteristic sign of toxic levels of prolonged bilirubin accumulation in the brain. Bf was shown to be a determinant of bilirubin toxicity in animal model of hyperbilirubinemia (Wennberg and Hance, 1986). Thus, Bf plays a key role in the pathogenesis of bilirubin-induced brain damage. However, Bf concentrations are not routinely evaluated in jaundiced patients (Ahlfors et al., 2006), and a reliable

marker to assess the state of patients and to predict damage, especially in jaundice newborns, is still needed.

1.3.6 Bilirubin-induced neurological dysfunction (BIND)

For the great majority of neonates the outcome of jaundice is benign, but prevention must be carried out to keep under control the potential neurodamage.

During neonatal jaundice UCB concentration may rise exceeding the binding capacity of albumin, and can reach life-threatening levels. In the past years, interest in bilirubin encephalopathy has been reawakened due to an increase in its prevalence (Bhutani et al., 2013; Kaplan and Hammerman, 2005). If untreated, newborns with very high UCB levels may eventually develop bilirubin-induced neurological dysfunction (BIND) in the CNS (Wennberg et al., 2006). Based on time of bilirubin exposure and symptoms, BIND can be divided into mild, moderate and severe BIND. Mild and moderate BIND symptoms are reversible, while severe BIND can lead to irreversible brain damage. Newborns that experience prolonged bilirubin toxicity show clinical features of lethargy, ophthalmoplegia (ocular muscle paralysis), high-pitch crying, opisthotonus (bowed body and rigid extremities or dystonia), and seizures, as well as mental retardation, and often death by kernicterus (Shapiro, 2003; Smitherman et al., 2006). In fact, in the developing brain, bilirubin targets specific regions such as basal ganglia, cochlear, and oculomotor nuclei and cerebellum, including granule and Purkinje neurons (Lauer and Spector, 2011; Watchko, 2006). Even moderate levels of UCB have been associated with developmental delay, attention-deficit disorders, autism, and isolated neural hearing loss (Shapiro, 2010). In any case, long-lasting exposure to high levels of bilirubin may lead to neurological sequelae, and it could have a permanent impact on the infant's learning and memory.

The degree of BIND in babies is measured by magnetic resonance images of the brain (Shah et al., 2003) and by brainstem auditory evoked potential (BAEPs, or auditory brainstem response ABRs), as the auditory system is particularly sensitive to bilirubin toxicity (Shapiro and Nakamura, 2001). Hence the response to auditory stimuli represents a reliable method that reflects neuronal activity.

Clearly, the detailed identification of the neurological events and molecular targets triggering bilirubin neurotoxicity will help to the understanding and management of BIND.

1.3.7 Kernicterus

The irreversible damage produced by prolonged exposure to high bilirubin levels is named ‘kernicterus’. Coined in 1903 by Christian Schmorl, the term kernicterus means "yellow kern," with kern referring to the most commonly afflicted region of the brain (i.e., the nuclear region).

The incidence of kernicterus in newborns with extreme hyperbilirubinemia is wide, reaching 10 per 100,000 live births in Western countries, while it raises up to 73 per 100,000 live birth in low- and middle-income countries (Bhutani et al., 2013; Greco et al., 2016). Death by kernicterus is ranked as one of the three top causes of death among African newborns (Olusanya et al., 2014). In preterm infants born before the 30^{th} week of gestation, the number of cases can considerably rise to 1.8 per 1000 live births (Morioka et al., 2015). In the 1980s and 1990s there was a resurgence of kernicterus in the United States and abroad, which has been attributed in part to early hospital discharge, the influence of managed care, and an increase in the number of breastfed infants, with a proportional increase in breastfeeding inadequacy in the first week of life (Moerschel et al., 2008).

A temporal window of CNS vulnerability to UCB toxicity have been suggested as the neurodevelopmental age at the time of UCB exposure influences the location of the selective damage (Conlee and Shapiro, 1997). While the auditory kernicterus subtype prevails in infants with peak levels of exposure to TB at earlier gestational ages, motor kernicterus subtype usually develops in infants with more than 34 weeks of gestation (Shapiro, 2010).

As previously mentioned, nomograms and guidelines were proposed for jaundiced newborn infants of 35 or more weeks of gestation to reduce the incidence of brain bilirubin damage and kernicterus (American Academy of Pediatrics, 2004). However, in sick and preterm infants, the absence of precise data on the prevalence of hyperbilirubinemia and the lack of proven predictive indices have made difficult to establish such guidelines.

1.4 Animal models to study hyperbilirubinemia

Several animal models have been generated to elucidate the molecular mechanisms of bilirubin neurotoxicity.

1.4.1 Non-genetic animal models of hyperbilirubinemia

There are some examples of animal models in which hyperbilirubinemia is artificially induced by bilirubin injection or by increasing haemolysis. These experimental methodologies help the investigation of bilirubin toxicity mechanisms, providing *in vivo* hyperbilirubinemic conditions and the related features of BIND and kernicterus. For instance, Gao and colleagues generated high levels of bilirubin by directly injecting bilirubin to mouse pups (intraperitoneal injection, i.p.) at postnatal day (P) 4 (Gao et al., 2011). More recently, Song and colleague generated a model of hyperbilirubinemia by the injection of bilirubin in the cistern magna of rat pups (Song et al., 2014), replicating kernicterus features.
Another model of neonatal jaundice was established by the administration of two consecutive i.p. injections of phenylhydrazine (PHZ) to wild type mice, which caused the increase in erythrocyte turnover leading to hyperbilirubinemia (Maity et al., 2013).

In addition to these transient hyperbilirubinemic models, there are different genetic models carrying the *Ugt1* mutation that resemble the CNSI. These animal models represent a strategic tool to understand the mechanism of bilirubin toxicity that affects jaundiced newborns.

1.4.2 Gunn rat

One of the most intensively studied models is the Gunn rat. In 1938, C.H. Gunn described a spontaneously jaundiced mutant strain of Wistar rats, which have a life-long, severe unconjugated hyperbilirubinemia (Gunn, 1938). The Gunn rat was recognized as an animal model for CNSI, when it was demonstrated that unconjugated hyperbilirubinemia in these animals was caused by the inherited inability to form bilirubin conjugates (Johnson et al., 1959). The alteration of the glucuronosylation system is caused by a one-base deletion in the exon 4 of the *Ugt1* locus that generates a premature stop codon by a frame shift in the open reading frame (ORF) and, consequently, the lack of the enzyme (Iyanagi et al., 1989). Homozygous mutant Gunn rats (jaundiced/jaundiced, or j/j) manifest a complete deficiency of hepatic UDP-glucuronosyl transferase, therefore showing high levels

of UCB. Since jj rat pups develop jaundice early after birth, they present cerebellar hypoplasia at P9, marked Granule cells (GCs) and Purkinje cells (PCs) loss and reduction in the cerebellar layer thickness (Conlee and Shapiro, 1997). Moreover, toxic bilirubin levels in Gunn rats cause alteration in BAEPs, underlining the brain impairment (Rice and Shapiro, 2008).

Hence, the Gunn rat represents a good model of bilirubin encephalopathy, neonatal jaundice and, specifically, CNSI (Chowdhury et al., 1993). However, the Gunn rat reproduces only some of the features of genetic hyperbilirubinemia. In fact, jj animals reach adulthood and are fertile if bilirubin levels remain unchallenged. Since jj rats have a un-lethal hyperbilirubinemic phenotype, drugs are often used to reproduce the acute hyperbilirubinemic condition, such as PHZ which increases haemolysis or sulphadimethoxine (Sulpha), a drug that displaces bilirubin from albumin in the circulation (Rice and Shapiro, 2008).

1.4.3 *Ugt1*$^{-/-}$ mouse model (gene disruption by a neomycin cassette)

The first engineered mouse model of hyperbilirubinemia was generated by Tukey's laboratory in 2008. By gene targeting, a neomycin cassette was introduced in the exon 4 of the *Ugt1* gene to disrupt the locus (Nguyen et al., 2008). Homozygous mutant mice show no activity of Ugt1a1 enzyme, resulting in increased levels of bilirubin and neonatal lethality, as these mice die within 2 weeks after birth. Two years later, in 2010, the same group generated a mouse strain presenting a milder phenotype of hyperbilirubinemia by the introduction of the *UGT1A1*28* allele, a common human genetic polymorphism in the *UGT1A1* promoter, into the *Ugt1*$^{-/-}$ strain, partially rescuing lethality. In fact, only 10% of this humanized *Ugt1* (*hUGT1*) mice experience toxic levels of bilirubin, resulting in seizure and death (Fujiwara et al., 2010).

Interestingly, these *hUGT1* mice allowed studying the relation between intestinal Ugt1a1 relevance and the effects of breastfeeding on the enzyme activity. Mutant mice receiving breast milk show decreased UGT1A1 activity and developed higher level of bilirubin compared to mice fed with formula (Fujiwara et al., 2012). In addition, the authors showed that the reduced enzyme activity involved the inhibition of the nuclear factor kappa-light-chain-enhancer of activated B cells (NFKβ), leading to hyperbilirubinemia, underlining the importance of the intestinal Ugt1a1 (Fujiwara et al., 2012).

By Cre-mediated recombination, two conditional knockouts were generated by the disruption of the *Ugt1* locus in the liver (*albumin*-Cre) or in the intestine (*villin*-Cre), to reveal the contribution of different organs to the bilirubin metabolism. Cre-mediated recombination of the *Ugt1*$^{F/F}$ mice (*Ugt1* intron 2 floxed/intron 4 floxed) was used to generate hepatocytes (*Ugt1*$^{\Delta Hep}$) or intestinal enterocytes (*Ugt1*$^{\Delta GI}$) deficient in Ugt1a1 activity. *Ugt1*$^{\Delta Hep}$ mice show much lower bilirubin levels compared to *Ugt1*$^{-/-}$ mice (TB was 2 vs 15 mg/dL, respectively), underling the importance of extrahepatic UGT1A1 activity, while the intestinal KO of *Ugt1* in *Ugt1*$^{\Delta GI}$ results in no abnormalities (Chen et al., 2013).

The *hUGT1* mice were also used to underscore the importance of the inflammatory response contribution, by mating them with a knock-out strain of the toll-like receptor 2 (TLR2). In fact, *hUGT1* mice reveal the activation of inflammatory players in the CNS, such as glia cells and inflammatory markers, while *hUGT1/TLR2*$^{-/-}$ mice show the absence of neuro-inflammatory response that resulted in increased death rate (Yueh et al., 2014). In addition, the analysis of *hUGT1* animals is characterized by the prevalence of astrocytes and microglia cells (Yueh et al., 2014). Two years later, the same group generated a liver-specific conditional *Ugt1a1* knockout mouse model, in which mice develop kernicterus. Reduced myelination, accompanied by increased astroglial and microglial reactivity, and marked PCs loss is observed in these mice (Barateiro et al., 2016).

1.4.4 *Ugt1*$^{-/-}$ mouse model (1 base deletion)

A mouse model of hyperbilirubinemia was also generated in my laboratory. In 2012, by gene targeting, Bortolussi and colleagues developed another mouse model bearing a one-base deletion in the exon 4 of the *Ugt1* gene, which results in a null mutation (Bortolussi et al., 2012). The mutation in the C57BL/6 strain background reproduces the major features of neonatal hyperbilirubinemia. In fact, consequent to the absence of Ugt1a1 bilirubin-glucuronosylation activity in *Ugt1*$^{-/-}$ mice, plasma TB levels rise immediately after birth leading to cerebellar hypoplasia, neuronal cell death and early lethality by kernicterus, with 50% mortality at P5 and no survivors after P11 (Bortolussi et al., 2012). The toxic levels of bilirubin in mutant mice produce neurodamage in the cerebellum, as cerebellar layers are reduced and PCs number is significantly less compared to wild type littermates. In addition, TUNEL assay in cerebellum showed increased cell death in *Ugt1*$^{-/-}$ animals (Bortolussi et

al., 2012). Phototherapy treatment (PT, Chapter 1.5.1.2) extends lifespan of C57BL/6 *Ugt1*$^{-/-}$ animals from 5 to 18 days (50% of survival), but was not sufficient to rescue their lethal phenotype (Bortolussi et al., 2012). By proteomic analysis, it was observed that hyperbilirubinemia impairs oxidoreductase activities and antioxidant processes. In addition, the activation of apoptosis by caspase 3 activation and the increased phosporylation of p38 are observed, resulting in the degeneration of PCs (Figure 4) (Bortolussi et al., 2015).

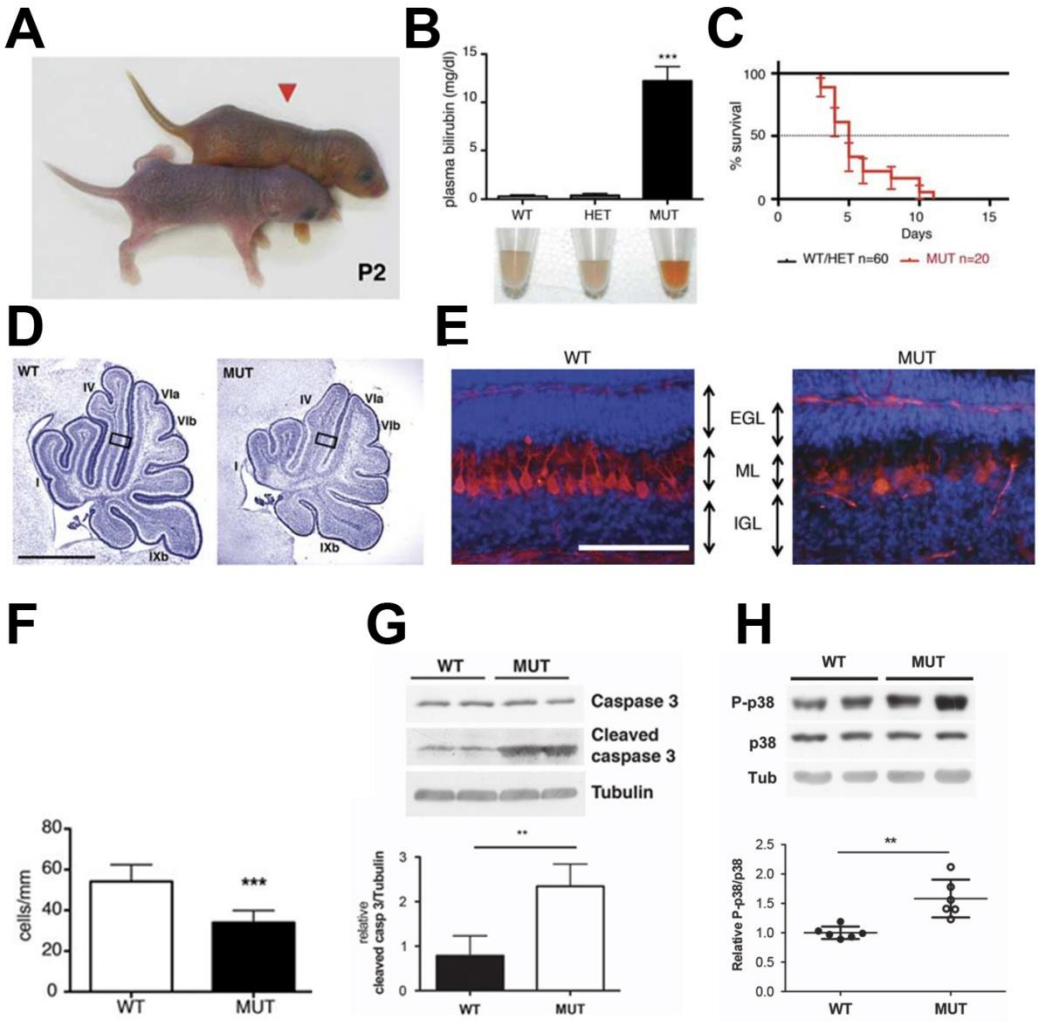

Figure 4. Hyperbilirubinemia features of *Ugt1*$^{-/-}$ mice in the C57BL/6 background strain. A) appearance of *Ugt1*$^{-/-}$ pup (MUT, red arrows) and WT at P2; **B)** TB levels (mg/dL) in wild type, heterozygous and *Ugt1*$^{-/-}$ mice at P5, representative plasma samples below; **C)** survival of *Ugt1*$^{-/-}$ mice in C57BL/6 background; **D)** representative images of cerebellar Nissl staining from WT and *Ugt1*$^{-/-}$ mice at P5 (scale bar 1000µm); **E)** representative images of fluorescent immunohistochemistry of WT and *Ugt1*$^{-/-}$ cerebella at P5, using Hoechst to stain nuclei (blue) and antibody anti-calbindin (red) to stain Purkinje cells; **F)** quantification of Purkinje cell density (cell/mm) at P5 (scale bar 100µm); **G)** WB of total cerebellar protein extracts using anti-cleaved caspase 3 and anti-total caspase 3 in WT and *Ugt1*$^{-/-}$ mice, and the relative quantification is represented below; **H)** WB of total cerebellar protein extracts using anti-P-p38 and anti-total p38 in WT and *Ugt1*$^{-/-}$ mice, and the relative quantification is represented below. Adapted from (Bortolussi et al., 2012, 2015).

When the mutation was transferred to the FVB/NJ background, homozygous mutant mice develop severe jaundice soon after birth and their mortality is delayed compared to the C57BL/6 strain, as the FVB/NJ-*Ugt1*$^{-/-}$ mice die within two weeks (50% of survival at P11), showing marked cerebellar impairment and neuronal cell death, with a prominent loss of PCs (Figure 5) (Bortolussi et al., 2014).

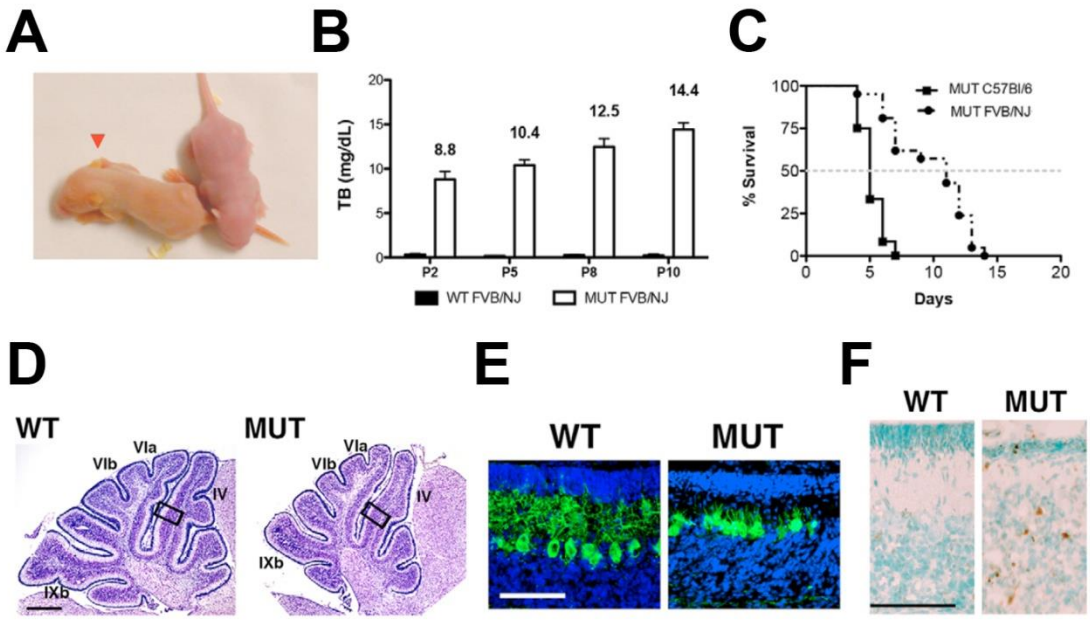

Figure 5. Hyperbilirubinemia features of *Ugt1*$^{-/-}$ mice in the FVB/NJ background strain. A) appearance of *Ugt1*$^{-/-}$ pup (MUT, red arrows) and WT at P2; **B)** TB levels (mg/dL) in wild type and *Ugt1*$^{-/-}$ mice at the indicated time points; **C)** survival of *Ugt1*$^{-/-}$ mice in C57BL/6 and FVB/NJ backgrounds; **D)** representative images of cerebellar Nissl staining from WT and *Ugt1*$^{-/-}$ mice at P8 (scale bar 200µm); **E)** representative images of fluorescent immunohistochemistry of WT and *Ugt1*$^{-/-}$ cerebella at P5, using Hoechst to stain nuclei (blue) and antibody anti-calbindin (green) to stain Purkinje cells (scale bar 50µm); **F)** TUNEL analysis. Positive cells are shown as brown dots; negative cells are counterstained with methyl green (scale bar 100µm). Adapted from (Bortolussi et al., 2014).

One of the advantages of these models resides in the possibility to modulate the severity of the phenotype by applying PT for different periods, allowing the study of physiological and biochemical implications of bilirubin toxicity at the desired developmental stage. It was demonstrated that PT treatment effectively prevents brain damage and results in the complete rescue of the lethal phenotype only in the FVB/NJ mutant animals, while C57BL/6 mutant mice show a more severe phenotype (Bortolussi et al., 2014). By PT modulation, a specific window of neuronal susceptibility to bilirubin is identified around P8 in the FVB/NJ *Ugt1*$^{-/-}$ mice, underling a different vulnerability of neurons to bilirubin. The PT application to FVB/NJ *Ugt1*$^{-/-}$

from birth to P8 does not prevent bilirubin neurodegenerative features, while the accumulation of BIND is not rescued when PT is applied from P8 to P20 (Bortolussi et al., 2014).
In addition, the importance of Bf in the outcome of BIND and death was also showed in FVB/NJ *Ugt1*$^{-/-}$ (see Results and Discussion Chapters for details).

1.5 Standard therapeutic treatments for hyperbilirubinemia

Several treatments have been proposed to avoid the risk of BIND. Standard therapies focus on the reduction of toxic UCB levels.

1.5.1 Phenobarbital treatment

The first clinical distinction between Crigler-Najjar syndrome types I and II has been based on the efficacy of phenobarbital therapy to lower plasma bilirubin levels. Phenobarbital increases the expression of *UGT1* genes (Argikar et al., 2009). In CNSII patients, the basal residual UGT1A1 activity is increased by the transcriptional induction of the *UGT1A1* gene by phenobarbital, maintaining bilirubin concentration below the neurotoxicity threshold (Jansen, 1999). Conversely, hyperbilirubinemia is unchanged by this treatment in CNSI patients, as there are no signs of increase in UGT1A1 activity. These patients are temporarily treated with phototherapy (see Chapter 1.5.2), as its effectiveness is reduced with age. The only causal treatment to cure CNSI, so far, is liver transplantation.

1.5.2 Phototherapy

Severe unconjugated hyperbilirubinemia is conventionally treated by intensive phototherapy (PT). Light energy (emission range 400-525 nm, peak emission: 450-460 nm) is absorbed by UCB as it circulates in skin capillaries, resulting in the conversion of insoluble bilirubin into water-soluble photoisomers that can be eliminated into the bile without the need of liver conjugation, or at smaller rate into the urine (Maisels and McDonagh, 2008). PT is generally very effective to prevent transient hyperbilirubinemia in healthy neonates, as the hepatic conjugation system rapidly matures.

The timing of PT intervention impacts on the outcome of preterm at risk infants. Indeed, the implementation of strategies to rapidly and effectively reduce the excessive bilirubin load prior to the onset of neurologic signs would prevent chronic post-icteric sequelae or kernicterus (Smitherman et al., 2006). Prophylactic phototherapy helps to maintain a lower serum bilirubin concentration and may have an effect on the rate of exchange transfusion. Despite PT effectiveness, the condition of neonatal jaundice may still require additional, potentially dangerous, exchange transfusion (ET, Chapter 1.5.4).

In Crigler–Najjar patients, the permanent unconjugated hyperbilirubinemia requires a consistent number of hours of phototherapy treatment per day (12-14h). However, there are different factors that affect the outcome of PT treatment with age, such as the growth of skin thickness, the increased pigmentation and the increment in the body surface/volume ratio. Thus, the blue light reaches the capillaries less efficiently, decreasing the PT efficacy. CNSI patients respond temporarily to PT and are at constant risk of developing brain damage unless liver transplantation is performed (Fagiuoli et al., 2013).

Experimental evidences of beneficial PT effects were also observed in animal models of hyperbilirubinemia. For instance, 24 hours of PT exposure between P4 and P11 prevent hypoplasia in the cerebellum of jj Gunn rat pups (Keino and Kashiwamata, 1989), while in the FVB/NJ *Ugt1*$^{-/-}$ mouse model, 15 days of PT application are necessary to completely rescue BIND and lethality (Bortolussi et al., 2014). This variability of PT efficacy in rescuing cerebellar abnormalities underlines the different degree of severity between the two hyperbilirubinemic models.

1.5.3 Immunoglobulins

As previously shown, blood incompatibility results in haemolysis and is, in consequence, an important risk factor to develop jaundice (Chapter 1.3.1 and Table 1). The combination of PT with intravenous injections of immunoglobulins against immune-mediated haemolysis (such as antibody against Rh or AB antigens) has been exploited in cases of hyperbilirubinemia induced by Rh and/or ABO blood incompatibility. It has been shown that intravenous immunoglobulin injections significantly reduced the need for exchange transfusion and the duration of PT in neonatal jaundice (Huizing et al., 2008).

1.5.4 Exchange transfusion

Jaundice is normally treated with PT, which has sufficient efficacy, convenience and high safety. However, to prevent or reduce bilirubin-induced brain damage, jaundiced infants who fail to respond to PT or are severely hyperbilirubinemic upon first presentation are treated with the more invasive and dangerous alternative such as exchange transfusion (ET). This procedure consists in the partial replacement of the patient blood (hyperbilirubinemic blood, as in the case of neonatal jaundice) with a compatible fresh one. ET is implemented only in specialized centres and carries a significant risk of morbidity and mortality, such as biochemical and haematological disturbances, vascular accidents, hypocalcaemia, necrotizing enterocollitis and cardiac complications (American Academy of Pediatrics, 2004; Bhutani and Wong, 2013). The overall mortality rate from the procedure ranges between 0.3% and 0.7%, having high variability among the different centres, but it can reach up to 17% in developing countries (Ibekwe et al., 2012). Adverse events, including catheter-related complications, sepsis, and thrombocytopenia may amount up to 36% (Davutoğlu et al., 2010; Owa et al., 2009).

Schreuder and colleagues provided proofs of the ET effectiveness in Gunn rats, showing that the combination of ET, PT and albumin administration strongly reduces plasma bilirubin levels of jj rats (Schreuder et al., 2013a).

It is expected that ET lowers bilirubin levels in a sufficient and quick manner. However, it has remained unclear whether ET could be successfully replaced by other more effective and less invasive treatments.

1.6 Experimental treatments

Standard treatments are usually very effective. Nevertheless, specific cases may require a different approach, in which experimental treatments may be combined with standard therapies to improve the outcome of neonatal hyperbilirubinemia. These experimental treatments can be divided in those pointing to avoid the toxic accumulation of UCB and those which confer neuroprotection without affecting TB levels

1.6.1 Orlistat and ursodeoxycholic acid

UCB can diffuse from the blood compartment into the intestinal lumen across the intestinal mucosa and it can be reabsorbed from the intestinal lumen. A possible implementation for standard therapies is the acceleration of UCB gastrointestinal transit by enhancing the efficacy of transmucosal bilirubin disposal.

Orlistat and ursodeoxycholic acid (UDCA) are compounds designed to increase the fecal disposal of UCB. The primary function of orlistat is to prevent the absorption of fats from the diet, whereas UDCA reduces the rate at which the intestine absorbs cholesterol molecules. It was shown that orlistat and UDCA administration lower plasma UCB concentrations via the enhancement of fecal excretion of UCB–bile salt complexes, being effective in bilirubin reduction in Gunn rats (Cuperus et al., 2009; Hafkamp et al., 2005) and Crigler-Najjar patients (Hafkamp et al., 2007).

Further studies are needed to exclude long-term side effects of these drugs, as both orlistat and UDCA showed hepatotoxic side effects, rising concerns of cost-effectiveness.

1.6.2 Human serum albumin

Not all neonates with severe hyperbilirubinemia develop bilirubin encephalopathy. Many factors may interact with the high TB concentrations, either preventing or predisposing to kernicterus. Among these factors, human serum albumin (HSA) plays an important role in the bilirubin pathway (Ahlfors, 2000; Dennery et al., 2001; Poland, 2002). In fact UCB binds to serum albumin and, in this form, it is transported to the liver. As long as the bilirubin is bound to albumin, UCB cannot cross the BBB and enter the brain (Odell, 1973). When bilirubin-binding capacity provided by plasma albumin is saturated, the unbound fraction (Bf), increases and accumulates in lipophilic tissues. In principle, increasing the plasma-binding capacity to UCB should mobilize bilirubin from tissues to plasma, preventing the neurodamage (Figure 6).

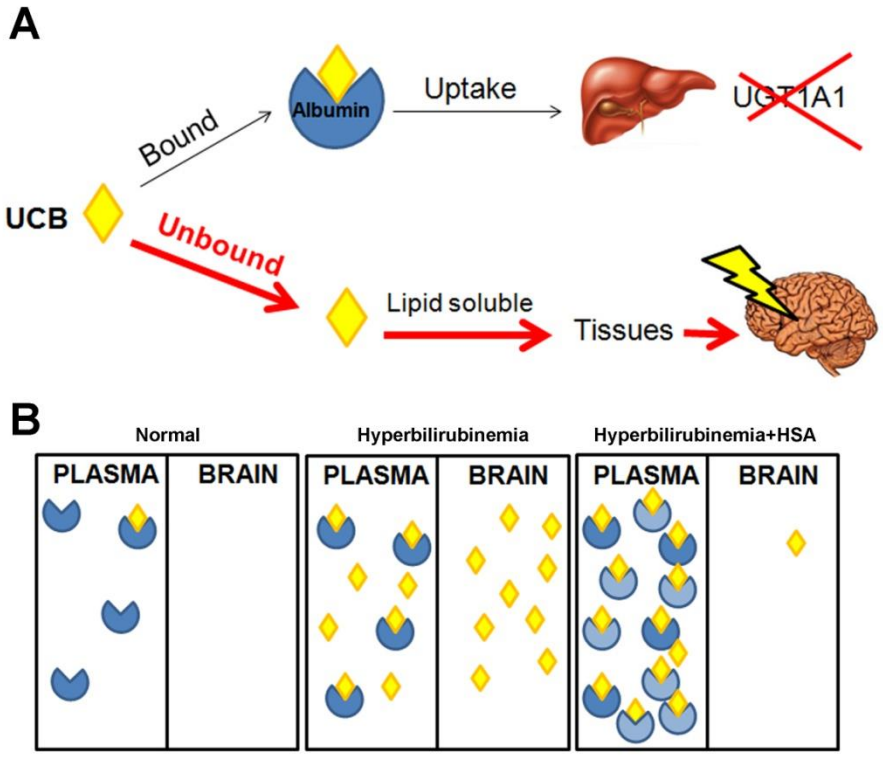

Figure 6. Rationale of HSA administration. A) Effect of UCB in case of glucuronosylation defects; **B)** Schematic representation of UCB mobilization from tissue to the newly supplied binding site in plasma

The albumin binding to bilirubin is less effective during the first post-natal days than in older infants or adults, as well as low serum albumin concentration. Thus even healthy and term neonates need a special consideration (Stevenson et al., 2004). Moreover, metabolic acidosis, infection, hyperoxia, prematurity and drugs or preservatives, including sulfisoxazole or benzyl alcohol may interfere with bilirubin-albumin binding or with the integrity of the blood–brain barrier (Connolly and Volpe, 1990).

Albumin infusion has long been used as an adjunct to PT or prior to ET to improve the outcome in the management of neonatal hyperbilirubinemia. The administration of 20% HSA solution significantly reduces post-ET bilirubin levels in term neonates (Shahian and Moslehi, 2010). In 2001, Hosono and colleagues showed that albumin priming may be effective for an immediate reduction in serum Bf values (Hosono et al., 2001a, 2002). Studies by Wood and colleagues have shown similar favourable results (Wood et al., 1970). Pre-ET, 5% albumin infusion in low birth weight neonates is significantly effective in reducing the post-ET UCB levels and the duration of post-exchange phototherapy (Mitra et al., 2011). Conversely, Chan and Schiff have reported no significant difference in the efficiency of bilirubin removal following albumin loading prior to exchange transfusion (Chan and Schiff, 1976).

Pre-clinical studies performed in adult Gunn rats demonstrated the short-term efficacy of a single albumin infusion. The group of Dr. Verkade showed that HSA efficiently lowers plasma Bf, brain bilirubin levels and prevents BAEPs (Cuperus et al., 2013; Schreuder et al., 2013b). Thus, HSA infusion to treat severe hyperbilirubinemic conditions may represent a safe and feasible approach. Deeper investigations are needed to clarify the role of Bf and the long-term effectiveness of HSA in tackling BIND during post-natal development of newborns at risk.

1.6.3 Minocycline

MNC is a second-generation tetracycline that has anti-inflammatory effects, which appear to be completely separated and distinct from its anti-microbial action (Ryan and Ashley, 1998). It is a small (495 kD), highly lipophilic molecule that crosses the BBB better than other tetracyclines (Macdonald et al., 1973).

MNC is readily absorbed from the gut after oral ingestion and, because of its low propensity to produce antibiotic resistance, it is commonly used in the management of chronic conditions such as acne and rosacea. This compound is well tolerated in teenagers and adults (according to registry records in the United Kingdom). For an average of 9 months, over 6 million individuals have been treated with MNC to cure acne. Overall, a good safety record for long-term clinical use has been established for MNC, justifying its intensive use for over 40 years (Yong et al., 2004). However, MNC has shown different side effects, such as hyperpigmentation, photosensibility, vestibular defects, hypersensitivity and tooth discoloration (Smith and Leyden, 2005).

The anti-inflammatory properties of MNC have been reported in various neurodegenerative conditions such as stroke (Yrjänheikki et al., 1999), Huntington's disease (HD) (Chen et al., 2000) and Parkinson's disease (PD) (Wu et al., 2002), especially by the inhibition of microglial inflammatory response. MNC exerts its anti-inflammatory actions by modulating microglia, immune cell activation and subsequent release of chemokines, lipid mediators of inflammation, matrix metalloproteinases (MMPs) and nitric oxide (NO) but also pro-inflammatory cytokines, such as tumor necrosis factor α (TNF-α), interleukin (IL) 1β (IL1β) and IL6 that are produced by microglial cells, astrocytes, neutrophils and macrophages (Stirling et al., 2005).

The neuroprotective properties of MNC have shown to be due in part to indirect effects in inhibiting glial (astrocytic/microglial) caspase 1 and inducible nitric oxide synthase (iNOS) activity (Wu et al., 2002; Yrjänheikki et al., 1999), although direct neuroprotective effects have also been observed (Lin et al., 2001, 2003).

Apoptosis of both neurons and glia occurs in a variety of neurodegenerative diseases and following CNS trauma (Ekshyyan and Aw, 2004). MNC is reported to decrease apoptotic neuronal cell death observed in several experimental models of neurodegeneration (Kim and Suh, 2009). In addition, MNC treatment delays mortality in the R6/2 mouse model of HD and amyotrophic lateral sclerosis (ALS), presumably by inhibiting caspase 1 and caspase 3 expression, as well as iNOS activity and cytochrome *c* release (Huang et al., 2009; Zhu et al., 2002).

In 2005, Lin and colleagues reported the first evidence of the *in vivo* effect of MNC on bilirubin-induced cerebellar hypoplasia, by the study of the Gunn rats. MNC treatment of homozygous Gunn rat pups almost completely prevents cerebellar hypoplasia and loss of cerebellar PCs and GCs, with no effect on total bilirubin levels. Exposure of cerebellar granule neurons (CGNs) to bilirubin results in a time-dependent phosphorylation of p38 mitogen-activated protein kinase (MAPK), which is inhibited by MNC treatment, suggesting a role for p38 MAPK activation in bilirubin neurotoxicity and the neuroprotective effects of MNC (Lin et al., 2005).

Further evidences on the effect of MNC on the attenuation of bilirubin neurotoxicity have been provided by the group of Shapiro, by its work on Gunn rats. First, the authors showed that MNC rescues bilirubin-induced alterations in acute BAEPs (Geiger et al., 2007). Later, a time-dependent, graded, neuroprotective effect of MNC was observed when the drug is administered after acute hyperbilirubinemia obtained by PHZ/Sulpha induction (Rice et al., 2011).

Recently, MNC administration to Gunn rats showed the amelioration of behavioural abnormalities. After MNC administration, it is observed the amelioration of performance in the open field, social interaction and prepulse inhibition tests, also underscoring the anti-psychotic effect of MNC (Liaury et al., 2014).

1.6.4 Other treatments

Other treatments have been experimented in combination with standard therapies to avoid toxic bilirubin levels in neonatal jaundice.

A promising therapy is the inhibition of heme oxygenase 1 (HO1) by metalloporphyrins (Mps). Mps target is the blockade of HO1 enzyme, which is the rate-limiting enzyme in the pathway of bilirubin production. The clinical efficacy of Mps is shown by the reduction of TB in neonatal haemolysis (Schulz et al., 2012). However, Mps may affect other enzymes and have some side effects, such as photosensibility, thus further studies on a modified version are required.
An additional experimentation on hyperbilirubinemia has been made by the use of ethanol extracts of *Phyllantus amarus* root. The authors showed the efficacy of this compound in reducing phenylhydrazine-induced neonatal jaundice in mice. In particular, the bilirubin lowering effect is achieved by the presence of gallic acid (Maity et al., 2013).

1.7 Mechanisms of bilirubin neurotoxicity

In this section, I will give an overview of the main mechanisms involved in bilirubin-induced neurological dysfunction.

1.7.1 Neurodegeneration

Neurodegeneration is the umbrella term for the neuronal progressive loss of structures or functions, including death. Since neurons renewal is tightly restricted, once developed, neurodegeneration strongly impacts on the CNS. Nowadays, the attention is mainly focused on conditions such as AD, HD, PD and ALS, which are the most intensively studied neurodegenerative diseases (Brettschneider et al., 2015).
However, in humans, many of the clinical and pathological features overlap between the different neurodegenerative diseases, leading to a misdiagnosis of the disease, but have neurodegeneration as a shared feature. To overcome such problems in the phenotypic identification of neurodegenerative diseases, animal models are useful tools to better characterize neurodegeneration (Harvey et al., 2012). Despite the extensive efforts made to elucidate the effects, the causes of neurodegeneration are often not completely understood and the identification of the key mechanisms initiating the diseases remains unclear.

Neurodegenerative diseases are not the only conditions in which the functionality of neurons is altered. In fact, neurodegeneration is also caused by all the events that in turn affect the neuron integrity and development. For instance, the lack of oxygen leads to dendrites loss and extensive fragmentation of the dendritic arbor (Wen et al., 2013), as well as in traumatic brain injury (Petzold et al., 2011), resulting in neuronal cell death.

High levels of bilirubin are also a cause of neurodegeneration. As mentioned before, genetic and non-genetic alterations of the bilirubin metabolism result in high levels of systemic UCB, affecting the developing CNS. Although transient, the phenomenon of neonatal jaundice may result in neurotoxic levels of bilirubin, thus affecting neurons. Neuronal cells are the target of bilirubin toxicity, due to the capacity of the yellow pigment to bind cellular membranes, specially the myelin-rich ones (Watchko and Tiribelli, 2013).

In fact, neurons are very susceptible to bilirubin, and UCB exposure causes the impairment of cellular morphology, resulting in the reduction of nodes and neurites extensions (Falcão et al., 2007; Vaz et al., 2010). Exposure to bilirubin also causes cell death both by apoptosis and necrosis (Grojean et al., 2001; Silva et al., 2001). The alteration of the redox status by UCB affects cellular viability (Tell and Gustincich, 2009). In fact, the decrease of mitochondrial membrane potential leads to cell energy failure producing the collapse of mitochondrial structures and the release of cytochrome c, then activating caspases and consequentially the programmed cell death (Rodrigues et al., 2002). Moreover, bilirubin has showed an impact on PCs degeneration in different models of hyperbilirubinemia (Barateiro et al., 2016; Bortolussi et al., 2012, 2014), and that the presynapsis of glutaminergic neurons are impaired by UCB (Haustein et al., 2010), giving additional *in vivo* evidences that bilirubin triggers neurodegeneration.

1.7.2 Oxidative stress

Oxidative stress is the result of the imbalance between the antioxidant defences in favour of the production of reactive oxygen species (ROS, more in general, free radicals) (Uttara et al., 2009). Free radicals are chemical species containing unpaired electrons. They can be products of the aerobic respiration, by-products released from chemical reactions or generated by external electromagnetic radiation. The unpaired number of electrons confers instability to the free radicals,

which, in turn, achieve a stable state passing the unpaired electron to other molecules. The interaction between free radicals and non-radicals molecules creates a free radical chain reaction, in which the instability of unpaired electrons is passed between molecules. If intense, the molecular instability may affect cellular homeostasis by overcoming the mechanism to counteract this kind of stress. Within cells, the excessive production of electrically instable molecules is avoided by the mitochondrial cytochrome oxidase, which transports the electrons without the release of reactive oxygen species. However, oxidative stress is detrimental for cells, as the oxidation of proteins, lipids and DNA may damage those molecules.

The levels of intracellular ROS are tightly regulated by cells. To overcome disproportionate free radicals production generated by toxic reactive oxygen metabolites and H_2O_2, different enzymes are involved in antioxidant defensive mechanisms, such as superoxide dismutase (SOD), glutathione peroxidase, catalase, thioredoxin and glutathione transferases, and HO1 (Cho et al., 2002). Moreover, non-enzymatic antioxidant molecules contribute to the protection from ROS. These compounds include β-carotene, vitamins C and E, uric acid and a tripeptide made of glutamine-cysteine-glycine (Birben et al., 2012).

One of the most intensively studied genes involved in the oxidative stress response is nuclear factor (erythroid-derived 2)-like 2 (Nrf2). When cells detect the stress, Nrf2 is activated and translocates from the cytoplasm into the nucleus, where it binds to the antioxidant response elements (ARE) in the upstream region of antioxidant genes, such as glutathione transferases and oxidoreductases and HO1 (Nguyen et al., 2003, 2009). Being an antioxidant enzyme, HO1 provides an important contribution in the bilirubin context, as it is a rate-limiting enzymes of the heme catabolism.

Mildly elevated bilirubin concentrations are considered beneficial, since UCB has antioxidant and cytoprotective properties (Stocker et al., 1987). However, high levels of bilirubin result in oxidative stress. *In vitro* experiments have shown that oxidative stress is a major mechanism involved in bilirubin neurotoxicity. ROS excess affects mitochondrial metabolism and glutathione homeostasis (Giraudi et al., 2011), generating cellular energetic crisis and the release of cytochrome c (Rodrigues et al., 2000) and Ca^{2+} perturbation (Stoeckius et al., 2012). The exposure of synaptosomes extracted from adult gerbils to bilirubin revealed the enhanced production of ROS, protein oxidation and lipid peroxidation (Brito et al., 2004). Similar results are highlighted in immortalized hepatoma cell lines, in which

the depolarization of the membranes leads to impaired homeostasis and caspase 9-induced apoptosis, further confirming the detrimental effect of excessive oxidative stress resulting from bilirubin exposure (Oakes and Bend, 2005). A microarray analysis performed on neuroblastoma cell lines showed the up-regulation of several molecular chaperones and oxido-reductase proteins, such as *protein disulfide isomerase family a 5* and *6*, and *endoplasmic reticulum oxidoreductase 1-like (ERO1L)* (Calligaris et al., 2009), being the latter one a chaperon protein involved in the folding of oxidated proteins.

Experiments performed in Gunn rat pups show that UCB induces lipid peroxidation (the oxidative degradation of lipids that result in cellular damage), as assessed by the determination of 4-hydroxy-2-nonenal levels in sulphadimethoxine-induced hyperbilirubinemia (Daood et al., 2012). My group showed that bilirubin affects antioxidant defences *in vivo* in the cerebellum of the C57BL/6 *Ugt1*$^{-/-}$ mouse model. In fact, by proteomic and expression analysis of affected cerebella we reported that Nrf2 expression is increased, while Sod1 levels are decreased (Bortolussi et al., 2015). In addition, it was shown an increased oxidation of peroxiredoxine 2 and 6 at protein upon bilirubin exposure. The reduction in antioxidant defences results in the increase of neuronal cell death (Bortolussi et al., 2015).

Other *in vivo* evidences of oxidative stress caused by bilirubin were shown in another mouse model of hyperbilirubinemia. The authors observed that elevated plasma UCB levels cause the increase in glutathione oxidation as well as in HO1 protein levels (Yueh et al., 2014).

Excessive oxidative stress triggered by bilirubin leads to neuronal cell death. During neurodegeneration, neurons lose their ability to sense the imbalanced metabolism of reactive oxygen production and, consequently, cell viability is affected by impaired oxidative stress (Figure 7) (Federico et al., 2012).

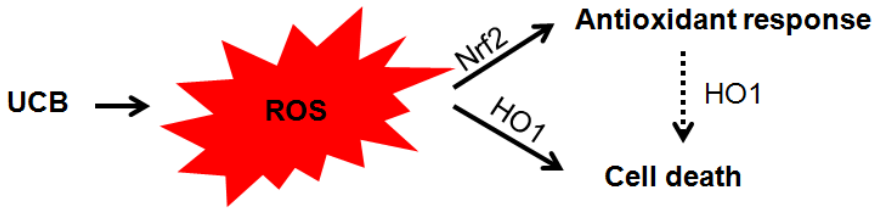

Figure 7. Bilirubin-induced oxidative stress. High levels of UCB generate an excess of free radical and ROS, activating the antioxidant response by Nrf2. During prolonged stage of stress, when cells are not able to counteract the oxidative stress, cell death is selected.

1.7.3 ER stress

The endoplasmic reticulum (ER) is a cell organelle involved in protein and lipid synthesis, composed by a network of branching tubules and sacs. It is contiguous to the nuclear envelope, and is present in the cytoplasm of all eukaryotic cells. Also, the ER is a dynamic store of calcium. Modifications of the cellular stability lead to an excess of unfolded proteins, a condition named ER stress, causing an accumulation of misfolded proteins.

The ER has a unique oxidizing-folding environment, and ROS may also come from the alteration of this cellular compartment, underlining a tight connection between oxidative stress and the ER.

During the initial phases of the loss of balance, cells activate a pro-survival pathway called unfolded protein response (UPR). Depending on the insult, the ER stress response takes place by the activation of one of the three major proteins (or the combination):

a) inositol requiring 1 (IRE1),

b) protein kinase RNA-like endoplasmic reticulum kinase (PERK)

c) activating transcription factor 6 (ATF6).

Each of the three main proteins has a different network cascade, and the activation of a preferential pathway is the result of different stresses (Doyle et al., 2011). In any case the aim of this activation is to reinstate the normal condition. The UPR activation delays the translation process to clear unfolded proteins and, at the same time, to induce the expression of genes involved in cell survival and protein degradation.

ER stress stimuli, such as the accumulation of unfolded proteins, cause the dissociation of an ER chaperone, glucose-regulated protein 78 (GRP78), from IRE1, PERK and ATF6, leading to the activation of the ER stress pathway (Doyle et al., 2011). GRP78 is also bound to the newly synthesized proteins, maintaining them in a competent state to allow the correct folding.

Generally, all these ER stress response pathways aim to restore the normal functionality of cells by the activation of UPR target genes. However, a sustained ER stress condition makes cells unable to reach back a steady state over time. In this case, the accumulation of unfolded proteins culminates with the activation of the apoptotic pathway. For instance, the activation of the two mediators C/EBP-Homologous Protein (CHOP) and cluster of differentiation (CD) 95/Fas (CD95/Fas) is involved in the apoptosis pathways selection through the activation of caspases

(Li et al., 2014; Peter et al., 2015). In addition, human cancer cells show that ER stress increased the transcription of important regulators, such as death receptor 5 (DR5), activating transcription factors 3 (ATF3) and 4 (ATF4), and CHOP (Liu et al., 2012). The activation of these genes results in apoptosis induced by the up-regulation of caspase 9, caspase 8 and caspase 3 (Liu et al., 2012).

ER stress is one of the key contributors to neurodegenerative disease (Oakes and Papa, 2015). In fact, AD, PD, ALS and HD but also other pathologies are characterized by the accumulation of abnormal protein aggregates, which affect the ER stability.

It was shown that bilirubin is involved in impairing ER homeostasis. In fact, when oligodendrocyte precursors are exposed to toxic UCB levels, ER stress is observed by the increase in GRP78, IRE1 and ATF6 expression (Barateiro et al., 2012). Other genes known to mediate ER-response, such as CHOP and ATF3, are up-regulated in response to high bilirubin levels in a transcriptome analysis performed in neuroblastoma cell lines (Calligaris et al., 2009). Microarray analysis of hepatoma cell lines incubated with toxic bilirubin levels revealed the activation of ER stress response. In particular, it was shown the up-regulation of GRP78, ATF3, CHOP expression and the activation of PERK pathway by its phosphorylation (Oakes and Bend, 2010), underling how ER stress contributes to UCB toxicity (Figure 8).

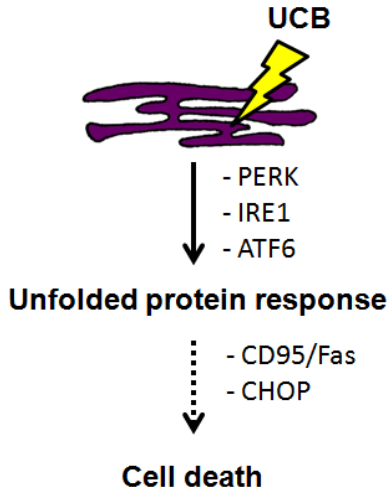

Figure 8. Bilirubin causes ER stress. ER stress response is produced by PERK, IRE1 or ATF6, which activate the unfolded protein response. Over prolonged bilirubin levels, CD95/Fas and/or CHOP are activated, leading to cell death.

The disruption of ER homeostasis leading to UPR activation, cellular energy failure and ROS production can also result in inflammation, a topic that will be discussed in the following Chapter.

1.7.4 Neuroinflammation

Neuroinflammation is used to describe the general inflammatory state that involves the brain and the spinal cord. Different factors mediate the degree of neuroinflammation, such as cytokines, chemokines, ROS and secondary messengers, but also the context, the nature of the insult and the duration of the inflammatory stimulus.

The CNS immune surveillance is provided mainly by CNS glia cells (microglia, astrocytes, macrophages and oligodendrocytes), but also by endothelial cells. The role of CNS inflammation is intended as protective, aiming to solve the impaired status generated by the stressor agents. However, prolonged neuroinflammatory response activation may exacerbate and amplify the damage by further increasing the activation of glia cells.

Microglia cells/macrophages migrating at the site of the injury can exert the opposite roles of repairing the damage or its intensification, depending on their activation status. The polarization of microglia/macrophages is important to define the different reactions at the site of interest. Once activated, glia cells produce different stimuli that define the neuroinflammatory responses. In fact, different types of peripheral macrophages have distinct functions depending on the surrounding environment and the duration of the injury: the inflammatory macrophages (M1 type microglia) and the anti-inflammatory macrophages (M2 type microglia). As a consequence, after an acute injury, the ratio of M1 and M2 microglia determines the direction of the response, whether pro-inflammatory or neuroprotective. The pro-inflammatory M1 phenotype is commonly associated with clearance of dead tissue (Kigerl et al., 2009; Martinez et al., 2006), while M2 neuroprotective macrophages facilitate the control and repair/regeneration of injured tissues, partially by reducing the inflammatory mediators (Kigerl et al., 2009; Martinez et al., 2006) (Table 3).

Table 3. M1 vs M2 microglia markers and effectors. M1 and M2 microglia express distinct molecular markers and produce different molecular effectors listed in the table.

	M1 type	M2 type
Molecular markers	CD11b CD32 CD68 CD86 Iba1	Arg1 MRC1 MRC2
Molecular effectors	IL1β IL6 IL18 iNOS TNFα	IL4 IL10

Neuroinflammation is a common feature of many neurodegenerative diseases (Frank-Cannon et al., 2009). In fact, the activated glia cells and their relative neuroinflammatory markers accumulate at the site of neurodegeneration.

Different investigations have been performed to study the effect of bilirubin on glia cells activation. *In vitro* experiments have shown that the exposure to bilirubin caused the activation of both astrocytes (Falcao et al., 2014; Fernandes et al., 2004, 2006, 2007a) and microglia (Fernandes and Brites, 2009; Gordo et al., 2006; Silva et al., 2010a), resulting in the release of inflammatory response mediators as IL1β, IL6, TNFα, NFKβ, glutamate and interferon γ (INFγ). Moreover, gliosis is a key feature of high levels of bilirubin *in vivo*, being astrocytes and microglia actively present in their brain of Gunn rat model (Liaury et al., 2012; Mikoshiba et al., 1980), as well as in a liver-specific Ugt1a1 conditional knockout mouse model (Barateiro et al., 2016; Yueh et al., 2014), in which astrocytes and microglia markers are up-regulated.

The increased presence of glia cells resulting from UCB neurotoxicity can consequently trigger the activation of key cellular and molecular factors of neuroinflammation that may result in neurodamage exacerbation and cell death (Figure 9). *In vivo*, it has been observed that bilirubin-induced glia cells activation triggers the up-regulation of IL1β, IL6 and TNFα (Yueh et al., 2014), which, in turn, affected neuron viability. Thus, by the production of neurotoxic inflammatory players, neuroinflammation exacerbates neurodegeneration leading to cell death.

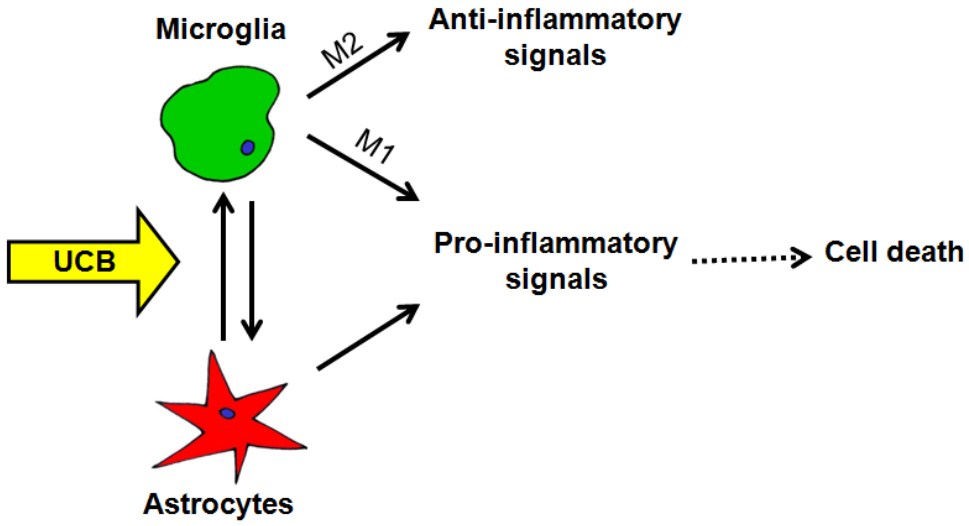

Figure 9. Bilirubin triggers neuroinflammation. Glia cells are activated after bilirubin exposure. Microglia can be polarized in the M2 type, showing anti-inflammatory properties. Astrocytes and M1 type microglia express pro-inflammatory signals leading to cell death.

Depending on the context, the modulation of inflammation is likely to decide the fate of neurons surrounded by glia cells. Thus, neuroinflammatory players may represent a strategic target for neurodegenerative disease.

1.7.5 Autophagy

Autophagy (from the Greek 'self-eating') is a cellular process which allows the orderly degradation of organelles and proteins. From an evolutionary point of view, this mechanism may represent the adaptation to the lack of nutrients. In fact, during starvation periods, the supplementation of energy and amino acids is provided by the activation of autophagy (Kuma et al., 2004). The basal autophagic activity is considered as a pro-survival mechanism, playing a cytoprotective role in response to stress factors. However, the impaired regulation of this process results in cell death through the activation of apoptosis (Scott et al., 2007). The inefficient clearance of the formed vesicles, the autophagosomes, leads to the alteration in the number of lysosomes within the cytoplasm that are detrimental to the cell homeostasis. Microtubule-associated protein 1A/1B-light chain 3 (LC3) is one of the key components in the formation of autophagosomes (Klionsky et al., 2009). The cytosolic LC3 (LC3I) is conjugated to phosphatidyelethanolamine to form the LC3-phophatidylethanolamine conjugate (LC3II), and LC3II is recruited on the

autophagosome. The fusion between autophagosomes with lysosomes generates the autolysosomes, and the hydrolases degrade the vesicle contents (Tanida et al., 2008). Hence, the ratio of LC3 isoforms represents a reliable marker to detect vesicles turnover.

Interestingly, mis-regulation of autophagy is involved in many different neurodegenerative disease, such as spinocerebellar ataxia, PD and HD (Rubinsztein et al., 2005).

In the context of bilirubin, few *in vitro* experiments showed the implication of autophagy activation in response to toxic bilirubin levels. Neuroblastoma cell lines incubated with bilirubin show the increased expression of regulation involved in the autophagic pathway, corresponding to the increase of important autophagy regulators (Calligaris et al., 2009). More recently, Palmela and colleagues showed the increase of LC3 ratio in brain microvascular endothelial cell (BMEC) cultures exposed to toxic bilirubin levels (Palmela et al., 2012). However, the two experiments underlined how this mechanism is activated only after prolonged bilirubin exposure, such as at the latest analysed time points.

So far, the role of autophagy was not investigated *in vivo*, thus further experiments are needed to elucidate the impact of autophagy in the developing brain exposed to bilirubin.

AIM OF THE THESIS

The aim of my PhD Thesis has been to characterize the bilirubin-induced neurological damage *in vivo* and to better understand the mechanisms of bilirubin neurotoxicity by the application of two different pharmacological treatments, such as the infusion of human serum albumin and the administration of MNC.

Since neonatal hyperbilirubinemia and the consequent death by kernicterus are still a concern, especially in low- and middle-income countries, a detailed description of the events leading to bilirubin neurotoxicity and death will give a further contribution to prevent the disease.

Taking advantage of the FVB/NJ *Ugt1*$^{-/-}$ mouse model, which resembles the human neonatal hyperbilirubinemia, it will be shown that free bilirubin is the cause of irreversible brain damage and death, and that these events can be prevented by increasing the bilirubin binding capacity in plasma.

Furthermore, I will elucidate the time-course of the molecular events at the onset of the neuropathological changes triggered by bilirubin.

Finally, I will use a neuroprotective and anti-inflammatory agent to explore the role of inflammation in the bilirubin neurotoxicity process.

MATERIALS AND METHODS

2.1 Chemicals and standard solutions:

2-butanol (Sigma-Aldrich)
Acetic acid (Sigma-Aldrich)
Albuman® (Sanquin, Amsterdam, the Netherlands)
Ascorbic acid (Sigma-Aldrich)
Bromo Cresol Green (Sigma-Aldrich)
Blue bromo Phenol (Sigma-Aldrich)
CCl_4 (Sigma-Aldrich)
Cresyl violet (Sigma-Aldrich)
dNTPs (Rovalab GmbH)
DOC (Sigma-Aldrich)
EDTA (Sigma-Aldrich)
EGTA (Sigma-Aldrich)
Ethanol (Sigma-Aldrich)
Glycine (Sigma-Aldrich)
Heparin (Sigma-Aldrich)
HPO_4 (Sigma-Aldrich)
KCl (Sigma-Aldrich)
KH_2PO_4 (Sigma-Aldrich)
Methanol (Sigma-Aldrich)
Minocin® (Teofarma, Pavia, Italy)
Na_2, HPO_4 (Sigma-Aldrich)
Na_3VO_4 (Sigma-Aldrich)
NaCl (Sigma-Aldrich)
NaN3 (Sigma-Aldrich)
NaF (Sigma-Aldrich)
NaPiro-P (Sigma-Aldrich)
NP-40 (Sigma-Aldrich)
PFA (Sigma-Aldrich)
phosphoSTOP (Roche)
Proteinase K (Roche)
SDS (Sigma-Aldrich)
SIGMAFAST protease inhibitors (Sigma-Aldrich)

Succinic acid (Sigma-Aldrich)
Sodium tetraborate (Sigma-Aldrich)
Tris (Invitrogen)
Triton-X 100 (Sigma-Aldrich)
Tween 20 (Sigma-Aldrich)
Xilene (Sigma-Aldrich)

10x protein loading buffer: 20 % SDS, 1 M DTT, 0.63 M Tris pH 7.0, 20 % BBP (dissolved in 60 % sucrose), 10 mM EDTA;
BCG solution: 26,2 mg of bromo cresol green, 24,4 mg of NaN_3, 2,214 g of Succinic Acid and 1 mL of Triton X-100 dissolved in 250 mL of dH_2O, pH 4.2;
Blotting Solution 1: 200 mM Tris, 10 % v/v Met-OH;
Blotting Solution 2: 25 mM Tris, 10 % v/v Met-OH;
Blotting Solution 3: 25 mM Tris, 40 mM Glycine 10 % v/v Met-OH;
Cresyl violet solution: 5 mg/mL cresyl violet in 0.3 % glacial acetic acid;
gDNA extraction buffer: 100 mM Tris pH 8.0, 5 mM EDTA pH 8.0, 0.2 % SDS, 200 mM NaCl and 100 µg/mL proteinase K;
PBS: 137 mM NaCl, 10 mM Na_2, HPO_4, 2.7 mM KCl, 2 mM KH_2PO_4, pH 7.4;
Perfusion solution: NaCl 0.9% w/v, 500 IU/mL heparin, 1 mg/mL ascorbic acid, 1 mg/mL EDTA;
Protein buffer: 150 mM NaCl, 1% NP-40, 0.5% DOC, 0.1% SDS, 50 mM Tris HCl pH 8.0, 2x protease inhibitors, 1 mM EGTA, 1 mM Na_3VO_4, 1 mM NaF, 1 mM NaPiro-P, 10 nM phosphoSTOP;
Running buffer 5X for SDS page: 30 g Tris, 147 g Glycine, 5 g SDS, dH_2O up to 1 L;
TBE buffer 5X: 1.1 M Tris, 900 mM Borate, 25 mM EDTA, pH 8.3;
TBS 1X: 50 mM Tris, 150 mM NaCl, pH 7.6, dH_2O up to 1 L;
TE Buffer: 10 mM Tris pH 8, 0.1 mM EDTA.

2.2 Animals

Ugt1$^{-/-}$ in FVB/NJ background was previously generated in Mouse Molecular Genetics group at the ICGEB (Bortolussi et al., 2014). Animals used in this study were at least 99.8% FVB/NJ genetic background, obtained after more than ten

backcrosses with wild type FVB/NJ mice. Homozygous mutant animals (*Ugt1*$^{-/-}$) were obtained from heterozygous (*Ugt1*$^{+/-}$) mating. Wild type (WT or *Ugt1*$^{+/+}$) littermates were used as control. Average litters were of 9-10 pups and loss of pups was not observed. Mice were housed and handled according to institutional guidelines, and experimental procedures approved by the International Centre for Genetic Engineering and Biotechnology (ICGEB) board, with the full respect of the EU Directive 2010/63/EU for animal experimentation. Mice were maintained at the ICGEB bio-experimentation facility in a temperature controlled environment with 12/12h hours of light/dark cycles and received a standard chow diet and water *ad libitum*.

2.3 Genomic DNA extraction from mouse tail biopsies

To obtain genomic DNA (gDNA) from tail biopsies, tissue from mice was digested overnight at 55°C in 600 µL of gDNA extraction buffer. The next day, dissolved tails were centrifuged for 15 min at 13200 rpm (Eppendorf 5145D, max. speed), and supernatant was transferred into a new tube and precipitated with an equal volume of 2-propanol. Tubes were centrifuged for 10 min at 13200 rpm, supernatant was discarded and pellets were rinsed once with 70% Et-OH. After 5 min centrifugation at 13200 rpm, pellets were air-dried and re-suspended with an appropriate volume of TE buffer. Solutions containing gDNA were then transferred to 65°C for 1 hour to facilitate dissolving. The gDNA was stored at room temperature until further use.

2.4 Polymerase chain reaction protocol to detect and discriminate different genotypes

GoTaq® Flexi DNA polymerase (Promega) was used for genotyping purposes. Polymerase chain reaction (PCR) was performed in 20 µL volume, 0.5 µL of gDNA were added. The PCR mix was composed as described below:

- 4 µL of 5x polymerase reaction buffer,
- 3 µL $MgCl_2$ 25 mM,
- 0.2 µL 100 nM dNTPs (25 mM stock),
- 0.1 µL of GoTaq® DNA Polymerase (0.25 units),

- 1 µL of primer forward (0.1 µg/µL),
- 1 µL of primer reverse (0.1 µg/µL),
- dH_2O to 20 µL.

Primers (EuroClone) used for genotyping are listed in Table 4 below.

Table 4. Primers for genotyping *Ugt1*$^{-/-}$ mouse model.

Gene	Oligo Name	Sequence (5'->3')	PCR Product	
			WT	*Ugt1*$^{-/-}$
mUGT1	EX4 SCREEN FOR	TCACCAGAGTAGGCATCTCATC	303	473
	UGT 9934 REV	GCTGTAAGACAATCTTCTCC		

The PCR thermo-cycler protocol to discriminate UGT genotype is reported below (Figure 10):

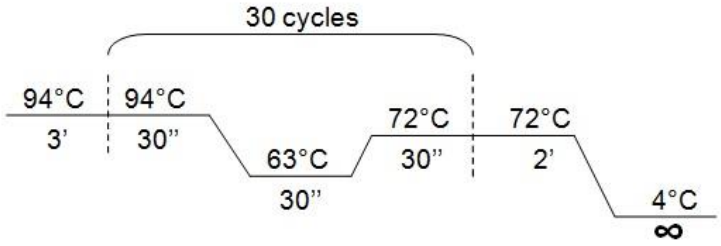

Figure 10. Scheme of PCR steps. Temperature and duration of the steps are reported.

PCR products were separated in an electrophoretic apparatus using a 2.0% agarose gel. Agarose was melted in 1x TBE buffer, which served as a running buffer as well. Prior to gel pouring, EuroSafe nucleic acid stain (EuroClone) was added for visualization of DNA fragments with UV transilluminator. To estimate the size of DNA fragments, 1 kb Plus molecular weight marker (Invitrogen) was run in parallel with DNA samples.

2.5 Animals treatments

Animals were treated as described in the following sub-chapters:

2.5.1 Phototherapy treatment

Phototherapy (PT) treatment was performed as previously described (Bortolussi et al., 2014). Newborn mice treated from postnatal day 0 (P0) to P10 with PT (P0-P10 PT) were exposed to blue fluorescent light (20 μW/cm^2/nm, Philips TL 20W/52 lamps; Philips, Amsterdam, The Netherlands) for 12 hours/day since birth for 10 days, then maintained under normal light conditions. PT treatment was synchronized with the light/dark cycle of the animal housing facility. Intensity of the PT unit was monitored periodically by Olympic Mark II Bili-Meter (Olympic Medical) to maintain standard conditions reported above.

2.5.2 Minocycline treatment

Fresh MNC (Minocin®, Teofarma; Pavia, Italy) was prepared every day and administered to lactating mothers starting on the parturition day, from P0 to P20. MNC was dissolved in water by gently mixing (in a 50 mL falcon) and then centrifuged 1 min at 1000 rpm to eliminate excipients, and then the correct dilution was reconstituted. Bottles were wrapped in aluminium foil to minimize exposure to light. The reference concentration (1X) was 0.842 mg/mL of MNC. Dams received 0.25X, 1X, 2X and 4X MNC concentrations.

2.5.3 Human serum albumin treatment

Newborn mice were intraperitoneally (i.p.) injected with human serum albumin (HSA) (Albuman®; solution for infusion, 200 g/L, fatty acid free, Sanquin, Amsterdam, The Netherlands). WT (injected control group) and *Ugt1*$^{-/-}$ mice were injected from P2 up P20, with 2.5 g/kg/48h, 5.0 g/kg/48h, 2.5 g/kg/24h, 5.0 g/kg/24h and 7.5 g/kg/24h of HSA. Animals treated every 48h received HSA administration at P2, P4, P6, P8, P10, P12, P14, P16, P18 and P20, while the 24h group every 24h, starting at P2 till P20.

2.5.4 Carbon tetrachloride treatment

Carbon tetrachloride (CCl_4) 1:10 v/v dissolved in corn oil, was i.p. injected in an adult WT mouse at 1 μL/g concentration, to generate liver damage (Domitrovi et al., 2009;

Yu et al., 2003). The day after plasma was collected. Alanine aminotransferase (ALT) and aspartate aminotransferase (AST) activities in plasma sample were assessed as described in the next chapters.

2.6 Biochemical analyses of plasma samples

Blood samples were collected at different time points in *Ugt1*$^{-/-}$ and WT littermates by cardiac puncture or decapitation into collection tubes containing 2 µL of EDTA (0.5M pH 8.0). Tubes were centrifuged for 15 min at 2000 rpm in a tabletop centrifuge (Eppendorf 5145D) and plasmas were transferred into new tubes. Before storing at -80°C, tubes were wrapped in aluminium foil to minimize exposure to light.

2.6.1 Plasma total bilirubin measurement

Total bilirubin (TB) determination in plasma was performed using Direct and Total Bilirubin Reagent kit (BQ Kits, San Diego, CA) adapting the method to reduce volumes (10 µL of plasma), but maintaining the original proportions, as previously described (Bortolussi et al., 2014). As quality control, three commercial bilirubin standards were included in each analysis: Control Serum I, Control Serum II and Bilirubin Calibrator (Diazyme Laboratories, Poway, CA). Absorbance values at 560 nm were obtained by using a multiplate reader (Perkin Elmer Envision Plate Reader, Walthman, MA). Briefly, samples were added to 140 µL of Buffer Reagent into a 96 wells plate (NUNC^{TM} plates), and 2.5 µL of nitrate reagents were added only in one of the two wells containing one the sample duplicates. The well with no nitrate reagent serves as background subtraction. Then 150 µL of methanol were added to start the reaction. Since the calibrator absorbance corresponds to 5 mg/dL, total bilirubin levels were calculated as follows:

$(A_{sample}-A_{blank})/(A_{calibrator}-A_{blank})*5= n$ (mg/dL)

2.6.2 Free bilirubin measurement

Free bilirubin (Bf) was determined in plasma samples by Dr. Henkjan Verkade laboratories (University of Groningen, Groningen, The Netherlands), using a Zone

Fluidics system (Global Flopro, Global Fia Inc, WA), as previously described by Ahlfors et al (Ahlfors et al., 2006).

2.6.3 Plasma albumin measurement

Plasma albumin levels were determined by modified bromocresol green (BCG) colorimetric method (Rodkey, 1965), adapting the method to use small plasma volumes (2 µL). Briefly, 200 µl of BCG solution were added to diluted samples (2 µL of plasma in 300 µL of dH_2O). Standard curve was obtained with different calibration points from 10 mg/mL of HSA solution. After 10 min at room temperature, absorbance values at 630 nm were recorded by the use of a multiplate reader (Perkin Elmer Envision Plate Reader, Walthman, MA). Plasma albumin levels were obtained by the interpolation of the samples absorbance with the standard curve.

2.6.4 Aminotransferases

Plasma aminotransferase activities were measured in albumin-treated and untreated animals. CCl_4-treated mouse plasma was used as a positive control for ALT and AST measurements.

2.6.4.1 ALT

Plasma ALT activity was measured with a Diagnostic ALT test kit (Sigma-Aldrich, Cat. No MAK052, St. Luis, MO), adapting the method to reduce volumes, but maintaining the same proportion. Briefly, a pyruvate standard solution was diluted in ALT Assay buffer, and, according to the calibration point, a standard curve was generated, while 5 µL of plasma were needed per sample. ALT Assay buffer was then loaded to reach a final total volume of 10 µL. Fifty µL of enzyme mix reaction was added to each sample. ALT mix was composed as follow:

- 43 µL of ALT Assay buffer,
- 1 µL of fluorescent peroxidase substrate,
- 1 µL of ALT Enzyme mix,
- 5 µL of ALT substrate.

Absorbance values at 570 nm were obtained by using a multiplate reader (Perkin Elmer Envision Plate Reader, Walthman, MA) at 37°C in a time-course read (every 2 min) for an interval of 20 min. ALT plasma activities were obtained by the interpolation of the samples absorbance with the standard curve generated in the recording window before the plateaux of the reaction.

2.6.4.2 AST

Plasma AST activity were measured with a Diagnostic AST test kit (Sigma-Aldrich, Cat. No MAK055, St. Luis, MO), adapting the method to reduce volumes, but maintaining the same proportion. Briefly, a glutamate standard solution was diluted in AST Assay buffer, and, according to the calibration point, standard curve was created, while 5 µL of plasma were needed per sample. AST Assay buffer was then loaded to reach a final total volume of 30 µL. 50 µL of enzyme mix reaction was added to each sample. AST mix was composed as follows:

- 43 µL of ALT Assay buffer,
- 1 µL of AST enzyme kit,
- 4 µL of AST developer,
- 5 µL of AST substrate.

Absorbance values at 450 nm were obtained by using a multiplate reader (Perkin Elmer Envision Plate Reader, Walthman, MA) at 37°C in a time-course read (every 2 min) for an interval of 20 min. AST plasma activities were obtained by the interpolation of the samples absorbance with the standard curve generated in the recording window before the plateaux of the reaction.

2.7 Tissue bilirubin measurement

Concentration of bilirubin in tissue was measured as described by Zelenka and colleagues (Zelenka et al., 2008). Measurements were performed by the laboratory of Prof. Libor Vitek, Charles University, Prague, CZ. Briefly, prior to organ collection animals were anesthetized, blood was collected by cardiac puncture in EDTA-containing syringes through the left ventricle. Immediately after, animals were perfused through the right ventricle with 10 mL of perfusion solution to wash out the residual blood from tissue. After perfusion organs were harvested, wrapped in

aluminium foil to minimize exposure to light, snap frozen in liquid nitrogen and stored at -80°C until measurements.

2.8 Preparation of total RNA from the mouse cerebellum

Total RNA was prepared with EuroGOLD TriFast solution (EuroClone, Milano, Italy). Extraction was performed according to instructions of the manufacturer. Integrity of extracted RNA was verified on 1% agarose gel.

2.8.1 Quantification and quality control of RNA

RNA concentrations were measured by NanoDrop™ 1000 spectrophotometer (Thermo Scientific) at 260 nm. Ratios of absorbance at 260 /280 nm and 260 nm/230 nm were used as indication of nucleic acids quality. RNA above 1.9 at 260/280 nm and 1.9-2.2 at 260/230 nm was considered of good quality.

2.8.2 Reverse transcription (RT)

For expression analysis by quantitative real-time RT-PCR (qRT-PCR), complementary DNA (cDNA) was prepared by reverse transcription of total RNA using M-MLV reverse transcriptase (Invitrogen), according to instructions of the manufacturer. Total RNA were retro-transcribed in a final volume of 12 µL as follow:

- 1 µg total RNA,
- 1 µL of 10 mM dNTP mix (10 mM of each dATP, dTTP, dCTP and dGTP at neutral pH),
- 5 µL of oligo dT (0.1 µg/µL)
- dH_2O up to 12 µL.

Mixture was heated to 65°C for 5 min and quickly chilled on ice. Then, 6 µL of a second mix were added. Mix was composed as follow:

- 4 µL of 5x First-Strand buffer
- 2 µL 0.1 M DTT

Samples were well mixed by pipetting and incubated for 2 min at 37°C, then 1 µL of M-MLV RT (200 units) was added, and incubated at 37°C for 1 hour. M-MLV RT was inactivated for 15 at 70°C. cDNA was kept at -20°C until further use.

2.9 Quantitative real-time RT-PCR

qRT-PCR was performed on the 96-well real-time PCR plate, using the iQ™ SYBR® Green Supermix (Bio-Rad) and a C1000 Thermal Cycler CFX96 Real Time System (Bio-Rad). The reaction mixture was in the final volume of 15 µL composed as follow:

- 7.5 µL IQ™ SYBR® Green Supermix 2x cocktail,
- 0.5 µL of primer forward (0.1 µg/µL),
- 0.5 µL of primer reverse (0.1 µg/µL),
- 5.5 µL of dH_2O,
- 1 µL of cDNA.

The protocol consisted of two steps, the amplification reaction and subsequent generation of melting curves of the PCR products. After one denaturation step at 98°C for 30 sec, 40 cycles of the following conditions were used for all reactions:

- denaturation step at 95°C for 5 sec
- annealing/extension at 62°C for 25 sec

After each cycle fluorescence was measured. After the amplification protocol PCR products were denatured for 10 sec at 95°C, then melt curve was generated by increasing temperature from 65°C to 95°C at 0.5°C increment every sec.
Before quantification analysis, the efficiency of primers was tested using a pool of cDNA derived from WT and *Ugt1*$^{-/-}$ cerebellum. Briefly, five serial 1:10 dilutions of cDNA were generated as a template to perform a calibration curve. The efficiency of the primers was derived from the slope of the curve (Figure 11A). Only primers whose efficiency was higher than 95% were used for quantification. Specificity was evaluated by melting curve profile from cDNA amplification products (Figure 11B). The melting curve was expected to show a single peak. Furthermore, 2.5% agarose gel was used to verify PCR product separation according to melting curve data.

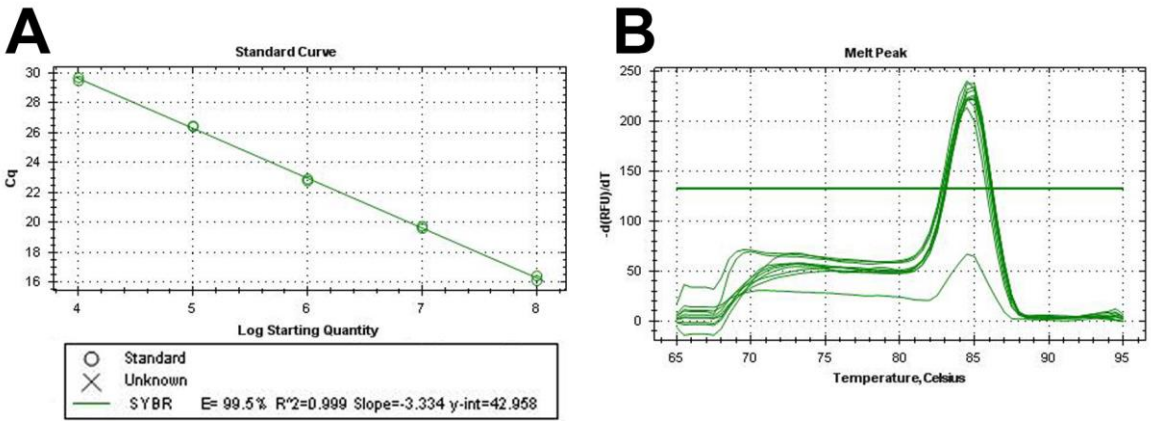

Figure 11. Primer pairs quality control. Example of quality control of GRP78 primer pairs. This procedure was performed for all sets of primers used in the analysis **A)** Efficiency of primer pairs derived from the slope generated by serial cDNA dilution templates. **B)** Melting curve profile of cDNA amplification, showing a single peak.

Primer pairs not matching efficiency or specificity requirements were discharged and a new set of primers was designed and tested. After the reactions, cDNA dilution vs. threshold cycle (C_t which the signal of the PCR product exceeds the background signal) was plotted. The primers used to quantify expression levels in this study are listed in Table 5.

Table 5. Mouse primers for qRT-PCR. Gene of interest, primer name, its 5'->3' sequence, and amplicon size.

Gene		Sequence (5'->3')	Length
Calbindin	FOR	TCTTGCTGCTCTTTCGATGC	186
	REV	TGAGGTCTGTGTACTCTGCTAG	
Neun	FOR	AGAAGCTGAATGGGACGATC	146
	REV	TTCAGGCCCATAGACTGTTC	
GFAP	FOR	TCGCCACCTACAGGAAATTG	148
	REV	ACGATGTTCCTCTTGAGGTG	
Iba1	FOR	AATGATGAGGATCTGCCGTC	201
	REV	AGTCAGAGTAGCTGAACGTC	
IL1b	FOR	GCAACTGTTCCTGAACTCAACT	161
	REV	ATCTTTTGGGGTCCGTCAACT	
IL6	FOR	CAACGATGATGCACTTGCAG	196
	REV	TCTGAAGGACTCTGGCTTTG	
IL10	FOR	GCCAAGCCTTATCGGAAATG	197
	REV	AATCACTCTTCACCTGCTCC	
INFγ	FOR	CACGGCACAGTCATTGAAAG	199
	REV	TTGCTGATGGCCTGATTGTC	
TLR2	FOR	GAGCATCCGAATTGCATCA	140
	REV	GAACAGCGTTTGCTGAAGAG	
iNOS	FOR	TGACACTCTTCACCACAAGG	146
	REV	AACTCAATGGCATGAGGCAG	
IL18	FOR	TTTGGCCGACTTCACTGTAC	178
	REV	ACAGCCAGTCCTCTTACTTC	
NFKβ	FOR	AGCAGGACATGGGATTTCAG	189
	REV	AGGTGGATGATGGCTAAGTG	
nNOS	FOR	TCCCATCACATACGGAAGTC	148
	REV	ATCTCCTTGTTCACCTCCTC	
MMP2	FOR	TTGCAGGAGACAAGTTCTGG	182
	REV	TTTGGTTCTCCAGCTTCAGG	
MMP9	FOR	CGCTCTGCATTTCTTCAAGG	228
	REV	ACCCAACTTATCCAGACTCC	
TNFα	FOR	TTCGAGTGACAAGCCTGTAG	154
	REV	AGACAAGGTACAACCCATCG	
CD68	FOR	TACCCAATTCAGGGTGGAAG	198
	REV	TGTATTCCACCGCCATGTAG	
CD86	FOR	TGTGTTCTGGAAACGGAGTC	164
	REV	CTGATTCGGCTTCTTGTGAC	

Gene		Sequence (5'->3')	Length
Arg1	FOR	GGAAAGCCAATGAAGAGCTG	171
	REV	GTGTTGATGTCAGTGTGAGC	
MRC2	FOR	TTGAGTCTTCGATGGCAGTG	193
	REV	TTTCCCTGGATGGTGTAGAC	
CHOP	FOR	ACCACACCTGAAAGCAGAAC	178
	REV	TCTTCCTCTTCGTTTCCTGG	
GRP94	FOR	AGCACATCTGGGAATCAGAC	194
	REV	TGCTACTCCACACGTAGATG	
GRP78	FOR	GTTCTTCAATGGCAAGGAGC	215
	REV	TGAGACTTCTTGGTGGGTAC	
P58^{IPK}	FOR	GTGGAGTAAATGCGGATGTG	203
	REV	CAATCACTTTGGTGAGGTCG	
FKBP1	FOR	AGAAACCGAAAGTCCTGTCC	181
	REV	TTTGGCCGAGTTCTATGACC	
ATF4	FOR	ATGGCCGGCTATGGATGAT	177
	REV	TCATCCAACGTGGTCAAGAG	
ATF3	FOR	CGCCATCCAGAATAAACACC	194
	REV	TATTTCTTTCTCGCCGCCTC	
DR5	FOR	ACTCTGTGCATTCGTCTCTC	181
	REV	AAAGGGCACTATGTCCGAAC	
CD95/FAS	FOR	AAGGGAAGGAGTACATGGAC	165
	REV	TGTTCACAGCCAGGAGAATC	
SOD	FOR	TACAACTCAGGTCGCTCTTC	228
	REV	CTTATTGAAGCCAAGCCAGC	
GPX1	FOR	ACACCGAGATGAACGATCTG	191
	REV	CACCATTCACTTCGCACTTC	
UPC2	FOR	GCTTTGAAGAACGAGACACC	198
	REV	CACATCTGTGGCCTTGAAAC	
ERO1L	FOR	ACCAGTGTGGAAGAAGAGAC	186
	REV	TCTTCAATGCGGTTGGCTTC	
HMGB	FOR	GCTTTGAAGAACGAGACACC	198
	REV	CACATCTGTGGCCTTGAAAC	
HO1	FOR	TTTCAGAAGGGTCAGGTGTC	112
	REV	AGACTGGGTTCTGCTTGTTG	
Gapdh	FOR	GCATGGACTGTGGTCATGAG	200
	REV	CCATCACCATCTTCCAGGAG	

Gapdh house-keeping gene expression was used to normalize gene of interest, applying the $\Delta\Delta C_t$ method to quantify the relative amount of expression. Briefly, the C_t of the reference amplicon is subtracted from C_t of the amplicon of interest to calculate ΔC_t of the sample. Then, the mean of ΔCt of WT samples is subtracted to each sample, obtaining $\Delta\Delta C_t$. $2^{\wedge\Delta\Delta Ct}$ represents the relative expression of each sample compared to the WT.

2.10 Preparation of total protein extracts

Tissue samples were homogenized in protein buffer with a mechanical homogenizer (IKA ULTRA-TURRAX T25) for 10-15 sec, then samples were centrifuged for 10 min at maximum speed at 4°C. Supernatants were transferred into a fresh tube and centrifuged for 10 min at maximum speed at 4°. Supernatants were again transferred into a fresh tube and stored at -80°C. Protein concentration was determined by Bradford protein assay (Bio-Rad) (Bradford, 1976) and samples analysed by Western blot (WB).

2.11 SDS-PAGE and Western blot

SDS-PAGE was used for separation of proteins. Polyacrylamide gels were cast with Protogel, a stabilized, ready to use 30 % (w/v) acrylamide/methylene biacrylamide solution (37.5:1 ratio, National diagnostics). Depending on size, proteins were spread on running gel from 8% to 15% (see Table 6).

Table 6. Stacking and running gel mixes. According to protein molecular weight, acrylamide varied from 8 % to 15 % for running gels.

	Stacking (mL)	**Running (mL)**			
		8%	**10%**	**12%**	**15%**
30% Acrylamide mix	1.6	2.6	3.3	4.0	5.0
1.5M Tris pH 8.0	-	2.5	2.5	2.5	2.5
0.5M Tris pH 6.8	1.5	-	-	-	-
dH_2O	6.0	4.9	4.1	3.4	2.4
10% SDS	0.1	0.1	0.1	0.1	0.1
10% APS	0.1	0.1	0.1	0.1	0.1

About 10 µL of N,N,N',N'-tetramethylethylenediamine (TEMED, Sigma-Aldrich) was added to initiate the polymerization. Gels were cast in vertical electrophoresis chamber and overlaid with H_2O-saturated 2-butanol to obtain a sharp interface. After the running gel polymerized, n-butanol was flushed with H_2O and stacking gel was cast (Table 6), and 20 µL of TEMED were added to initiate polymerization.
Samples were mixed with 10x protein loading buffer and dH_2O to reach about 30 µL of final volume, denatured for 5 min at 95°C, cooled on ice and loaded onto a gel, with protein marker Sharpmass V Plus (Euroclone) to estimate protein size. Twenty

to 40 µg of total proteins from tissue samples were loaded. Gels were run in 1X running buffer at 30 mA until the dye ran out of gel.

For WB analysis, proteins were transferred onto a nitrocellulose membrane using Lightning Blot™ System (Perkin Elmer). Briefly, three layers of 3mm paper were soaked in Blotting Solution 1. In parallel nitrocellulose membrane was rinsed and activated in Blotting Solution 2 and other three layers of 3MM paper soaked in Blotting Solution 3. Blotting was run for 30 min at 27 V. The transfer was verified by Ponceau S staining (Sigma) and scanned to keep a reference of the run. After complete Ponceau S washing out, membranes were blocked 1 hour at room temperature with appropriate blocking solution, then o/n with primary antibody at 4°C (Table 7). The day after, membranes were washed 3 times for 5 min with 1X PBS 0.1 % Tween and incubated with the corresponding secondary antibody for one hour. After 3 washing steps for 5 min, the reaction was developed with ECL system (Amersham Biosciences).

Table 7. Summary of the antibodies used in WB and IF. Antibody name, company name, molecular weight (kD), dilutions for WB and IF, and secondary antibody are indicated.

Antibody	**Company**	**MW (kD)**	**Dilution**		**2nd antibody**
			WB	**IF**	
Calbindin 1	Synaptic Systems	27	1:3000	1:200	α-rabbit/α-mouse
NeuN	Millipore	46-48	1:2000	1:200	α-rabbit
cleaved caspase 3	Cell Signaling	17	1:500	-	α-rabbit
total caspase 3	Santa Cruz Biotechnology	32	1:800	-	α-rabbit
GFAP	Sigma	52	1:2000	1:200	α-mouse
Iba1	WAKO	17	1:1000	1:200	α-rabbit
MBP	Millipore	14-17-18-21	1:2000	1:200	α-rabbit
LC3	Sigma	17-19	1:2000	-	α-rabbit
Tubulin	Developmental Study Hybridoma	55	1:4000	-	α-mouse

2.12 Histological analysis

Histological and immunofluorescence (IF) analysis of brain samples was performed as previously described (Bortolussi et al., 2014). Brains were removed from the skull and fixed in 4 % PFA-PBS o/n at 4°C. The day after, PFA solution was removed and brains were crio-preserved at 4°C in 20% sucrose and 0.02% NaN_3 in PBS until

slicing. For slicing, brains were frozen in cryostat embedding medium (Killik, Bio-optica) and sliced in 14 µm thick sagittal sections in a cryostat. Slices were gently located on gelatinized slides. Slides were air dried for about 30 min and then stored at -20°C until use.
The study was performed in a double-blind fashion: the genotype of the animals and the treatment were unknown to the surgeon, while a different investigator analysed the data. Measurements were averaged for each animal.

2.12.1 Nissl staining

Slides were air-dried for about 30 min, then rehydrated in 1X PBS for about 20 min and dipped in cresyl violet solution for 5 min at 37°C. Next steps were performed as follow:

- 2 min in dH_2O (x2)
- 3 min in 50 % Et-OH and 50 % dH_2O
- 3 min in 100 % Et-OH
- 3 min in 50 % Et-OH and 50 % xylene
- 3 min in 100 % xylene

Then, slides were mounted in Eukitt (Fluka, St Louis, MO). Images were acquired on Nikon Eclipse E-800 microscope equipped with a charge-coupled device camera (DMX 1200F; Nikon Amstelveen, The Netherlands). Digital images were collected using ACT-1 (Nikon) software.

2.12.2 Immunofluorescence analysis

To perform analysis of IF, slides were first air-dried for about 30 min, then rehydrated in 1X PBS for 20 min. After blocking (bovine serum albumin, BSA, or normal goat serum, NGS), specimens were incubated with the primary antibody (see dilutions in Table 5) 2 hours at RT. After 3×5 min washes with blocking solution, specimens were incubated with secondary antibody (Alexa Fluor; Invitrogen Carlsbad, CA) for 2 hours at RT. Nuclei were visualized by addition of Hoechst (10 µg/ml, Invitrogen) for 5 min after secondary antibody solution.

Images were acquired with a Nikon Eclipse E-800 epifluorescent microscope equipped with a charge-coupled device camera (DMX 1200F; Nikon Amstelveen, The Netherlands). Digital images were collected using ACT-1 (Nikon) software. Calbindin-positive Purkinje cells (PCs) number was calculated as previously described (Bortolussi et al., 2012) by counting cells in sections located in the vermis region of the cerebellum. PCs number was expressed as linear density (cell/mm).

2.13 Rotarod test

The coordination and balance ability of mice were tested on a rotating cylinder with an accelerating apparatus, as previously described (Bortolussi et al., 2014). Behavioural studies were performed as previously described (Chauhan et al., 2005). The animals were allowed to acclimate to the testing room for 1 hour prior to the test. Before testing the apparatus was cleaned with H_2O and 50% Et-OH to remove odours, which could affect the behavioural analysis of the following animal. After the adaptation period animals were trained with three trials at constant speed:

- slow (2.8 rpm) for 1 min,
- moderate (5.5 rpm) for 1 min,
- fast (8.0 rpm), for 1 min.

After the training session mice were subjected to three trials of accelerating rotarod test with a linear increase in rotating speed from 2.5 rpm to 48 rpm over a 5 min period and the latency to fall was recorded. Analysis was performed for two consecutive days. The second day, animals were tested after 1 hour of acclimation, then were tested without training session. Tracks and order of animals was changed between the two days of test. Results represent the average of the three trials of day 1 mediate by the average the three trials of the day 2.

2.14 Open field test

Open field (OF) test was performed as previously described (Chauhan et al., 2005). Mice 6-8 weeks old were analysed in the open field test, using an open rectangular box (60 cm wide × 60 cm long × 30 cm high) made of transparent Plexiglas. The animals experienced 1 hour of acclimation in the testing room before final test was performed. After each animal the OF equipment was cleaned with H_2O and 50% Et-OH to remove odours, which could affect the behavioural analysis of the animal. At

the time of the test, each mouse was placed individually in the centre of the field and it was recorded for a total period of uninterrupted 20 min. For analysis purpose the arena was divided as follow: 'peripheral' corresponded to the outer two rows of squares (outer 12 cm), 'central' to the central 24×24 cm square and the 'median' area corresponded to one square width ring (6 cm) located between the external and internal areas (Figure 12). All testing was conducted in the same period of the day (between 15:00 and 18:00 h).

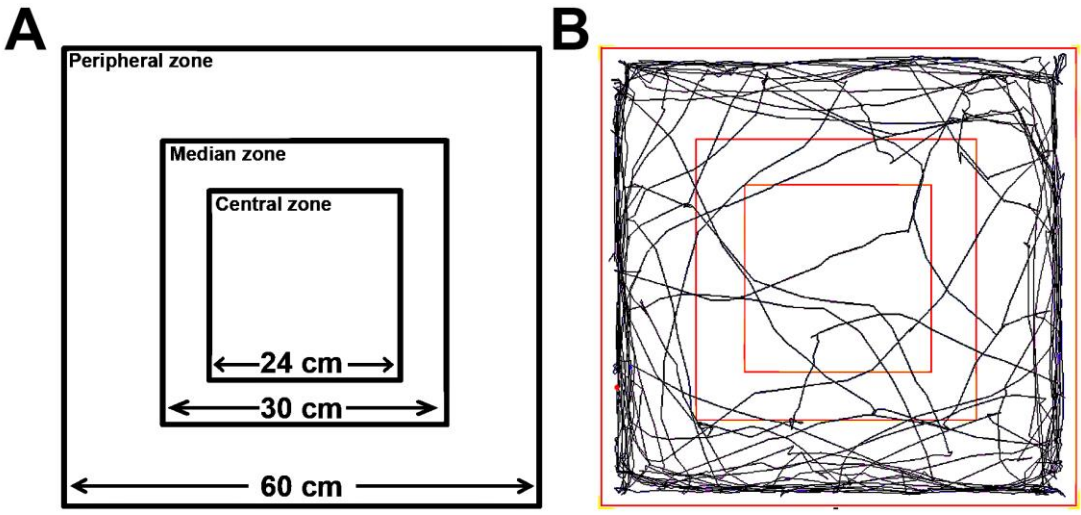

Figure 12. Open field test arena. A) Name and dimension of the different arena zones are indicated. **B)** Representative mice track after 5 minutes, according to Any-maze software**.**

Different parameters were analysed:

1) *activity* parameters:
   a) the total distance travelled,
   b) time and distance spent in the zones,
   c) zones crossover (defined as all four paws crossing the line),
2) *anxiety* parameters:
   a) number of rearing (raising both forefeet off the ground and extension of the body),
   b) number of groomings (hygiene and caring of the body surface),
   c) fecal bolus events.

Activity data were analysed by Any-maze software (Ugo Basile Instruments, kindly provided by E. Tongiorgi, University of Trieste, Italy). After the zone settings, the software generates an excel file containing the values for each mouse parameter. Each group was mediated by its number of animals.

Anxiety parameters were reported manually by examining video record, and values were mediated by each group.

2.15 Statistics

The Prism package (GraphPad Software, La Jolla, CA) was used to analyse the data. All the results are expressed as mean ± s.d. Values of $p<0.05$ were considered statistically significant. Depending on the experimental design, Student's *t*-test, one-way ANOVA or two-way ANOVA with Bonferroni's post-hoc comparison tests were used, as indicated in the legends to the figures and text. Correlation analyses were done using the Pearson coefficient to assess the linearity between two variables and calculate two-tailed p value (95% of confidence interval).

2.16 Collaborators

Giulia Bortolussi performed some of the IF experiments (Figures 30C-D, 31C-D, 32C-D, 47C, 48C and 49C). Jana Jašprovà performed the measurement of UCB content in tissues (Figures 19, 25 and 26). Andrea B. Schreuder performed plasma measurement of Bf (Figures 20 and 24C).

RESULTS

3.1 Albumin supplementation demonstrates that Bf is the cause of bilirubin neurotoxicity

Bilirubin neurotoxicity, caused by the fraction of UCB not bound to albumin (Bf), occurs when unbound bilirubin is present at high levels as observed in neonatal unconjugated hyperbilirubinemia. In this condition, free bilirubin crosses the blood-brain barrier (BBB) causing brain damage and, if untreated, death by kernicterus. The routine therapy to treat neonatal hyperbilirubinemia is phototherapy (PT), while exchange transfusion (ET) is performed in unresponsive cases. However, the ET procedure is carried out only in specialized centres and has significant risk of morbidity and mortality. It is reasonable to hypothesized that increasing bilirubin-binding capacity in plasma by HSA administration may result in the mobilization of Bf from tissues to plasma, reducing bilirubin toxicity. However, therapeutic administration of HSA to lower bilirubin neurotoxicity risks is not well recognized in the clinical practice due to the absence of reliable scientific evidence of its potential benefit, together with the lack of markers to monitor bilirubin toxicity risks. Thus, the determination of the potential beneficial properties of HSA administration needs a deeper investigation.

The goal of this study is to test the potential of HSA administration to reduce neurological damage and mortality and in the *Ugt1*$^{-/-}$ mouse model of neonatal hyperbilirubinemia.

3.1.1 Experimental plan

With the aim of increasing plasma bilirubin-binding capacity and determining its potential beneficial effects in the protection from bilirubin neurotoxicity, HSA was intraperitoneally (i.p.) administered to wild type (WT) and *Ugt1*$^{-/-}$ pups starting from post-natal day 2 (P2) to P20 (corresponding to the day of weaning).

I selected increasing doses of HSA: 2.5 g/kg, 5.0 g/kg, and 7.5 g/kg and two frequencies of administration: daily (24h) and every two days (48h).

Survival, animal weight and general aspect, of the mice were monitored daily. As shown in Figure 13, plasma and tissue samples were collected at the indicated time points (P15, P16 and at P30), while rotarod test was performed at P30.

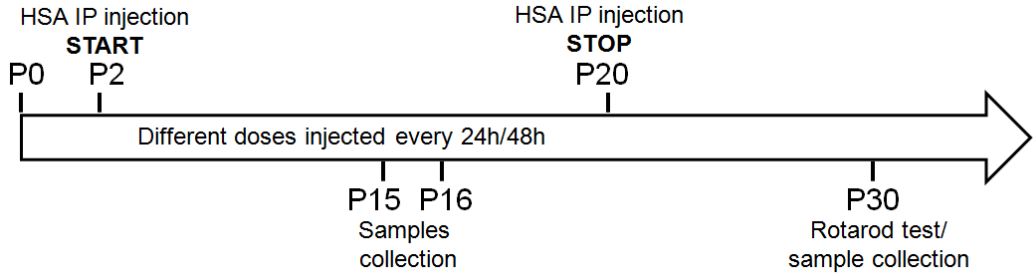

Figure 13. HSA experimental plan. Mice were i.p. injected with different doses of HSA (2.5, 5.0 and 7.5 g/kg) from P2 to P20. HSA was administered at two different frequencies, daily or every 48 hours. Samples were collected at P15, P16 and P30, and rotarod test was performed at P30.

3.1.2 Survival of the HSA-treated *Ugt1*$^{-/-}$ mice

I performed a dose-response experiment to determine whether HSA administration extended survival of *Ugt1*$^{-/-}$ mice. Administration of 2.5 g/kg and 5.0 g/kg HSA doses every 48 hours (HSA 2.5/48h and HSA 5.0/48h, respectively) resulted in delayed mortality of mutant mice (50% survival at P17 and P18, respectively, Fig. 14), but all *Ugt1*$^{-/-}$ mice died before day 27 after birth.

Considering the positive results obtained with the HSA administration every 48 hours, the frequency of the injections was increased to one every 24 hours. Daily 2.5 g/kg HSA administration (HSA 2.5/24h) resulted in increased survival of *Ugt1*$^{-/-}$ mice compared with the previous doses, reaching 50% of mutant mice survival at P22, with one out of 11 treated mice surviving beyond P30.

When I further increased the dose of HSA daily administration, I observed that HSA 5.0 g/kg/24h (HSA 5.0/24h) was the minimum dose able to rescue almost all mutant mice (14 out of 15 mice, 93.3%; Figure 14, blue line). In parallel, a higher HSA dose was also tested (7.5 g/kg injection every 24h: HSA 7.5/24h), resulting in the successful rescue of almost all *Ugt1*$^{-/-}$ mice beyond P30 (11 out of 12 mice, 91.7%; Figure 14, dark blue line).

To note, all the different HSA doses did not affect the survival of WT animals, resulting in 100% of survival, even at the highest dose (HSA 7.5/24h).

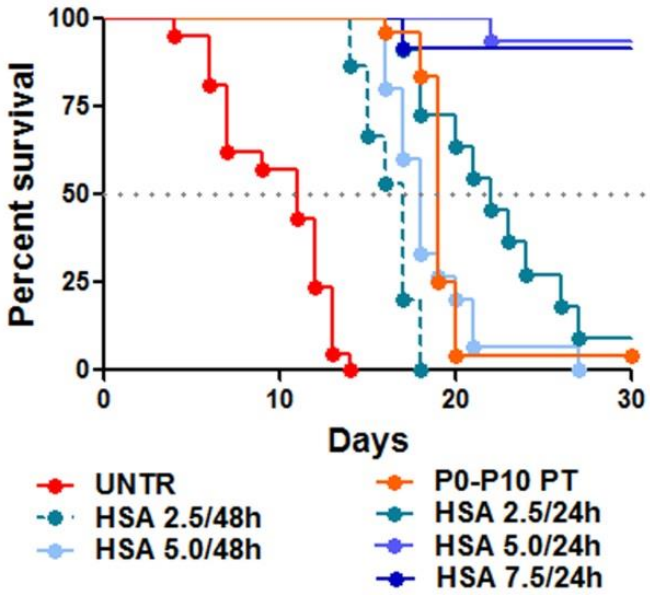

Figure 14. Survival of HSA-treated *Ugt1*$^{-/-}$ mice. Kaplan-Meier of HSA treatment. The line colour/type indicates the different treatments (red line, untreated (UNTR) *Ugt1*$^{-/-}$ mice; orange line, P0-P10 PT-treated *Ugt1*$^{-/-}$ mice; other lines, HSA treatments). Log-rank (Mantel-Cox) test, $p<0.0001$, each HSA treatment vs UNTR. The number of animals per treatment is as follows: UNTR (n=21), P0-P10 PT (n=24), HSA 2.5/48h (n=15), HSA 2.5/24h (n=11), HSA 5.0/48h (n=15), HSA 5.0/24h (n=15), HSA 7.5/24h (n=12).

Since untreated *Ugt1*$^{-/-}$ mice did not survive longer than P15 (Bortolussi et al., 2014), it was not possible to use these animals as the untreated control group to be compared with HSA-treated *Ugt1*$^{-/-}$ mice. Therefore, as control group I selected an experimental condition that allows mutant animals to survive longer. *Ugt1*$^{-/-}$ mice were temporarily treated with PT since birth up to P10 (P0-P10 PT), and then transferred to normal light conditions. After discontinuation of the PT treatment, bilirubin rapidly raised reaching toxic levels, and only ~5% of P0-P10 PT-treated *Ugt1*$^{-/-}$ mice survived after P30 (Fig. 14, orange line).

3.1.3 Assessment of the HSA-treatment side effects

To assess the potential side effects of albumin administration on pup's health, HSA-treated WT and *Ugt1*$^{-/-}$ littermates were daily monitored. As shown in Figure 15, no obvious alteration in the weight curve of mutant and WT mice treated with HSA 7.5/24h were observed, the highest dose tested.

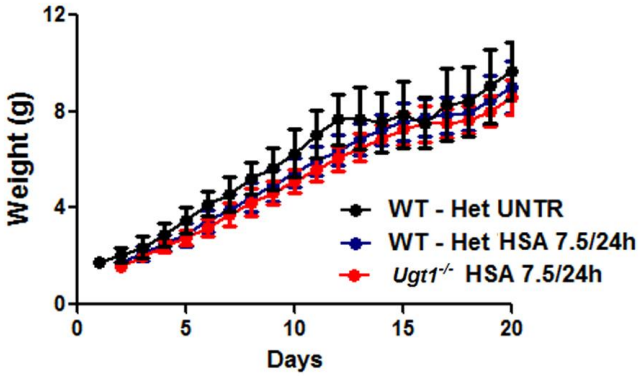

Figure 15. Weight curve of HSA-treated mice. Weight of untreated (UNTR), wild type/heterozygous (WT – Het) and *Ugt1*$^{-/-}$ littermates treated with the highest dose of HSA (daily injected HSA 7.5 g/kg) was monitored. Values represent mean ± s.d. (g). Two-way ANOVA, Bonferroni's post test, not significant; average of analysed families per treatment n=7).

To determine whether HSA treatment may lead to liver damage, alanine aminotransferase (ALT) were analysed at P15. In addition, to exclude a possible damage on muscular tissue aspartate aminotransferase (AST) activity was analysed in WT and *Ugt1*$^{-/-}$ littermates treated with the highest dose. As positive control, animals were treated with carbon tetrachloride (CCl_4), a compound known to induce liver damage (Domitrovi et al., 2009).

No significant change in the ALT and AST activities were observed between the injected and non-injected groups, indicating the absence of liver or muscle damage caused by HSA daily treatment (Figure 16).

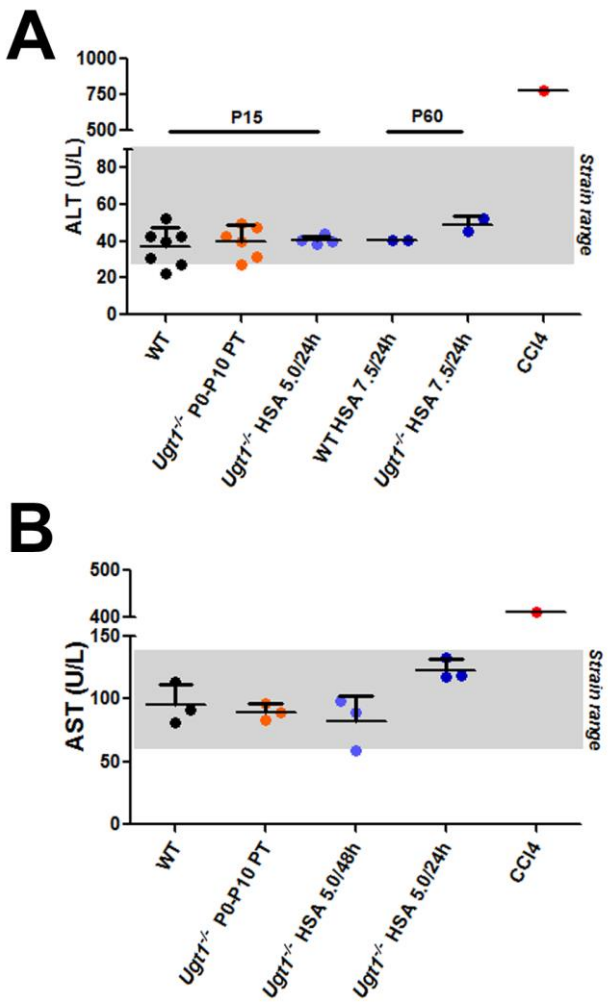

Figure 16. HSA administration has no effect on transaminases activity in HSA-treated *Ugt1*$^{-/-}$ mice. A) ALT were analysed at P15 on plasma of untreated and P0-P10 PT- and HSA 5.0/24h-treated mice, and at P60 on littermates treated with HSA 7.5/24h. **B)** AST levels were analysed at P15 on WT, P0-P10 PT-, HSA 5.0/48h- and HSA 5.0/24h-treated *Ugt1*$^{-/-}$ mice. Plasma from a CCl_4-treated mouse (red point) was used as a positive control of increased ALT and AST levels. Values represent mean ± s.d. (U/L). Each dot corresponds to a single animal.

3.1.4 Effects of HSA administration on plasma levels

To have a deeper insight on the events occurring after HSA supplementation that resulted in the survival of *Ugt1*$^{-/-}$ mice, plasma albumin levels were analysed at P15. HSA treatment increased plasma albumin concentration in a dose-dependent manner, from the basal level of control and P0-P10 PT-treated mice (~17 g/L) to a maximum concentration observed in 7.5/24h-treated animals (~36 g/L; Figure 17A). To note, no differences in basal albumin concentration between P0-P10 PT-treated WT and *Ugt1*$^{-/-}$ mice were observed. In addition, no differences in plasma albumin levels were observed between control and *Ugt1*$^{-/-}$ mice undergoing the same treatment.

Next, the effects of HSA administration on plasma total bilirubin (TB) levels was determined at P15. Since untreated mutant mice do not survive up to this time point, P0-P10 PT-treated *Ugt1*$^{-/-}$ mice were considered as the reference value for the untreated group. In those animals, PT was discontinued at P10 and, after 5 days in normal light, their plasma bilirubin values reached the steady state (Bortolussi et al., 2014). Albumin treatment resulted in an increase of plasma bilirubin concentration in *Ugt1*$^{-/-}$ mice, reaching values of up to 100% higher than in controls (P0-P10 PT vs HSA 7.5/24h; TB 15 mg/dL vs 30 mg/dL, respectively, Figure 17B). Notably, HSA administration did not alter the plasma bilirubin levels of WT treated mice, which showed TB levels similar to those of P0-P10 PT-treated WT mice (Table 8).

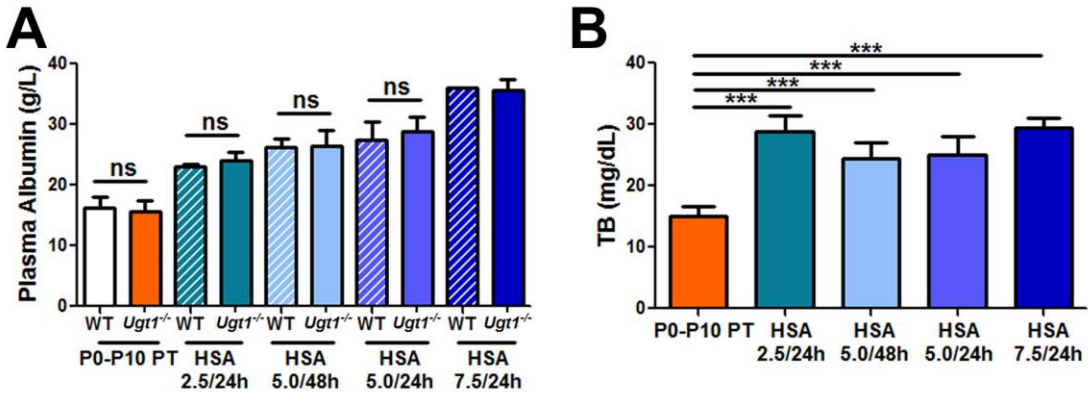

Figure 17. Dose-dependent effect of HSA administration on plasma values 24 hours after last injection. At P15, plasma levels were analysed to assess the effect of albumin administration in all the conditions. **A)** Plasma albumin levels. Values represent mean ± s.d.(g/L). Student *t*-test; ns, not significant. **B)** TB levels of mutant animals in all the conditions at P15. Values represent mean ± s.d.(mg/dL). One-way ANOVA test, ***p<0.001. The number of animals was ≥ 3 in all the experiments and conditions, except for WT HSA 7.5/24h which represents 1 sample.

Table 8. Plasma total bilirubin and albumin levels. The number of animals is indicated between parentheses. *** indicates a $p < 0.001$ (*t*-test between WT and *Ugt1*$^{-/-}$ mice, within each treatment). ND, not determined as untreated *Ugt1*$^{-/-}$ do not survive up to P30.

		TB (mg/dL)			Plasma albumin (g/L)	
Treatment	**Age**	**WT**	***Ugt1*$^{-/-}$**		**WT**	***Ugt1*$^{-/-}$**
P0-P10 PT	**P15**	0.2 ± 0.1 (20)	14.9 ± 1.6 (21)***		16.2 ± 1.8 (20)	15.7 ± 2.1 (21) ns
HSA 2.5 g/kg/24h	**P15**	0.6 ± 0.1 (5)	28.8 ± 2.6 (7)***		22.9 ± 0.5 (5)	24.1 ± 1.4 (7) ns
HSA 5.0 g/kg/48h	**P15**	0.5 ± 0.1 (4)	24.3 ± 2.6 (15)***		26.1 ± 1.4 (4)	26.4 ± 2.6 (15) ns
HSA 5.0 g/kg/24h	**P15**	0.7 ± 0.1 (5)	25.1 ± 2.8 (15)***		27.4 ± 2.9 (5)	28.9 ± 2.2 (15) ns
HSA 7.5 g/kg/24h	**P15**	1.7 (1)	29.4 ± 1.6 (3)		35.9 ± 0 (1)	35.3 ± 1.1 (3)
P0-P10 PT	**P16**	0.2 ± 0.1 (7)	19.3 ± 3.5 (6)***		16.2 ± 1.1 (7)	15.8 ± 2.8 (6) ns
HSA 5.0 g/kg/48h	**P16**	0.3 ± 0.2 (7)	27.7 ± 2.8 (14)***		24.2 ± 4.2 (7)	21.7 ± 4.1 (14) ns
HSA 5.0 g/kg/24h	**P16**	0.8 ± 0.2 (6)	31.2 ± 4.2 (7)***		29.1 ± 4.4 (6)	29.5 ± 4.6 (7) ns
Untreated	**P30**	0.1 ± 0.1 (4)	ND		18.3 ± 1.8 (4)	ND
HSA 5 g/kg/24h	**P30**	0.1 ± 0 (5)	8.2 ± 1.2 (7)***		19.2 ± 1.5 (7)	16.7 ± 2.0 (7) ns
HSA 7.5 g/kg/24h	**P30**	0.1 ± 0 (5)	7.4 ± 1.05 (6)***		18.7 ± 2.3 (6)	17.9 ± 1.7 (6) ns

3.1.5 Effects of HSA administration in the first 24 hours after injection

The obtained results underscored the importance of administration frequency in the HSA-treatment. Daily administration of HSA 5.0 g/kg was the minimal dose resulting in virtually complete survival of *Ugt1*$^{-/-}$ mice (14 out of 15 mice, 93.3% survivors; Figure 14), while the same dose administered every 48 hours resulted in the death of all mutant animals. This striking difference led me to investigate the reasons for the opposite outcomes of the two administration frequencies of the same HSA dose. At P15 I demonstrated a strong correlation between plasma albumin and plasma TB levels among the control, 5.0/24h and 5.0/48h groups (Figure 18), indicating that higher albumin binding sites in plasma were associated with higher bilirubin levels in plasma.

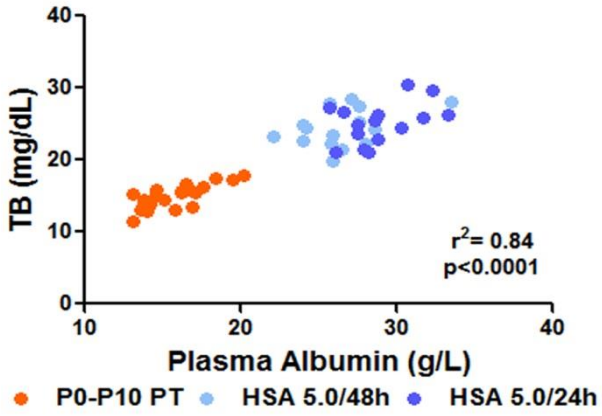

Figure 18. Correlation plot of plasma albumin and TB. At P15, Plasma albumin levels were correlated to TB levels between P0-P10 PT-, HSA 5.0/48h- and HSA 5.0/24h-treated *Ugt1*$^{-/-}$ animals. Each dot corresponds to a single animal. Correlation test, Pearson's coefficient.

Since bilirubin preferentially accumulates in the brain, causing neurotoxicity, forebrain (FB) and cerebellum (CB) were collected at P15 (24 hours after the last administration given at P14, for both HSA-treated groups) from P0-P10 PT-, 5.0/48h- and 5.0/24h-treated *Ugt1*$^{-/-}$ mice and tissue bilirubin content was quantified. Tissue bilirubin determination was carried out by Jana Jašprovà, member of the group of Prof. Libor Vitek at Charles University in Prague (CZ).

Twenty-four hours after last albumin supplementation, both HSA treatments were effective in lowering brain bilirubin content at P15, both in FB and CB. In fact, brain bilirubin content in HSA 5.0/48- and HSA 5.0/24-treated *Ugt1*$^{-/-}$ dropped 30-40% compared to P0-P10 PT-control mice (Fig. 19). Surprisingly, at this time point I did not observe any difference in tissue bilirubin levels between HSA 5.0/48- and HSA 5.0/24-treated *Ugt1*$^{-/-}$ mice.

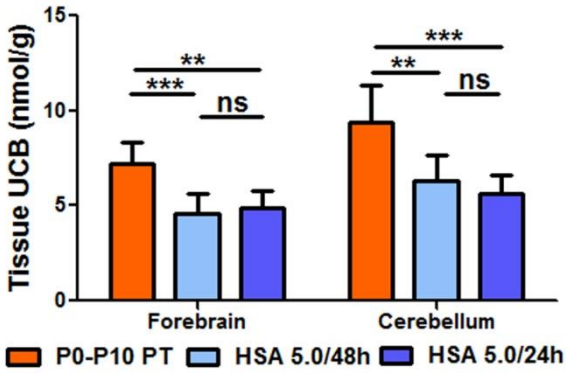

Figure 19. Effect of HSA administration on brain bilirubin content. At P15, forebrain and cerebellum UCB content was analysed in P0-P10 PT-, HSA 5.0/48h- and HSA 5.0/24h-treated *Ugt1*$^{-/-}$ animals. Values represent mean ± s.d. (nmol/mg). One-way ANOVA test, ***p*<0.01, ****p*<0.001. The number of animals was ≥ 6 in all the experiments and conditions.

Next, Andrea Schreuder, member of the Dr. Henkjan Verkade laboratory (University of Groningen, Groningen, The Netherlands), determined plasma concentrations of the free fraction of bilirubin (Bf), which is considered the fraction of bilirubin capable of crossing the blood-brain barrier and inducing neuro-damage. At P15, a clear effect of albumin administration on Bf reduction was observed (Figure 20). Bf in HSA-treated mutant animals was about 1/3 compared to the P0-P10 PT *Ugt1*$^{-/-}$ control group. Interestingly, there was no difference between the 5.0/24h- and the 5.0/48h-treated groups, which received different frequencies of injection.

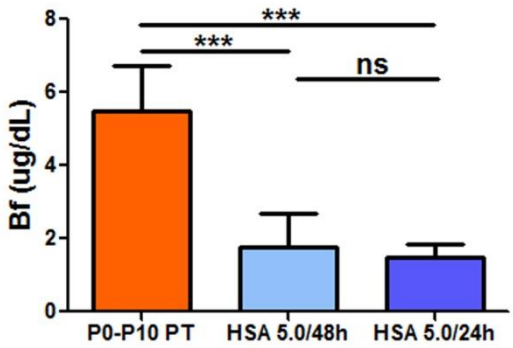

Figure 20. Effect of HSA administration on Bf. At P15, the free fraction of bilirubin (Bf) was analysed in plasma samples of P0-P10 PT-, HSA 5.0/48h- and HSA 5.0/24h-treated *Ugt1*$^{-/-}$ animals. Values represent mean ± s.d.(µg/dL). One-way ANOVA test, ****p*<0.001. The number of animals was ≥ 8 in all the conditions.

Overall, this set of experiments showed that albumin supplementation increases the bilirubin-binding capacity in plasma, significantly mobilizing the free fraction of bilirubin from tissue to plasma.

Thus, to assess the degree of neurological damage induced by bilirubin, at P15 I performed histological analysis of WT and *Ugt1*$^{-/-}$ mice cerebellum, the most affected brain region (Bortolussi et al., 2014). Brain sections were stained with Nissl, then the thickness of the cerebellar layers was measured (Figure 21). Cerebellar layers of HSA 5.0/24h-treated *Ugt1*$^{-/-}$ mice were indistinguishable from WT, while an important reduction of the layers' depth was observed in the HSA 5.0/48h-treated group (50% reduction in the internal granular layer (IGL)-thickness and molecular layer (ML)-thickness, Figure 21A). As previously observed, the P0-P10 PT treatment was sufficient to prevent major abnormalities in cerebellar development (Figure 21A) (Bortolussi et al., 2014).

As Purkinje cells (PCs) are one of the most vulnerable cerebellar cell types, immunostaining was performed to assess their morphology and cell number. Calbindin-specific staining of PCs showed a 40-50% reduction in PCs number and their dendritic arborization in HSA 5.0/48h-treated *Ugt1*$^{-/-}$ mice (Figure 21B). On the contrary, normal PCs density and dendritic growth in both P0-P10 PT- and HSA 5.0/24h-treated mutant animals was detected (Figure 21B), confirming the absence of neurological damage in *Ugt1*$^{-/-}$ mice rescued by the HSA 5.0/24h treatment.

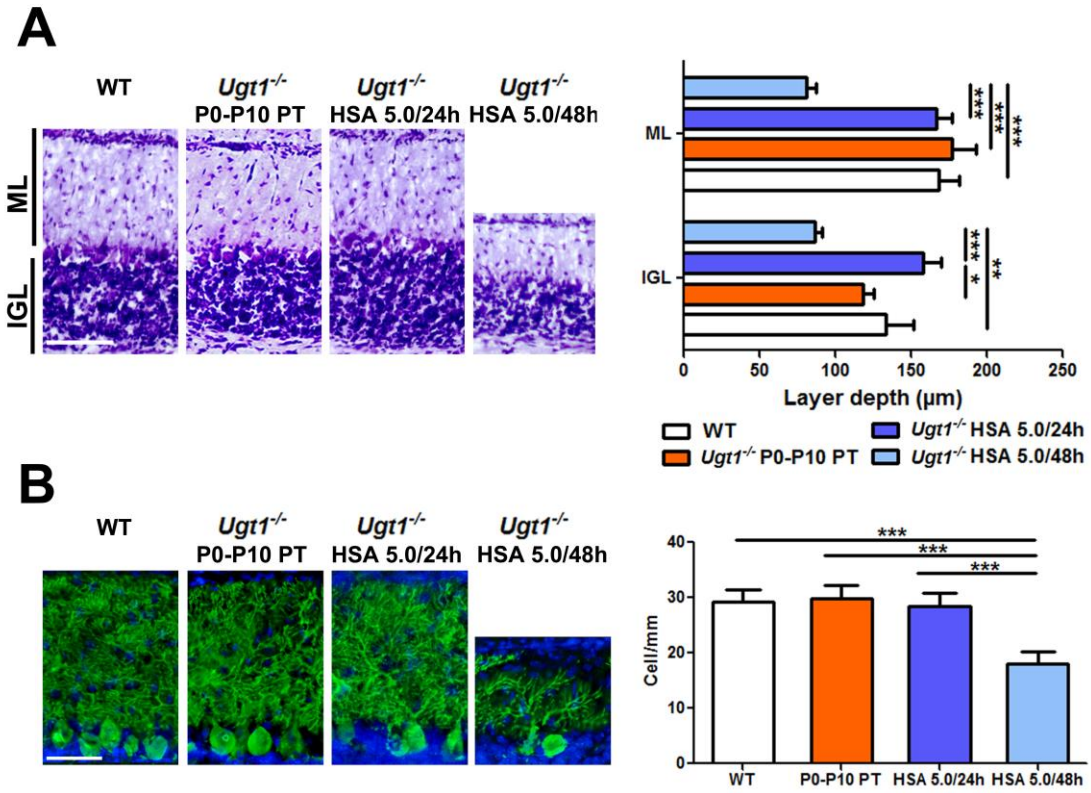

Figure 21. Neurological assessment of HSA treatment. Cerebellar analysis at P15 of WT, P0-P10 PT-, HSA 5.0/48h- and HSA 5.0/24h-treated *Ugt1*$^{-/-}$ animals. **A)** Left panel, representative sections stained with Nissl staining. Right panel, quantification of layers. Values represent mean ± s.d.(µm). IGL, internal granular layer; ML, molecular layer. Scale bar 100 µm. **B)** Left panel, representative immunohistochemisrty using anti-calbindin antibody (green) to stain PCs, nuclei were stained with Hoechst (blue). Scale bar 50 µm. Right panel, PCs quantification. Values represent mean ± s.d.(cell/mm). One-way ANOVA test, **p*<0.05 ***p*<0.01, ****p*<0.001. The number of animals was ≥ 8 in all the conditions.

3.1.6 Long-term effects of HSA administration in rescued *Ugt1*$^{-/-}$ mice

To further assess the long-term effectiveness of HSA administration, animal plasma samples were analysed at P30. Ten days after the last injection, plasma albumin concentration in HSA treated *Ugt1*$^{-/-}$ mice returned to the WT basal levels (Figure 22A), while plasma TB levels remained high (Figure 22B). To analyse the integrity of cerebellar architecture in mutant mice after the discontinuation of HSA treatment (P20), Nissl staining was also performed at one month of age (Figure 22C). Once again, rescued *Ugt1*$^{-/-}$ mice (HSA 5.0/24h- and HSA 7.5/24h-treated mutant mice) showed no differences compared to WT animal.

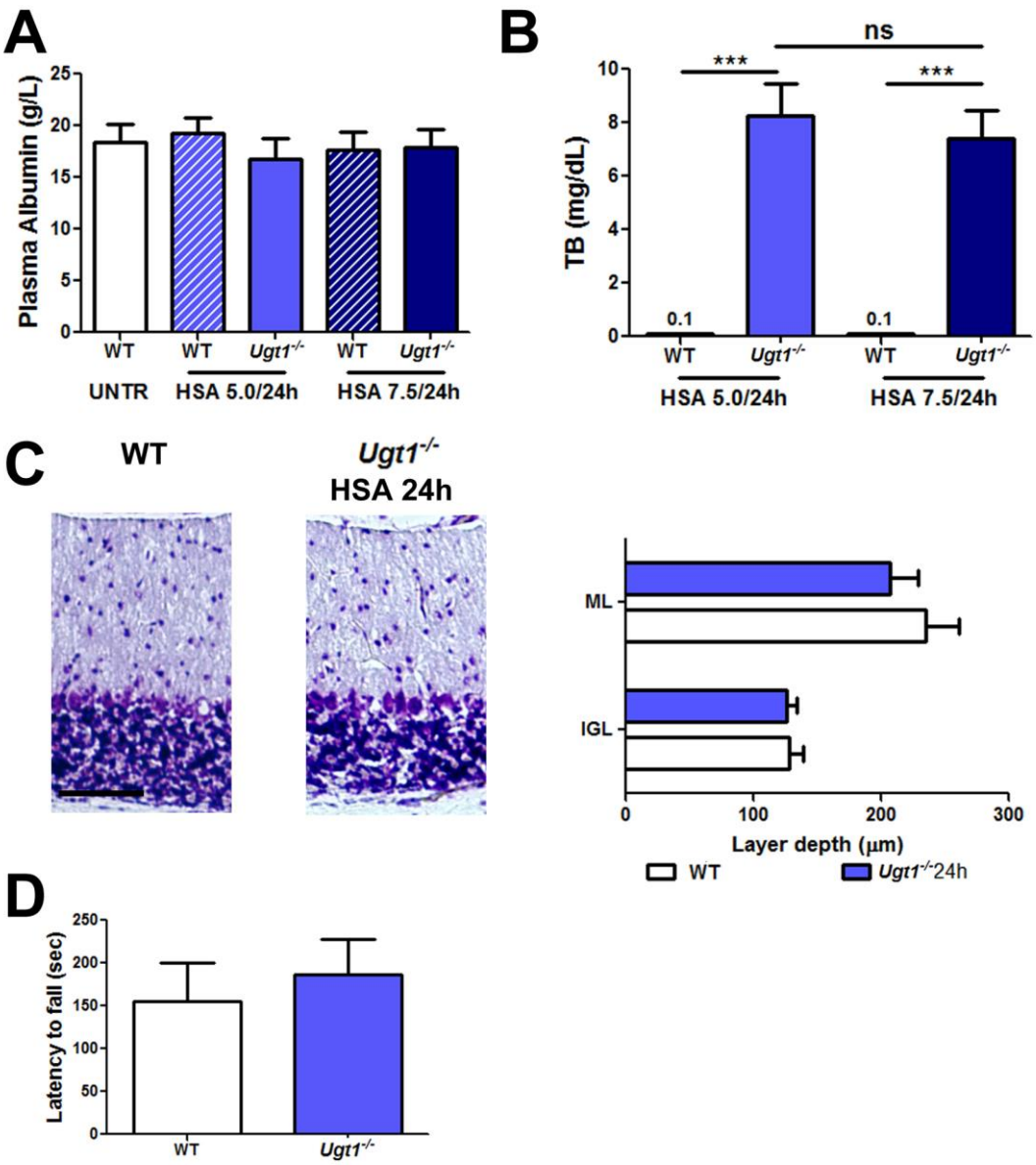

Figure 22. Long term evaluation of rescued mutant mice. A) Plasma albumin levels (g/L) and **B)** TB levels (mg/dL) at P30 in untreated WT, HSA 5.0/24h-treated animals and HSA 7.5/24h-treated animals. **C)** Left panel, representative sections from untreated WT and HSA 5.0/24h-treated *Ugt1*$^{-/-}$ animals, stained with Nissl staining. Right panel, quantification of layers (µm). The number of animals was ≥ 3 in all the conditions. **D)** Rotarod test (s) performed at P30 in WT (n=24) and rescued *Ugt1*$^{-/-}$ animals (n=20). For all the experiments values represent mean ± s.d. Student *t*-test, ***p<0.001; ns, not significant.

Since the cerebellum is the region of brain responsible for motor coordination (Fine et al., 2002) and toxic levels of bilirubin severely affect cerebellar architecture, rescued *Ugt1*$^{-/-}$ animals were tested by rotarod test to assess their motor-coordination abilities on a rotating rod at one month of age. Rescued mutant mice did not show any obvious impairment, as they performed as well as untreated WT (Figure 22D).

In line with the histological analysis, these results confirmed that repeated HSA

administration confers long-term protection from BIND.

3.1.7 The second 24 hours after HSA administration are crucial

Since the histological and survival differences between the HSA 5.0/24h and HSA 5.0/48h-treated *Ugt1*$^{-/-}$ mice were not supported by any difference in the parameters determined at P15 (TB, Bf and tissue bilirubin), I hypothesized that this incongruity could be related to the timing of albumin administration. In fact, at P15 both groups had received the last HSA dose 24h before the day of sacrifice.

Therefore, the second 24 hours after i.p. HSA administration in the HSA 5.0/48h group were investigated by sacrificing both treated groups at P16. At this time point, the HSA 5.0/48h group received the last HSA injection at P14, that corresponded to 48 hours before the analysis. Conversely, only 24 hours passed for the HSA 5.0/24h-treated animals that received the last injection at P15 (Figure 23).

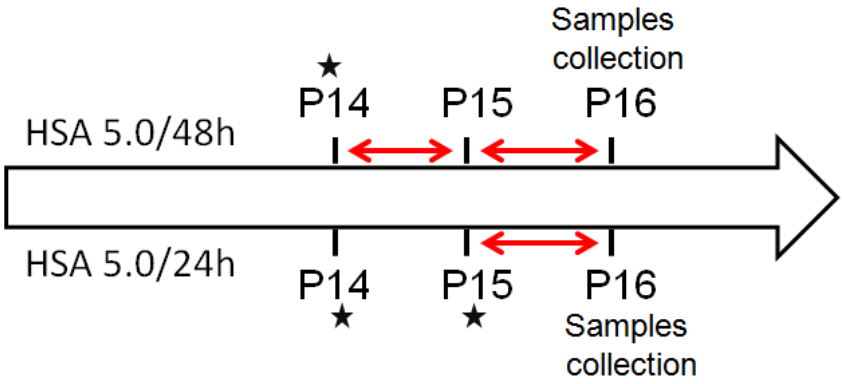

Figure 23. The second 24h after albumin administration. At P15, all the treated mice received last injection 24h before (at P14 injection is represented by the black stars). At P16, *Ugt1*$^{-/-}$ mice injected every 48h (upper side of timeline arrow) spent a second temporal window of 24h (red arrow) with no albumin administration, while mice treated with daily HSA administration (lower side of timeline arrow) received last injection at P15 (second black star). Thus, *Ugt1*$^{-/-}$ treated with HSA 5.0/24h experienced only 24h (red arrow) before sample collection, while *Ugt1*$^{-/-}$ mice treated with HSA 5.0/48h lacked albumin supplementation for 48 hours (two red arrows).

Therefore, plasma TB levels were determined at P16 in *Ugt1*$^{-/-}$ mice. The analysis showed a physiological increase in TB concentration for all the three condition (Figure 24A). Interestingly, the plasma albumin determination showed that HSA 5.0/48h-treated mice experienced a significant reduction of about 20-25% between

P15 and P16 (Figure 24B). On the contrary, no differences were observed for the P0-P10 PT-treated group, in which the albumin levels did not change. No differences in the plasma albumin levels of the 5.0/24h-treated *Ugt1*$^{-/-}$ mice were observed between P15 and P16, which also remained high (Figure 24B).

The decrease in plasma albumin levels in HSA 5.0/48h group led me to analyse plasma Bf values at P16 (Figure 24C). Notably, 48 hours after the last injection, given at P14 in the HSA 5.0/48h-treated group, Bf values triplicated in this group compared to the analyses at P15, reaching values similar to those of the P0-P10 PT control group. In contrast, Bf plasma levels remained steady and low in the HSA 5.0/24h-treated *Ugt1*$^{-/-}$ mice.

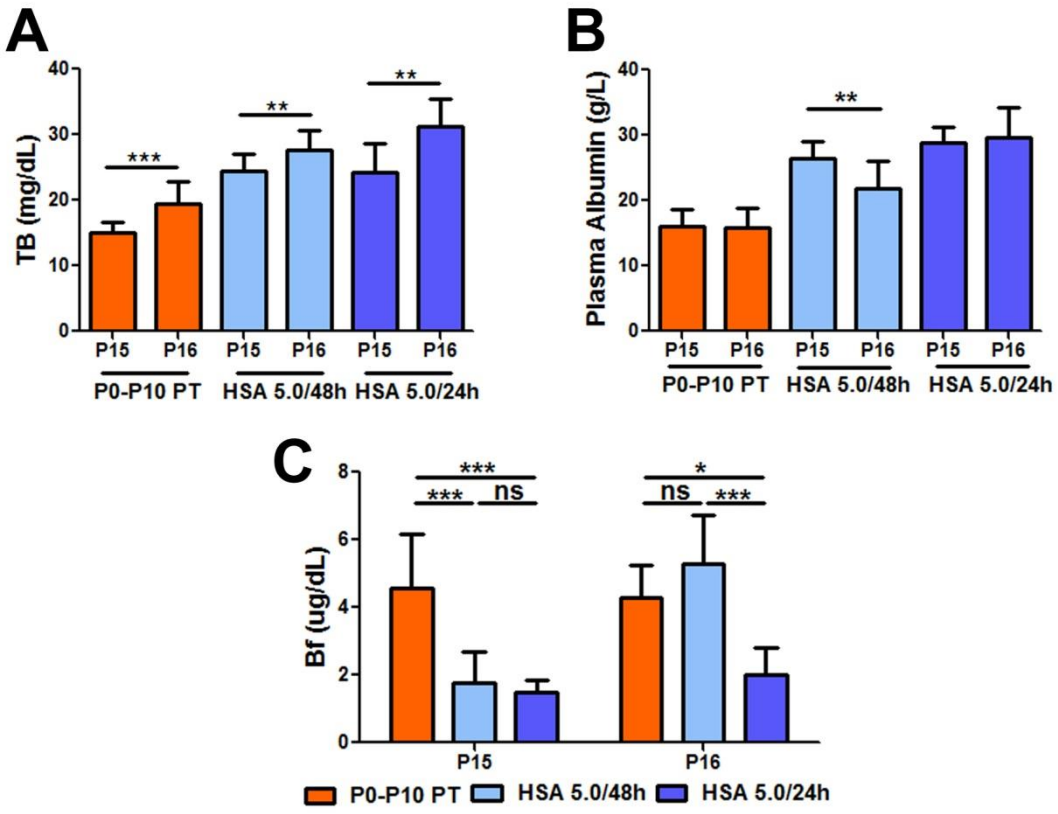

Figure 24. Comparison of plasma albumin, TB and Bf between P15 and P16. **A)** TB levels (mg/dL), **B)** Plasma albumin levels (g/L) and **C)** Bf measurement (μg/dL) in P0-P10 PT-, HSA 5.0/48h- and HSA 5.0/24h-treated *Ugt1*$^{-/-}$ animals at P15 and P16. For all the experiments values represent mean ± s.d. Student *t*-test, ***p*<0.01, ****p*<0.001. One-way ANOVA test, **p*<0.05****p*<0.001, ns not significant. The number of animals was ≥ 6 in all the experiments and conditions.

Because of this impressive increase of Bf in plasma, tissue bilirubin was determined at P16 (Figure 25). P0-P10 PT control group showed a significant increase of free bilirubin content both in the forebrain and in cerebellum, probably associated with the physiological raise in TB plasma levels between P15 and P16. Moreover, in the

5.0/48h-treated group tissue bilirubin rose significantly, by duplicating in FB and almost triplicating in CB bilirubin content. In contrast, no variations were found in tissue UCB in the HSA 5.0/24h group, strongly indicating that daily HSA infusions can keep under safe therapeutic levels tissue UCB, avoiding bilirubin toxicity and neurological damage.

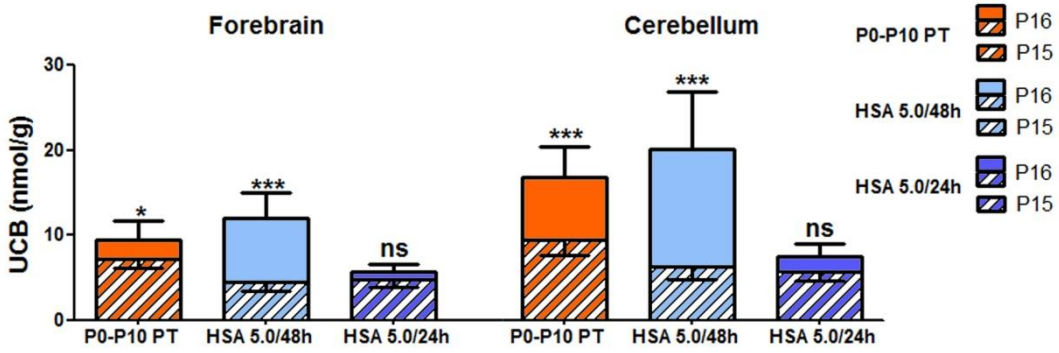

Figure 25. Tissue bilirubin increment at P16. UCB content in forebrain (left side) and cerebellum (right side) of *Ugt1*$^{-/-}$ animals. The whole bars, stripped plus full colored, represent UCB levels at P16 while the stripped bars represent the amount of UCB at P15. The full colored bars represent the increment of UCB levels from P15 to P16. Values represent mean ± s.d. (nmol/g). Student *t*-test, *p<0.05, ***p<0.001, ns not significant. The number of animals was ≥ 6 in all the experiments and conditions.

To further assess the effects of albumin administration, bilirubin levels were analysed in liver (LIV) and skeletal muscle (SM), two tissues normally not susceptible to bilirubin toxicity. As shown in Figure 26, although no differences were observed in LIV bilirubin content, P0-P10 PT-treated *Ugt1*$^{-/-}$ showed an increase in SM bilirubin levels, probably coupled with the physiologic increase in plasma bilirubin. Notably, bilirubin content in HSA 5.0/48-treated group significantly increased only in LIV, while no changes in SM were observed. Importantly, bilirubin levels in liver and SM of *Ugt1*$^{-/-}$ mice treated daily with HSA 5.0 g/kg were stable between P15 and P16, underlining the beneficial effects of albumin administration.

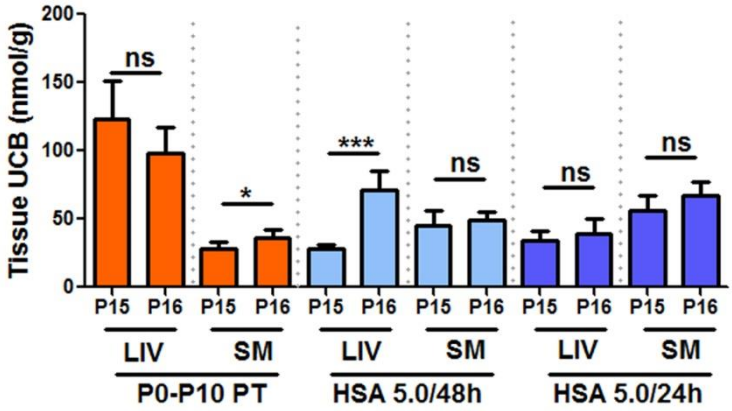

Figure 26. Effect of HSA on liver and skeletal muscle. At P15 and P16, tissue UCB content was performed in LIV and SM of *Ugt1*$^{-/-}$ mice. Values represent mean ± s.d. (nmol/g). Student *t*-test, **p*<0.05, ****p*<0.001, ns not significant. The number of animals was ≥ 6 in all the experiments and conditions.

3.1.8 Predictive markers of bilirubin-induced neurological dysfunction

I finally evaluated which parameter better predicted neurological damage and survival. Individual cerebellar bilirubin levels were plotted as function of plasma TB concentration, bilirubin/albumin (B/A) ratio or Bf obtained at P16 from the P0-P10 PT, HSA 5.0/24h and HSA 5.0/48h groups. I used tissue bilirubin in the cerebellum as a direct indicator of neurological damage, since cerebellum is the most affected region of the brain.

The distribution of the data in the P0-P10 PT, HSA 5.0/48h and 5.0/24h groups of TB and B/A ratio plots overlapped among the groups and poorly correlated with cerebellar bilirubin content (Figure 27A and 27B; r2=0.08 and 0.35, respectively; *p*=0.2, *p*<0.01, respectively, Correlation test, Pearson's coefficient). The predictor value of these two plots was very low (i.e., *Ugt1*$^{-/-}$ animals of the control and HSA 5.0/48h groups were not separated from the HSA 5.0/24h group that results in survival of mutant mice).

Conversely, the Bf plot clearly showed that the data from the HSA 5.0/24h group formed a distinct cluster, clearly separated from the two other groups (P0-P10 PT and HSA 5.0/48h) (Figure 27C, r^2=0.62, *p*<0.0001, Correlation test, Pearson's coefficient), supporting a high predictor value of Bf.

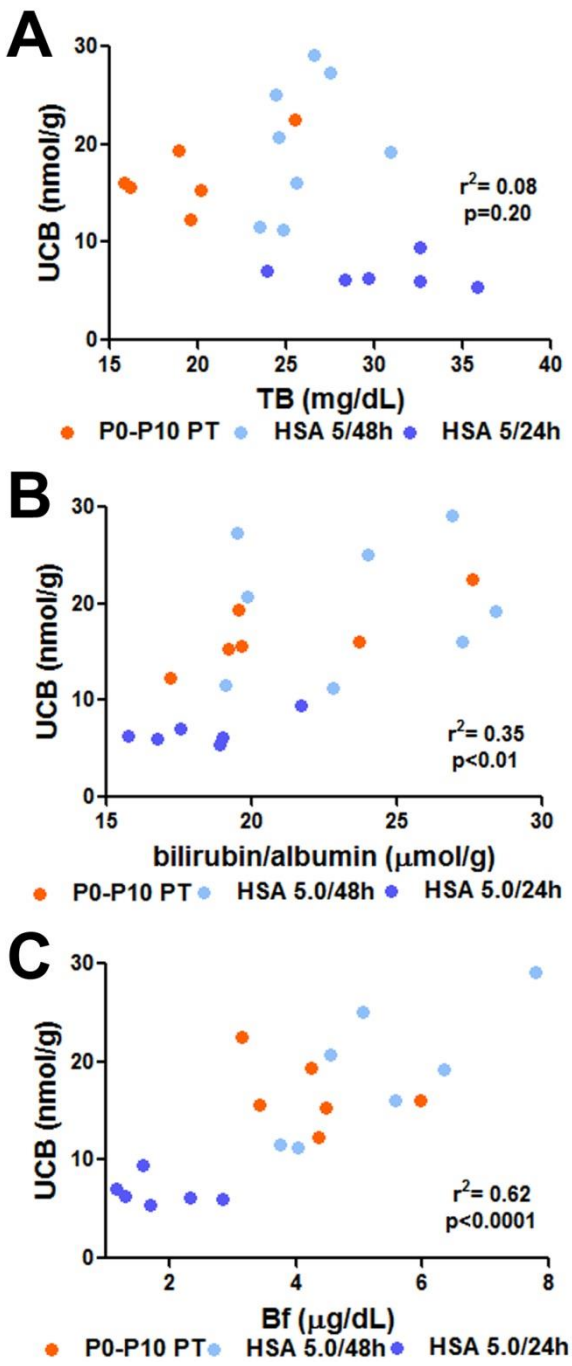

Figure 27. Plasma markers of bilirubin toxicity. Correlation of **A)** TB (mg/dL), **B)** Bilirubin/albumin (B/A) ratio (µmol/g) and **C)** Bf levels (µg/dL) with cerebellar UCB content (nmol/g), as a measure of bilirubin induced damage. Each dot represents a single animal. Correlation test, Pearson's coefficient.

In conclusion, as determined at P16, this set of correlation experiments indicated that Bf is the best predictor of bilirubin neurotoxicity among the most relevant markers used in clinics.

3.2 Molecular basis of neurotoxicity in neonatal hyperbilirubinemia

Despite intensive studies, cellular and molecular events leading to irreversible BIND remained not fully understood. The purpose of this investigation is the identification of the neurological events preceding and leading to BIND.

3.2.1. Experimental plan

As a further effort to deeper investigate the mechanisms leading to bilirubin neurotoxicity, it was performed a time-course analysis of *Ugt1*$^{-/-}$ animals at three different time points: P5, at the onset of the pathology; P8 (Figure 28A), as a more advanced pathological condition, shown to be a key time point reversible by PT application in a low proportion of mice (Bortolussi et al., 2014); and finally P10, as the latest and most severe analysed phase, the day before the observed 50 % mortality of *Ugt1*$^{-/-}$ mice (P11, Figure 28B). At the indicated time points I studied bilirubin susceptibility of different neuronal cell types, such as PCs and Granule cells (GCs).

In addition, to illustrate a comprehensive landscape of bilirubin neurotoxicity effects it was investigated the activation of different mechanisms induced by bilirubin, such as neuroinflammation and its relative markers, endoplasmic reticulum (ER) and oxidative stress.

3.2.2. Susceptibility to bilirubin depends on the neuronal type and its developmental stage

One of the major features of BIND is neurodegeneration, a mechanism that involves the collapse of neuronal cell structure and cell death (Haustein et al., 2010). A previous work from Mouse Molecular Genetics lab has shown that apoptosis, assessed by caspase 3 activation at P4, is induced by hyperbilirubinemia in the cerebellum of C57BL/6 *Ugt1*$^{-/-}$ mice (Bortolussi et al., 2015), a mouse strain carrying the same genetic mutation but showing a more severe phenotype (Bortolussi et al., 2012). Hence, I investigated the activation of the apoptotic pathway in FVB/NJ *Ugt1*$^{-/-}$ mice and their WT littermates by Western blot (WB) analysis. On the contrary to what observed at P4 in the C57BL/6 strain (Bortolussi et al., 2015), no increase in

caspase 3 cleavage was shown at P5, while a two-fold increase was observed at P8 (Figure 28C).

To assess bilirubin-induced neurological damage at cerebellar level, brain sections of *Ugt1*$^{-/-}$ mice were stained with Nissl staining at P8 and P10 (Figures 28D and 28E, respectively). Next, layers' thickness was quantified in WT and *Ugt1*$^{-/-}$ pups, showing a significant reduction in the EGL and ML at both P8 and P10. I observed a ~ 45% reduction of EGL-thickness at both time points analysed, while ML-thickness was reduced by 25% at P8 and by 34% at P10 in *Ugt1*$^{-/-}$ mice (Figure 28D and 28E, respectively). Furthermore, the internal granular layer (IGL)-thickness was reduced only at P10, in which *Ugt1*$^{-/-}$ presented 25% reduction compared to WT littermates (Figure 28E).

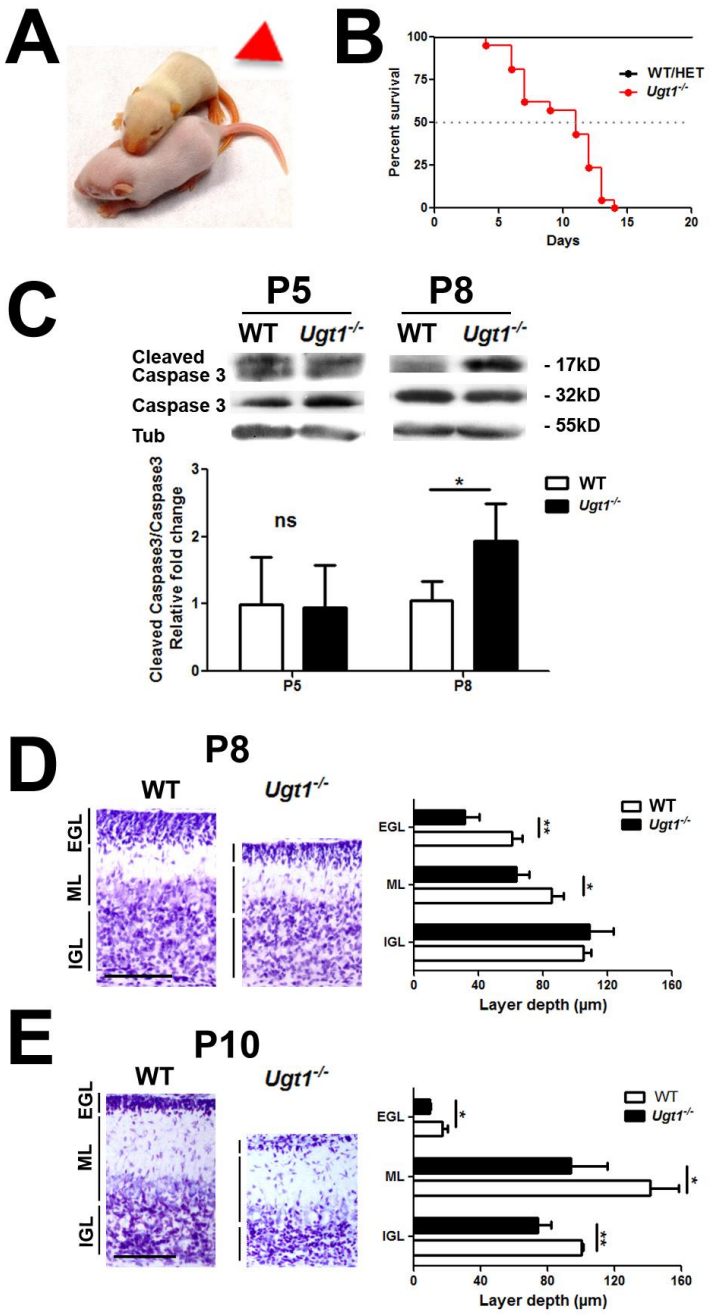

Figure 28. Neurological characterization of the FVB/NJ *Ugt1*$^{-/-}$ mice. A) Jaundiced *Ugt1*$^{-/-}$ mouse (red arrowed) and WT littermate appearance at P8. **B)** Kaplan-Meier survival curve of *Ugt1*$^{-/-}$ (red line, n=21) and Ugt1$^{+/-}$ and Ugt1$^{+/+}$ (WT/HET, n=59). **C)** WB analysis using an anti-cleaved and -total caspase 3 antibodies on total cerebellum protein extract at P5 and P8 of WT and *Ugt1*$^{-/-}$ mice. β-tubulin was used as loading control. **D)** Left panel, Nissl staining of cerebellar layers at P8. Scale bar 100 μm. Right panel, layer depth quantification of WT and *Ugt1*$^{-/-}$ (μm). **E)** Left panel, Nissl staining of cerebellar layers at P10. Scale bar 100 μm. Right panel, layer depth quantification of WT and *Ugt1*$^{-/-}$ (μm). For all the graphs values represent mean ± s.d. Student *t*-test, **p*< 0.05, ***p*<0.01, ns not significant. The number of WT and *Ugt1*$^{-/-}$ was ≥ 3 in all the experiments and time points. EGL, external germinal layer; IGL internal granular layer; ML, molecular layer.

To have a deeper insight about the effects of bilirubin neurotoxicity, different types of cerebellar neurons were investigated. By real-time RT-PCR, WB and IF, it was first estimated bilirubin detrimental effects on PCs by the analysis of calbindin1, a PCs-specific marker (Whitney et al., 2008). A significant reduction of *calbindin* mRNA levels was observed only at P10, although a non-statistically significant decrease was also evident in the earlier time points analysed in *Ugt1*$^{-/-}$ mice (Figure 29A). Then, protein levels were analysed by WB analysis using an anti-calbindin specific antibody. It was observed a minor reduction in calbindin levels at P5, while a significant reduction in mutant cerebellar protein extracts was observed in *Ugt1*$^{-/-}$ mice compared to WT at P8 and P10, showing 56% and 61% decrease, respectively (Figure 29B).

IF experiments (Figure 29C and 29D) confirmed the results obtained by RT-PCR and WB, showing a 30% and 50% reduction in PCs number at P8 and P10, respectively (Figure 29D), and the almost complete absence of the PCs' dendritic arbor in *Ugt1*$^{-/-}$ mice.

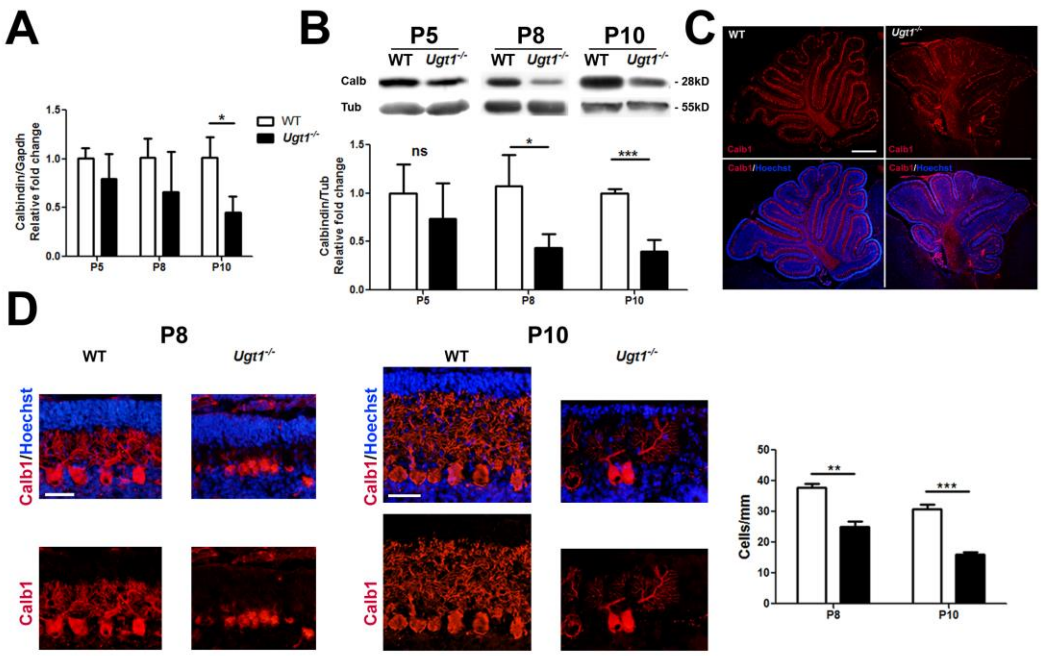

Figure 29. Bilirubin affects PCs dendritic arborization and survival. A) Time-course of *calbindin* mRNA expression levels at P5, P8 and P10 in total RNA preparations of WT and *Ugt1*$^{-/-}$ cerebella. **B)** WB analysis of total cerebellum protein extracts using an anti-calbindin antibody at indicated time points of WT and *Ugt1*$^{-/-}$ mice. β-tubulin was used as loading control. **C)** Low-magnification images at P10 of representative IF of WT and *Ugt1*$^{-/-}$ cerebellum sections using anti-calbindin antibody (red) to highlight PCs. Hoechst (blue) was used to mark nuclei. Scale bar: 500 µm. **D)** High-magnification images of cerebellar sections from WT and *Ugt1*$^{-/-}$ mice at P8 and P10, using an anti-calbindin antibody (red) to highlight PCs. Hoechst (blue) was used to mark nuclei. Scale bar: 50 µm. The quantification of PCs number at P8 and P10 of WT and *Ugt1*$^{-/-}$ mice is represented in the bar graph (cell/mm). For all the experiments values represent mean ± s.d. Student *t*-test, **p*< 0.05, ***p*<0.01, ****p*<0.001, ns not significant. The number of WT and *Ugt1*$^{-/-}$ was ≥ 3 in all the experiments and time points.

Next, to determine whether bilirubin affected mature cerebellar GCs, it was analysed the nuclear protein NeuN, since its expression in the cerebellum is restricted to differentiated granule neurons (Sarnat et al., 1998). *NeuN* expression levels were not affected in *Ugt1*$^{-/-}$ mice compared to WT animals at all time points analysed, as determined by real-time RT-PCR (Figure 30A). WB experiments confirmed the mRNA expression results, as it was observed no changes in protein levels of NeuN of cerebellar extracts from *Ugt1*$^{-/-}$ and WT mice at P5, P8 and P10 (Figure 30B). IF analysis performed at P8 and P10 (Figure 30C and 30D) showed no obvious reduction in cell density of neurons located in the IGL, indicating that chronic exposure to bilirubin in *Ugt1*$^{-/-}$ mice did not affect differentiated granule cells survival.

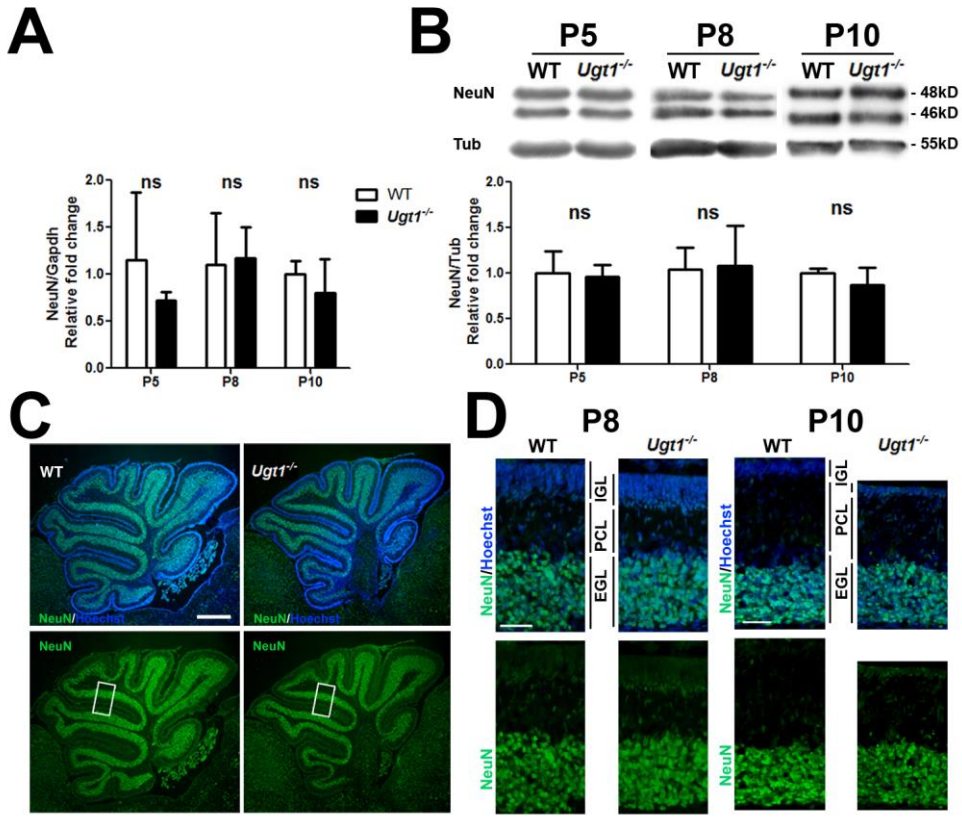

Figure 30. Bilirubin does not affect survival of differentiated granule cells. A) Time-course of *NeuN* mRNA expression levels at P5, P8 and P10 in total RNA preparations of WT and *Ugt1*$^{-/-}$ cerebella. **B)** WB analysis of total cerebellum protein extracts using an anti-NeuN antibody at indicated time points of WT and *Ugt1*$^{-/-}$ mice. β-tubulin was used as loading control. **C)** Low-magnification images of total cerebellum at P10. Representative IF of WT and *Ugt1*$^{-/-}$ cerebellum sections using anti-NeuN antibody (green) to stain differentiated granule cells. Hoechst (blue) was used to mark nuclei. Scale bar: 500 µm. **D)** High-magnification images of fields indicated in panel C from WT and *Ugt1*$^{-/-}$ mice at P8 and P10, using anti-NeuN antibody (green) Hoechst (blue) was used to mark nuclei. Scale bar: 50 µm. For all the experiments values represent mean ± s.d. Student *t*-test, ns not significant. The number of WT and *Ugt1*$^{-/-}$ was ≥ 3 in all the experiments and time points.

Collectively, this set of experiments underscored the importance of the neuronal cell type and the related developmental stage in response to bilirubin neurotoxicity.

3.2.3. Bilirubin-induced gliosis in *Ugt1*$^{-/-}$ mice cerebella

It has been observed the association of neurotoxicity and neuroinflammation in a humanized mouse model of neonatal hyperbilirubinemia, expressing the human *Ugt1* locus in a mouse *Ugt1* null background (*hUGT1*) (Yueh et al., 2014). Since only 8-10% of *hUGT1* die by bilirubin neurotoxicity and several differences exist between Yueh mice and the model I studied, my work was focused on the study of

neuroinflammation, investigating whether an increase in inflammatory markers could be coupled to bilirubin-induced neurodegeneration and death in the *Ugt1*$^{-/-}$ mouse model of severe neonatal hyperbilirubinemia.

First, to determine the astrocyte response to bilirubin the levels of glial fibrillary acidic protein (GFAP), an astrocyte-specific marker (Sofroniew and Vinters, 2010) were assessed. The time-course analysis of *GFAP* mRNA expression levels revealed no alterations in the earliest time point (P5, Figure 31A). Conversely, a 3- and 7-fold *GFAP* mRNA level increase was detected in *Ugt1*$^{-/-}$ mice at P8 and P10, respectively (Figure 31A). WB analysis of cerebellar protein extracts confirmed the increase in mRNA expression, showing no differences were observed at P5, but a 2- to 3-fold increase at P8 and P10 in *Ugt1*$^{-/-}$ pups (Figure 31B).

IF analysis at P8 and at P10 on cerebellar sections of WT and *Ugt1*$^{-/-}$ littermates showed the localization of GFAP positive signal (glial scar) in proximity to cerebellar fissures in which PCs loss was more evident, such as fissures IV to VIII (Figure 31C). The higher magnification analysis performed at P8 and P10 (Figure 31D) confirmed the previous observation, as GFAP-positive cells correlated with the time-dependent loss of PCs.

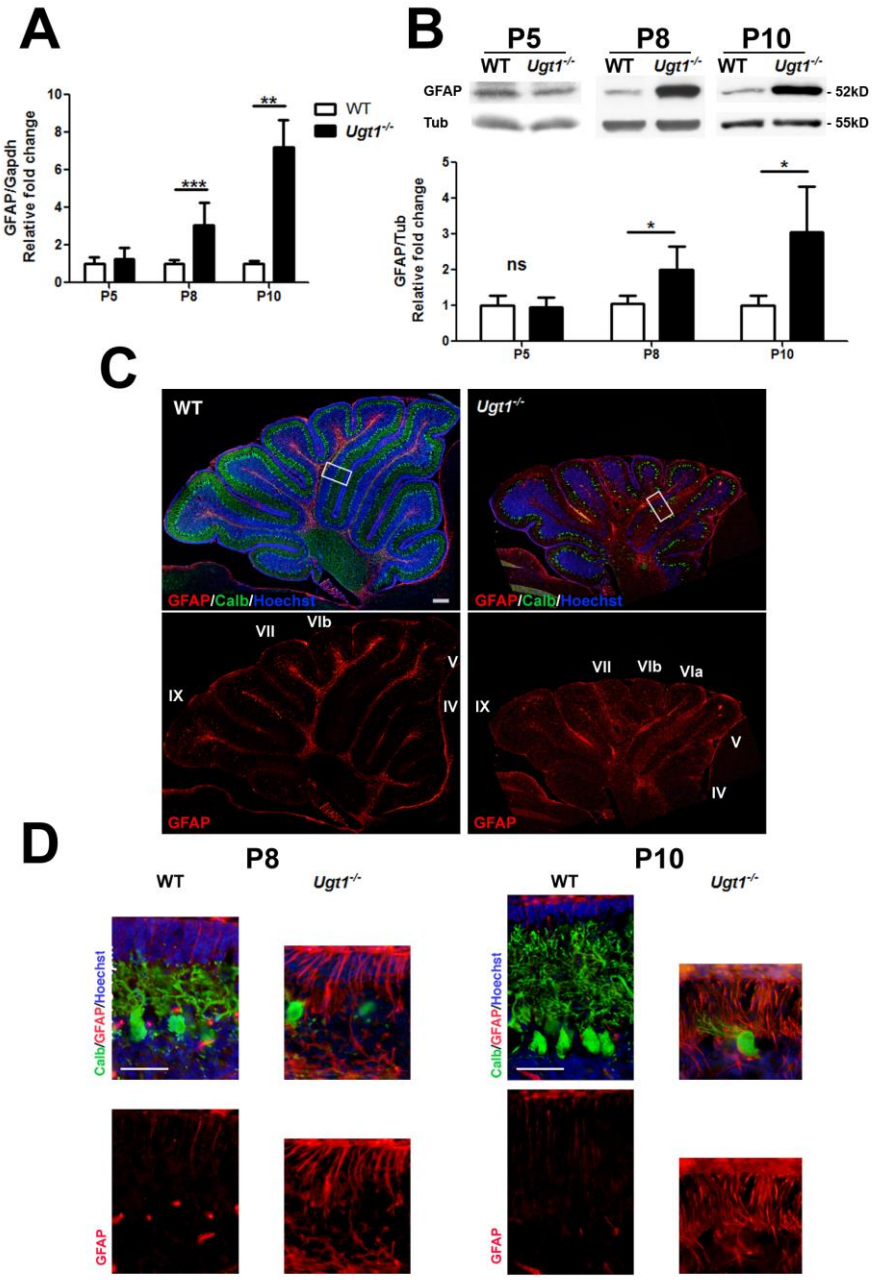

Figure 31. Bilirubin triggers the activation of astrocytes. A) Time-course of *GFAP* mRNA expression levels at P5, P8 and P10 in total RNA preparations of WT and *Ugt1*$^{-/-}$ cerebella. **B)** WB analysis of total cerebellum protein extracts using an anti-GFAP antibody at indicated time points of WT and *Ugt1*$^{-/-}$ mice. β-tubulin was used as loading control. **C)** Low-magnification images of representative IF from WT and *Ugt1*$^{-/-}$ cerebellum sections using anti-GFAP antibody (red) to detect astrocytes, co-stained with an anti-calbindin antibody (green) to highlight PCs. Hoechst (blue) was used to mark nuclei. Scale bar: 200 µm. Boxed areas indicate fields shown in Figure 2B. IV, VI, VIa, VIb, VII and IX indicate the cerebellar fissures. **D)** High-magnification images of boxed areas indicated in panel C. Scale bar: 50 µm. For all the experiments values represent mean ± s.d. Student *t*-test, **p*< 0.05, ***p*<0.01, ****p*<0.001, ns not significant. The number of WT and *Ugt1*$^{-/-}$ was ≥ 3 in all the experiments and time points.

Next, to determine the cerebellar microglia response to bilirubin, it was analysed the ionized calcium-binding adapter molecule 1 (Iba1) as a cell-specific marker of microglia (Ito et al., 1998). Real-time RT-PCR showed no alterations in *Iba1* mRNA levels at P5 (Figure 32A). By contrast, I observed an increase in *Iba1* mRNA expression starting from P8 (Figure 32A), with Iba1 cerebellar levels in hyperbilirubinemic *Ugt1*$^{-/-}$ mice that doubled those of WT littermates. In addition, bilirubin triggered a three-fold increase in *Iba1* mRNA levels at P10 (Figure 32A). It was observed a delay in protein expression, in comparison to mRNA levels, as WB analysis revealed a two-fold increase in Iba1 only at P10 (Figure 32B). IF staining performed at P10 (Figure 32C) showed an evident increase in Iba1 signal in mutant cerebella. Furthermore, cerebellar regions in which PCs neurodegeneration was more marked also showed an increase in Iba1 positive cells. In fact, only a few microglia-positive cells were present in these areas at P8; while a stronger signal was observed at P10 (Figure 32D).

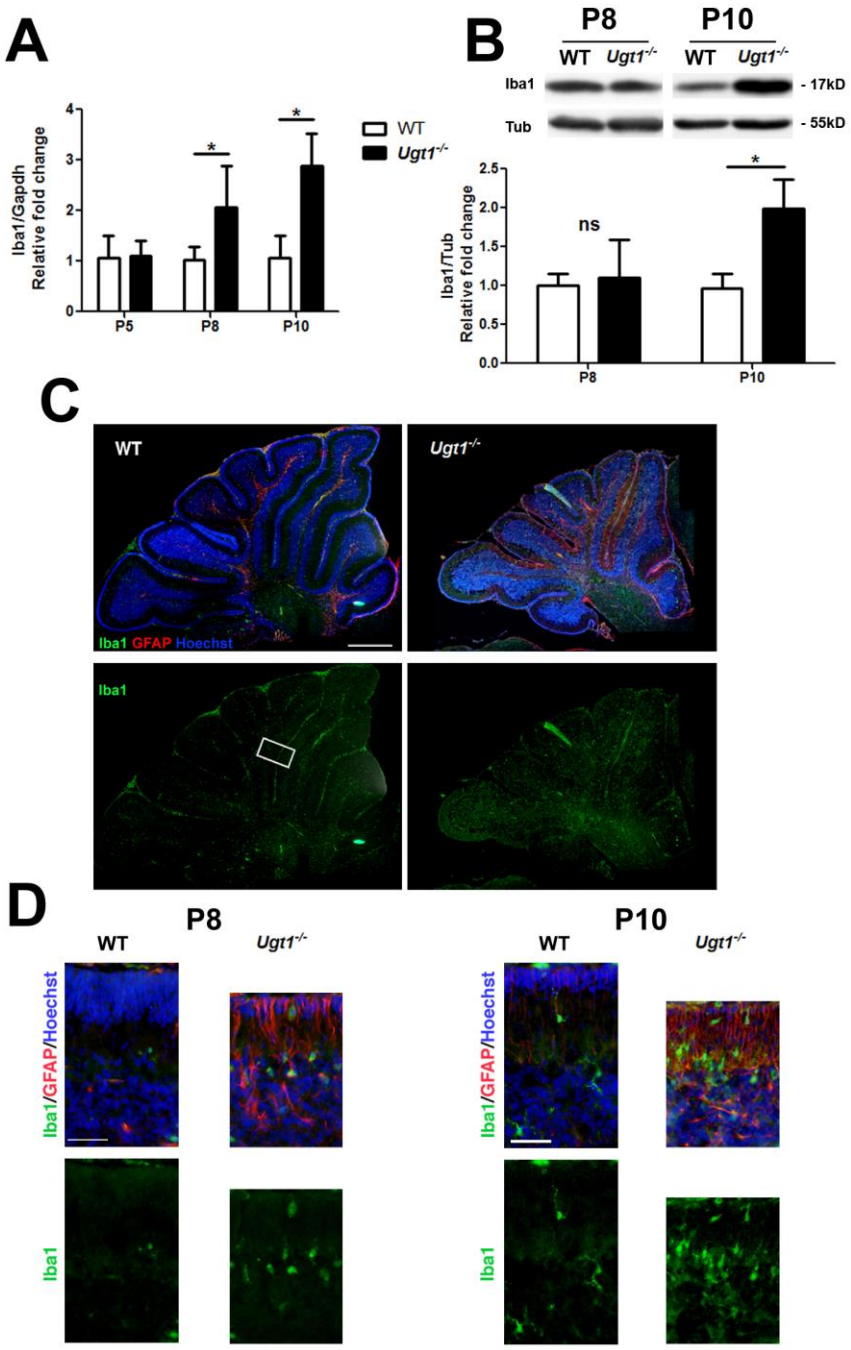

Figure 32. Bilirubin triggers the activation of microglia. A) Time-course of *Iba1* mRNA expression levels at P5, P8 and P10 in total RNA preparations of WT and *Ugt1*$^{-/-}$ cerebella. **B)** WB analysis of total cerebellum protein extracts using an anti-Iba1 antibody at indicated time points of WT and *Ugt1*$^{-/-}$ mice. β-tubulin was used as loading control. **C)** Low-magnification images of P10, IF from of WT and *Ugt1*$^{-/-}$ cerebellum sections using anti-Iba1 antibody (green) to detect microglia-positive cell, co-stained with an anti-GFAP antibody (red) to highlight astrocytes. Hoechst (blue) was used to mark nuclei. Scale bar: 500 μm. **D)** High-magnification images of boxed areas indicated in panel C. Representative IF of cerebellar sections at P8 and P10 from WT and *Ugt1*$^{-/-}$ mice Scale bar: 50 μm. For all the experiments values represent mean ± s.d. Student *t*-test, **p*< 0.05, ***p*<0.01, ****p*<0.001, ns not significant. The number of WT and *Ugt1*$^{-/-}$ was ≥ 3 in all the experiments and time points.

3.2.4 Time-dependent decrease of M2 is inversely proportional to M1 activation

The inflammatory response typically involves the resident population of tissue macrophages. Macrophages states can be divided in two main types: M1 and M2, which correspond to inflammatory and neuroprotective ones, respectively. To better characterize microglia activation during prolonged bilirubin exposure, it was performed a real-time RT-PCR analysis of molecular markers that discriminate microglia/macrophage states. These markers are key features of the pro-inflammatory M1 type of microglia (*cluster of differentiation* (*CD*) *68* and *86*) and the anti-inflammatory M2 type of microglia [*mannose receptor complex* (*MRC*) *1* and *2* and *arginase 1* (*Arg1*)].

A marker of neuro-inflammatory (M1 type) microglia, *CD68*, showed 2.1-, 2.5- and 3.5-fold increase at P5, P8 and P10, respectively, compared to WT levels (Figure 33). On the contrary, the expression analysis of *CD86*, another component of M1 type microglia, revealed that mRNA levels of *Ugt1*$^{-/-}$ mice were similar to those of WT littermates.

By contrast, real-time RT-PCR analysis revealed an inverted trend for the M2 type, which is the neuroprotective counterpart of microglia. *MRC1* and *Arg1* in mutant mice showed decreased expression over time, while *MRC2* was significantly activated only at P8 (Figure 33).

Since the transition from M2 to M1 phenotype is generally associated with inflammation-induced pathologies, taken together these data indicate that exposure to bilirubin triggers activation of pro-inflammatory microglia and a parallel decrease in the neuroprotective one.

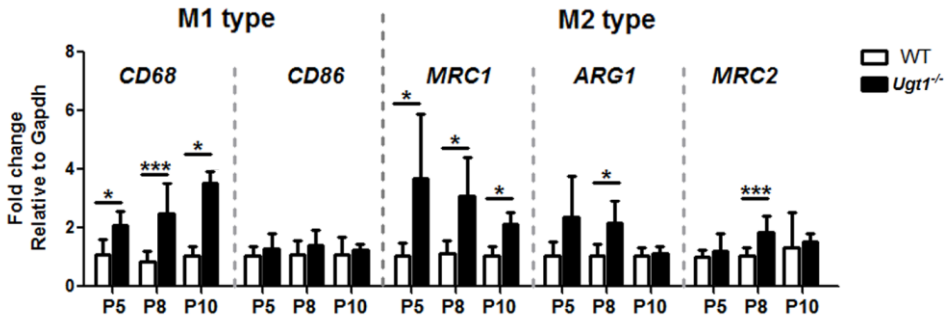

Figure 33. Bilirubin induces activation of pro-inflammatory microglia. Time-course of mRNA expression levels of M1 and M2 microglia markers. WT and *Ugt1*$^{-/-}$ mice mRNA cerebellar expression levels of *CD68*, *CD86*, *MRC1*, *Arg1* and *MRC2* were analysed at the indicated time points. Values represent the mean ± s.d. Student *t*-test, **p*< 0.05, ****p*<0.001. The number of WT and *Ugt1*$^{-/-}$ was ≥ 3 in all the experiments and time points.

3.2.5 Amplifiers genes of bilirubin-induces inflammatory response

To be effective, the immune response must be amplified by the recruitment of additional cells to the site of 'injury". Important players of this response are cytokines (e.g. INFγ, TNFα and ILs) and chemokines that also serve to recruit additional immune cells. Moreover, during the inflammatory process other inflammatory players may influence substrate metabolism, cell mobility, phagocytosis, intracellular killing and antigen presentation.

Thus, some of these inflammatory markers were analysed by real-time RT-PCR [*interleukin* (*IL*) *1β*, *IL6*, *IL10*, *interferon γ* (*INFγ*), *Toll-like receptor 2* (*TLR2*), *inducible nitric oxide synthase* (*iNOS*), *neuronal NOS* (*nNOS*), *IL18*, *nuclear factor kappa-light-chain-enhancer of activated B cells* (*NFKβ*), *matrix metalloproteinases 2* (*MMP2*) and *9* (*MMP9*) and *tumor necrosis factor α* (*TNFα*)].

As shown in Figure 34, it was not possible to detect several cytokines and inflammatory markers known to be involved in response to the bilirubin insult (Figure 34A). To rule out technical problems limiting the detection of inflammatory markers, dendritic cells (DCs) treated with LPS for 24 hours were used as positive control. Few candidate genes were below the detection limit in cerebellar RNA extracts (Figure 34A), showing a technically clear product only in DCs RNA extracts (such as IL1β, Figure 34B), while all the other candidate genes used in this study showed a clear product both in DCs and cerebellar RNA extracts (such as TNFα, Figure 34C).

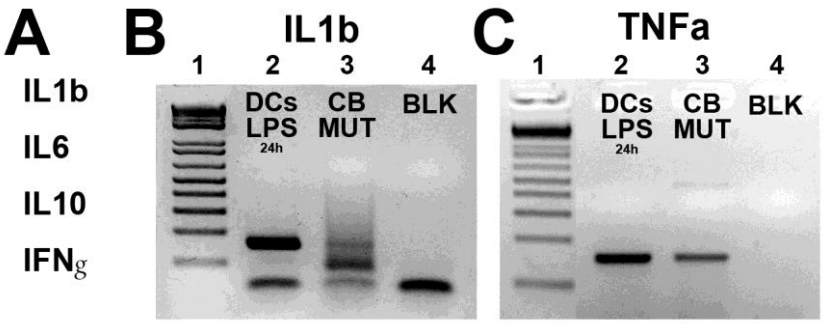

Figure 34. Inflammatory markers screening. A) List of mRNAs that were not detected by qRT-PCR in cerebellar total RNA extracts. **B)** Example of expression levels under the detection limit of the technique. PCR product of *IL1β* mRNA expression. As positive control dendritic cells (DCs) were treated with LPS for 24 hours. **C)** Example of detectable mRNA, *TNFα* expression. Lane 1: 1Kb ladder; lane 2: PCR product from dendritic cells (DCs) treated with LPS for 24h; lane 3: CB, cerebellar total RNA extract; lane 4, blank.

The analysis of inflammatory markers by real-time RT-PCR revealed an early response of *IL18* and *NFKβ* to bilirubin accumulation (Figure 35), as they were significantly up-regulated at P5 (Figure 35A). Prolonged exposure to bilirubin levels, such as at the second analysed time point (P8), led to a mild but significant expression of the inflammatory mediators *nNOS*, *MMP2* and *MMP9* in *Ugt1*$^{-/-}$ mice compared to WT animals (Figure 35A). Only in very severe conditions (P10) where cerebellar architecture appeared to be compromised and enhanced gliosis was observed, the *TNFα* mRNA was strongly up-regulated (up to ~10 times), coupled with increased *NFKβ* expression (Figure 35A). However, other markers involved in the inflammatory processes, such as *TLR2* and *iNOS*, were not regulated by bilirubin exposure at any time point analysed in the *Ugt1*$^{-/-}$ mouse model (Figure 35B).

Since neuroinflammation appeared to importantly contribute to each stage of bilirubin neurotoxicity, these expression data emphasized the complexity of the inflammatory response triggered by bilirubin *in vivo*.

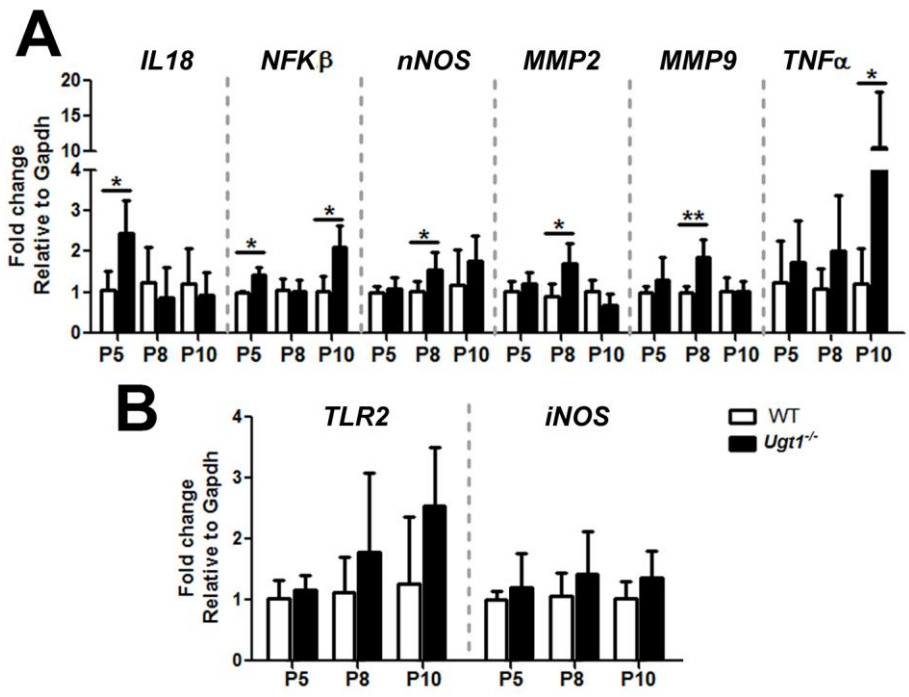

Figure 35. Relative mRNA expression of inflammatory markers. A) WT and *Ugt1*$^{-/-}$ mice mRNA cerebellar expression levels of *IL18, NFKβ, nNOS, MMP2, MMP9* and *TNFα* were analysed at the indicated time points. **B)** WT and *Ugt1*$^{-/-}$ mice mRNA cerebellar expression levels of *TLR2* and *iNOS* were analysed at the indicated time points. Values represent the mean ± s.d. Student *t*-test, **p*< 0.05, ***p*<0.01. The number of WT and *Ugt1*$^{-/-}$ was ≥ 3 in all the experiments and time points.

3.2.6 Early stages of BIND are characterized by ER and oxidative stress activation

Among others, two mechanisms are supposed to have important roles in bilirubin neurotoxicity: ER and oxidative stress responses. In fact, it has been shown that bilirubin triggers ER stress *in vitro* (Barateiro et al., 2012). In addition, the alteration of normal homeostasis elicited by bilirubin exposure led to the interference of oxidative protein folding resulting in ER stress (Bortolussi et al., 2015).

At the onset of the disease, at P5, it was observed the activation of ER stress markers coupled with *IL18* and *NFKβ* up-regulation in *Ugt1*$^{-/-}$ mice compared to WT animals. As determined by real-time RT-PCR analysis, a significant increase in mRNA levels of *activating transcription factor* (*ATF*) *3*, *C/EBP-homologous protein* (*CHOP*) and *CD95/Fas* was observed in *Ugt1*$^{-/-}$ cerebella (Figure 36A). To note, the activation of these ER stress responders was not just related to the initial stage of the disease, but their mRNA levels further increased over time. However, other

players of established/canonical ER stress pathways were not modified along the analysis in the *Ugt1*$^{-/-}$ mouse model [e.g. *glucose-regulated protein 78* (*GRP78*), *ATF4*, Figure 36B], giving additional proof on the multifaceted mechanisms associated to hyperbilirubinemia, in which not always the canonical pathways are followed, at least in mRNA expression levels of *Ugt1*$^{-/-}$ mouse model.

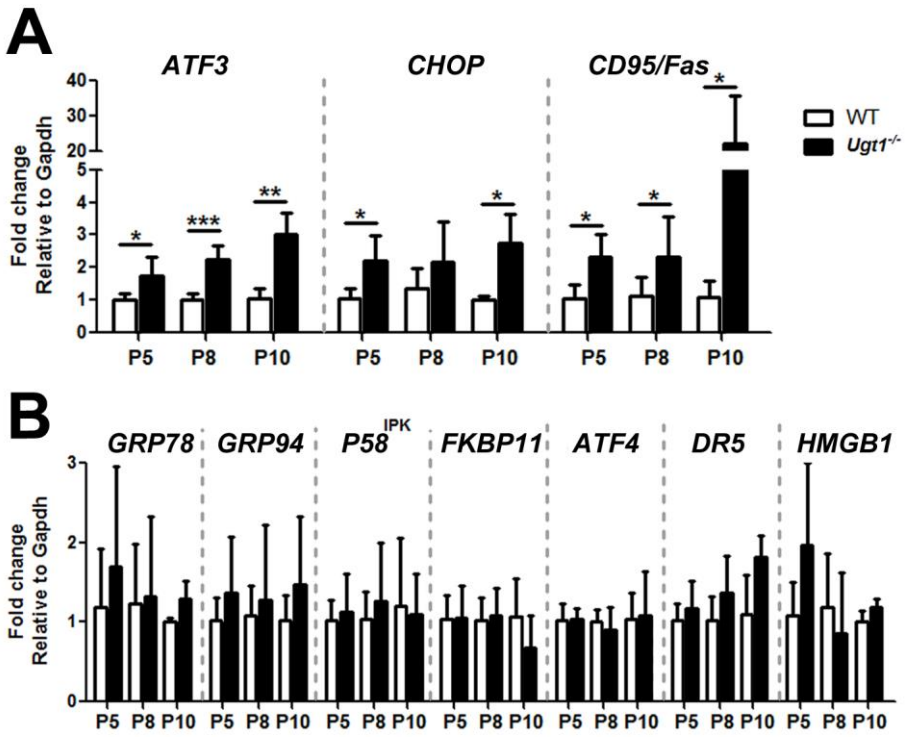

Figure 36. Time-course of mRNA expression levels of ER stress-related markers. A) WT and *Ugt1*$^{-/-}$ mice mRNA cerebellar expression levels of *ATF3, CHOP* and *CD95/Fas* were analysed at the indicated time points. **B)** WT and *Ugt1*$^{-/-}$ mice mRNA cerebellar expression levels of *GRP78, GRP94, P58*^{IPK}, *FKBP11, ATF4, DR5* and *HMGB1* were analysed at the indicated time points. Values represent the mean ± s.d. Student *t*-test, **p*< 0.05, ***p*<0.01, ****p*<0.001. The number of WT and *Ugt1*$^{-/-}$ was ≥ 3 in all the experiments and time points.

Since a prominent ER stress response was observed, I next focused my attention on oxidative stress, which is considered a major process affected by bilirubin. Real time RT-PCR showed the early expression (P5) of an important transcription factor involved in cellular response to oxidative stress, *nuclear factor (erythroid-derived 2)-like 2* (*Nrf2*) (Figure 37A). After peaking at P5, *Nrf2* mRNA levels at P8 and P10 in *Ugt1*$^{-/-}$ animals were similar to those of WT mice. Interestingly, the *Ugt1*$^{-/-}$ cerebellar mRNA expression of *heme oxygenase 1* (*HO1*), a key enzyme in heme catabolism, increased in a time-dependent manner, starting from P8 up to ~10 times more than WT levels at P10 (Figure 37A). However, differences in other markers of oxidative stress were not detectable (Figure 37B).

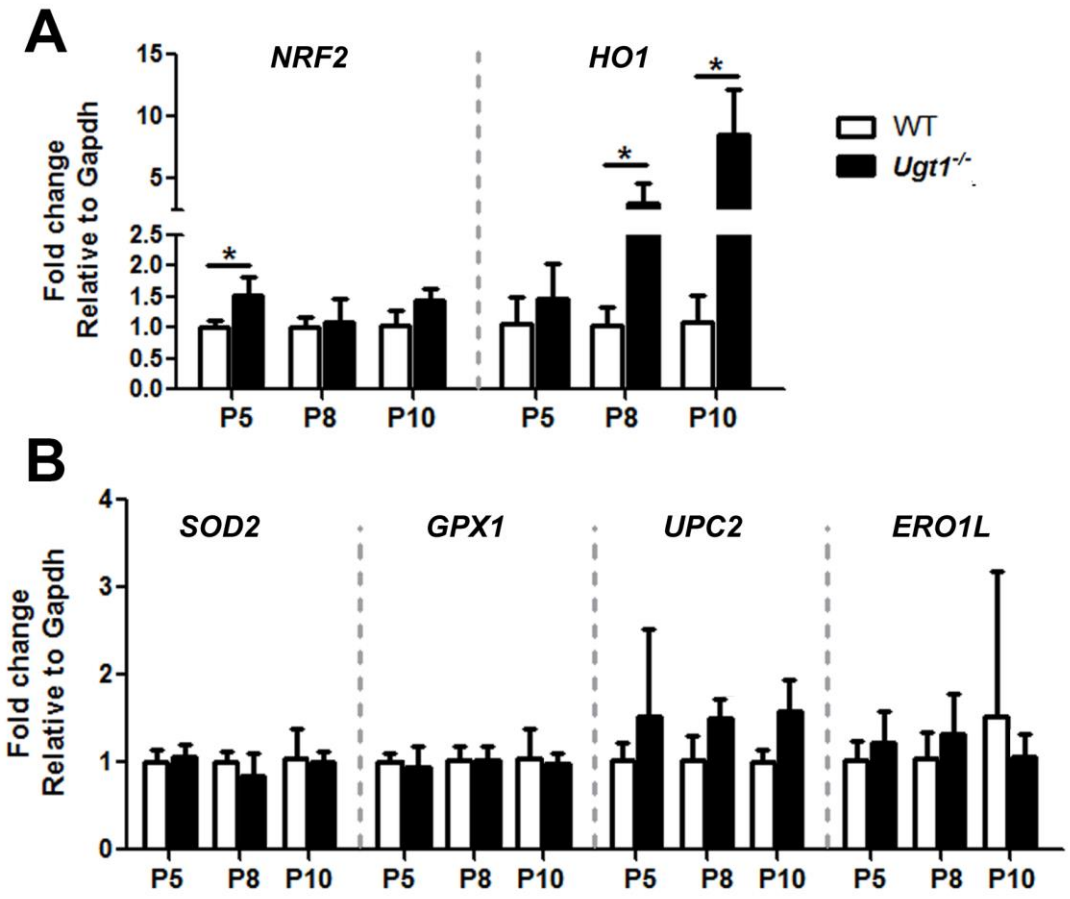

Figure 37. Time-course of mRNA expression levels of oxidative stress-related markers. A) WT and *Ugt1*$^{-/-}$ mice mRNA cerebellar expression levels of *Nrf2* and *HO1* were analysed at the indicated time points. **B)** WT and *Ugt1*$^{-/-}$ mice mRNA cerebellar expression levels of *SOD2, GPX1, UPC2* and *ERO1L* were analysed at the indicated time points. Values represent the mean ± s.d. Student *t*-test, **p*< 0.05. The number of WT and *Ugt1*$^{-/-}$ was ≥ 3 in all the experiments and time points.

3.2.7 Autophagy is a late event triggered by bilirubin

Finally, by anti-microtubule-associated protein 1A/1B-light chain 3 (LC3) antibody WB analysis was performed to determine whether autophagy is triggered in vivo by hyperbilirubinemia. Levels of LC3-II form, as a marker of activated autophagy, were quantified and normalized to LC3-I, the unconjugated form (Klionsky et al., 2009). WB analysis performed in cerebellar total extracts showed no differences at P5 and P8, but there was a significant increase in the LC3-II/LC3-I ratio in *Ugt1*$^{-/-}$ animals at P10 (Figure 38), corresponding to most severe time point analysed.

These data showed, for the first time *in vivo*, that the autophagy is altered at least in our mouse model of severe neonatal hyperbilirubinemia. In fact, the increase of LC3-II was observed in mutant mice corresponded to an increase of the vesicles number. Further studies are needed to elucidate whether the number of vesicles correspond to an anti- or a pro-survival mechanism in the *Ugt1*$^{-/-}$ mouse model.

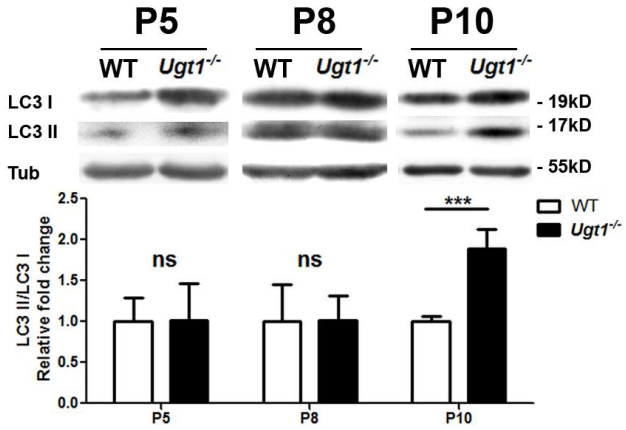

Figure 38. Autophagy is a late event in bilirubin toxicity. WB analysis of total cerebellum protein extracts using an anti-LC3 antibody at P5, P8 and P10 of WT and *Ugt1*$^{-/-}$ mice. β-tubulin was used as a loading control. Lower panel: densitometric quantification of the bands; results are expressed as the mean of the LC3 II/I ratio. Values represent the mean ± s.d. Student *t*-test, ****p*<0.001, ns not significant. P5: WT n=3; *Ugt1*$^{-/-}$ n=5; P8: WT n=4, *Ugt1*$^{-/-}$ n=4; P10: WT n=3; *Ugt1*$^{-/-}$ n=5.

Summarizing, the time-course analysis of hyperbilirubinemic mutants cerebella presented here indicated that bilirubin toxicity first triggers ER stress and oxidative stress activation. Prolonged high levels of bilirubin resulted in neurodegeneration. Over time, gliosis and inflammatory markers up-regulation took place as a consequence of neurodegeneration, particularly in those regions where the damage was more evident, leading to the generation of a glial scar. Autophagy was observed only in the phases prior to mice death. The FVB/NJ *Ugt1*$^{-/-}$ characterization over time may further help the clarification of bilirubin detrimental effects.

3.3 Mitigation of neuroinflammation by minocycline treatment ameliorates bilirubin neurotoxicity

To get a deeper insight in the bilirubin-mediated toxicity mechanisms and to estimate the contribution of inflammation to bilirubin neurotoxicity and death, *Ugt1*$^{-/-}$ and WT mice were treated with MNC, a second-generation tetracycline having anti-inflammatory and neuroprotective properties (Ryan and Ashley, 1998). MNC is particularly suitable for treating neurological diseases because it efficiently crosses the BBB (Macdonald et al., 1973). A previous study has shown the beneficial effects of MNC treatment in a non-lethal model of bilirubin neurotoxicity (Lin et al., 2005). Hence, the MNC potential in the prevention of the neurotoxic effects of bilirubin was tested in the lethal *Ugt1*$^{-/-}$ mouse model.

3.3.1 MNC treatment improves survival of the *Ugt1*$^{-/-}$ mice

To determine the effects of MNC administration on the survival of *Ugt1*$^{-/-}$ mice, MNC was administered in the drinking water of heterozygous lactating dams, which had been mated with heterozygous males to generate *Ugt1*$^{-/-}$ pups. Fresh MNC solutions (MNC 0.2X, MNC 1X, MNC 2X or MNC 4X; 0.842 mg of MNC/mL of drinking water=1X) were prepared daily and bottles were kept covered from light with aluminium foil. The MNC treatment started the day of birth and lasted till weaning (from P0 to P20, according to pups lifetime); plasma and brain samples were collected at P8 and at P15, and behavioural tests were performed on rescued animals as indicated in the timetable of the experimental plan (Figure 39A).

I observed that MNC administration increased the survival of treated mutant mice in a dose-dependent manner (Figure 39B). Compared to the untreated animals (Figure 39B, red line), the MNC 0.2X treatment (Figure 39B, light green line) did not produce any significant improvement in survival. Instead, the MNC 1X treatment shifted significantly the survival of mutant mice, as 50% of survival was observed at P16 (Figure 39B, green line). The increase of MNC concentration resulted in a consistent dose-dependent delay in the mortality, as observed in MNC 2X- and MNC 4X-treated *Ugt1*$^{-/-}$ mice, in which 50% of survival was observed at P21 and at P24, respectively (Figure 39B, dark green and very dark green lines). Importantly, the two highest MNC doses partially rescued the lethal phenotype. In fact about ~ 15%

and ~ 30% of treated *Ugt1*$^{-/-}$ mice survived over one month of age, when treated with the MNC 2X and MNC 4X, respectively (Figure 39B).

All the different MNC doses did not affect the survival of WT animals, resulting in 100% of survival, even at the highest MNC concentration (MNC 4X).

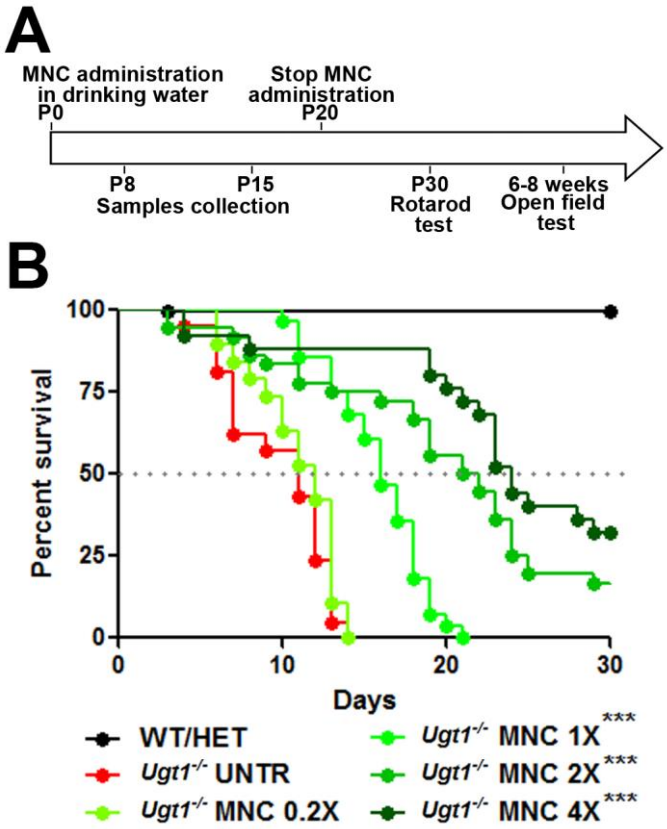

Figure 39. Experimental plan and survival of MNC-treated *Ugt1*$^{-/-}$. A) MNC was administered from P0 to P20. Rescued animals were tested with behavioural tests at P30 by rotarod test, and between the 6th and the 8th week of life by open field test. Samples were collected at P8 and P15. **B)** Kaplan-Meier survival curve of MNC treatment. The line colour/type indicates the different treatments (WT/heterozygous mice, black line; *Ugt1*$^{-/-}$ UNTR, red line; *Ugt1*$^{-/-}$ MNC 0.2X, light green line; *Ugt1*$^{-/-}$ MNC 1X, green line; *Ugt1*$^{-/-}$ MNC 2X, dark green line; *Ugt1*$^{-/-}$ MNC 4X, very dark green line). ****p*<0.0001, Log-rank (Mantel-Cox) test vs UNTR mutants. The number of animals per treatment is as follows: untreated WT (n=51) an *Ugt1*$^{-/-}$ (n=21); *Ugt1*$^{-/-}$ MNC 0.2X (n=19); *Ugt1*$^{-/-}$ MNC 1X (n=28); *Ugt1*$^{-/-}$ MNC 2X (n=36); *Ugt1*$^{-/-}$ MNC 4X (n=25). MNC 0.2X survival curve was performed by two other members of Mouse Molecular Genetics group: Elena Martinelli and Giulia Bortolussi.

3.3.2 Evaluation of MNC effect on mice health

Next, I analysed whether water consumption of dams could be affected by the presence of MNC in the drinking water. MNC daily intake (mL/day) was monitored for 2 weeks and compared to untreated controls receiving only water (Figure 40). no statistical difference in the amount of water consumption at any time and MNC dose analysed was reported. This observation is particularly important because a modification of liquid intake by the mothers could directly affect milk production. Consequently, a decreased intake by mother could impact on the amount of milk drunk by pups and their growth, in addition to undetermined changes in the MNC dose taken by the pups.

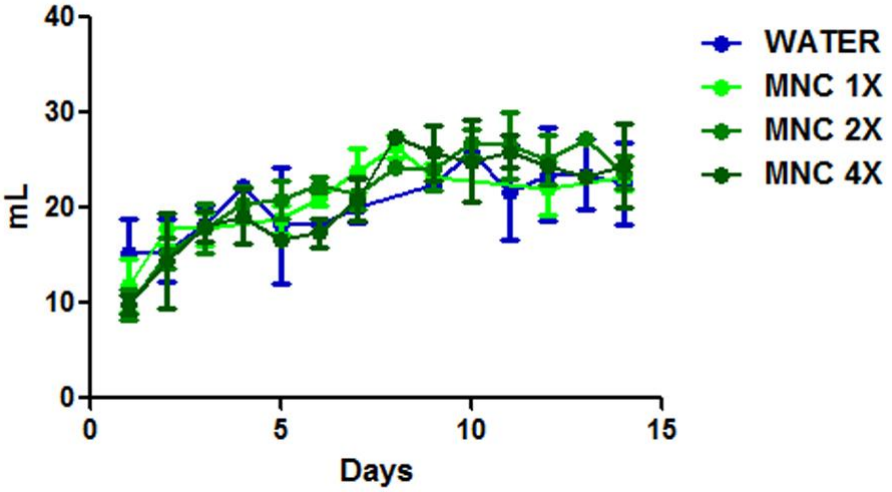

Figure 40. Effect of MNC on liquid consumption. MNC was dissolved in water and its daily consumption was compared to that of dams receiving only water. The colour indicates the different liquid consumptions (Water, blue line; MNC 1X, light green; MNC 2X, dark green; MNC 4X, very dark green). Values represent the mean ± s.d. (mL). Number of tested dams was ≥ 3 in all the conditions. Two-way ANOVA, Bonferroni's post test, not significant.

To verify if MNC affected the health status of the pups during their post-natal development, WT and *Ugt1*$^{-/-}$-treated pups were daily weighted (Figure 41). It was observed a dose/response effect of MNC on WT and *Ugt1*$^{-/-}$ littermates weight during the first 10 days of treatment, starting from P5 and P4 in WT and *Ugt1*$^{-/-}$ littermates, respectively (Figure 41A and 41B). However, their weight recovered after the discontinuation of the treatment reaching the levels of WT untreated controls (Figure 41C and 41D).

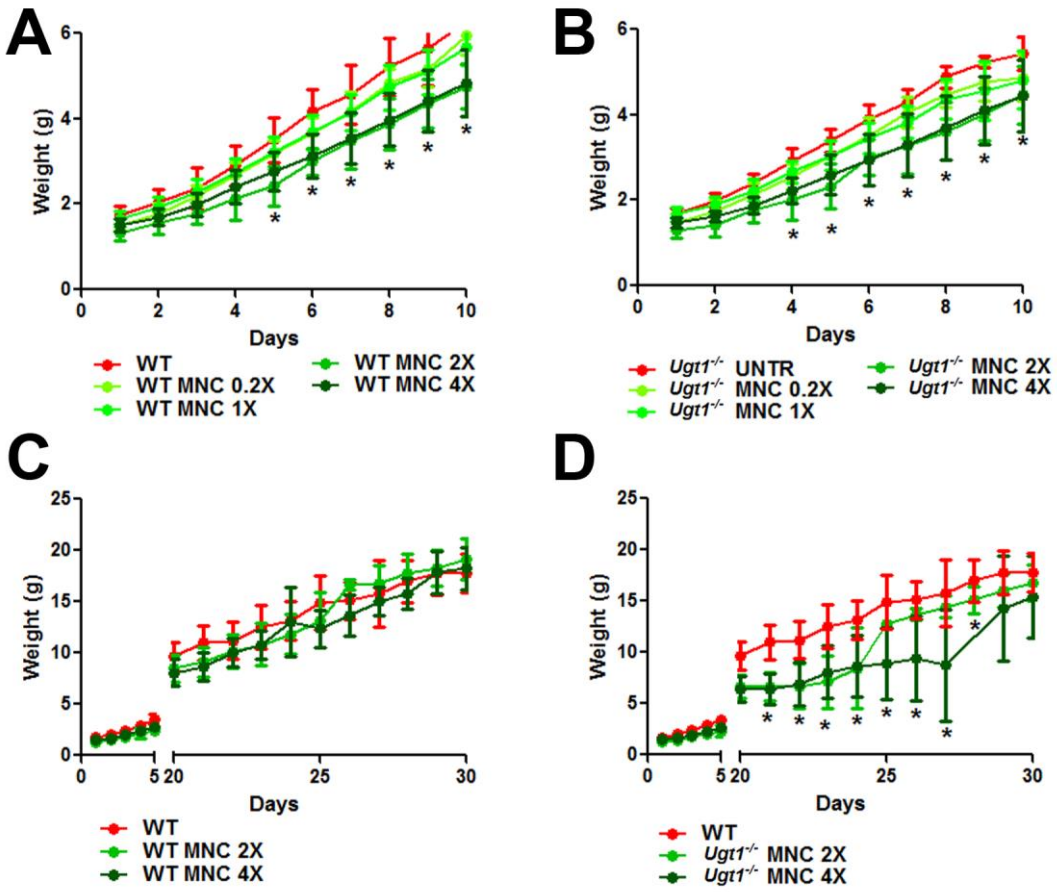

Figure 41. Effect of MNC on mice weight along the first month of life. A-B) Time-course of mice weight from P0 to P10, in WT and *Ugt1*$^{-/-}$. Untreated WT, WT MNC 0.2X, WT MNC 1X, WT MNC 2X and WT MNC 4X. Two-way ANOVA, *$p \leq 0.05$ for the highest treatments compared to untreated WT. **C-D)** Time-course of mice weight from P20 to P30, (after MNC discontinuation at P20) in WT and *Ugt1*$^{-/-}$. Untreated WT (n=51), *Ugt1*$^{-/-}$ (n=21); MNC 0.2X-treated WT (n=119), *Ugt1*$^{-/-}$ (n=19); MNC 1X-treated WT-H (n=83), *Ugt1*$^{-/-}$ (n=28); MNC 2X-treated WT-H (n=116), *Ugt1*$^{-/-}$ (n=36); MNC 4X-treated WT-H (n=54), *Ugt1*$^{-/-}$ (n=25). Values represent the mean ± s.d. (g). Two-way ANOVA, Bonferroni's post test, *$p \leq 0.05$ for the highest treatments compared to untreated WT A), C) and D), compared to untreated *Ugt1*$^{-/-}$ for B).

3.3.3 MNC administration does not affect bilirubin and albumin plasma values

As previously reported, untreated *Ugt1*$^{-/-}$ mice showed elevated levels of plasma TB (Bortolussi et al., 2014). Since MNC-treated mutant mice survived longer than untreated ones, it was verified whether the increased survival of MNC-treated *Ugt1*$^{-/-}$ mice could be the result of a systemic decrease of bilirubin levels. Plasma TB levels of MNC-treated *Ugt1*$^{-/-}$ mice at P8 were equivalent to those of the untreated mutants, and no differences were observed between the distinct MNC treatments at P15 (Figure 42A). Likewise, plasma albumin levels of treated animals were also

similar to untreated WT mice, confirming that MNC treatment did not affect plasma albumin levels, both at P8 and P15 (Figure 42B). These findings demonstrated that the efficacy of MNC did not stand in decreasing plasma bilirubin levels.

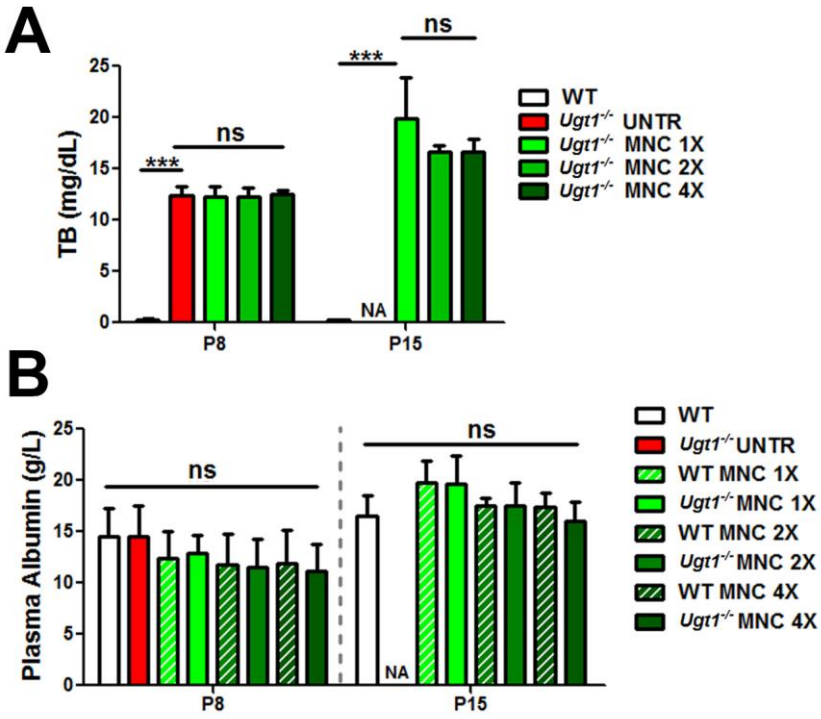

Figure 42. Plasma bilirubin and albumin levels in MNC-trated mice. A) Plasma TB of WT and *Ugt1*$^{-/-}$ mice were analysed at P8 and 15. **B)** Plasma albumin measurement (g/L) at P8 and P15 in MNC-treated animals. One-way ANOVA test, ***p<0.001, ns not significant; NA not available. For all the experiments values represent mean ± s.d. (mg/dL). The number of animals was ≥ 4 in all the experiments, conditions and time points.

3.3.4 Motor-coordination and activity parameters of MNC rescued *Ugt1*$^{-/-}$ mice are comparable to WT mice, but anxiety features are only partially rescued

Since bilirubin neurotoxicity affects cerebellar development and architecture, it was determined the degree of the functional rescue in *Ugt1*$^{-/-}$ mice treated with MNC. For this purpose, I performed specific behavioural tests designed to assess locomotor activity, motor coordination and balance, all functions in which the cerebellum has a key role. Mice were treated as described in Figure 39A, and their performance were tested in rotarod test (to assess motor coordination and balance, Figure 43) and open field (OF) test (to assess spontaneous activity, such as general locomotor activity levels and anxiety, Figure 44).

At one month of age, rescued *Ugt1*$^{-/-}$-MNC mice performed as well as untreated WT on the rotating rod (Figure 43) indicating no obvious motor-coordination impairment.

In addition, MNC treatment did not affect WT-MNC mice performance, which was similar to that of untreated WT mice.

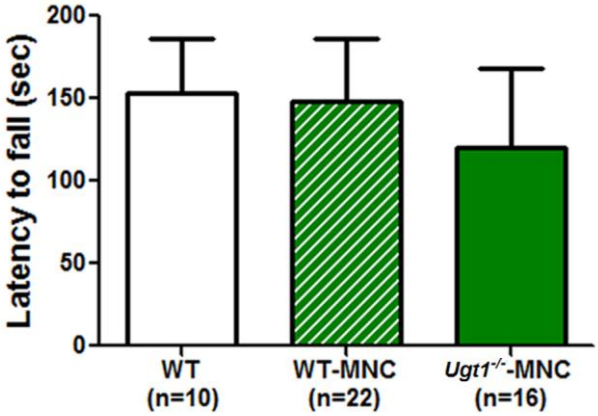

Figure 43. Performance of MNC-treated mice on the rotating rotarod. At P30, Untreated WT, MNC-treated WT and rescued *Ugt1*$^{-/-}$ mice were analysed by rotarod test. Values represent the mean ± s.d. (s). One-way ANOVA test, ns, not significative. WT (n=10), WT-MNC (n=22) and *Ugt1*$^{-/-}$-MNC (n=16).

Then, the spontaneous activity of 6-8 weeks old animals was determined with the OF test. Two types of parameters were analysed:

- *activity parameters*: covered distance (m), number of entries in the different zones of the arena (peripheral, medial and central zone), and time spent in the different zones (%);
- *anxiety parameters*: self-grooming (hygiene and caring for the body surface), rearing (standing on the rear limbs) and number of stool (as a measure of stress).

Importantly, no differences in *activity parameters* among the three groups were observed (WT, WT-MNC and *Ugt1*$^{-/-}$-MNC). Indeed, untreated WT and MNC-treated animals showed similar total travelled distance and number of entries in the different zones of the arena (Figures 44A and 44B, respectively). However, it was observed a minor although significant decrease in the time spent in the peripheral zone by the MNC-treated *Ugt1*$^{-/-}$ mice (Figure 44C).

Then, the *anxiety parameters* were measured in the three groups. The number of grooming events was comparable among the three groups (Figure 44D). Conversely, significant differences were observed in the number of rearing events and in the number of mice droppings in the group of MNC-treated *Ugt1*$^{-/-}$ mice

(Figure 44E and 44F, respectively). Importantly, no differences between untreated and MNC-treated WT indicated that MNC treatment did not affect any of the tested behavioural parameters of non-hyperbilirubinemic mice. On the other hand, anxiety parameters were influenced and compromised by bilirubin neurotoxicity in MNC-treated *Ugt1*$^{-/-}$ mice, confirming the partial rescue potential of MNC.

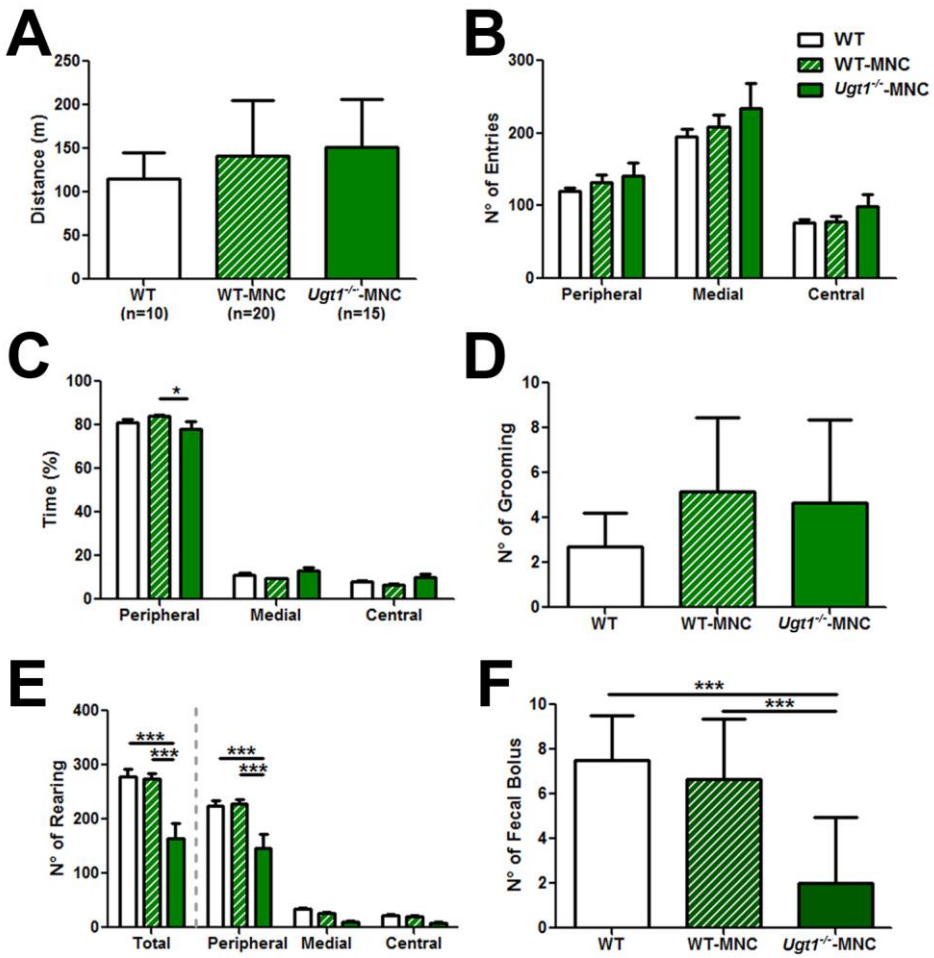

Figure 44. Spontaneus activity of MNC-treated animals in the Open Field test. 6-8 weeks old untreated WT, MNC-treated WT and rescued *Ugt1*$^{-/-}$ mice were analysed by open field test. *Activity parameters*: **A)** total travelled distance (m), **B)** number of entries in the different zones and **C)** time spent in the different zones (%); *anxiety parameters*: **D)** number of rearing, **E)** number of grooming and **F)** number of droppings. For all the experiments values represent the mean ± s.d. One-way ANOVA, **p*<0.05, ****p*<0.001. WT (n=10), WT-MNC (n=20) and *Ugt1*$^{-/-}$-MNC (n=15).

3.3.5 Minocycline reduces apoptosis and protects cerebellar neurons

In light of the results shown in the previous chapter concerning untreated *Ugt1*$^{-/-}$ animals (3.2 Molecular basis of neurotoxicity in neonatal hyperbilirubinemia), it was analysed the neuroprotective effects of MNC on cerebellar neurons at P8 and P15.

Untreated samples at P8 were compared with animals treated with MNC 4X, the dose showing the maximum rescuing capacity. However, since untreated *Ugt1*$^{-/-}$ animals did not survive over P14 (Figure 39B, red line), to evaluate the effects of MNC administration over prolonged bilirubin exposure, such as at P15, I selected as a control group an experimental condition that allowed the animals to survive longer, such as MNC 1X, showing no variation in bilirubin levels over time and treatment.

First, I focused my attention on neurodegeneration and apoptosis by determining the cleaved /total caspase 3 ratio in the cerebellum of treated and untreated mice at the indicated time points. It was observed a trend of apoptosis reduction in cerebellar extracts of MNC 4X-treated *Ugt1*$^{-/-}$ mice compared to untreated *Ugt1*$^{-/-}$ controls at P8 (Figures 45A), although this difference was not statistically significant. At P15, the high levels of apoptosis present in the cerebella of *Ugt1*$^{-/-}$ mice treated with the lowest dose (MNC 1X, 2-fold increase compared to WT) were reduced to WT levels in the *Ugt1*$^{-/-}$ mice treated with the highest one (MNC 4X, Figure 45B).

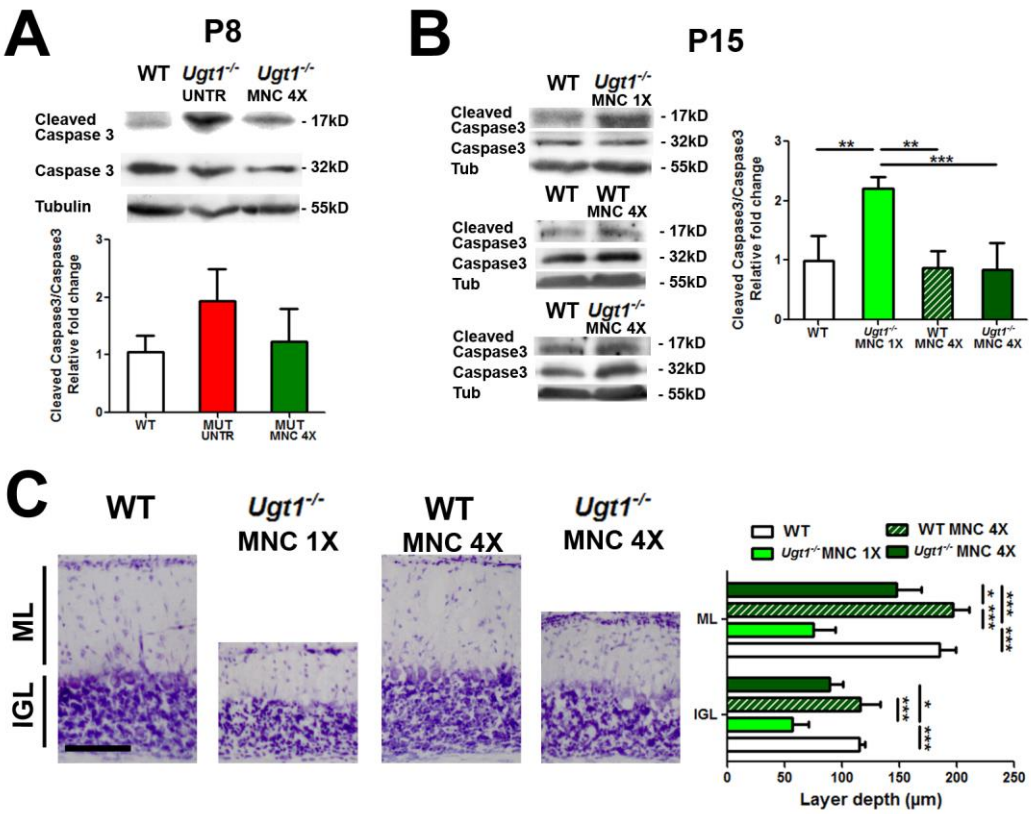

Figure 45. Effect of MNC on apoptosis and cerebellar morphology. WB analysis using an anti-cleaved and –total caspase 3 antibody on total cerebellum protein extract **A)** at P8 and **B)** at P15 of untreated and treated mice. The bar graphs show the mean of cleaved/total caspase 3 ratio of the bands. β-tubulin was used as loading control. **C)** Left panel, Nissl staining of cerebellar layers at P15 of WT, *Ugt1*$^{-/-}$ MNC 1X, WT MNC 4X and *Ugt1*$^{-/-}$ MNC 4X. Scale bar 100 µm. Right panel, layer depth quantification (µm). For all the experiments values represent mean ± s.d. One-way ANOVA, *p< 0.05, **p<0.01, ***p<0.001. The number of animals was ≥ 3 in all the experiments and conditions.

Histological evaluation of cerebellar architecture at P15 showed that the MNC 1X dose was not sufficient to rescue the defects in cerebellar morphology. In fact, MNC 1X-treated *Ugt1*$^{-/-}$ mice carried a significant decrease in ML- and IGL-thickness (60% and 50% of reduction, respectively, compared to WT), resulting in a total cerebellar layer reduction of 57% compared to WT, as determined by Nissl staining (Figure 45C). In contrast, MNC 4X-treated *Ugt1*$^{-/-}$ mice showed a significant increase in the ML- and IGL-thicknesses compared to MNC 1X-treated *Ugt1*$^{-/-}$ mice (respectively 50% and 40% of reduction in *Ugt1*$^{-/-}$ treated with MNC 1X vs MNC 4X), indicating a dose dependent positive effect of MNC on cerebellar neurons. Despite the important protective effect observed in MNC 4X-treated *Ugt1*$^{-/-}$ mice, layer thickness in those animals was still significantly different from WT animals (25%

whole cerebellar layer reduction). In addition, MNC 4X-treated WT mice did not differ in the cerebellar architecture compared to untreated WT mice.

Importantly, PCs analyses revealed a dose-dependent effect of MNC on cell survival and dendritic arborization, well correlating with apoptosis inhibition observed by WB analysis. MNC administration resulted in similar calbindin content in MNC 4X-treated compared to untreated *Ugt1*$^{-/-}$ animals at P8 (Figure 46A), suggesting the absence of a positive effect of the drug on PCs. However, analysis performed at P15 showed 75% decrease in calbindin content in the cerebellum of MNC 1X-treated *Ugt1*$^{-/-}$ mice, but only 50% of calbindin reduction was observed in MNC 4X-treated *Ugt1*$^{-/-}$ animals (Figure 46B). Moreover, the IF analysis of cerebellar sections using anti-calbindin antibody showed that PCs number was decreased only in the MNC 1X- but not in MNC 4X-treated *Ugt1*$^{-/-}$ mice, which showed the same PCs density of WT animals (Figure 46C). The analysis of PCs morphology indicated that the decrease in calbindin content observed in MNC 4X-treated *Ugt1*$^{-/-}$ mice was due to reduction in dendritic arborisation, well correlating with the reduction in calbindin levels determined by WB analysis in both P8 and P15 cerebellar extracts.

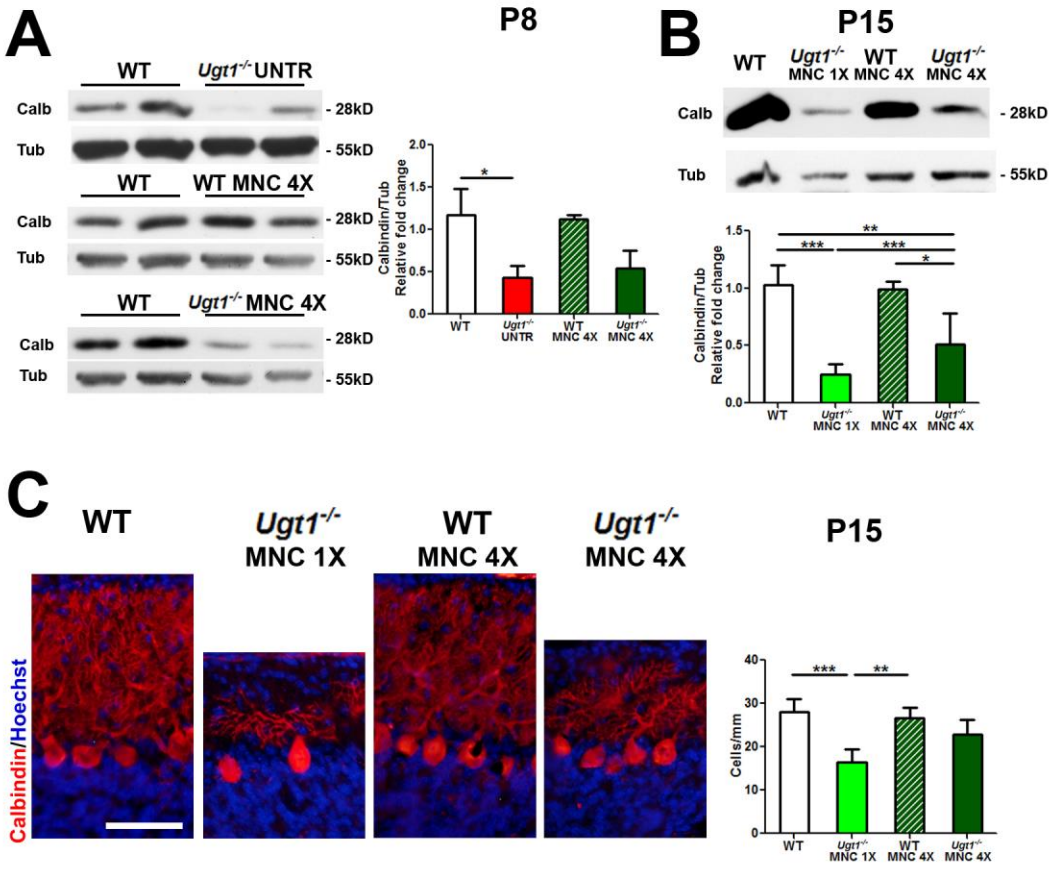

Figure 46. Effect of MNC on PCs. WB analysis using an anti-calbindin antibody on total cerebellum protein extract **A)** at P8 and **B)** at P15 of untreated and treated mice. β-tubulin was used as loading control. **C)** Left panel, representative fluorescent immunohistochemistry of cerebellar sections from WT, *Ugt1*$^{-/-}$ MNC 1X, WT MNC 4X and *Ugt1*$^{-/-}$ MNC 4X at P15, using an anti-calbindin antibody (red) to highlight PCs. Hoechst (blue) was used to mark nuclei. Scale bar: 50 µm. Right panel, the quantification of PCs number is represented in the bar graph (cell/mm). For all the experiments values represent mean ± s.d. One-way ANOVA, **p*< 0.05, ***p*<0.01, ****p*<0.001. The number of animals was ≥ 3 in all the experiments and conditions.

To analyse the bilirubin effect on other neuronal types in response to MNC administration, anti-NeuN antibody was used to elucidate the GCs outcome (Figure 47). As determined by WB, at P8 it was observed no differences in NeuN content both in MNC-treated and untreated *Ugt1*$^{-/-}$ mice (Figure 47A). Instead, a significant reduction of NeuN content was observed at P15 (Figure 47B), and further confirmed by IF (Figure 47C), but MNC 4X-treated *Ugt1*$^{-/-}$ mice showed cerebellar NeuN levels similar to WT mice.

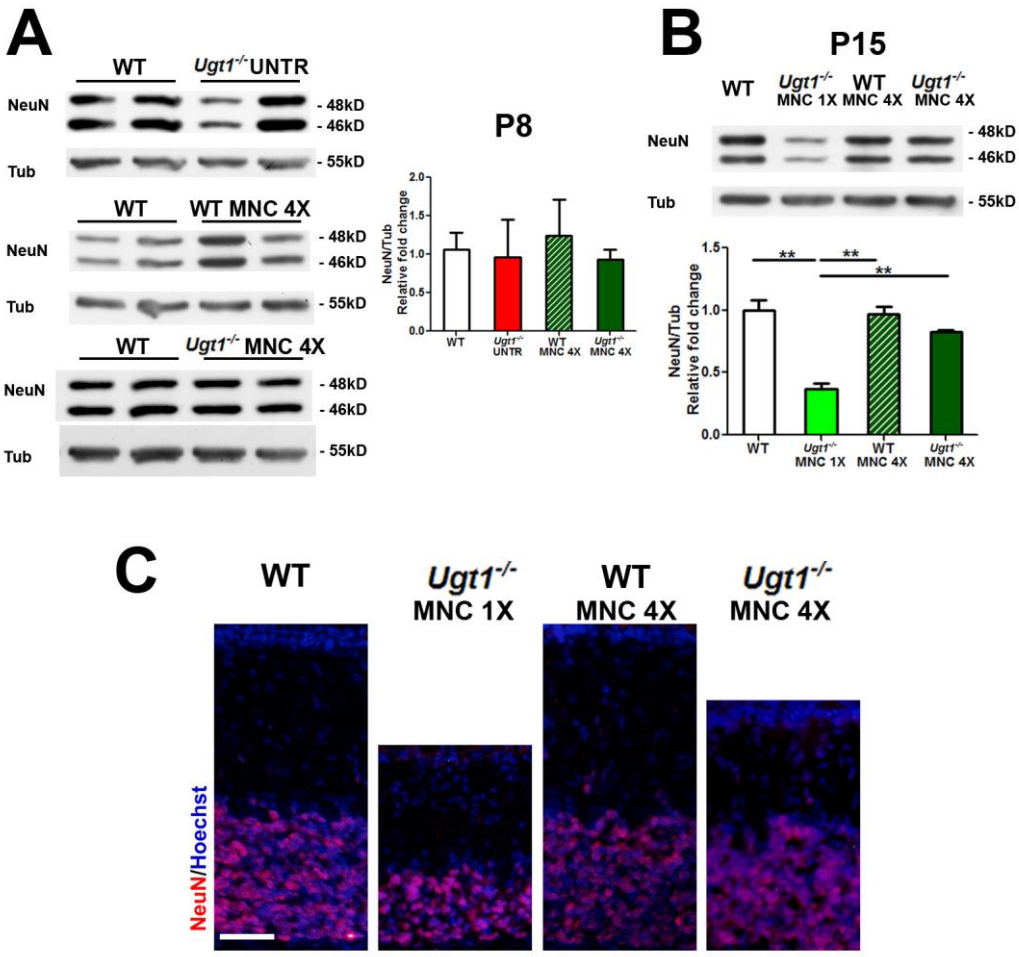

Figure 47. Effect of MNC on GCs. WB analysis using an anti-NeuN antibody on total cerebellum protein extract **A)** at P8 and **B)** at P15 of untreated and treated mice. β-tubulin was used as loading control. **C)** Representative fluorescent immunohistochemistry of cerebellar sections from WT, *Ugt1*$^{-/-}$ MNC 1X, WT MNC 4X and *Ugt1*$^{-/-}$ MNC 4X at P15, using an anti-NeuN antibody (green) to highlight GCs. Hoechst (blue) was used to mark nuclei. Scale bar: 50 µm. For all the experiments values represent mean ± s.d. One-way ANOVA, $^{**}p<0.01$. The number of animals was ≥ 3 in all the experiments and conditions. The IF analysis was performed by Giulia Bortolussi, a member of the Mouse Molecular Genetics group.

Taken together, this set of experiments demonstrated the dose-dependent effect of MNC in protecting cerebellar neurons from bilirubin-induced neurodegeneration.

3.3.6 MNC attenuates neuro-inflammation in the cerebellum of mutant mice

Since the anti-inflammatory properties of MNC are well-known, it was examined whether MNC treatment could affect astrocytes and glia activation also in the hyperbilirubinemic context.

First, I focused my attention on astrocytes. As determined by WB analysis, at P8 I observed increased cerebellar GFAP content in MNC 4X-treated *Ugt1*$^{-/-}$ mice, although this difference was not statistically significant compared to untreated WT mice (Figure 48A). Importantly, WB analyses performed at P15 revealed a marked astrocytosis in MNC 1X-treated *Ugt1*$^{-/-}$ mice, while GFAP levels were reduced down to WT levels in *Ugt1*$^{-/-}$ mice treated with the highest MNC dose (Figure 48B). The IF analysis confirmed the absence of astrocyte activation (Figure 48C), previously observed by WB analysis at P15 in MNC 4X-treated *Ugt1*$^{-/-}$ mice, confirming the potent anti-inflammatory properties of MNC.

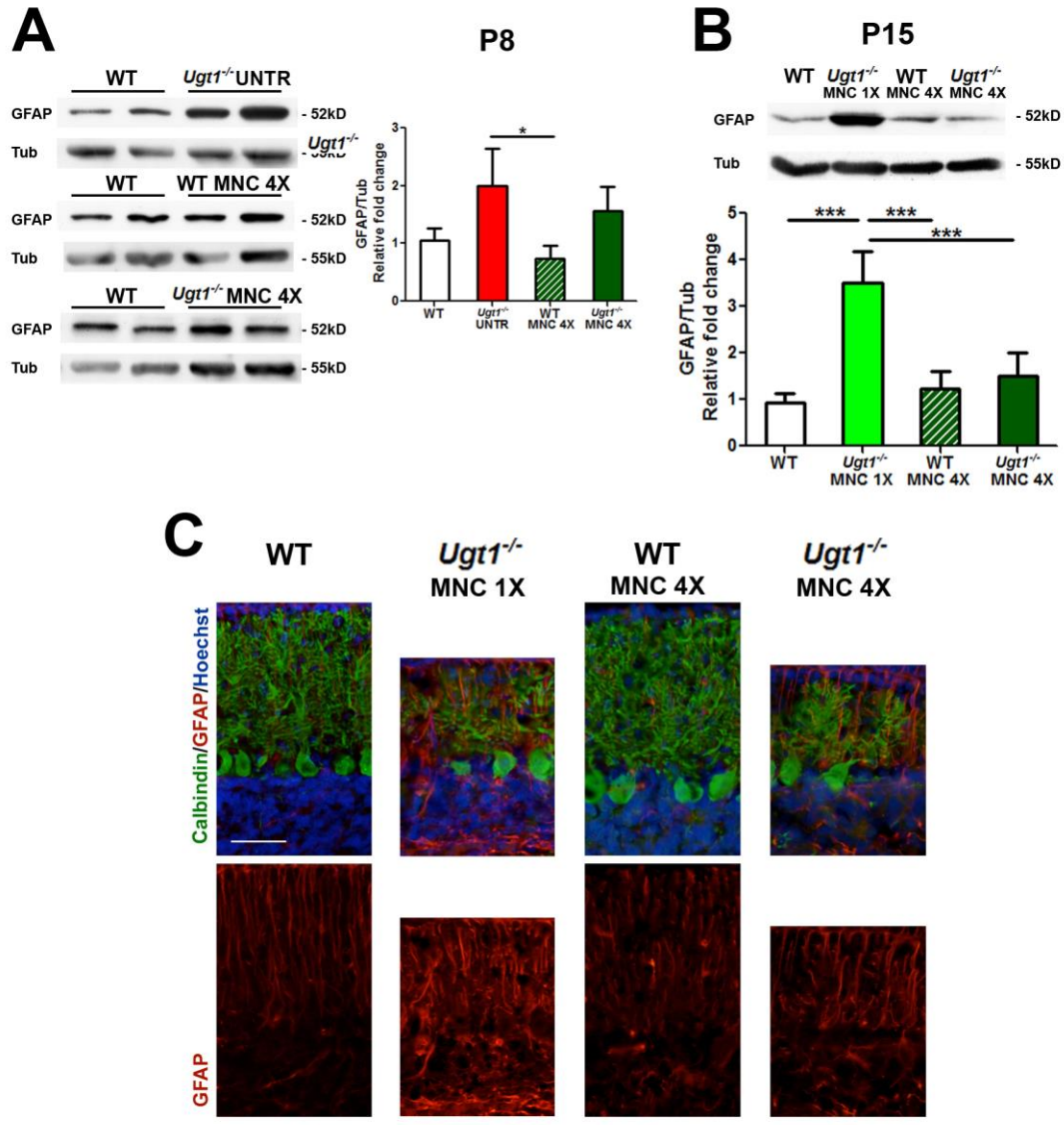

Figure 48. Effect of MNC on astrocytes. WB analysis using an anti-GFAP antibody on total cerebellum protein extract **A)** at P8 and **B)** at P15 of untreated and treated mice. β-tubulin was used as loading control. **C)** Representative fluorescent immunohistochemistry of cerebellar sections at P15 from WT, *Ugt1*$^{-/-}$ MNC 1X, WT MNC 4X and *Ugt1*$^{-/-}$ MNC 4X using anti-GFAP antibody (red) to detect astrocytes, co-stained with an anti-calbindin antibody (green) to highlight PCs. Hoechst (blue) was used to mark nuclei. Scale bar: 50 µm. For all the experiments values represent mean ± s.d. One-way ANOVA, **p*< 0.05, ****p*<0.001. The number of animals was ≥ 3 in all the experiments and conditions. The IF analysis was performed by Giulia Bortolussi, a member of the Mouse Molecular Genetics group.

The dose-dependent anti-inflammatory action of MNC was further corroborated by the study of microglia. Real-time RT-PCR experiments performed at P8 revealed no effects of MNC on *Iba1* mRNA levels, which were highly expressed in both MNC-treated and untreated *Ugt1*$^{-/-}$ mice (Figure 49A), indicating the absence of MNC effects on treated *Ugt1*$^{-/-}$ animals at the earlier selected time point. However, at a later time point (P15), the MNC treatment resulted in a dose-dependent reduction

of microglia activation, as assessed by WB of Iba1 cerebellar content (Figure 49B). These results were confirmed by IF analysis using anti-Iba1 antibody performed at the same time point (Figures 49C). In fact, the IF analysis showed an increase in Iba1-positive cells in MNC 1X-treated *Ugt1*$^{-/-}$ mice, while their number was reduced to WT levels in MNC 4X-treated *Ugt1*$^{-/-}$ mice.

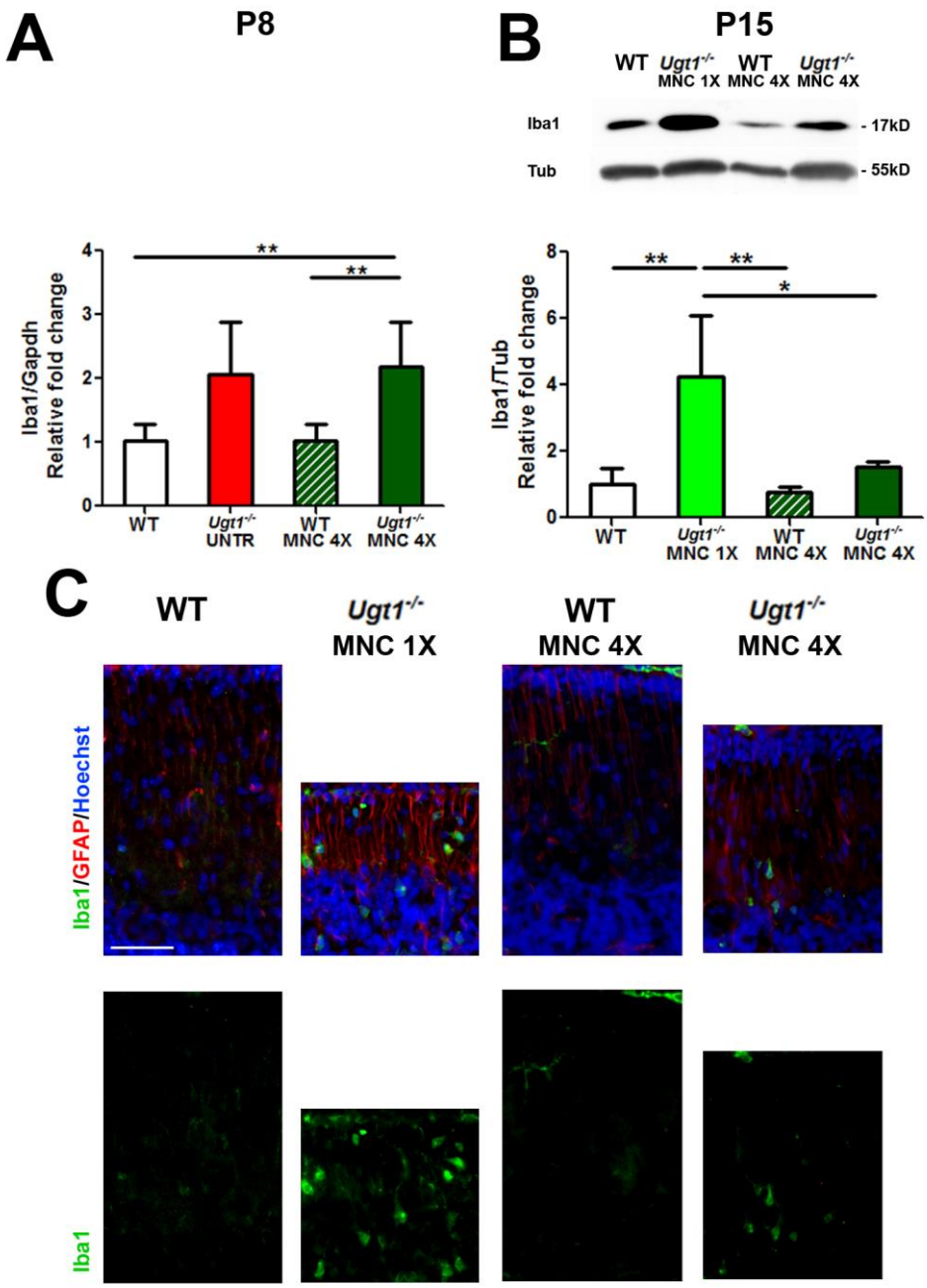

Figure 49. Effect of MNC on microglia cells. A) Real-time PCR analysis of *Iba1* expression levels at P8 and **B)** WB analysis using an anti-Iba1 antibody at P15 on total cerebellum protein extract of untreated and treated mice. β-tubulin was used as loading control. **C)** Representative IF of cerebellar sections at P15 from WT, *Ugt1*$^{-/-}$ MNC 1X, WT MNC 4X and *Ugt1*$^{-/-}$ MNC 4X using anti-Iba1 antibody (green) to detect microglia-positive cells, co-stained with an anti-GFAP antibody (red) to highlight astrocytes. Hoechst (blue) was used to mark nuclei. Scale bar: 50 µm. For all the experiments values represent mean ± s.d. One-way ANOVA, **p*< 0.05, ***p*<0.01. The number of animals was ≥ 3 in all the experiments and conditions. The IF analysis was performed by Giulia Bortolussi, a member of the Mouse Molecular Genetics group.

3.3.7 MNC attenuates M1 but not M2 microglia activation

To better determine the microglia/macrophage activation states and to characterize more in detail glia activation, some of the key markers of M1 and M2 microglia were analysed by real-time RT-PCR experiments on cerebellar total RNA preparations at P15 (Figure 50). Interestingly, MNC decreased M1 microglia (neuro-inflammatory) activation in a dose-dependent manner, as determined by *CD68* and *CD86* mRNA expression levels.

In contrast, the *MRC1* and *MRC2* markers of M2 microglia (neuro-protective) were activated in response to bilirubin and only the levels of *MRC1* partially decreased after MNC-4X administration.

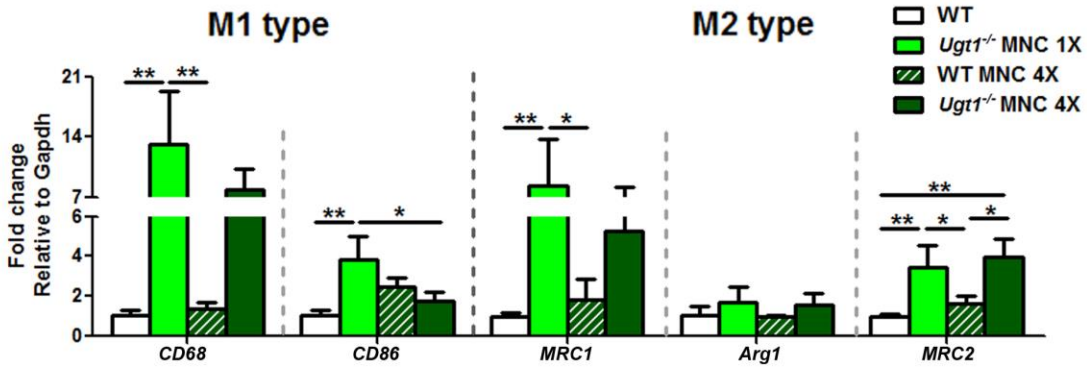

Figure 50. MNC effect on M1 and M2 microglia markers. WT, *Ugt1*$^{-/-}$ MNC 1X, WT MNC 4X and *Ugt1*$^{-/-}$ MNC 4X mRNA cerebellar expression levels of *CD68, CD86, MRC1, Arg1* and *MRC2* were analysed at P15. Values represent the mean ± s.d. One-way ANOVA, **p*< 0.05, ***p*<0.01. The number of animals was ≥ 3 in all the experiments.

3.3.8 MNC attenuates inflammatory mediators

Next, it was investigated the anti-inflammatory effects of MNC on different markers involved in the neuro-inflammation pathway at P15.

Interestingly, *IL18* expression levels were not affected by MNC administration even at the highest dose tested (Figure 51A). In contrast, the highest dose of MNC decreased the expression levels of all the other inflammatory mediators analysed in treated *Ugt1*$^{-/-}$ mice. In particular, the expression levels of *NFKβ* were reduced to WT baseline, while those of *TNFα* were drastically reduced, although without reaching WT values. Real-time RT-PCR analysis of *MMP2* and *MMP9* also showed a dose-dependent down-regulation of their mRNA levels in MNC 4X-treated mutant mice (Figure 51A), well correlating with the decrease in microglia cells observed by

IF analysis (Figure 49). Importantly, *TLR2* expression was increased about 20 times the WT levels at P15 in MNC 1X-treated *Ugt1*$^{-/-}$ animals, but the MNC 4X treatment resulted in a 65% decrease in MNC 4X-treated *Ugt1*$^{-/-}$ mice (Figure 51B). No differences in the expression levels of *iNOS*, *nNOS* were observed at any dose analysed (Figure 51B).

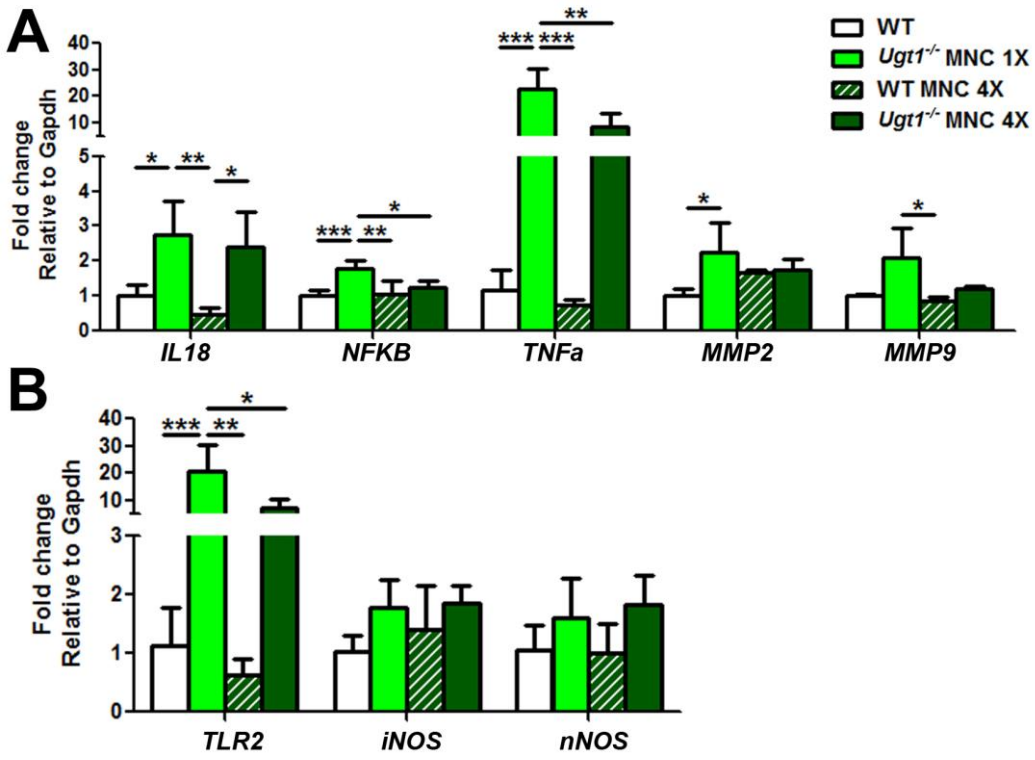

Figure 51. Effect of MNC on inflammatory markers. WT, *Ugt1*$^{-/-}$ MNC 1X, WT MNC 4X and *Ugt1*$^{-/-}$ MNC 4X mRNA cerebellar expression levels of **A)** *IL18, NFKβ, TNFα, MMP2,* and *MMP9*; **B)** *TLR2, iNOS* and *nNOS* were analysed at P15. Values represent the mean ± s.d. One-way ANOVA, **p*< 0.05, ***p*<0.01, ****p*<0.001. The number of animals was ≥ 3 in all the experiments.

These findings suggested that the activation of a prominent inflammatory response occurred in presence of neuro-apoptosis and that inhibition of neuro-inflammation ameliorated the neurodegenerative phenotype induced by bilirubin.

3.3.9 MNC effect on ER and oxidative stress

Since it was previously observed the involvement of ER stress in bilirubin neurotoxicity (Chapter 3.2.6), the effect of MNC administration on ER stress response related genes at P15 was investigated. Bilirubin activated the ER stress

response at P15, as determined by real-time RT-PCR in the *Ugt1*$^{-/-}$ animals treated with the lower dose of MNC. MNC 4X treatment effectively abolished the activation of *ATF3*, *GRP78*, *CD95* and *P58*^{IPK} (Figure 52A). In contrast, *CHOP*, high mobility group box 1 (*HMGB1*), *GRP94*, death receptor 5 (*DR5*) and *FK506* binding protein 11 (*FKBP11*) were unaffected by the MNC treatment at any of the doses analysed (Figure 52B), pointing out that ER stress is present at later stages (P15) and that the MNC treatment was not sufficient to fully counteract ER triggered by bilirubin.

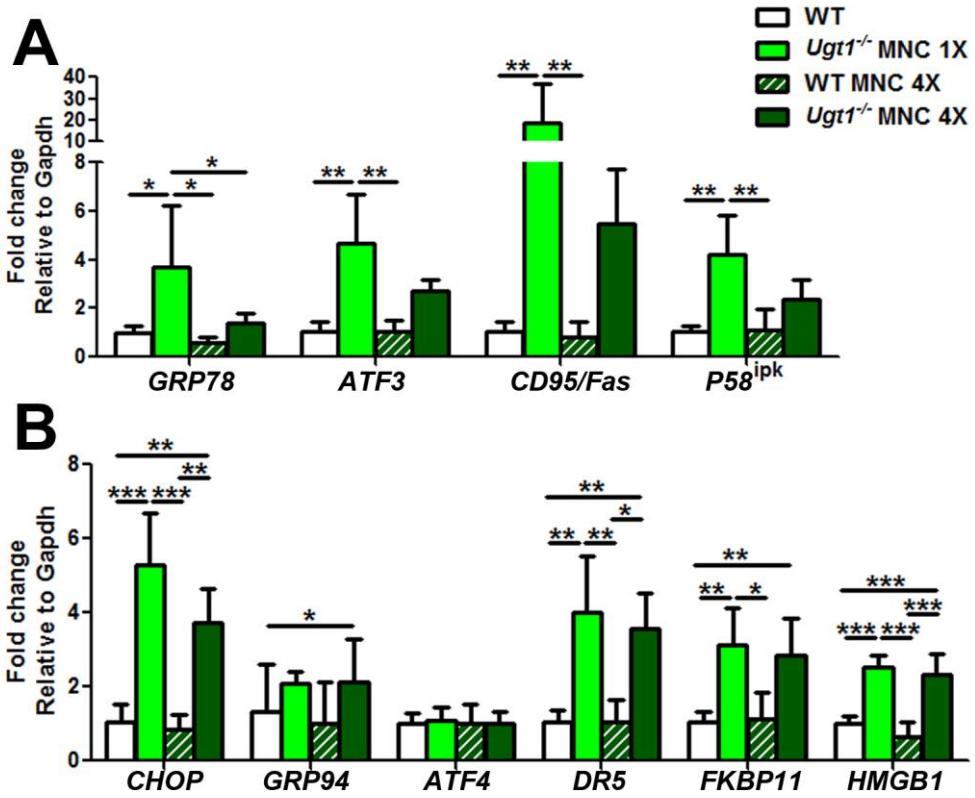

Figure 52. Effect of MNC on ER stress-related genes. WT, *Ugt1*$^{-/-}$ MNC 1X, WT MNC 4X and *Ugt1*$^{-/-}$ MNC 4X mRNA cerebellar expression levels of **A)** *ATF3, GRP78, CD95/Fas, P58*^{IPK}, **B)** *CHOP, GRP94, ATF4, DR5 FKBP11* and *HMGB1* were analysed at P15. Values represent the mean ± s.d. One-way ANOVA, **p*< 0.05, ***p*<0.01, ****p*<0.001. The number of animals was ≥ 3 in all the experiments.

Finally, due to the tight connection between ER stress and oxidative stress previously highlighted, it was evaluated the response of oxidative stress related genes to MNC treatment. Interestingly, at P15, *Nrf2* mRNA levels in MNC-treated *Ugt1*$^{-/-}$ animals were similar to those observed in WT cerebella, while HO1 expression was increased about 8 times in MNC 1X- treated *Ugt1*$^{-/-}$ mice. MNC 4X treatment of *Ugt1*$^{-/-}$ animals resulted in a 50% reduction of *HO-1* levels, without reaching WT levels (Figure 53A). Furthermore, *UPC2* and *ERO1L* mRNA

expression levels were increased in response to bilirubin in MNC 1X-treated mice, but were not diminished in MNC 4X-treated *Ugt1*$^{-/-}$ mice (Figure 53B). Finally, no differences in *GPX1* and *SOD2* expression were observed at any MNC dose tested (Figure 53B).

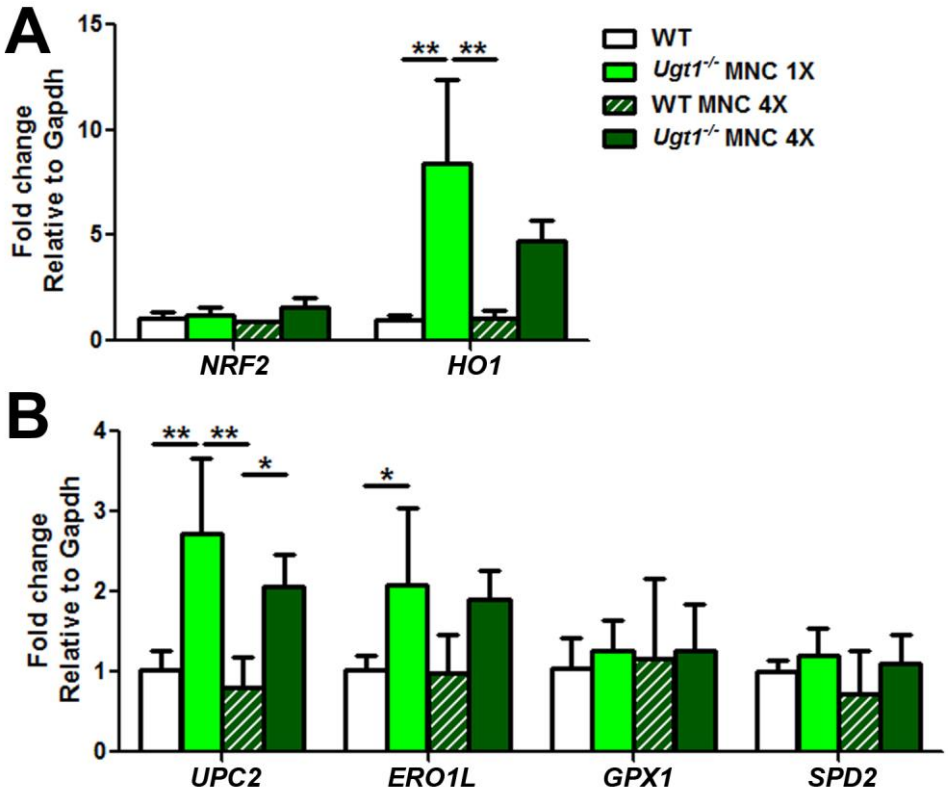

Figure 53. Effect of MNC on relative mRNA expression of oxidative stress-related genes. WT, *Ugt1*$^{-/-}$ MNC 1X, WT MNC 4X and *Ugt1*$^{-/-}$ MNC 4X mRNA cerebellar expression levels of **A)** *Nrf2* and *HO1*; **B)** *UPC2, ERO1L, GPX1* and *SOD2* were analysed at P15. Values represent the mean ± s.d. One-way ANOVA, **p*< 0.05, ***p*<0.01, ****p*<0.001. The number of animals was ≥ 3 in all the experiments.

In conclusion, these results confirmed the potent anti-inflammatory effect of MNC underscoring its potential use in attenuating bilirubin toxicity. In fact, MNC administration resulted in increased survival of the hyperbilirubinemic mice. This treatment reduced cell death and neurodegeneration, with the concomitant down-regulation of neuroinflammation. However, it seems clear that bilirubin affects several pathways at different cellular levels. Thus, the partial rescue achieved by MNC supports the concept that a drug with a wider effect, or the combination with others reducing ER stress, may further ameliorate the bilirubin-induced neurological damage.

In fact, since ER stress was only partially attenuated by MNC, I speculate about the relevance of ER stress contribution to neurons imbalance that results in cerebellar damage and death in a fraction of the MNC-treated *Ugt1*$^{-/-}$ animals.

DISCUSSION

4.1 Albumin supplementation studies demonstrate that Bf is the cause of bilirubin neurotoxicity

In this chapter, it was elucidated the role of Bf as the cause of BIND. The data presented in this study provide experimental support to the effectiveness of the HSA supplementation to prevent neonatal neurological damage and death, by increasing bilirubin-binding capacity in plasma.

4.1.1 Previous studies in Gunn rats

It has been previously demonstrated that HSA effectively decreases bilirubin toxicity in the brain of the hyperbilirubinemic Gunn rat model. However, the Gunn rat phenotype is not usually associated with kernicterus, mutant animals reach adulthood without any sign of toxicity and they are able to reproduce. Neurotoxic levels of bilirubin in the Gunn rat are usually induced by increasing haemolysis using phenylhydrazine (PHZ) or by displacing bilirubin from circulating albumin using sulphadimethoxine (Sulpha) (Rose and Wisniewski, 1959). Cuperus and colleagues showed that a single albumin injection combined with PT lowers the brain bilirubin and Bf levels of Gunn rats (Cuperus et al., 2013). In the acute hyperbilirubinemia condition induced by PHZ, HSA is effective only in combination with PT. Further evidences of HSA beneficial roles on hyperbilirubinemic Gunn rats were given by Schreuder and colleagues, demonstrating that a single albumin injection prevents BAEPs in the jj pups treated with PHZ or Sulpha (Schreuder et al., 2013b). In this study, animals are selected according to their TB levels, reducing the variability, and sacrificed 48h after a single HSA injection. Therefore, both the potential beneficial effects of HSA administration during neonatal development and a comprehensive long-term landscape of HSA potential were still missing.

4.1.2 Proof of principle in *Ugt1*$^{-/-}$ mouse model

Daily HSA treatment of *Ugt1*$^{-/-}$ mouse model resulted in a crucial step forward to understand the role of Bf in BIND. It was demonstrated that repeated albumin infusions during postnatal development were necessary and sufficient to rescue not

only neurological damage, but also lethality that characterizes hyperbilirubinemic *Ugt1*$^{-/-}$ animals used in this study.

Moreover, the importance of the experiments relied in the fact that no PT was applied to *Ugt1*$^{-/-}$ mice. The exclusive albumin supplementation increased plasma bilirubin-binding capacity, positively affecting *Ugt1*$^{-/-}$ mice outcome.

This study on albumin administration provides additional support to the concept that over-supplementation of bilirubin-binding sites results in the mobilization of bilirubin from tissues to plasma (Figure 54).

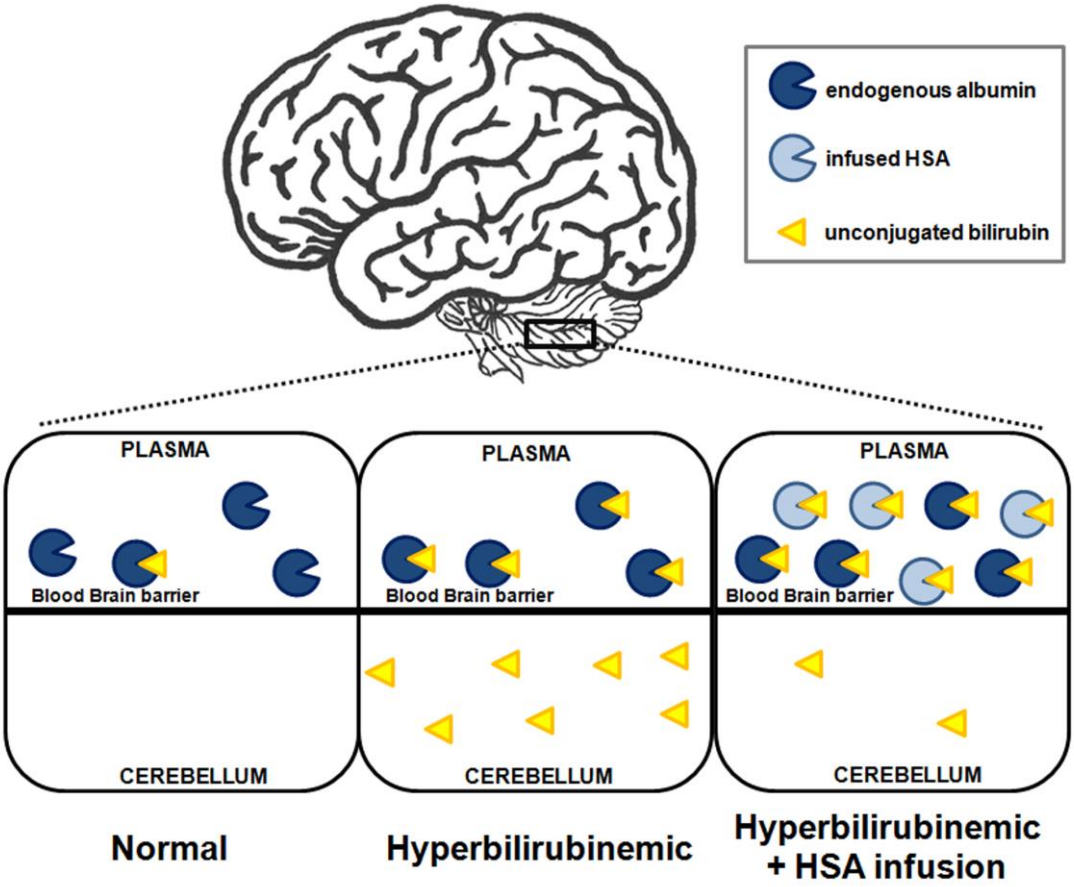

Figure 54. Model of the bilirubin-binding capacity in plasma in hyperbilirubinemic condition. In normal conditions, the bilirubin-binding capacity provided by albumin exceeds the amount of UCB (left). In severe hyperbilirubinemic conditions, UCB levels outnumber the albumin-binding capacity, and the excess of UCB (free bilirubin) solubilizes in lipid-rich tissues, such as the brain and cerebellum (center), resulting in neurotoxicity. When the bilirubin-binding capacity is artificially increased by HSA administration, bilirubin is mobilized from the tissues to the plasma compartment, leading to an increased UCB levels in plasma, and consequential safe levels of tissue UCB (right). The mobilization prevents the neurodamage, and results in the survival of treated *Ugt1*$^{-/-}$ mice.

The effectiveness of HSA administration in mobilizing bilirubin from tissues to plasma was also evident by the impressive increase in plasma TB in treated

animals. Despite this remarkable increase in TB, plasma Bf levels significantly dropped. Indeed, the therapeutic efficacy of albumin administration was consequent to the reduction in the Bf concentration by the increased bilirubin-binding capacity in plasma.

4.1.3 HSA long-term effectiveness

Most strikingly, HSA-treated animals survived without any adverse effect despite very high levels of plasma TB, consequent to the mobilization of UCB from tissues. In addition, I observed neither alterations in the growth curve of treated WT and *Ugt1*$^{-/-}$ littermates, even with the highest dose (HSA 7.5 g/kg/24h), nor significant transaminases activation (Figure 16).
Ten days after HSA treatment discontinuation (at P30), rescued *Ugt1*$^{-/-}$ mice showed no abnormalities in motor coordination skills, no cerebellum architecture impairment and normal albumin levels, although the extreme hyperbilirubinemia in the plasma compartment (Figure 22B). These findings underline the fact that brain susceptibility to bilirubin neurotoxicity is correlated to developmental stages, as previously suggested (Bortolussi et al., 2014).

4.1.4 Frequency of HSA administration is crucial

Importantly, it was shown that the frequency of administration was a very critical parameter to determine *Ugt1*$^{-/-}$ mice fate. In fact, daily supplementation of HSA 5.0 g/kg increased bilirubin-binding sites in plasma and reasonably lowered Bf levels, guaranteeing normal brain development and survival, according to the dose. In contrast, the same dose of albumin administered every 48 h was not sufficient to prevent the increase of Bf in the brain, resulting in severe neurological damage and death. It is important to note that the plasma levels of albumin significantly decreased during the second day after administration (in the HSA 5.0 g/kg/48h groups), resulting in a critical increase in tissue UCB (Figure 25). Likewise, these events probably represent the cause of the failure of this therapy.

4.1.5 Albumin half-life

Since monomeric albumin life-time in humans is reported in the range of 28-36 days (Fanali et al., 2012), the decrease of plasma albumin concentration two days after the previous administration remains unclear. Several works based on analbuminemic patients and adult Gunn rats have reported that, despite plasma albumin levels peaked immediately after infusion, albumin substantially decreases 24h after the treatment, (Cuperus et al., 2013; Greissman et al., 1996), while that of mice infused with mouse albumin is 35h (Chaudhury et al., 2003). The reason of such short half-life could be related to albumin redistribution in the extravascular space of different body compartments, leading to a reduction in the plasma levels, and/or to a faster degradation due to species-specific differences (Andersen et al., 2010). However, the first hypothesis may be ruled out by the frequency of the infusions in the experimental model that was performed.

4.1.6 Doses and routes of administration

Cerebellar abnormalities and mortality were rescued in *Ugt1*$^{-/-}$ mice with the dosage scheme of daily infusion of 5.0 g/kg of HSA. Similar results were also obtained with a higher dose (7.5 g/kg/24h). Usually, the clinical route of administration and dosage employed in neonates are different to the ones applied in this study, such as about 1 g/kg, administered by intravenous (i.v.) injection (Hosono et al., 2001b). However there are reported cases in which a higher doses, up to 2 g/kg, were applied without evident adverse effects (Wood et al., 1970). Similarly, no obvious secondary side effects were observed after albumin administration, even when WT and *Ugt1*$^{-/-}$ littermates were treated with the highest dose (7.5 g/kg every 24 h).

Since the route of administration is different, a comparison of dose administration between mice and neonates is not trivial. Neonates usually undergo i.v. administration; due to the reduced size of mice (about 2 g at P2), i.p. injection was adopted. The latter procedure results in a slower HSA availability in the intravascular compartment, although a higher volume can be used for the purpose. Differently, i.v. administration renders the compound immediately active. Therefore, it is reasonable to hypothesize that that lower but more frequent doses of HSA using i.v. as privileged way of administration may result in a similar rate of survival to those obtained with 5.0 g/kg daily i.p. infusion.

Lower i.v. doses of HSA combined with intensive PT may limit the concerns raised by the high HSA application used in this model. However, a deeper investigation concerning the potential benefits of HSA treatment is needed in human jaundiced babies, particularly regarding preterm infants with very low birth weight, as they are the most affected by bilirubin neurotoxicity.

4.1.7 Predictive markers of BIND

4.1.7.1 Total bilirubin (TB)

The decision to treat hyperbilirubinemic newborns is conventionally based on TB levels. However, there is not a generalized consensus on the threshold TB levels. The guidelines of different countries suggest to apply therapeutic protocols to avoid bilirubin neurotoxicity at different TB levels (Yu et al., 2014) and clinical studies in jaundiced babies suggest that TB levels over value of ~20 mg/dL are poor discriminators to determine the individual risk of developing BIND (see chapter 1.3.3) (Ahlfors and Parker, 2008). However, the administration of albumin to prevent brain damage elicited the increase of plasma TB levels. Therefore, the use of TB as an estimator of BIND may be misled after the HSA treatment, indicating the clinical need for different and more specific parameters.

4.1.7.2 Bilirubin/albumin (B/A) ratio

In neonates, the ratio of bilirubin to albumin (B/A) has been proposed as a valid parameter to assess bilirubin neurotoxicity risk (Ahlfors, 1994). Also the guidelines of the American Academy of Pediatrics support the routine B/A ratio endorsement to determine the threshold for ET (Ahlfors, 1994; American Academy of Pediatrics, 2004). The correlation test performed in this study indicated that the B/A ratio poorly correlated with neurological damage and death in this mouse model (Figure 27B). Although a slight better correlation was obtained counterpointing B/A and cerebellar UCB levels (compared to TB), several samples were still overlapping among the groups. In fact, similarly to the TB values, the B/A ratio did not accurately discriminate the fate of the different groups of mice.

In line with these observation, a recent clinical study, the BARTrial, showed comparable effects in the management of hyperbilirubinemia in preterm infants to prevent neurodevelopmental damage by the use of TB and B/A ratio (Hulzebos et al., 2014). However, it has to be considered that the artificial increase in plasma

albumin concentration in my experimental protocol affected TB levels and, consequently, it may have also affected the B/A ratio.

4.1.7.3 Free bilirubin (Bf)

In this study, it was shown that plasma Bf, strongly correlated with UCB brain concentration, providing a further proof that Bf is the most accurate indicator of the neurological damage risk (Figure 27C).

The potential use of Bf as BIND predictor has been widely investigated in human patients (Ahlfors and Parker, 2008). The authors showed that, in a newborn population, Bf correlates better than TB with defects in auditory brainstem response (ABR) generated by bilirubin neurotoxicity. In addition, another study performed in infants with extremely low birth weight revealed the Bf association with death or adverse neurodevelopmental outcomes (Oh et al., 2010), and that Bf, rather than TB, better correlates with neurological complications. A recent study concerning extremely low birth weight Japanese infants confirmed the association between high levels of Bf and kernicterus (Morioka et al., 2015).

However, the use of Bf is not widely employed due to the technical difficulties to set up a robust and simple assay (McDonagh and Maisels, 2006). In this study it was employed the method described by Alhfors (Ahlfors et al., 2006), which consists in a modified peroxidase test performed using Zone Fluidics. Compared to previous peroxidase test methods, peroxidase test using Zone Fluidics reduces samples volume and their dilutions. Moreover, the automated procedure decreases the manual bias, and represents a more consistent and reliable range of measurement. However, the intrinsic properties of this method are not devoid of imprecision, since different factors, like haemoglobin, can interfere with the measurement.

4.1.8 HSA administration as a potential alternative to ET

HSA administration can clearly protect brain from bilirubin neurotoxicity and save lives, at least in *Ugt1*$^{-/-}$ mouse model of severe neonatal hyperbilirubinemia. One of the most striking findings of this project is that albumin beneficial effects were obtained without any other concomitant therapy, such as PT which produces a hypobilirubinemic effect. Thus, it is reasonable to assume that, if coupled with PT, this procedure could be applied in those PT-unresponsive acute cases that may result in kernicterus. In addition, HSA administration offers an alternative to ET.

The potential of albumin administration combined with PT in lowering Bf concentration has been shown in a preclinical rat model (Cuperus et al., 2013; Schreuder et al., 2013b). It is reasonable to speculate that the synergistic effect of intensive PT and frequent albumin administration may result in a feasible and more effective procedure for neonates with acute hyperbilirubinemia. However, due to methodological and technical reasons, Bf is consider unreliable by some experts (McDonagh and Maisels, 2006).

In line with our results, Hosono and colleagues (Hosono et al., 2001b) showed promising results by a single albumin infusion at the beginning of the PT treatment. In fact, the albumin-PT-treated babies show reduced Bf compared to the ones treated only with PT. Moreover, the follow-up study showed decreased ABR abnormalities in infants in which PT is also implemented with HSA (Hosono et al., 2002). The results obtained in my Thesis, combined to those described above (Hosono et al., 2001b, 2002), support the speculation that a similar or higher therapeutic effect could be obtained if less concentrated but more frequent doses are administered to the *Ugt1*$^{-/-}$ pups, concomitant with PT application.

HSA supplementation may also be helpful when ET is not easily or rapidly possible, as in situations in which patient-related factors or lack of infrastructures/expertise might not make ET implementable. ET is normally carried out only in specialized centre, but it has different risks of complications, especially in developing countries, where morbidity and mortality rates are remarkable (Ibekwe et al., 2012). In fact, not only the procedure *per se* presents complications, but also the interval between the decision to implement ET and the actual ET procedure is a significant constraint (Mabogunje et al., 2016). HSA infusion could easily complement intensive PT, since albumin is at the reach of most neonatal care units, and risks of complications in the application of this procedure are very rare (Vincent et al., 2003), although clinical trials on newborns with extreme low birth weight are needed.

In conclusion, HSA infusion exerts important beneficial effects in the severe acute phase of neonatal hyperbilirubinemia and Crigler-Najjar patients. Albumin administration could be a valid alternative in borderline situations where ET is required, since it prevents and/or decreases bilirubin accumulation in brain tissue. It was demonstrated that frequency of administration and dosage are crucial parameters to achieve full efficacy. Finally, these data provide evidence that plasma Bf level is the best marker to predict the risk of high bilirubin brain content and

consequential BIND, in the *Ugt1*$^{-/-}$ lethal mouse model. I strongly support further survey of albumin therapy, such as randomized clinical trials, to validate these data.

4.2 Bilirubin neurotoxicity is the result of concerted pathways mis-regulation

The aim of this section was to temporally characterize the molecular events activated in the developing cerebellum upon high bilirubin levels, which define the lethal mouse model of neonatal hyperbilirubinemia.

This set of experiments showed the concomitant activation of a wide variety of mechanisms activated by the long-term exposure to high bilirubin levels in the cerebellum of *Ugt1*$^{-/-}$ pups, ranging from ER and oxidative stress to inflammation and neurodegeneration. From the time perspective, in the early stages of the disease are characterized by ER and oxidative stress responses activation, consequentially affecting developing neurons' survival. At later stages, when apoptosis occurred in neurons, the rise of a prominent inflammatory response was observed, as well as the generation of a glial scar. In the final stages of the disease, the autophagy pathway was activated by bilirubin-induced neurotoxicity (Figure 55).

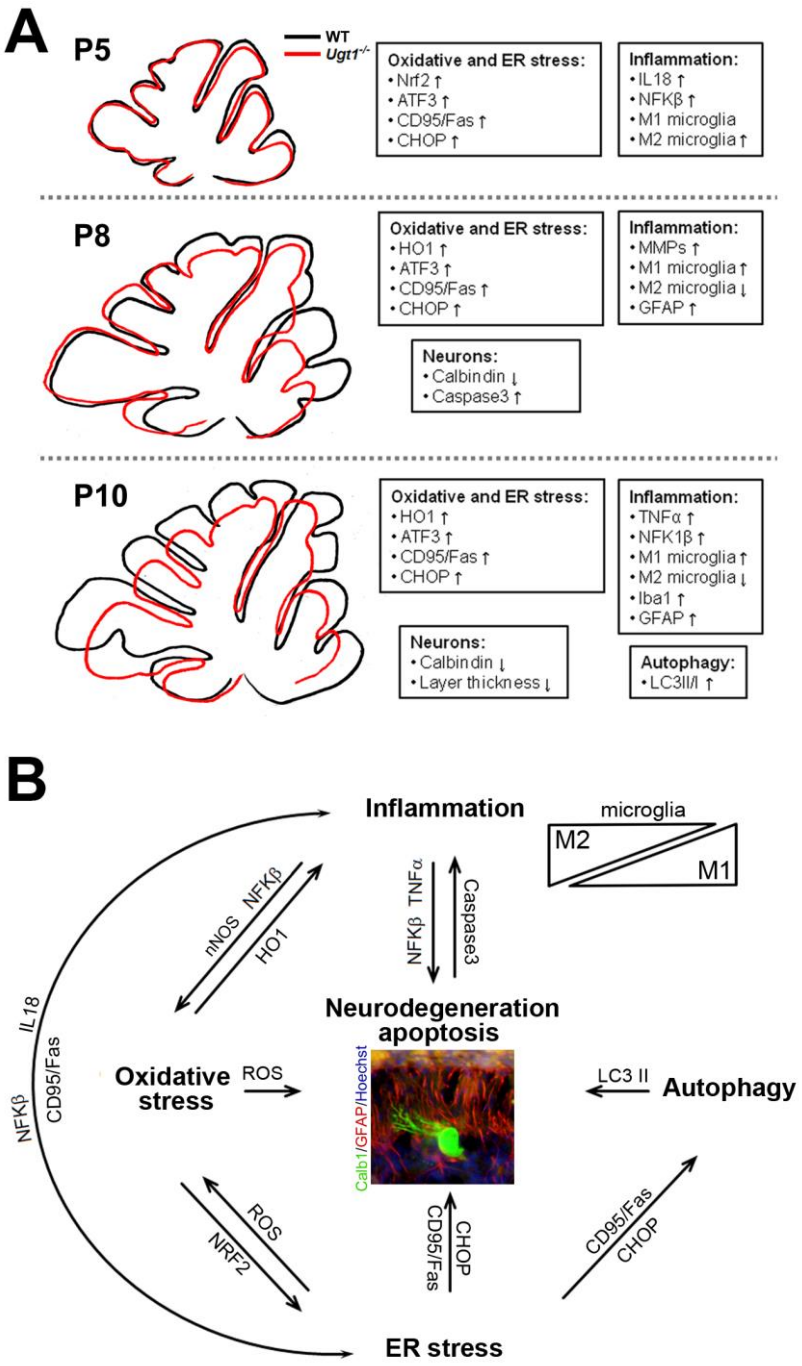

Figure 55. **Time-line of the molecular events leading to bilirubin-mediated neurodegeneration in the *Ugt1*$^{-/-}$ mouse model of neonatal hyperbilirubinemia. A)** The three sequential phases of the disease progression are indicated: P5, P8 and P10. Representative cartoons show the morphology of cerebellar sections from WT (black line) and *Ugt1*$^{-/-}$ (red line). Boxes indicate the main pathways and molecular players affected by bilirubin. B) Proposed interplay between the molecular events leading to cerebellar neurodegeneration. Bold font indicates main mechanisms involved in the onset of the disease; arrows and molecular markers indicate the interconnection between different mechanisms. An image of a neurodegenerated Purkinje neuron (stained with Calb1, green) surrounded by glial scar (stained with GFAP, red) is represented.

4.2.1 Neurodegeneration and neuro-apoptosis

Neurons are particularly vulnerable to insults because of their high metabolic rate and their restricted cell renewal. During cerebellar development of *Ugt1*$^{-/-}$ mice, high levels of bilirubin led to a progressively enhanced neurodegeneration. In the cerebellum, the neurodegenerative phenotype is characterized by reduced arborization of PC and cell loss (Figure 29). In contrast, no neurodegenerative effect at any time point analysed was observed in mature granule cells (Figure 30). These evidences are in agreement with previous observations in both C57BL/6 and FVB/NJ strains of the *Ugt1*$^{-/-}$ mouse model (Bortolussi et al., 2012, 2014, 2015).

My group showed that the absence of bilirubin conjugation in the C57BL/6 *Ugt1*$^{-/-}$ strain of mice resulted in an increase in TB, and in the accumulation of bilirubin in the brain. High levels of bilirubin lead to impaired cerebellar architecture and neuronal cell death, resulting in neonatal lethality and showing 50% of survival at P5 (Bortolussi et al., 2012). In addition, it was shown that only PCs own a neurodegenerative phenotype (Figure 4) (Bortolussi et al., 2015). On the other hand, further insights in bilirubin neurotoxicity mechanisms were obtained by the study of the FVB/NJ *Ugt1*$^{-/-}$ mouse strain (Figure 5). This model shows a delayed lethality, allowing the identification of a specific window of brain susceptibility to bilirubin. In fact, high bilirubin levels result in cerebellar damage of untreated *Ugt1*$^{-/-}$ animals at P8. The application of phototherapy (PT) over the first 8 days of life (P0-P8 PT) or starting from P8 to P20 (P8-P20 PT) does not rescue the lethality of mice, underling a critical window of susceptibility of brain during this developmental stage (Bortolussi et al., 2014).

These results obtained by PT modulation supports the concept that bilirubin susceptibility depends on the cell type and developmental stage, affecting survival of neuronal precursors by impairing their neurogenesis, arborization and synaptic connectivity (Falcão et al., 2007; Fernandes et al., 2009). *In vitro* experiments performed by the group of Prof. Brites showed that immature neurons are particularly sensitive to bilirubin and inflammatory agents (e.g. TNFα), resulting in decreased neurites outgrowth and increased apoptosis rate (Falcão et al., 2007). Bilirubin exposure reduces viability of proliferating neuronal precursors (Fernandes et al., 2009), thus indicating that bilirubin exerts a detrimental effect on undifferentiated neurons during brain development. In addition, bilirubin affects other cell types in the CNS, such as oligodendrocyte precursor cells, by delayed

differentiation, reduced number of mature oligodendrocytes, decreased number of internodes and their relative myelin length (Barateiro et al., 2013).

4.2.2 Oxidative stress response

Due to its antioxidant and cytoprotective properties, low bilirubin concentrations are considered beneficial (Stocker et al., 1987). However, higher levels of bilirubin impair cell homeostasis, placing jaundice babies at risk during neonatal severe hyperbilirubinemia. It has been shown that toxic bilirubin concentrations lead to oxidative stress response *in vitro*, and the abrogation of nitric oxide (NO) production extends the survival of cell cultures of rat neurons (Brito et al., 2008b). Further demonstration on oxidative stress involvment were given by Brito and colleagues (Brito et al., 2008a), showing that oxidative stress response is impaired not only in neuronal cell cultures, but also in rat cortical cerebrum astrocyte cultures, although the latter cell type appears to be less sensitive to bilirubin incubation. In addition to these *in vitro* evidences, it is important to underline that the CNS is particularly sensible to oxidative stress, and neurodegeneration occurs when reactive oxygen species (ROS) production overwhelms antioxidant defences (Fischer and Maier, 2015).

In the *Ugt1*$^{-/-}$ mouse model, mutant animals showed increased ROS production that resulted in the up-regulation of *Nrf2* gene expression. As a key transcription factor activated in response to stress conditions, Nrf2 translocates in to the nucleus, where it transactivates antioxidant regulated genes (ARE) (Giudice et al., 2010), such as cyto-protective enzymes. Accordingly, after *Nrf2* stimulation by bilirubin, it was observed the up-regulation of *HO-1* expression levels during the more advanced stages of the disease analysed (such as P8 and P10) (Figure 37A).

These findings support previous *in vitro* and *in vivo* studies, showing that the redox-sensitive pathway is not sufficient to protect neurons over the prolonged oxidative stress induced by bilirubin (Calligaris et al., 2009; Giraudi et al., 2011; Rodrigues et al., 2000; Stoeckius et al., 2012).

As a consequence of the cell damage, the mitochondrial apoptotic pathway is activated (Brites, 2011), resulting in increased oxidative stress and cellular redox status imbalance (Qaisiya et al., 2014; Tell and Gustincich, 2009). However, in the cerebellum of *Ugt1*$^{-/-}$ mice it was not observed the regulation of the mitochondrial *superoxide dismutase 2* (*SOD2*), nor an impaired expression of mitochondrial

cytochromes (data not shown), suggesting that compensatory mechanisms in response to the lack of conjugation system are exerted through a different pathway, at least in this mouse model.

In vivo evidences obtained in other animal models of systemic hyperbilirubinemia showed that oxidative stress is a key event of neurotoxicity. In line with my results, the severe hyperbilirubinemia that characterizes *Ugt1*$^{-/-}$ mice in the C57BL/6 background also leads to the overexpression of *Nrf2* (Bortolussi et al., 2015). The group of Tukey showed that bilirubin activates *HO1* expression in another mouse model lacking UGT1A1 activity (Nguyen et al., 2008; Yueh et al., 2014), underscoring the importance of its activation pathway as an adaptive response to oxidative stress. However, the pharmacological reduction of lipid peroxidation is not sufficient to prevent BIND in the hyperbilirubinemic Gunn rat (Daood et al., 2012), supporting the concept that, despite its importance, oxidative stress partially contributes to bilirubin neurotoxicity.

4.2.3 UPR and ER stress response

Given the close connection of oxidative stress and ER stress, I investigated whether the unfolded protein response (UPR) and impairment of ER balance occurred *in vivo* as a consequence of bilirubin toxicity.

The results showed a significant induction of key markers of ER stress in response to high bilirubin levels, such as *ATF3*, *CD95/Fas* and *CHOP* (Figure 36A). However, others genes related to UPR and ER stress showed no changes in their transcriptional levels (*GPR78*, *GRP94*, *P58*^{IPK}, *FKBP11* and *DR5*) at any time point analysed (Figure 36B). In particular, it was recently reported the activation of ER stress in response to bilirubin in *in vitro* oligodendrocyte cell cultures, resulting in the up-regulation of *GRP78* (Barateiro et al., 2012). Many ER stress related genes were shown to be up-regulated in a transcriptome analyses performed on neuroblastoma cell line incubated with bilirubin, such as *ATF4*, *GRP94* and *ERO1L* (Calligaris et al., 2009). The latter, being involved in oxidative protein folding, underlines the close connection between ER and oxidative stress. Anyhow, cerebellar analysis did not show the activation of any of the selected genes in *Ugt1*$^{-/-}$ mice compared to WT littermates.

In line with these observations, genes known to mediate ER-response, such as *CHOP* and *ATF3*, are up-regulated in a transcriptome analysis of neuroblastoma

and hepatoma cell lines in response to high bilirubin levels (Calligaris et al., 2009; Oakes and Bend, 2010). The continuous rise of bilirubin levels over time in the FVB/NJ *Ugt1*$^{-/-}$ mouse model causes an impairment in cell homeostasis (Bortolussi et al., 2014). Neurons are not able to revert ER stress, as suggested by the up-regulated expression of effector genes like *CD95/Fas* and *CHOP*, resulting in death by apoptosis of susceptible cells. The activation of ER stress may trigger the PERK-mediated pathway (Chaudhari et al., 2014; Kim et al., 2009), leading to the apoptotic pathway, as evidenced by increased *CHOP* and *CD95/Fas* expression and caspase 3 cleavage (Figure 36A and 28C, respectively).

The early and progressive up-regulation of *CHOP* and *ATF3* observed in the *Ugt1*$^{-/-}$ mouse model may reflect the precocity of the ER stress response, indicating that neurons have already activated ER stress response after the initial phases of bilirubin accumulation. Taken together, these *in vivo* observations suggest that ER stress is a key initial event that causes neuro-apoptosis and has an important contribution in the overall process that results in lethality by hyperbilirubinemia.

4.2.4 Inflammatory mediators

As shown in the previous chapter, ER stress was a critical process involved in bilirubin lethality of the neonatal hyperbilirubinemia mouse model. Since the activation of ER stress can critically regulate inflammation, particularly through ROS production (Chaudhari et al., 2014), it was then analysed the contribution of inflammatory players to the exacerbation of bilirubin-induced cerebellar damage. In fact, in addition to ER and oxidative stress stimuli, also in the nervous system the degeneration of neurons can stimulate inflammation. Neuroinflammation can be activated by different mechanisms, such as the signals deriving from injured neurons, the accumulation of misfolded or modified proteins, and/or the imbalance between pro- and anti-inflammatory processes.

I showed that two well-known inflammatory mediators, *NFKβ* and *IL18*, were early responders to high bilirubin levels at the onset of the disease (Figure 35).

NFKβ can have both neuroprotective and neurotoxic roles, since this transcription factor plays a bivalent function depending on the kinetics and the expression in the injured tissue. NFKβ is essential in the regulation of inflammation and oxidative stress when activated as a defence response to stress stimuli, but it is also involved in processes such as apoptosis, proliferation and differentiation to establish cellular

fate (Pizzi and Spano, 2006). Pathological conditions like ischemia, trauma or different types of neurodegenerative disease activate NFKβ (Fischer and Maier, 2015), but its role is also important in non-neurodegenerative disease like diabetes (Tersey et al., 2012). In fact, NFKβ mediates the activation of genes that boost oxidative stress, inflammation and apoptosis (Chaudhari et al., 2014). In line with these observations, it was shown the exacerbation of neurotoxicity at P10, the most severe condition analysed. At this stage, the parallel increase in *HO1* expression levels, neurodegeneration, astrocytosis and gliosis was observed.

Matrix metalloproteinases (MMPs) are also important in the context of neuropathology by their contribution to demyelination, perpetuation of inflammation and neurotoxicity (Yong et al., 2001). It was observed a transient activation of the matrix metalloproteinases *MMP2* and *MMP9* in the hyperbilirubinemic pups used in this study (Figure 35). MMPs activation was observed in primary rat cultures of brain microvascular endothelial cells (BMCE) incubated with bilirubin (Cardoso et al., 2012) and, in agreement with my observation, MMPs activation in BMCE decreases over time. Interestingly, it was observed that UCB decreases MMP2 and MMP9 activity of isolated murine splenic lymphocytes across monolayers of murine endothelial cells (Keshavan et al., 2005). This effect may be due to the antioxidant properties of bilirubin, since the incubation of endothelial cells was performed at low bilirubin levels.

According to Silva and colleagues, the MMPs activity could be the result of NFKβ activation, since microglia cells treated with bilirubin show the increased activity of MMP2 and MMP9 following *NFKβ* over-expression (Silva et al., 2010a). Moreover, the concomitant up-regulation of MMPs and Iba1 expression at P8 may be determinant to the activation of the inflammatory process.

IL18 is involved in the modulation of different cellular mechanisms in the brain. In fact, this interleukin is important in the propagation of apoptosis in the developing brain and also in the regulation of inflammatory and cytotoxic pathways in hyperoxia-induced neurodegeneration (Felderhoff-Mueser et al., 2005). The correlation between ER stress, inflammation and neuro-apoptosis is suggested by the fact that IL18 maturation is mediated by CD95/Fas signalling (Bossaller et al., 2012), underscoring how different stimuli contribute to hyperbilirubinemia in a multifaceted manner. Several factors underline the discrepancy between *in vitro* and *in vivo* data. In fact, *in vitro* primary cultures do not resemble the intensity of the insult, the complex network formed by the interplay between different cell types, and the brain

developmental status. IL18 is a key example of this concept, since it is highly expressed in the early post-natal stages of brain development, but it is down-regulated and almost absent in the adult brain (Felderhoff-Mueser et al., 2005). To my knowledge, this is the first report showing the activation of *IL18* and *NFKβ* induced by bilirubin in an *in vivo* model of neonatal hyperbilirubinemia.

TNFα was activated in the latest and most severe phases that characterize the disease states of the *Ugt1*$^{-/-}$ pups. TNFα is a key factor released in the CNS by activated microglia and astrocytes, and mediates the amplification of neuro-inflammatory events contributing to the initiation of the apoptotic cascade. As in the cases of NFKβ and IL18, many neurodegenerative conditions such as ALS, PD and HD, show the up-regulation of *TNFα* (Olmos and Llado, 2014). Studies performed on astrocytes and microglia primary cultures showed the release of the pro-inflammatory cytokines TNFα and IL1β after bilirubin incubation (Fernandes et al., 2004; Gordo et al., 2006). In our studies, *TNFα* expression was increased at the later analysed stage (Figure 35), in line with experiments performed in primary cell cultures of astrocytes treated with bilirubin (Fernandes and Brites, 2009). In the same study, the activation of other well-known pro-inflammatory mediators, such as IL1β, IL6 and INFγ, was less pronounced (Fernandes and Brites, 2009). Unexpectedly, it was not possible to detect IL1β, IL6, IL10 and INFγ in the cerebellum of FVB/NJ *Ugt1*$^{-/-}$ and WT mice (Figure 34). Nonetheless, the network of interrelated mechanisms resulting from different studies on hyperbilirubinemia will require further *in vivo* experimentation to evaluate and assess the role of distinct pathways in this multifaceted disease.

4.2.5 Implication of inflammatory cell mediators

The main effectors of innate immune response in the CNS are microglia and astrocytes, whose activation is particularly evident in response to neurodegeneration.

Hyperbilirubinemia triggered the activation of both astrocytes and microglia in the cerebellum of *Ugt1*$^{-/-}$ mice. It was observed a prominent activation of GFAP expression compared to WT mice in the most compromised conditions (P8 and P10, Figure 31), while Iba1 expression was also increased but less prominently and in the latest analysed time point (P10, Figure 32).

The effect of bilirubin activation on these two cell types has been reported both *in vitro* and *in vivo*. *In vitro* experiments showed the activation of glia cells in response to toxic bilirubin levels (Brites, 2012). However, the role of glia activation is still controversial. In fact, the beneficial effect of astrocytes in protecting neurons when challenged by bilirubin was reported (Falcao et al., 2013). On the other hand, longer exposure to bilirubin showed that astrocytes critically worsen the viability of neurons (Falcão et al., 2014). *In vivo* studies on Gunn rat cerebellum indicated that the increase in GFAP content is a common trait of hyperbilirubinemia (Mikoshiba et al., 1980). Moreover, astrocytes activation was also shown in a liver-specific *Ugt1a1* conditional knockout mouse model (Barateiro et al., 2016; Yueh et al., 2014). In both works, the authors showed that at P14, GFAP is increased in response to bilirubin more than 15 times by expression analysis, and a 6-fold increase by IF analysis when compared to their control, being astrocytes the main effectors of HO1 production. In addition, primary cultures of astrocytes are the main effectors for HO1 production (Yueh et al., 2014).

According to my results, Yueh and colleagues also reported the involvement of glia by Iba1 activation, as shown by a 3-fold increase in Iba1 expression. The analysis of microglia primary cell cultures revealed that Iba1-positive cells are mostly responsible for the increase in pro-inflammatory cytokines (Yueh et al., 2014).

Importantly, the role of TLR2 in activation of inflammatory response was demonstrated in the context of bilirubin damage to brain. Hyperbilirubinemic *Ugt1a1*$^{-/-}$ *TLR2*$^{-/-}$ mice are characterized by the block of inflammatory activation that results in increased mortality, underlining the importance of inflammatory response in the context of bilirubin toxicity (Yueh et al., 2014). However, despite the activation of inflammatory response in the *Ugt1*$^{-/-}$ mouse model, no differences in *TLR2* regulation in response to bilirubin were observed (Figure 35B). The reason of this discrepancy could rely on the fact that Yueh and colleagues´ analysis was performed at a later time point, namely P14, or could be due to intrinsic differences in the models. Although the mouse model characterized by Yueh and colleagues showed lower levels of TB, it is reasonable to hypothesize that the level and duration of the bilirubin insult in the two models may produce differences in *TLR2* regulation.

Furthermore, it was studied the role of different types of microglia that are activated during the disease progression. In fact, the interplay between M1 and M2 microglia was never investigated in context of bilirubin toxicity. The activation of M2 microglia, such as *MRC1* expression, was observed at the early stages of the disease.

However, the up-regulation decreased over time, as the severity of the *Ugt1*$^{-/-}$ mice phenotype increased (Figure 33). On the contrary, it was reported the opposite trend of M1 microglia activation, being progressively activated at later stages, as determined by the M1 markers, such as *Iba1* and *CD68* (Figure 33). Similar inverse interplays between M1 and M2 microglia were also observed after traumatic brain injury (TBI) (Hsieh et al., 2013) and spinal cord injury (SCI) (Kigerl et al., 2009). In fact, both works showed the activation and localization of M2 microglia subset at the site of injury. This activation decreases over time, while the M1 subset expression is increased, promoting neurotoxicity and exacerbating damage. In particular, in the SCI mouse model a transient activation of iNOS is reported, in agreement to the results obtained in the *Ugt1*$^{-/-}$ mouse model, in which iNOS up-regulation was observed in the central analysed time point, at P8 (Figure 35). However, in contrast with my observation, the *CD86* progressive up-regulation was also reported by Kigerl and colleagues (Kigerl et al., 2009). These discrepancies underline the complex nature of events present in the different disease states modifying microglia states and their functions.

Nonetheless, as the M2 microglia subset promotes the CNS repair, its identification and stimulation may open a new clinical strategy using the M2 anti-inflammatory microglia as a therapeutic target.

4.2.6 Autophagy is the final deathblow

Autophagy, or cellular self-digestion, is a cellular pathway involved in protein and organelle degradation by lysosomes. It allows the maintenance of cellular homeostasis by preventing the accumulation of misfolded proteins or damaged organelles (i.e. mitochondria) (Mizushima et al., 2008).

As recently shown, autophagy is a key defence mechanism against neurodegenerative diseases and its deregulation is crucial to decide cell fate. In fact, although it is considered as a mediator of programmed cell death (Hsieh et al., 2009), the activation of autophagy pathway may also lead to a pro-survival mechanism activation (Levine and Yuan, 2005).

Since the close connection between oxidative stress, neuro-apoptosis, inflammation and autophagy, I investigated the autophagic response in the hyperbilirubinemic context by the analyses of LC3. It was observed the late activation of autophagy in the cerebellum of the *Ugt1*$^{-/-}$ mice, being LC3 activated only at P10 (Figure 38).

Previous *in vitro* experiments are in line with my observation (Calligaris et al., 2009; Palmela et al., 2012). In fact, the autophagy pathway activation is reported in neuroblastoma and endothelial cell lines treated with high levels of bilirubin (Bf=100-140 nM), but only at later stages of the analyses (24-72h), when cell death is evident.

Interestingly, the strong induction of Fas/CD95 in the cerebellum of $Ugt1^{-/-}$ mice upon bilirubin exposure (Figure 36A) may represent the link between autophagy and ER stress. In fact, the overexpression of CD95/Fas in HeLa triggers cell death not only by caspase-mediated apoptosis, but also by stimulating autophagy through MAPK pathway (Zhang et al., 2008). Furthermore, CHOP is required for the transcriptional increase of genes responsible for the correct autophagosome formation, once again underlining the tight connection between ER stress and autophagy (B'Chir et al., 2013).

Altogether, these results indicate that autophagy is the last pro-survival mechanism activated to overcome bilirubin cellular stress. Importantly, this is the first time that autophagy is observed *in vivo*, as a response to hyperbilirubinemia toxicity.

4.2.7 Future directions

The dissection of the molecular mechanisms of hyperbilirubinemia revealed the complexity of such multifaceted disease. In fact, the response to bilirubin toxicity consists in the activation of different pathways that are simultaneously regulated, rather than being activated in a sequential time frame. At the onset of the disease ER stress and inflammation appear to be the most prominent processes leading to neurodegeneration. The detailed determination of the mechanisms involved in the hyperbilirubinemic condition is essential to set up and develop potential therapeutic strategies against bilirubin-induced brain damage.

Further studies are needed to demonstrate whether modulation of one or more of them are required to reduce neurodegeneration and death, before this knowledge can be translated to patients.

4.3 MNC decreases neurodegeneration and neuroinflammation resulting in increased lifespan and partial rescue of neonatal hyperbilirubinemia lethality

To obtain deeper insights in bilirubin neurotoxicity mechanisms mutant mice were treated with MNC, a known compound with anti-inflammatory and neuroprotective properties. In fact, MNC administration throughout lactating dams decreased neurodegeneration and neuroinflammation, and increased the lifespan of *Ugt1*$^{-/-}$ pups. As a result, it was obtained a partial rescue of the lethal outcome triggered by severe neonatal hyperbilirubinemia.

4.3.1 MNC lifespan extension

Treatment of the lactating mothers with increasing MNC dosage resulted in the lifespan extension of *Ugt1*$^{-/-}$ pups, shifting the 50% of survival from P11 in untreated mutant animals to P26 in mice treated with the highest MNC dose (Figure 39). Moreover, 20 days of MNC administration rescued lethality of 15% and 30% of mutant animals treated with MNC 2X and MNC 4X, respectively, underscoring the beneficial potentiality of this treatment. The *in vivo* wide beneficial effects of MNC on survival have been shown in several mouse models of neurodegeneration, ranging from multiple sclerosis (MS) to spinal cord injury, from ALS to HD, PD and AD (Kim and Suh, 2009). For example, two different groups working on ALS showed the efficacy of MNC in increasing the lifespan of SOD^{G93A} mice, which exhibit a motor neuron-specific neurodegeneration (Kobayashi et al., 2013; Zhang et al., 2003). However, the age of animals and route of administration were different from those used in this Thesis, as these studies were performed in adult mice treated with several i.p. injections per week.

On the other hand, the role of MNC is controversial, since different groups have shown it has negative effects on survival. A recent work from Pinkernelle and colleagues showed the deleterious effect of MNC administration on motor neurons in *ex vivo* organotypic rat spinal cord cultures (Pinkernelle et al., 2013). In addition, *in vivo* negative effects of high MNC doses were shown in the R6/2 mouse model of HD (Menalled et al., 2010), as mice survival was reduced. Since HD affects neuron viability in different regions of the brain compared to bilirubin, which affects preferentially the cerebellum, further studies are needed to elucidate the impact of MNC on survival in different disease contexts.

4.3.2 MNC route of administration

The route of MNC administration is particularly important for the treatment efficacy. Fagan and colleagues suggested the use of i.v. MNC administration to obtain reliable results in a brain injury model, as MNC half-life in plasma is ~3 hours post injection (Fagan et al., 2004). To note, most of the work performed on rodent models of neurodegeneration takes advantage of single or double i.p. injections, preferentially evaluating the outcome shortly after 'injury' (Plane et al., 2010).

Since repeated i.p. or i.v. injection of P0 pups is impracticable (the weight of pups is about 1.0-1.5 g at birth), I used the approach already employed by Lin et al with Gunn rat pups (Lin et al., 2005), by daily administering fresh MNC dissolved in the drinking water to the lactating mothers. However, in that study MNC is administrated also after weaning on, till the day of sacrifice; the drug is dissolved in water with the addition of sucrose to favour the intake (Lin et al., 2005). In contrast, in my study sucrose supplementation was omitted, since it was observed no difference between the sole intake of water and the water-MNC solution (Figure 40). In line with my data, Hinwood and colleagues observed that 40 mg/kg/day of MNC administration does not modify water consumption of treated adult rats (Hinwood et al., 2012). Unaffected drinking rate is particularly important for the homogeneity of the experiment, not only because the amount of milk drunk may affect the effective MNC dosage in pups, but also because it may have a direct effect on the general conditions (dehydration, strength to milk, etc.) of pups affecting their growth and severity of the disease.

The lowest dose of MNC able to extend lifespan was 0.84 mg/mL (corresponding to MNC 1X), while the highest consisted in 3.36 mg/mL (MNC 4X). No negative effects were observed by this MNC dose except the decrease in weight growth (discussed below), but it cannot be excluded that higher MNC doses may have a detrimental effect on pups. For example, in another model and species, a single i.p. MNC administration of high doses (500 mg/kg) results in the death of hyperbilirubinemic rat pups (Geiger et al., 2007). However, it is difficult to assess the exact quantity of drug intake by pups and final effective dose, due to the several passages of MNC (from mother to pups) and lack of information of MNC concentration in the milk, that add complexity to the calculation.

The usual dosage of MNC to treat acne in adult is 200 mg/day. Lin and colleagues showed that about 22.5 mg/day of mothers intake results in 1.46 µg/g of brain MNC concentration in treated pups (Lin et al., 2005). It is reasonable that, considering the

different size of mice and rats brains, and the higher drug doses given to the mothers, MNC concentration in the brain of *Ugt1*$^{-/-}$ pups may result even higher. However, such hypothesized high concentration, correlated with survival, underlines the severity of *Ugt1*$^{-/-}$ mice phenotype compared to the one of hyperbilirubinemic Gunn rat pups.

A comparison between animal model and human is hardly practicable, since MNC is not recommended for the use in children below the age of 8 years old. In a recent work on children with an average of 8 years old affected by Angelman syndrome (a rare genetic disorder characterized by a deletion in the chromosome 15 causing neurodevelopmental disorder) indicated that 8 weeks of oral MNC administration (3 mg/kg/day) are well tolerated, also showing beneficial effects of the drug on cognitive impairment (Grieco et al., 2014). However, solid and reliable data on MNC concentration in babies' brain are still missing.

4.3.3 MNC side effects

MNC administration has different effects in the outcome of neurodegenerative disorders, depending on the type of the disease and the age of subjects. As many other antibiotics, the use of MNC is discouraged in infants or pregnant woman. In fact, being ion chelators, tetracyclines act as calcium phosphate binder, allowing the aggregates deposition in teeth and bones, thus impairing their growth (Buller et al., 2008). In the *Ugt1*$^{-/-}$ mouse model, a decrease in the weight growth curve was observed during the treatment in MNC-treated WT and mutant mice, when compared with untreated WT mice (Figure 41). This effect was transient and the weight recovered after MNC discontinuation. This is in contrast to what observed by Hinwood and colleagues when MNC was administered in the drinking water to 70 days old rats exposed to chronic psychological stress (Hinwood et al., 2012). In fact, they showed that the stress affects weight gain of rats but MNC does not. This effect may be due to the different age of the animals, as in my experiment pups received milk from mothers since birth, while Hinwood treated adult rats. Interestingly, MNC does not affect the pups' growth in a rat model of neonatal stroke. After focal cerebral ischemia-reperfusion, P7 rat pups treated with PBS show no differences with littermates treated with i.p. injection of MNC, regardless if single or triple injection (Fox et al., 2005).

One important difference may stand in the frequency of MNC administration, which was given just once or three times, in comparison with the continuous administration in my experimental protocol. It cannot be excluded that the antimicrobial effect may influence digestion of milk in pups, thus affecting their growth.

The majority of the MNC 2X- and 4X-treated *Ugt1*$^{-/-}$ animals begun to die after MNC discontinuation, as shown in the survival curve (Figure 39). Moribund animals lost weight, thus affecting the weight curve in the temporal window from P20 (at the time of MNC discontinuation) to P30 (Figure 41C and 41D). It is reasonable to think that a more prolonged MNC administration could further extend *Ugt1*$^{-/-}$ mice lifespan, but a different way of administration (e.g. gavage, i.p. or i.v. administration) would be required.

One of the most surprising beneficial properties of MNC was the ability to rescue animals without modifying bilirubin plasma levels. In fact, treated and untreated animals had high and unaffected TB levels (Figure 42), similarly to the bilirubin determination performed on Gunn rats (Lin et al., 2005), indicating no effect of MNC on systemic bilirubin levels.

I did not observe any obvious secondary effect in the MNC-treated mice, but I cannot rule out an increase in transaminases levels in mice treated with MNC. However, since the administration of MNC 10 mg/kg results in decreased transaminases activation in a mouse model of hemorrhagic shock (Kholmukhamedov et al., 2014), it can be speculated that this phenomenon may not occur in *Ugt1*$^{-/-}$ mice treated with MNC.

4.3.4 Timing of administration is crucial to obtain MNC beneficial effects

Recent evidences pointed to the importance of the timing of MNC administration, i.e., whether administration is performed during the pre- or the post-symptomatic condition. In fact, it was observed that MNC beneficial properties are most significant when the drug is administered close to the moment of 'injury'. This effect was particularly evident in the case of acute hyperbilirubinemia, as the efficacy of MNC was tested in Gunn rat pups (at P16) with acute bilirubin levels generated by with sulpha. The late administration of MNC (120 min after sulpha) does not rescue the alterations in BAEPs caused by the bilirubin peak, while pups with early i.p. MNC supplementation (30 min after sulpha) show no abnormalities (Rice et al., 2011). Hence, the effect of MNC early administration to Gunn rats was remarkable.

However, important differences exist between the work of Rice and colleagues and the work performed in this Thesis. In fact, the damage in the Gunn pups was produced by the pharmacological increase of bilirubin levels, resembling an acute phase, while hyperbilirubinemia was genetically induced and the *Ugt1*$^{-/-}$ mice used in my study showed chronic high TB. Nonetheless, MNC administration from the day of birth resulted in amelioration of the lethal phenotype of *Ugt1*$^{-/-}$ mice, suggesting that, although hyperbilirubinemia was chronic, the preventive use of MNC is effective in rescuing animals.

4.3.5 MNC effectively reduces neurodegeneration

As shown in the section 3.2, neurodegeneration is a key event caused by bilirubin. At P15, *Ugt1*$^{-/-}$ mice used in this study showed a severely impaired cerebellum, resulting in the reduction of 57% of cerebellar layer thickness in mice treated with the lowest analysed dose (MNC 1X). In contrast, MNC 4X-treated *Ugt1*$^{-/-}$ animals had a 50% increase in the total cerebellar thickness compared to mutant receiving the MNC 1X dose (Figure 43C). The prevention of cerebellar abnormalities by MNC was also shown in a neonatal rat model of hyperoxia, in which i.p. MNC injection reduced cerebellar impairment in rat pups exposed to 80% of O_2 (Scheuer et al., 2015). In addition, my results are in agreement with the work of Lin and colleagues, who showed that administration of MNC to dams (at lower doses compared to this study) retrieves cerebellar abnormities of Gunn rat pups (Lin et al., 2005). However, as mentioned before, Gunn rats showed a milder neurological phenotype, survive and reach adulthood without any treatment; thus, the estimation of the MNC benefit on rats' survival is not possible to determine. The less severe phenotype combined with the administration of MNC after weaning may account for the complete rescue of both the cerebellar hypoplasia and PCs number. In the same work it was shown that the *in vivo* administration of MNC decreases the activation of p38 in cerebellar extracts of hyperbilirubinemic Gunn rat pups, adding further insights in the anti-inflammatory properties of MNC (Lin et al., 2005).

The trend showing a reduction in apoptosis after MNC 4X treatment observed at P8 (Figure 45A) was very significant at P15, as cleaved-caspase 3 levels decreased to WT levels in MNC 4X-treated *Ugt1*$^{-/-}$ animals (Figure 45B). It was previously shown that, among its beneficial properties, MNC inhibits the cytochrome *c* release from mitochondria in an *in vivo* model of ALS, in primary cortical neurons and in isolated

mitochondria, thus directly affecting caspase 3 activation (Zhu et al., 2002). In addition, my result is in line with those of Wang and colleagues, who demonstrated caspase 3 reduction in both *in vitro* and *in vivo* models of ALS and HD (Wang et al., 2003). A more recent report showed that MNC inhibits apoptosis by reducing caspase 3 cleavage, protecting a human dopaminergic cell line challenged with a neurotoxic inducer (Ossola et al., 2012).

It is straightforward to predict that the reduction of cerebellar apoptosis will result in an increase of the final number of neurons. In fact, it was observed that the neuroprotective properties of MNC on GCs of MNC 4X-treated *Ugt1*$^{-/-}$mice resulted in an increase in Granule neurons number, since they were increased more than 2 times compared to mutant mice treated with the lower dose of MNC (Figure 47). This is in contrast to what observed by Cheng and colleagues, showing that MNC treatment is not sufficient to rescue NeuN content and cell death upon induction of *Dicer* knocking-out (a mouse model of neurodegeneration) in the hippocampus (Cheng et al., 2015). Interestingly, in untreated *Ugt1*$^{-/-}$ mice GCs were not affected, even after ten days of severe hyperbilirubinemia (P10) (Figure 30). Therefore, it is reasonable to hypothesise that this cell type may be affected by a more prolonged bilirubin exposure, as clear differences were present at P15 in MNC 1X-treated *Ugt1*$^{-/-}$mice (Figure 47). It should be considered that the MNC effects may depend on the cell-type and the nature of the insult, accounting for different neuroprotective outcomes, as Chen and colleagues focused their attention on hippocampal neurons (Cheng et al., 2015), while in my study the analysis was performed on cerebellar neurons.

MNC also partially rescued MNC 4X-treated *Ugt1*$^{-/-}$ animals from PCs loss by bilirubin toxicity. In fact, it was observed decreased cerebellar calbindin content down to 50% and reduced arborization (Figure 46), but PCs density of mutant mice treated with the highest dose was comparable to WT. The potential neuroprotective properties of MNC on these important neurons were also shown in Gunn rats, where pups have same PCs number compared to WT when treated with the drug (Lin et al., 2005). The cerebellum is the organ implicated in movement and motor coordination and, remarkably, the rescued *Ugt1*$^{-/-}$ animals were able to perform the rotarod test as well as WT animals (Figure 43), suggesting that the number of viable PCs, despite their reduced arborisation, is an important factor affecting the cerebellar function.

4.3.6 MNC attenuation of inflammation ameliorates neurodegenerative disease

The wide anti-inflammatory effects of MNC were shown in many neurodegenerative diseases (Kim and Suh, 2009). In the *Ugt1*$^{-/-}$ mouse model, the bilirubin-induced activation of cells involved in the glial scar process in untreated *Ugt1*$^{-/-}$ mice was significantly reduced after MNC 4X treatment. In fact, at P15 both the levels of the GFAP and Iba1 cerebellar markers of inflammation were decreased in MNC 4X-treated mutant animals, compared to mice treated with the lowest dose of MNC, almost reaching WT levels (Figure 48 and 49). These observations are in line with the decreased number of astrocyte and microglia cells observed in a *Dicer* KO mouse model of neurodegeneration after MNC treatment (Cheng et al., 2015). Interestingly, MNC shows a beneficial impact in modulating retrovirus-induced neurodegeneration. MNC protects neuronal cells from the detrimental effects of co-cultured astrocytes infected (and consequentially activated) with *ts1* virus, a virus that selectively infects astrocytes (Kuang et al., 2009). However, MNC modulation of the neuroinflammatory players depends on the disease. In fact, no reduction in astrocytosis is observed when LPS is injected in the brain of rat pups treated with MNC but, instead, the treatment results in a reduction in microgliosis (Fan et al., 2005).

It is plausible that, since gliosis influences neuronal development, the reduction in gliosis impacts on neurons, spines generation and arborisation, as shown in MNC 4X-treated *Ugt1*$^{-/-}$ mice. These results underline both the anti-inflammatory effects of MNC, and that the reduction of the inflammatory response is important to ensure brain development.

4.3.7 M1 and M2 microglia

Microglia modulation is very important in the outcome of brain injury, as differences in microglia polarization can determine the fate of neurons (Michell-Robinson et al., 2015). It was shown that bilirubin triggered the progressive activation of pro-inflammatory M1 type microglia (inversely proportional to M2 type microglia, the neuro-protective one) from P5 to P10 in untreated mutant mice (Figure 33), leading to damage exacerbation, as increased gliosis formed the glial scar.

At P15, *Ugt1*$^{-/-}$ mice treated with MNC 4X showed a reduction in the M1 microglia (Figure 50). This result is in line with what observed by Kobayashi and colleagues,

showing a decreased expression of M1 microglia markers by MNC treatment, both in *in vivo* and *in vitro* models. In fact, MNC treatment reduces Iba1, CD68 and CD86 levels contributing to lifespan extension in a mouse model of ALS, while primary cultured microglia cells treated with LPS show decreased expression of *CD86* after MNC treatment (Kobayashi et al., 2013). It is reasonable that attenuation of M1 microglia may contribute to a better outcome also in *Ugt1*$^{-/-}$ hyperbilirubinemic mice. Since MNC abolished microglia activation, it was studied its effect on M2 type microglia by investigating the expression of *MRC1* and *MRC2*, two membrane receptors involved in the resolution of the inflammatory state by M2 microglia. The dose-dependent reduction in *MRC1* well correlated with the general anti-inflammatory effect of MNC. On the other hand, *MRC2* was up-regulated both in MNC 1X- and MNC 4X-treated *Ugt1*$^{-/-}$ animals. I can be speculated that MNC had no effect in reducing *MRC2* activation, as observed in a rat model of depression in which MNC does not affect this gene up-regulation (Burke et al., 2014). Interestingly, MNC had no effect on M2 expression in the ALS mouse model mentioned above, since M2 markers up-regulation is found in both MNC-treated and untreated mice (Kobayashi et al., 2013). However, neonatal hyperbilirubinemia and ALS greatly differ by their onset during life. This feature might reflect the different effects of MNC on M2 microglia regulation and, consequentially, the outcome of treated mice.

MNC effect on microglia is still controversial. Liu and colleagues showed that, although MNC protects neuronal precursor cell cultures from LPS-activated microglia toxic effects, it also suppresses the differentiation toward neurons, being toxic to neuronal undifferentiated cell types at high concentration (Liu et al., 2013). Once again, the time of administration appears crucial for the disease outcome. For example, in an ALS mouse model, the markers of glia activation are not increased after pre-symptomatic administration of MNC. Conversely, post-symptomatic drug treatment triggers a further up-regulation of the already activated astrocytes and microglia, exacerbating the course of the disease (Keller et al., 2011). Hence, further studies are needed to elucidate the mechanism of MNC on microglia polarization.

4.3.8 Markers of inflammation

Among the molecular effectors of inflammation triggered by bilirubin, it was observed a dose-dependent reduction of many transcripts belonging to the

inflammatory pathway (e.g., *NFKβ*, *TNFα*, *MMPs*, *NOSs* and *TLR2*, Figure 49) after MNC administration.

To note, one of the most common examined marker of bilirubin-induced neuroinflammation is IL1β (Fernandes and Brites, 2009; Yueh et al., 2014). Unexpectedly, I was not able to clearly detect the mRNA of *IL1β* in the cerebellum of mice in the FVB/NJ strain (Figure 34). Thus, the role of IL18, another key cytokine belonging to the IL1 superfamily, was investigated. In contrast with other inflammatory markers, only *IL18* was up-regulated in the all MNC-treated *Ugt1*$^{-/-}$ mice. This observation is in line with results obtained in MNC-treated P7 rat pups after cerebral ischemia-reperfusion. In fact, 24h after the transient middle cerebral artery occlusion, MNC does not affect *IL18* levels in brain compared to PBS treated rat pups (Fox et al., 2005). In my study, the prolonged activation of *IL18* is of great importance, because its up-regulation could highlight other mechanisms involved in brain damage triggered by bilirubin.

NFKβ is one of the key markers involved in bilirubin-induced neuroinflammation. In fact, it was activated in MNC 1X-treated *Ugt1*$^{-/-}$ animals and effectively reduced to WT levels in MNC 4X-treated *Ugt1*$^{-/-}$ mice. A similar trend was also observed when MNC was administered to *in vitro* cultures of microglia cells stimulated with LPS (Kobayashi et al., 2013) and in an *in vivo* model of AD triggered by a diabetic metabolic disorder (Cai et al., 2011). In the context of bilirubin, different *in vitro* studies on inflammatory cells incubated with bilirubin revealed the contribution of NFKβ to the damage, both in astrocytes (Falcao et al., 2007; Fernandes et al., 2006, 2007b) and microglia (Silva et al., 2010b). Although modest, the reduction of *NFKβ* in MNC 4X-treated *Ugt1*$^{-/-}$ mice was significant and may contribute to their extended survival.

Neuron viability is particularly susceptible to TNFα (Oldreive and Doherty, 2010). As shown before in this study, the late expression of *TNFα* in untreated hyperbilirubinemic *Ugt1*$^{-/-}$ mice correlated with the disease severity (Figure 35). Importantly, a drastic reduction in *TNFα* expression was observed at P15 in MNC 4X-treated *Ugt1*$^{-/-}$ mice compared to MNC 1X-treated mutant mice. Likewise, MNC treatment attenuated *TNFα* overexpression in a wide variety of neurodegenerative conditions, like osmotic demyelination syndrome (Suzuki et al., 2010), hyperoxia (Scheuer et al., 2015), schizophrenia (Mattei et al., 2014), β-amyloid-related disorders (Cai et al., 2011) and epilepsy (Abraham et al., 2012). In addition, rat astrocytes cell cultures incubated with bilirubin show increased *TNFα* levels

(Fernandes et al., 2004, 2011). In light of the TNFα relevance in the context of bilirubin, I speculate that the enduring activation of *TNFα* may account, at least in part, for the percentage of MNC 4X-treated mutant mice not surviving the treatment. Also nitric oxide synthase (NOS) activation is considered as a major causative reason for the pathogenesis of neurodegenerative diseases (Yuste et al., 2015). Other experiments showed the activation of *neuronal NOS* (*nNOS*) in neuronal cell cultures incubated with bilirubin, which promotes cells dysfunction and death (Brito et al., 2010). The *inducible NOS* (*iNOS*) activation was shown to be up-regulated by bilirubin exposure in endothelial cell cultures (Mazzone et al., 2010), suggesting that regulation of NO production is important for cell viability. Although MNC is known to reduce NOS activation in microglia cells (Wu et al., 2002), even after prolonged exposure to high bilirubin levels it could not be observed the activation of *NOS*, regardless of being the inducible or neuronal NOS. It is reasonable to conclude that NO production is not a leading mechanism in bilirubin toxicity, at least in this animal model of neonatal hyperbilirubinemia.

The importance of TLR2 response was shown in the *Ugt1* conditional knockout mouse model, as deficiency of *TLR2* leads to the absence of neuroinflammatory response, resulting in premature death of hyperbilirubinemic animals (Yueh et al., 2014). In line with Yueh and colleagues, it was observed a 10- to 20-fold up-regulation of *TLR2* expression in mutant mice compared to WT animals at roughly similar developmental stages (P14 and P15, respectively). Conversely, untreated *Ugt1*$^{-/-}$ animals did not show *TLR2* up-regulation at any of the analysed time points (Figure 35B). Taken together, these data indicate that *TLR2* activation occurs over prolonged bilirubin levels. Pre-treatment with MNC of Balb/C mice receiving i.p. injections of LPS results in decreased *TLR2* expression (Henry et al., 2008). Accordingly, in my study the anti-inflammatory effect of MNC resulted in a 60% reduction of TLR2 expression in *Ugt1*$^{-/-}$ mice treated with the highest MNC dose. Interestingly, Hu and colleagues revealed the close connection between TLR2 and the matrix metalloproteinases (MMPs) pathway, as *in vivo* TLR2 deficiency attenuates the expression of microglia *MMPs*. The up-regulation of MMPs by TLR2 activation in *in vitro* glioma cells was reduced by MNC administration (Hu et al., 2014). As mentioned in the chapter 4.2.4, MMPs activation is an important mechanism involved in various neurodegenerative diseases, since they contribute to neuroinflammation (Yong et al., 2001). It was observed the dose-dependent reduction of *MMP2* and *MMP9* expression in MNC 4X-treated mutant animals, in

line with *in vivo* ischemic stroke rat model evidences, in which the gelatinolytic activity of MMPs is reduced by MNC (Machado et al., 2006). My observation, together with the aforementioned evidences, pointed to the relevance of the TLR2 pathway as a potential target to reduce neurodegenerative consequences.

Collectively, glia cells analysis and inflammatory markers investigation underscored that the reduction of the inflammatory response by MNC contributes to the amelioration of the lethal phenotype in *Ugt1*$^{-/-}$ mice. Since neurodegeneration and neuroinflammation are tightly connected and it is difficult to distinguish a specific pattern in a time-dependent manner, further efforts are needed to clarify whether the inhibition of gliosis exerted by MNC directly affects cell death or it is a consequence of the prevention of neurodegeneration.

4.3.9 Bilirubin alters anxiety but not activity parameters in MNC rescued animals

Since bilirubin affects cerebellar development, and the cerebellum is the organ responsible for movement and motor coordination, behaviours of rescued *Ugt1*$^{-/-}$ animals were tested. However, untreated mutant mice did not survive over P14, thus the “untreated” control to compare *Ugt1*$^{-/-}$ mice improvement by MNC treatment was missing.

Overall, the behaviour of MNC-treated mutant animals was similar to untreated WT animals. In particular, despite high levels of bilirubin and their consequences on brain morphology impairment (Figure 45C), the rotarod test showed that MNC-rescued *Ugt1*$^{-/-}$ animals performed as well as WT littermates (Figure 43). My results are in line with those observed in a mouse model of chronic cannabis exposure, which results in cerebellar dysfunction due to activation of neuroinflammatory players, thus affecting fine motor coordination (Cutando et al., 2013). Cutando and colleagues showed that MNC administration rescues motor coordination performance of mice affected by THC-induced cerebellar deficit (Cutando et al., 2013). These observations underline the relevance of MNC administration in the amelioration of cerebellar dysfunction.

Most of the parameters analysed in the OF test were similar to WT, confirming the results of MNC-treated *Ugt1*$^{-/-}$ mice on motor-coordination performance. In fact, activity parameters of treated *Ugt1*$^{-/-}$ mice (total travelled distance and number of

entries in the different zones of the arena, Figure 44A and 44B, respectively) were similar to those of treated and untreated WT mice. The rescuing potential of activity parameters was also evident in a mouse model of intracerebral haemorrhage. In fact, after surgery, total travelled distance of MNC-treated mice is similar to non-operated mice, and differs from mice treated with saline solution (Xue et al., 2010). The most evident differences in rescued *Ugt1*$^{-/-}$ mice were shown in anxiety parameters compared to both treated and untreated WT. Different number of rearing events and stools production indicated an alteration in exploratory behaviour and fear (Figure 44E and 44F). These results are in line with works performed on hyperbilirubinemic Gunn rats by Liaury, suggesting that bilirubin-induced glia activation may promote cognitive impairment and anxiety features (Liaury et al., 2012, 2014). A further indication to explain different anxiety behaviours could come from what observed in the earlier analysed time point. In fact, at P8 GFAP protein (Figure 48A) and Iba1 mRNA levels (Figure 49A) in the cerebellum were similar to hyperbilirubinemic untreated *Ugt1*$^{-/-}$ animals, suggesting that MNC needs time to establish its anti-inflammatory properties. Thus, differences in the anxiety behaviours of rescued *Ugt1*$^{-/-}$ animals may be related to this incomplete protection from neuroinflammation during the first days after birth. Beside these analysed parameters, further experiments will be required to better determine the causes of the behavioural impairment of MNC-treated *Ugt1*$^{-/-}$ survivors.

4.3.10 Effects of MNC on oxidative and ER stress

Gene expression analysis of oxidative stress markers in treated mutant mice revealed that most of them were increased upon the treatment with the lowest dose of MNC and never reached the values of WT controls, even at the higher dose of MNC (such as *HO1*, *UPC2* and *ERO1L*, Figure 53), once again underscoring the importance of oxidative stress in the progression of the pathology.
Differently to what observed in the untreated *Ugt1*$^{-/-}$ animals at P5 (Figure 37A), *Nrf2* was not regulated by bilirubin or by MNC at P15 (Figure 53). The role of Nrf2 is usually associated to the increase in antioxidant defences to compensate oxidative stress, and MNC stimulates Nrf2 to promote protection, as demonstrated by Kuang and colleagues (Kuang et al., 2009). In fact, using an *in vitro* model of virus-induced neurodegeneration, they showed that MNC administration restores Nrf2 protein levels of infected primary astrocytes to the levels of uninfected ones. I speculate

that the contribution of *Nrf2* in the *Ugt1*$^{-/-}$ mouse model of neonatal hyperbilirubinemia could be minor or restricted only to the initial stages of the disease, while in later stages other players, such as HO1, are involved in the anti-oxidant response to bilirubin stress. In fact, expression analysis of *HO1* revealed an 8-fold increase in cerebella of MNC 1X-treated mutant mice, while these levels were reduced to 5-fold increase upon MNC 4X treatment compared to WT animals levels, showing an important trend of decreased activation. These data are in agreement with *in vivo* experiments performed in a rat model of PD induced by zinc administration (Kumar et al., 2015) and in a rat model of hepatic encephalopathy (Gamal et al., 2014), in which MNC reduces *HO1* expression levels. Taken together, these data indicates that MNC pleiotropic effect may involve also the attenuation of oxidative stress by decreasing the bilirubin-induced *HO1* activation.

As described in the section 3.2.6, ER stress is one of the initial events leading to cell impairment by the increase of its activation in parallel with disease progression (Figure 34), thus, contributing to the onset of BIND. The majority of ER stress markers were up-regulated in the mice treated with the lowest dose of MNC, indicating that ER stress is an important molecular mechanism accounting for bilirubin-induced toxicity. Although MNC treatment decreased the expression of some of the investigated ER stress related genes (Figure 50A), many others were not affected by MNC administration even at the highest dose (MNC 4X) (Figure 50B), underling the poor effect of the drug on the modulation of the ER stress pathway.

The MNC effect on ER stress is controversial. Depending on the context, MNC treatment resulted in different responses of the main ER stress effectors. In an *in vitro* model of PD, rat neuron cell cultures treated with paraquat showed a decreased expression of *CHOP* and *GRP78* when MNC is administered (Huang et al., 2012). On the contrary, Liu and colleagues showed both *in vitro* and *in vivo* that the MNC treatment of glioma cells results in the increased expression of the above-mentioned ER-stress related markers (Liu et al., 2013). Thus, as also suggested by Kyuhou and colleagues (Kyuhou et al., 2006), it can be speculated that ER stress is one of the key event leading to neurodegeneration, by its continuous neuron homeostasis impairment, and MNC has only a partial effect in the attenuation of this pathway.

4.3.11 MNC administration could open future therapeutic approaches for neonatal hyperbilirubinemia

MNC was shown to be effective as it partially rescued the lethal phenotype of FVB *Ugt1*$^{-/-}$ mice used in this study. In order to increase the efficiency of the therapy to treat the acute phase of hyperbilirubinemia, the combination of MNC administration (even at lower doses) with other therapies may represent a possible approach. Unfortunately, one of the side effect of MNC is the photo-sensibility (Kestel, 1981), thus a possible combination with PT to reduce bilirubin neurotoxicity is excluded.
A number of efforts have been made to design a modified version of MNC, trying to eliminate the antimicrobial activity, without losing the neuroprotective and anti-inflammatory properties. Regrettably, results are not striking. For example, the modified MNC 12S-hydroxy-1,12-pyrazolinomynocycline (PMIN) was shown to reduce lipid peroxidation, but no effect on BIND rescue was obtained, as observed in hyperbilirubinemic Gunn rats (Daood et al., 2012). In fact, despite PMIN has no antimicrobial activity, it was shown to be a non-chelating drug, lacking MMPs inhibitory activity (Lertvorachon et al., 2005). Furthermore, CMT-3 6-dimethyl-6-deoxy-4-de(dimethylamino) tetracycline, known as COL3, showed properties resembling the non-antimicrobial activity of MNC (Edan et al., 2013). Even though the beneficial features were replicated, also the undesired side effect of COL3 was photosensitivity, similarly to MNC. Thus, further efforts are needed to generate novel drugs owing higher specificity to target brain disease and fewer side effects.

Nonetheless, this set of experiments revealed that ER stress seems a predominant feature of hyperbilirubinemia. Thus, a drug owing wider potential effects may be more effective in acute condition to prevent BIND.

CONCLUSIONS

BIND and kernicterus are still a “silent” cause of significant neonatal morbidity and mortality in low- and middle-income countries, and a concern in western countries. The understanding of the mechanisms resulting in bilirubin neurotoxicity is essential to prevent brain damage and death of hyperbilirubinemic babies. In this Thesis, it was shown that bilirubin neurotoxicity is the result of concerted deregulation of different mechanisms. In fact, the *in vivo* time-course analysis revealed that neuroinflammation, ER and oxidative stress are activated at the onset of the pathology. Marked neuroinflammation coupled to neurodegeneration exacerbate the disease course, leading to mis-regulation of the autophagy pathway prior to death.

The use of MNC, a neuroprotector compound having anti-inflammatory properties, resulted in the partial rescue of the lethal phenotype by reducing neuronal cell death and decreasing neuroinflammation, revealing the prevalence of ER stress in bilirubin-induced neurological damage. However, the partial rescue of *Ugt1*$^{-/-}$ mice underscores the complexity of such multifaceted disease, supporting the concept that the combined administration of a neuroprotector compound with a drug able to attenuate ER stress may result in the complete prevention of BIND.

In addition, I contributed to clarify the potential of HSA administration in reducing bilirubin neurotoxicity and mortality during the neonatal period. In this work, I showed that plasma Bf is the most accurate clinical parameter to indicate bilirubin neurotoxicity, as it strongly correlates with UCB accumulation in the brain of hyperbilirubinemic mice. Furthermore, it was demonstrated that repeated albumin administration, as the sole therapy, prevented bilirubin accumulation in the brain tissue, resulting in the absence of brain abnormalities and the complete rescue of the lethal phenotype. HSA could be a valid therapeutic alternative to the unresponsive and acute cases of hyperbilirubinemia, to avoid or delay ET.

BIBLIOGRAPHY

Abraham, J., Fox, P.D., Condello, C., Bartolini, A., and Koh, S. (2012). Minocycline attenuates microglia activation and blocks the long-term epileptogenic effects of early-life seizures. Neurobiol. Dis. *46*, 425–430.

Ahlfors, C.E. (1994). Criteria for exchange transfusion in jaundiced newborns. Pediatrics *93*, 488–494.

Ahlfors, C.E. (2000). Unbound bilirubin associated with kernicterus: a historical approach. J. Pediatr. *137*, 540–544.

Ahlfors, C.E., and Parker, A.E. (2008). Unbound bilirubin concentration is associated with abnormal automated auditory brainstem response for jaundiced newborns. Pediatrics *121*, 976–978.

Ahlfors, C.E., Marshall, G.D., Wolcott, D.K., Olson, D.C., and Van Overmeire, B. (2006). Measurement of unbound bilirubin by the peroxidase test using Zone Fluidics. Clin. Chim. Acta. *365*, 78–85.

American Academy of Pediatrics (2004). Managment of Hyperbilirubinemia in the newborns infant 35 or more weeks of gestation. Pediatrics *114*, 297–316.

Amin, S.B., Ahlfors, C., Orlando, M.S., Dalzell, L.E., Merle, K.S., and Guillet, R. (2001). Bilirubin and serial auditory brainstem responses in premature infants. Pediatrics *107*, 664–670.

Andersen, J.T., Daba, M.B., Berntzen, G., Michaelsen, T.E., and Sandlie, I. (2010). Cross-species binding analyses of mouse and human neonatal Fc receptor show dramatic differences in immunoglobulin G and albumin binding. J. Biol. Chem. *285*, 4826–4836.

Ardakani, S.B., Dana, V.G., Ziaee, V., Ashtiani, M.-T.H., Djavid, G.E., and Alijani, M. (2011). Bilirubin/Albumin Ratio for Predicting Acute Bilirubin-induced Neurologic Dysfunction. Iran. J. Pediatr. *21*, 28–32.

Argikar, U.A., Senekeo-Effenberger, K., Larson, E.E., Tukey, R.H., and Remmel, R.P. (2009). Studies on induction of lamotrigine metabolism in transgenic UGT1 mice. Xenobiotica. *39*, 826–835.

Arias, I.M. (1962). Chronic unconjugated hyperbilirubinemia without overt signs of hemolysis in adolescents and adults. J. Clin. Invest. *41*, 2233–2245.

Arias, I.M., Gartner, L.M., Seifter, S., and Furman, M. (1964). Prolonged Neonatal Unconjugated Hyperbilirubinemia Associated with Breast Feeding and a Steroid, Pregnane-3 (Alpha), 20 (Beta)-Diol, in Maternal Milk That Inhibits Glucuronide Formation In Vitro*. J. Clin. Invest. *43*, 2037–2047.

B'Chir, W., Maurin, A.C., Carraro, V., Averous, J., Jousse, C., Muranishi, Y., Parry, L., Stepien, G., Fafournoux, P., and Bruhat, A. (2013). The eIF2α/ATF4 pathway is essential for stress-induced autophagy gene expression. Nucleic Acids Res. *41*, 7683–7699.

Barateiro, A., Vaz, A.R., Silva, S.L., Fernandes, A., and Brites, D. (2012). ER

stress, mitochondrial dysfunction and calpain/jnk activation are involved in oligodendrocyte precursor cell death by unconjugated bilirubin. NeuroMolecular Med. *14*, 285–302.

Barateiro, A., Miron, V.E., Santos, S.D., Relvas, J.B., Fernandes, A., Ffrench-Constant, C., and Brites, D. (2013). Unconjugated bilirubin restricts oligodendrocyte differentiation and axonal myelination. Mol. Neurobiol. *47*, 632–644.

Barateiro, A., Chen, S., Yueh, M.-F., Fernandes, A., Domingues, H.S., Relvas, J., Barbier, O., Nguyen, N., Tukey, R.H., and Brites, D. (2016). Reduced Myelination and Increased Glia Reactivity Resulting from Severe Neonatal Hyperbilirubinemia. Mol. Pharmacol. *89*, 84–93.

Bhutani, V.K., and Wong, R.J. (2013). Bilirubin neurotoxicity in preterm infants: risk and prevention. J. Clin. Neonatol. *2*, 61–69.

Bhutani, V.K., Zipursky, A., Blencowe, H., Khanna, R., Sgro, M., Ebbesen, F., Bell, J., Mori, R., Slusher, T.M., Fahmy, N., et al. (2013). Neonatal hyperbilirubinemia and Rhesus disease of the newborn: incidence and impairment estimates for 2010 at regional and global levels. Pediatr. Res. *74 Suppl 1*, 86–100.

Biran, V., Verney, C., and Ferriero, D.M. (2012). Perinatal cerebellar injury in human and animal models. Neurol. Res. Int. *2012*, 858929.

Birben, E., Sahiner, U.M., Sackesen, C., Erzurum, S., and Kalayci, O. (2012). Oxidative stress and antioxidant defense. World Allergy Organ. J. *5*, 9–19.

Bortolussi, G., Zentilin, L., Baj, G., Giraudi, P., Bellarosa, C., Giacca, M., Tiribelli, C., and Muro, A.F. (2012). Rescue of bilirubin-induced neonatal lethality in a mouse model of Crigler-Najjar syndrome type I by AAV9-mediated gene transfer. FASEB J. *26*, 1052–1063.

Bortolussi, G., Baj, G., Vodret, S., Viviani, G., Bittolo, T., and Muro, A.F. (2014). Age-dependent pattern of cerebellar susceptibility to bilirubin neurotoxicity in vivo. Dis. Model. Mech. 1057–1068.

Bortolussi, G., Codarin, E., Antoniali, G., Vascotto, C., Vodret, S., Arena, S., Cesaratto, L., Scaloni, A., Tell, G., and Muro, a F. (2015). Impairment of enzymatic antioxidant defenses is associated with bilirubin-induced neuronal cell death in the cerebellum of Ugt1 KO mice. Cell Death Dis. *6*, e1739.

Bosma, P.J. (2003). Inherited disorders of bilirubin metabolism. J. Hepatol. *38*, 107–117.

Bosma, P.J., Seppen, J., Goldhoorn, B., Bakker, C., Oude Elferink, R.P., Chowdhury, J.R., Chowdhury, N.R., and Jansen, P.L. (1994). Bilirubin UDP-glucuronosyltransferase 1 is the only relevant bilirubin glucuronidating isoform in man. J. Biol. Chem. *269*, 17960–17964.

Bossaller, L., Chiang, P.-I., Schmidt-Lauber, C., Ganesan, S., Kaiser, W.J., Rathinam, V. a K., Mocarski, E.S., Subramanian, D., Green, D.R., Silverman, N., et al. (2012). Cutting edge: FAS (CD95) mediates noncanonical IL-1β and IL-18 maturation via caspase-8 in an RIP3-independent manner. J. Immunol. *189*,

5508–5512.

Bradford, M.M. (1976). A rapid and sensitive method for the quantitation of microgram quantities of protein utilizing the principle of protein-dye binding. Anal. Biochem. *72*, 248–254.

Brettschneider, J., Tredici, K. Del, Lee, V.M.-Y.Y., and Trojanowski, J.Q. (2015). Spreading of pathology in neurodegenerative diseases: a focus on human studies. Nat. Rev. Neurosci. *16*, 109–120.

Brites, D. (2011). Bilirubin Injury to Neurons and Glial Cells : New Players , Novel Targets , and Newer Insights. YSPER *35*, 114–120.

Brites, D. (2012). The evolving landscape of neurotoxicity by unconjugated bilirubin : role of glial cells and inflammation. Front. Pharmacol. *3*, 1–27.

Brito, M.A., Brites, D., and Butterfield, D.A. (2004). A link between hyperbilirubinemia, oxidative stress and injury to neocortical synaptosomes. Brain Res. *1026*, 33–43.

Brito, M.A., Rosa, A.I., Falc??o, A.S., Fernandes, A., Silva, R.F.M., Butterfield, D.A., and Brites, D. (2008a). Unconjugated bilirubin differentially affects the redox status of neuronal and astroglial cells. Neurobiol. Dis. *29*, 30–40.

Brito, M. a, Lima, S., Fernandes, A., Falcão, A.S., Silva, R.F.M., Butterfield, D.A., and Brites, D. (2008b). Bilirubin injury to neurons: contribution of oxidative stress and rescue by glycoursodeoxycholic acid. Neurotoxicology *29*, 259–269.

Brito, M. a, Vaz, A.R., Silva, S.L., Falcão, A.S., Fernandes, A., Silva, R.F.M., and Brites, D. (2010). N-methyl-aspartate receptor and neuronal nitric oxide synthase activation mediate bilirubin-induced neurotoxicity. Mol. Med. *16*, 372–380.

Buckley, D.B., and Klaassen, C.D. (2007). Tissue- and Gender-Specific mRNA Expression of UDP-Glucornosyltransferases (UGTs) in Mice. Drug Metab. Dispos. *35*, 121–127.

Buller, K.M., Carty, M.L., Reinebrant, H.E., and Wixey, J.A. (2008). Minocycline : A Neuroprotective Agent for Hypoxic-Ischemic Brain Injury in the Neonate ? J. Neurosci. Res. *608*, 599–608.

Burke, N.N., Kerr, D.M., Moriarty, O., Finn, D.P., and Roche, M. (2014). Minocycline modulates neuropathic pain behaviour and cortical M1-M2 microglial gene expression in a rat model of depression. Brain. Behav. Immun. *42*, 147–156.

Cai, Z., Zhao, Y., Yao, S., and Zhao, B. (2011). Increases in B-amyloid protein in the hippocampus caused by diabetic metabolic disorder are blocked by minocycline through inhibition of NF-kB pathway activation. Pharmacol. Reports *63*, 381–391.

Calligaris, R., Bellarosa, C., Foti, R., Roncaglia, P., Giraudi, P., Krmac, H., Tiribelli, C., and Gustincich, S. (2009). A transcriptome analysis identifies molecular effectors of unconjugated bilirubin in human neuroblastoma SH-SY5Y cells. BMC Genomics *10*, 543.

Cardoso, F.L., Kittel, A., Veszelka, S., Palmela, I., Toth, A., Brites, D., Deli, M.A.,

and Brito, M.A. (2012). Exposure to lipopolysaccharide and/or unconjugated bilirubin impair the integrity and function of brain microvascular endothelial cells. PLoS One *7*, 1–14.

Chan, G., and Schiff, D. (1976). Variance in albumin loading in exchange transfusions. J. Pediatr. *88*, 609–613.

Chaudhari, N., Talwar, P., Parimisetty, A., Lefebvre d'Hellencourt, C., and Ravanan, P. (2014). A molecular web: endoplasmic reticulum stress, inflammation, and oxidative stress. Front. Cell. Neurosci. *8*, 213.

Chaudhury, C., Mehnaz, S., Robinson, J.M., Hayton, W.L., Pearl, D.K., Roopenian, D.C., and Anderson, C.L. (2003). The major histocompatibility complex-related Fc receptor for IgG (FcRn) binds albumin and prolongs its lifespan. J. Exp. Med. *197*, 315–322.

Chauhan, A.K., Moretti, F.A., Iaconcig, A., Baralle, F.E., and Muro, A.F. (2005). Impaired motor coordination in mice lacking the EDA exon of the fibronectin gene. Behav. Brain Res. *161*, 31–38.

Chen, M., Ona, V.O., Li, M., Ferrante, R.J., Fink, K.B., Zhu, S., Bian, J., Guo, L., Farrell, L.A., Hersch, S.M., et al. (2000). Minocycline inhibits caspase-1 and caspase-3 expression and delays mortality in a transgenic mouse model of Huntington disease. Nat. Med. *6*, 797–801.

Chen, S., Yueh, M.-F., Bigo, C., Barbier, O., Wang, K., Karin, M., Nguyen, N., and Tukey, R.H. (2013). Intestinal glucuronidation protects against chemotherapy-induced toxicity by irinotecan (CPT-11). Proc. Natl. Acad. Sci. U. S. A. *110*, 19143–19148.

Cheng, S., Hou, J., Zhang, C., Xu, C., Wang, L., Zou, X., Yu, H., Shi, Y., Yin, Z., and Chen, G. (2015). Minocycline reduces neuroinflammation but does not ameliorate neuron loss in a mouse model of neurodegeneration. Sci. Rep. *5*, 10535.

Cho, H.-Y., Jedlicka, A.E., Reddy, S.P.M., Kensler, T.W., Yamamoto, M., Zhang, L.-Y., and Kleeberger, S.R. (2002). Role of NRF2 in protection against hyperoxic lung injury in mice. Am. J. Respir. Cell Mol. Biol. *26*, 175–182.

Chowdhury, J.R., Kondapalli, R., and Chowdhury, N.R. (1993). Gunn rat: a model for inherited deficiency of bilirubin glucuronidation. Adv. Vet. Sci. Comp. Med. *37*, 149–173.

Conlee, J.W., and Shapiro, S.M. (1997). Development of cerebellar hypoplasia in jaundiced Gunn rats: a quantitative light microscopic analysis. Acta Neuropathol. *93*, 450–460.

Connolly, A.M., and Volpe, J.J. (1990). Clinical features of bilirubin encephalopathy. Clin. Perinatol. *17*, 371–379.

Coughtrie, M.W., Burchell, B., Leakey, J.E., and Hume, R. (1988). The inadequacy of perinatal glucuronidation: immunoblot analysis of the developmental expression of individual UDP-glucuronosyltransferase isoenzymes in rat and human liver microsomes. Mol. Pharmacol. *34*, 729–735.

Crigler, J.F., and Najjar, V.A. (1952). Congenital familial nonhemolytic jaundice with kernicterus. Pediatrics *10*, 169–180.

Cuperus, F.J.C., Hafkamp, A.M., Havinga, R., Vitek, L., Zelenka, J., Tiribelli, C., Ostrow, J.D., and Verkade, H.J. (2009). Effective treatment of unconjugated hyperbilirubinemia with oral bile salts in Gunn rats. Gastroenterology *136*, 673–82.e1.

Cuperus, F.J.C., Schreuder, A.B., Imhoff, D.E. Van, Vitek, L., Vanikova, J., Konickova, R., Ahlfors, C.E., Hulzebos, C. V, and Verkade, H.J. (2013). Beyond plasma bilirubin : The effects of phototherapy and albumin on brain bilirubin levels in Gunn rats. J. Hepatol. *58*, 134–140.

Cutando, L., Busquets-Garcia, A., Puighermanal, E., Gomis-Gonz??lez, M., Delgado-Garc??a, J.M., Gruart, A., Maldonado, R., and Ozaita, A. (2013). Microglial activation underlies cerebellar deficits produced by repeated cannabis exposure. J. Clin. Invest. *123*, 2816–2831.

Daood, M.J., Hoyson, M., and Watchko, J.F. (2012). Lipid peroxidation is not the primary mechanism of bilirubin-induced neurologic dysfunction in jaundiced Gunn rat pups. Pediatr. Res. *72*, 455–459.

Davutoğlu, M., Garipardiç, M., Güler, E., Karabiber, H., and Erhan, D. (2010). The etiology of severe neonatal hyperbilirubinemia and complications of exchange transfusion. Turk. J. Pediatr. *52*, 163–166.

Dennery, P.A., Seidman, D.S., and Stevenson, D.K. (2001). Neonatal hyperbilirubinemia. N. Engl. J. Med. *344*, 581–590.

Domitrovi, R., Jakovac, H., Tomac, J., and Ivana, Š. (2009). Liver fi brosis in mice induced by carbon tetrachloride and its reversion by luteolin. *241*, 311–321.

Doyle, K.M., Kennedy, D., Gorman, A.M., Gupta, S., Healy, S.J.M., and Samali, A. (2011). Unfolded proteins and endoplasmic reticulum stress in neurodegenerative disorders. J. Cell. Mol. Med. *15*, 2025–2039.

Edan, R.A., Luqmani, Y. a, and Masocha, W. (2013). COL-3, a Chemically Modified Tetracycline, Inhibits Lipopolysaccharide-Induced Microglia Activation and Cytokine Expression in the Brain. PLoS One *8*, e57827.

Ekshyyan, O., and Aw, T.Y. (2004). Apoptosis: a key in neurodegenerative disorders. Curr. Neurovasc. Res. *1*, 355–371.

Erlinger, S., Arias, I.M., and Dhumeaux, D. (2014). Inherited disorders of bilirubin transport and conjugation: new insights into molecular mechanisms and consequences. Gastroenterology *146*, 1625–1638.

Escobar, G.J., Greene, J.D., Hulac, P., Kincannon, E., Bischoff, K., Gardner, M.N., Armstrong, M. a, and France, E.K. (2005). Rehospitalisation after birth hospitalisation: patterns among infants of all gestations. Arch. Dis. Child. *90*, 125–131.

Fagan, S.C., Edwards, D.J., Borlongan, C. V., Xu, L., Arora, A., Feuerstein, G., and Hess, D.C. (2004). Optimal delivery of minocycline to the brain: Implication for

human studies of acute neuroprotection. Exp. Neurol. *186*, 248–251.

Fagiuoli, S., Daina, E., D'Antiga, L., Colledan, M., and Remuzzi, G. (2013). Monogenic diseases that can be cured by liver transplantation. J. Hepatol. *59*, 595–612.

Falcao, A.S., Silva, R.F.M., Fernandes, A., Brito, M.A., and Brites, D. (2007). Influence of hypoxia and ischemia preconditioning on bilirubin damage to astrocytes. Brain Res. *1149*, 191–199.

Falcao, A.S., Silva, R.F.M., Vaz, A.R., Silva, S.L., Fernandes, A., and Brites, D. (2013). Cross-talk between neurons and astrocytes in response to bilirubin: Early beneficial effects. Neurochem. Res. *38*, 644–659.

Falcao, A.S., Silva, R.F.M., Vaz, A.R., Gomes, C., Fernandes, A., Barateiro, A., Tiribelli, C., and Brites, D. (2014). Cross-talk between neurons and astrocytes in response to bilirubin: Adverse secondary impacts. Neurotox. Res. *26*, 1–15.

Falcão, A.S., Silva, R.F.M., Pancadas, S., Fernandes, A., Brito, M. a, and Brites, D. (2007). Apoptosis and impairment of neurite network by short exposure of immature rat cortical neurons to unconjugated bilirubin increase with cell differentiation and are additionally enhanced by an inflammatory stimulus. J. Neurosci. Res. *85*, 1229–1239.

Falcão, A.S., Silva, R.F.M., Vaz, A.R., Gomes, C., Fernandes, A., Barateiro, A., Tiribelli, C., and Brites, D. (2014). Cross-talk between neurons and astrocytes in response to bilirubin: adverse secondary impacts. Neurotox. Res. *26*, 1–15.

Fan, L.-W., Pang, Y., Lin, S., Rhodes, P.G., and Cai, Z. (2005). Minocycline attenuates lipopolysaccharide-induced white matter injury in the neonatal rat brain. Neuroscience *133*, 159–168.

Fanali, G., Trezza, V., Marino, M., Fasano, M., and Ascenzi, P. (2012). Human serum albumin : From bench to bedside. Mol. Aspects Med. *33*, 209–290.

Federico, A., Cardaioli, E., Da Pozzo, P., Formichi, P., Gallus, G.N., and Radi, E. (2012). Mitochondria, oxidative stress and neurodegeneration. J. Neurol. Sci. *322*, 254–262.

Felderhoff-Mueser, U., Schmidt, O.I., Oberholzer, A., Bührer, C., and Stahel, P.F. (2005). IL-18: A key player in neuroinflammation and neurodegeneration? Trends Neurosci. *28*, 487–493.

Fernandes, A., and Brites, D. (2009). Contribution of inflammatory processes to nerve cell toxicity by bilirubin and efficacy of potential therapeutic agents. Curr. Pharm. Des. *15*, 2915–2926.

Fernandes, A., Silva, R.F.M., Falcao, A.S., Brito, M.A., and Brites, D. (2004). Cytokine production, glutamate release and cell death in rat cultured astrocytes treated with unconjugated bilirubin and LPS. J. Neuroimmunol. *153*, 64–75.

Fernandes, A., Falcao, A.S., Silva, R.F.M., Gordo, A.C., Gama, M.J., Brito, M.A., and Brites, D. (2006). Inflammatory signalling pathways involved in astroglial activation by unconjugated bilirubin. J. Neurochem. *96*, 1667–1679.

Fernandes, A., Falcao, A.S., Silva, R.F.M., Brito, M.A., and Brites, D. (2007a). MAPKs are key players in mediating cytokine release and cell death induced by unconjugated bilirubin in cultured rat cortical astrocytes. Eur. J. Neurosci. *25*, 1058–1068.

Fernandes, A., Falcão, A.S., Silva, R.F.M., Brito, M. a., and Brites, D. (2007b). MAPKs are key players in mediating cytokine release and cell death induced by unconjugated bilirubin in cultured rat cortical astrocytes. Eur. J. Neurosci. *25*, 1058–1068.

Fernandes, A., Falc??o, A.S., Abranches, E., Bekman, E., Henrique, D., Lanier, L.M., and Brites, D. (2009). Bilirubin as a determinant for altered neurogenesis, neuritogenesis, and synaptogenesis. Dev. Neurobiol. *69*, 568–582.

Fernandes, A., Barateiro, A., Sofia, A.N.A., Ao, F., Silva, S.L., Vaz, A.N.A.R., Brito, M.A., Fernando, R.U.I., Silva, M., and Brites, D. (2011). Astrocyte Reactivity to Unconjugated Bilirubin Requires TNF- a and IL-1 b Receptor Signaling Pathways. *25*, 14–25.

Fine, E.J., Ionita, C.C., and Lohr, L. (2002). The history of the development of the cerebellar examination. Semin. Neurol. *22*, 375–384.

Fischer, R., and Maier, O. (2015). Interrelation of Oxidative Stress and Inflammation in Neurodegenerative Disease : Role of TNF. Oxid. Med. Cell. Longev. 1–18.

Fisher, M.B., Paine, M.F., Strelevitz, T.J., and Wrighton, S.A. (2001). The role of hepatic and extrahepatic UDP-glucuronosyltransferases in human drug metabolism. Drug Metab. Rev. *33*, 273–297.

Fonnum, F., and Lock, E. a (2000). Cerebellum as a target for toxic substances. Toxicol. Lett. *112–113*, 9–16.

Fox, C., Dingman, A., Derugin, N., Wendland, M.F., Manabat, C., Ji, S., Ferriero, D.M., and Vexler, Z.S. (2005). Minocycline confers early but transient protection in the immature brain following focal cerebral ischemia-reperfusion. J. Cereb. Blood Flow Metab. *25*, 1138–1149.

Frank-Cannon, T.C., Alto, L.T., McAlpine, F.E., and Tansey, M.G. (2009). Does neuroinflammation fan the flame in neurodegenerative diseases? Mol. Neurodegener. *4*, 47.

Fujiwara, R., Nguyen, N., Chen, S., and Tukey, R.H. (2010). Developmental hyperbilirubinemia and CNS toxicity in mice humanized with the UDP glucuronosyltransferase 1 (UGT1) locus. Proc. Natl. Acad. Sci. U. S. A. *107*, 5024–5029.

Fujiwara, R., Chen, S., Karin, M., and Tukey, R.H. (2012). Reduced Expression of UGT1A1 in Intestines of Humanized UGT1 Mice via Inactivation of NF-κB Leads to Hyperbilirubinemia. Gastroenterology *1*, 109–118.

Gamal, M., Abdel Wahab, Z., Eshra, M., Rashed, L., and Sharawy, N. (2014). Comparative neuroprotective effects of dexamethasone and minocycline during hepatic encephalopathy. Neurol. Res. Int. *2014*.

Gamaleldin, R., Iskander, I., Seoud, I., Aboraya, H., Aravkin, A., Sampson, P.D., and Wennberg, R.P. (2011). Risk factors for neurotoxicity in newborns with severe neonatal hyperbilirubinemia. Pediatrics *128*, e925-31.

Gao, X., Yang, X., and Zhang, B. (2011). Neuroprotection of taurine against bilirubin-induced elevation of apoptosis and intracellular free calcium ion in vivo. Toxicol. Mech. Methods *21*, 383–387.

Geiger, A.S., Rice, A.C., and Shapiro, S.M. (2007). Minocycline blocks acute bilirubin-induced neurological dysfunction in jaundiced Gunn rats. Neonatology *92*, 219–226.

Giraudi, P.J., Bellarosa, C., Coda-Zabetta, C.D., Peruzzo, P., and Tiribelli, C. (2011). Functional induction of the cystine-glutamate exchanger system X c- activity in SH-SY5Y cells by unconjugated bilirubin. PLoS One *6*.

Giudice, A., Arra, C., and Turco, M.C. (2010). Review of molecular mechanisms involved in the activation of the Nrf2-ARE signaling pathway by chemopreventive agents. Methods Mol. Biol. *647*, 37–74.

Gong, Q.H., Cho, J.W., Huang, T., Potter, C., Gholami, N., Basu, N.K., Kubota, S., Carvalho, S., Pennington, M.W., Owens, I.S., et al. (2001). Thirteen UDPglucuronosyltransferase genes are encoded at the human UGT1 gene complex locus. Pharmacogenetics *11*, 357–368.

Gordo, A.C., Falca, A.S., Fernandes, A., Brito, M.A., Silva, R.F.M., and Brites, D. (2006). Unconjugated Bilirubin Activates and Damages Microglia. *201*, 194–201.

Greco, C., Arnolda, G., Boo, N.-Y., Iskander, I.F., Okolo, A.A., Rohsiswatmo, R., Shapiro, S.M., Watchko, J., Wennberg, R.P., Tiribelli, C., et al. (2016). Neonatal Jaundice in Low- and Middle-Income Countries: Lessons and Future Directions from the 2015 Don Ostrow Trieste Yellow Retreat. Neonatology 172–180.

Greissman, A., Silver, P., Nimkoff, L., and Sagy, M. (1996). Albumin bolus administration versus continuous infusion in critically ill hypoalbuminemic pediatric patients. Intensive Care Med. *22*, 495–499.

Grieco, J.C., Ciarlone, S.L., Gieron-Korthals, M., Schoenberg, M.R., Smith, A.G., Philpot, R.M., Heussler, H.S., Banko, J.L., and Weeber, E.J. (2014). An open-label pilot trial of minocycline in children as a treatment for Angelman syndrome. BMC Neurol. *14*, 232.

Grojean, S., Lievre, V., Koziel, V., Vert, P., and Daval, J.L. (2001). Bilirubin exerts additional toxic effects in hypoxic cultured neurons from the developing rat brain by the recruitment of glutamate neurotoxicity. Pediatr. Res. *49*, 507–513.

Gunn, C.H. (1938). Hereditary acholuric jaundice in a New Mutant Strain of Rats. J. Hered. 137–139.

Hafkamp, A.M., Havinga, R., Sinaasappel, M., and Verkade, H.J. (2005). Effective oral treatment of unconjugated hyperbilirubinemia in Gunn rats. Hepatology *41*, 526–534.

Hafkamp, A.M., Nelisse-Haak, R., Sinaasappel, M., Oude Elferink, R.P.J., and

Verkade, H.J. (2007). Orlistat treatment of unconjugated hyperbilirubinemia in Crigler-Najjar disease: a randomized controlled trial. Pediatr. Res. *62*, 725–730.

Harvey, B.K., Richie, C.T., Hoffer, B.J., and Airavaara, M. (2012). Transgenic animal models of neurodegeneration based on human genetic studies. J. Neural Transm. *118*, 27–45.

Haustein, M.D., Read, D.J., Steinert, J.R., Pilati, N., Dinsdale, D., and Forsythe, I.D. (2010). Acute hyperbilirubinaemia induces presynaptic neurodegeneration at a central glutamatergic synapse. J. Physiol. *588*, 4683–4693.

Henry, C.J., Huang, Y., Wynne, A., Hanke, M., Himler, J., Bailey, M.T., Sheridan, J.F., and Godbout, J.P. (2008). Minocycline attenuates lipopolysaccharide (LPS)-induced neuroinflammation, sickness behavior, and anhedonia. J. Neuroinflammation *5*, 15.

Hinwood, M., Morandini, J., Day, T.A., and Walker, F.R. (2012). Evidence that microglia mediate the neurobiological effects of chronic psychological stress on the medial prefrontal cortex. Cereb. Cortex *22*, 1442–1454.

Hosono, S., Ohno, T., Kimoto, H., Nagoshi, R.E.N., Neonatology, D., and Children, S. (2001a). Effects of albumin infusion therapy on total and unbound bilirubin values in term infants with intensive phototherapy. 8–11.

Hosono, S., Ohno, T., Kimoto, H., Nagoshi, R., Shimizu, M., and Nozawa, M. (2001b). Effects of albumin infusion therapy on total and unbound bilirubin values in term infants with intensive phototherapy. Pediatr. Int. *43*, 8–11.

Hosono, S., Ohno, T., Kimoto, H., Nagoshi, R., Shimizu, M., Nozawa, M., and Harada, K. (2002). Follow-up study of auditory brainstem responses in infants with high unbound bilirubin levels treated with albumin infusion therapy. Pediatr. Int. *44*, 488–492.

Hsieh, C.L., Kim, C.C., Ryba, B.E., Niemi, E.C., Bando, J.K., Locksley, R.M., Liu, J., Nakamura, M.C., and Seaman, W.E. (2013). Traumatic brain injury induces macrophage subsets in the brain. Eur. J. Immunol. *43*, 2010–2022.

Hsieh, Y.-C., Athar, M., and Chaudry, I.H. (2009). When apoptosis meets autophagy: deciding cell fate after trauma and sepsis. Trends Mol. Med. *15*, 129–138.

Hu, F., Ku, M.C., Markovic, D., Dzaye, O.D., Lehnardt, S., Synowitz, M., Wolf, S.A., and Kettenmann, H. (2014). Glioma-associated microglial MMP9 expression is upregulated by TLR2 signaling and sensitive to minocycline. Int. J. Cancer *135*, 2569–2578.

Huang, C.L., Lee, Y.C., Yang, Y.C., Kuo, T.Y., and Huang, N.K. (2012). Minocycline prevents paraquat-induced cell death through attenuating endoplasmic reticulum stress and mitochondrial dysfunction. Toxicol. Lett. *209*, 203–210.

Huang, T.-Y., Chu, H.-C., Lin, Y.-L., Lin, C.-K., Hsieh, T.-Y., Chang, W.-K., Chao, Y.-C., and Liao, C.-L. (2009). Minocycline attenuates experimental colitis in mice by blocking expression of inducible nitric oxide synthase and matrix

metalloproteinases. Toxicol. Appl. Pharmacol. *237*, 69–82.

Huizing, K.M.N., Røislien, J., and Hansen, T.W.R. (2008). Intravenous immune globulin reduces the need for exchange transfusions in Rhesus and AB0 incompatibility. Acta Paediatr. Int. J. Paediatr. *97*, 1362–1365.

Hulzebos, C. V, Dijk, P.H., Imhoff, D.E. Van, Bos, A.F., Lopriore, E., Offringa, M., Ruiter, S.A.J., Braeckel, K.N.J.A. Van, Krabbe, P.F.M., Quik, E.H., et al. (2014). The Bilirubin Albumin Ratio in the Management of Hyperbilirubinemia in Preterm Infants to Improve Neurodevelopmental Outcome : A Randomized Controlled Trial – BARTrial. *9*, 1–7.

Ibekwe, R.C., Ibekwe, M.U., and Muoneke, V.U. (2012). Outcome of exchange blood transfusions done for neonatal jaundice in abakaliki, South eastern Nigeria. J. Clin. Neonatol. *1*, 34–37.

Ito, D., Imai, Y., Ohsawa, K., Nakajima, K., Fukuuchi, Y., and Kohsaka, S. (1998). Microglia-specific localisation of a novel calcium binding protein, Iba1. Mol. Brain Res. *57*, 1–9.

Iyanagi, T., Watanabe, T., and Uchiyama, Y. (1989). The 3-methylcholanthrene-inducible UDP-glucuronosyltransferase deficiency in the hyperbilirubinemic rat (Gunn rat) is caused by a -1 frameshift mutation. J. Biol. Chem. *264*, 21302–21307.

Jangi, S., Otterbein, L., and Robson, S. (2013). The molecular basis for the immunomodulatory activities of unconjugated bilirubin. Int. J. Biochem. Cell Biol. *45*, 2843–2851.

Jansen, P.L. (1999). Diagnosis and management of Crigler-Najjar syndrome. Eur. J. Pediatr. *158 Suppl*, S89-94.

Johnson, L., Sarmiento, F., Blanc, W.A., and Day, R. (1959). Kernicterus in rats with an inherited deficiency of glucuronyl transferase. AMA. J. Dis. Child. *97*, 591–608.

Kaplan, M., and Hammerman, C. (2005). Understanding severe hyperbilirubinemia and preventing kernicterus: adjuncts in the interpretation of neonatal serum bilirubin. Clin. Chim. Acta. *356*, 9–21.

Keino, H., and Kashiwamata, S. (1989). Critical period of bilirubin-induced cerebellar hypoplasia in a new Sprague-Dawley strain of jaundiced Gunn rats. Neurosci. Res. *6*, 209–215.

Keller, A.F., Gravel, M., and Kriz, J. (2011). Treatment with minocycline after disease onset alters astrocyte reactivity and increases microgliosis in SOD1 mutant mice. Exp. Neurol. *228*, 69–79.

Keshavan, P., Schwemberger, S.J., Smith, D.L.H., Babcock, G.F., and Zucker, S.D. (2004). Unconjugated bilirubin induces apoptosis in colon cancer cells by triggering mitochondrial depolarization. Int. J. Cancer *112*, 433–445.

Keshavan, P., Deem, T.L., Schwemberger, S.J., Babcock, G.F., Cook-Mills, J.M., and Zucker, S.D. (2005). Unconjugated Bilirubin Inhibits VCAM-1-Mediated

Transendothelial Leukocyte Migration. J. Immunol. *174*, 3709–3718.

Kestel, J.L. (1981). Photo-onycholysis from minocycline. Side effects of minocycline therapy. Cutis *28*, 53–54.

Kholmukhamedov, A., Czerny, C., Hu, J., Schwartz, J., Zhong, Z., and Lemasters, J.J. (2014). Minocycline and doxycycline, but not tetracycline, mitigate liver and kidney injury after hemorrhagic shock/resuscitation. Shock *42*, 256–263.

Kigerl, K.A., Gensel, J.C., Ankeny, D.P., Alexander, J.K., Donnelly, D.J., and Popovich, P.G. (2009). Identification of two distinct macrophage subsets with divergent effects causing either neurotoxicity or regeneration in the injured mouse spinal cord. J. Neurosci. *29*, 13435–13444.

Kim, H.-S., and Suh, Y.-H. (2009). Minocycline and neurodegenerative diseases. Behav. Brain Res. *196*, 168–179.

Kim, K.H., Jeong, J.Y., Surh, Y.J., and Kim, K.W. (2009). Expression of stress-response ATF3 is mediated by Nrf2 in astrocytes. Nucleic Acids Res. *38*, 48–59.

Klionsky, D.J., Abeliovich, H., Agostinis, P., Agrawal, D.K., Aliev, G., Askew, D.S., Baba, M., Baehrecke, E.H., Bahr, B.A., Ballabio, A., et al. (2009). Guidelines for the use and interpretation of assays for monitoring autophagy in higher eukaryotes. *4*, 151–175.

Kobayashi, K., Imagama, S., Ohgomori, T., Hirano, K., Uchimura, K., Sakamoto, K., Hirakawa, A., Takeuchi, H., Suzumura, A., Ishiguro, N., et al. (2013). Minocycline selectively inhibits M1 polarization of microglia. Cell Death Dis. *4*, e525.

Kuang, X., Scofield, V.L., Yan, M., Stoica, G., Liu, N., and Wong, P.K.Y. (2009). Attenuation of oxidative stress, inflammation and apoptosis by minocycline prevents retrovirus-induced neurodegeneration in mice. Brain Res. *1286*, 174–184.

Kuma, A., Hatano, M., Matsui, M., Yamamoto, A., Nakaya, H., Yoshimori, T., Ohsumi, Y., Tokuhisa, T., and Mizushima, N. (2004). The role of autophagy during the early neonatal starvation period. Nature *432*, 1032–1036.

Kumar, V., Singh, B.K., Chauhan, A.K., Singh, D., Patel, D.K., and Singh, C. (2015). Minocycline Rescues from Zinc-Induced Nigrostriatal Dopaminergic Neurodegeneration: Biochemical and Molecular Interventions. Mol. Neurobiol. *53*, 2761–2777.

Kyuhou, S., Kato, N., and Gemba, H. (2006). Emergence of endoplasmic reticulum stress and activated microglia in Purkinje cell degeneration mice. Neurosci. Lett. *396*, 91–96.

Lauer, B.J., and Spector, N.D. (2011). Hyperbilirubinemia in the newborn. Pediatr. Rev. *32*, 341–349.

Lertvorachon, J., Kim, J.P., Soldatov, D. V., Boyd, J., Roman, G., Sung, J.C., Popek, T., Jung, Y.S., Lau, P.C.K., and Konishi, Y. (2005). 1,12-Substituted tetracyclines as antioxidant agents. Bioorganic Med. Chem. *13*, 4627–4637.

Levine, B., and Yuan, J. (2005). Autophagy in cell death: an innocent convict? J. Clin. Invest. *115*, 2679–2688.

Li, Y., Guo, Y., Tang, J., Jiang, J., and Chen, Z. (2014). New insights into the roles of CHOP-induced apoptosis in ER stress Structure and Properties of C / EBP Homologous Protein Roles of CHOP in ER Stress-Mediated Apoptosis. *46*, 629–640.

Liaury, K., Miyaoka, T., Tsumori, T., Furuya, M., Wake, R., Ieda, M., Tsuchie, K., Taki, M., Ishihara, K., Tanra, A.J., et al. (2012). Morphological features of microglial cells in the hippocampal dentate gyrus of Gunn rat: a possible schizophrenia animal model. J. Neuroinflammation *9*, 56.

Liaury, K., Miyaoka, T., Tsumori, T., Furuya, M., Hashioka, S., Wake, R., Tsuchie, K., Fukushima, M., Limoa, E., Tanra, A.J., et al. (2014). Minocycline improves recognition memory and attenuates microglial activation in Gunn rat: A possible hyperbilirubinemia-induced animal model of schizophrenia. Prog. Neuro-Psychopharmacology Biol. Psychiatry *50*, 184–190.

Lin, S., Zhang, Y., Dodel, R., Farlow, M.R., Paul, S.M., and Du, Y. (2001). Minocycline blocks nitric oxide-induced neurotoxicity by inhibition p38 MAP kinase in rat cerebellar granule neurons. Neurosci. Lett. *315*, 61–64.

Lin, S., Yan, C., Wei, X., Paul, S.M., and Du, Y. (2003). p38 MAP kinase mediates bilirubin-induced neuronal death of cultured rat cerebellar granule neurons. Neurosci. Lett. *353*, 209–212.

Lin, S., Wei, X., Bales, K.R., Paul, A.B.C., Ma, Z., Yan, G., Paul, S.M., and Du, Y. (2005). Minocycline blocks bilirubin neurotoxicity and prevents hyperbilirubinemia-induced cerebellar hypoplasia in the Gunn rat. Eur. J. Neurosci. *22*, 21–27.

Liu, G., Su, L., Hao, X., Zhong, N., Zhong, D., Singhal, S., and Liu, X. (2012). Salermide up-regulates death receptor 5 expression through the ATF4-ATF3-CHOP axis and leads to apoptosis in human cancer cells. J. Cell. Mol. Med. *16*, 1618–1628.

Liu, X., Su, H., Chu, T.H., Guo, A., and Wu, W. (2013). Minocycline inhibited pro-apoptotic effect of microglia on neuronal progenitor cells and protected their neuronal differentiation in vitro - Liu.pdf. Neurosci. Lett. 30–36.

London, I.M.., West, R.., Shemin, D.., and Rittenberg, D. (1950). On the origin of bile pigment in normal man. J. Biol. Chem. *184*, 351–358.

Mabogunje, C.A., Olaifa, S.M., and Olusanya, B.O. (2016). Facility-based constraints to exchange transfusions for neonatal hyperbilirubinemia in resource-limited settings. World J. Clin. Pediatr. *5*, 182.

Macdonald, H., Kelly, R.G., Allen, E.S., Noble, J.F., and Kanegis, L.A. (1973). Pharmacokinetic studies on minocycline in man. Clin. Pharmacol. Ther. *14*, 852–861.

Machado, L.S., Kozak, A., Ergul, A., Hess, D.C., Borlongan, C. V, and Fagan, S.C. (2006). Delayed minocycline inhibits ischemia-activated matrix metalloproteinases 2 and 9 after experimental stroke. BMC Neurosci. *7*, 56.

Mackenzie, P.I., Gregory, P.A., Lewinsky, R.H., Yasmin, S.N., Height, T., McKinnon, R.A., and Gardner-Stephen, D.A. (2005). Polymorphic variations in the expression of the chemical detoxifying UDP glucuronosyltransferases. Toxicol. Appl. Pharmacol. *207*, 77–83.

Maisels, M.J., and McDonagh, A.F. (2008). Phototherapy for neonatal jaundice. N. Engl. J. Med. *358*, 920–928.

Maisels, M.J., Watchko, J.F., Bhutani, V.K., and Stevenson, D.K. (2012). An approach to the management of hyperbilirubinemia in the preterm infant less than 35 weeks of gestation. J. Perinatol. *32*, 660–664.

Maity, S., Nag, N., Chatterjee, S., Adhikari, S., and Mazumder, S. (2013). Bilirubin clearance and antioxidant activities of ethanol extract of Phyllanthus amarus root in phenylhydrazine-induced neonatal jaundice in mice. J. Physiol. Biochem. *69*, 467–476.

Martinez, F.O., Gordon, S., Locati, M., and Mantovani, A. (2006). Transcriptional Profiling of the Human Monocyte-to-Macrophage Differentiation and Polarization: New Molecules and Patterns of Gene Expression. J. Immunol. *177*, 7303–7311.

Mattei, D., Djodari-Irani, A., Hadar, R., Pelz, A., de Coss??o, L.F., Goetz, T., Matyash, M., Kettenmann, H., Winter, C., and Wolf, S.A. (2014). Minocycline rescues decrease in neurogenesis, increase in microglia cytokines and deficits in sensorimotor gating in an animal model of schizophrenia. Brain. Behav. Immun. *38*, 175–184.

Mazzone, G.L., Rigato, I., and Tiribelli, C. (2010). Unconjugated bilirubin modulates nitric oxide production via iNOS regulation. Biosci. Trends *4*, 244–248.

McDonagh, A.F., and Maisels, M.J. (2006). Bilirubin unbound: déjà vu all over again? Pediatrics *117*, 523–525.

Menalled, L.B., Patry, M., Ragland, N., Lowden, P.A.S., Goodman, J., Minnich, J., Zahasky, B., Park, L., Leeds, J., Howland, D., et al. (2010). Comprehensive behavioral testing in the R6/2 mouse model of Huntington's disease shows no benefit from CoQ10 or minocycline. PLoS One *5*.

Michell-Robinson, M.A., Touil, H., Healy, L.M., Owen, D.R., Durafourt, B.A., Bar-Or, A., Antel, J.P., and Moore, C.S. (2015). Roles of microglia in brain development, tissue maintenance and repair. Brain *138*, 1138–1159.

Mikoshiba, K., Kohsaka, S., Takamatsu, K., and Tsukada, Y. (1980). Cerebellar hypoplasia in the Gunn rat with hereditary hyperbilirubinemia: immunohistochemical and neurochemical studies. J. Neurochem. *35*, 1309–1318.

Mitra, S., Samanta, M., Sarkar, M., De, A.K., and Chatterjee, S. (2011). Pre-exchange 5% albumin infusion in low birth weight neonates with intensive phototherapy failure--a randomized controlled trial. J. Trop. Pediatr. *57*, 217–221.

Mizushima, N., Levine, B., Cuervo, A.M., and Klionsky, D.J. (2008). Autophagy fights disease through cellular self-digestion. Nature *451*, 1069–1075.

Moerschel, S.K., Cianciaruso, L.B., and Tracy, L.R. (2008). A practical approach to

neonatal jaundice. Am. Fam. Physician *77*, 1255–1262.

Morioka, I., Nakamura, H., Koda, T., Yokota, T., Okada, H., Katayama, Y., Kunikata, T., Kondo, M., Nakamura, M., Hosono, S., et al. (2015). Current incidence of clinical kernicterus in preterm infants in Japan. Pediatr. Int. *57*, 494–497.

Muchowski, K.E. (2014). Evaluation and treatment of neonatal hyperbilirubinemia. Am. Fam. Physician *89*, 873–878.

Newman, T.B., Liljestrand, P., and Escobar, G.J. (2003). Infants with bilirubin levels of 30 mg/dL or more in a large managed care organization. Pediatrics *111*, 1303–1311.

Nguyen, N., Bonzo, J. a, Chen, S., Chouinard, S., Kelner, M.J., Hardiman, G., Bélanger, A., and Tukey, R.H. (2008). Disruption of the ugt1 locus in mice resembles human Crigler-Najjar type I disease. J. Biol. Chem. *283*, 7901–7911.

Nguyen, T., Sherratt, P.J., and Pickett, C.B. (2003). Regulatory Mechanisms Controlling Gene Expression Mediated By the Antioxidant Response Element. Annu. Rev. Pharmacol. Toxicol. *43*, 233–260.

Nguyen, T., Nioi, P., and Pickett, C.B. (2009). The Nrf2-Antioxidant Response Element Signaling Pathway and Its Activation by Oxidative Stress. J. Biol. Chem. *284*, 13291–13295.

Oakes, G.H., and Bend, J.R. (2005). Early steps in bilirubin-mediated apoptosis in murine hepatoma (Hepa 1c1c7) cells are characterized by aryl hydrocarbon receptor-independent oxidative stress and activation of the mitochondrial pathway. J. Biochem. Mol. Toxicol. *19*, 244–255.

Oakes, G.H., and Bend, J.R. (2010). Global changes in gene regulation demonstrate that unconjugated bilirubin is able to upregulate and activate select components of the endoplasmic reticulum stress response pathway. J. Biochem. Mol. Toxicol. *24*, 73–88.

Oakes, S.A., and Papa, F.R. (2015). The role of endoplasmic reticulum stress in human pathology. Annu. Rev. Pathol. *10*, 173–194.

Odell, G.B. (1973). Influence of binding on the toxicity of bilirubin. Ann. N. Y. Acad. Sci. *226*, 225–237.

Oh, W., Stevenson, D.K., Tyson, J.E., Morris, B.H., Ahlfors, C.E., Bender, G.J., Wong, R.J., Perritt, R., Vohr, B.R., Van Meurs, K.P., et al. (2010). Influence of clinical status on the association between plasma total and unbound bilirubin and death or adverse neurodevelopmental outcomes in extremely low birth weight infants. Acta Paediatr *99*, 673–678.

Okumura, A., Kidokoro, H., Shoji, H., Nakazawa, T., Mimaki, M., Fujii, K., Oba, H., and Shimizu, T. (2009). Kernicterus in preterm infants. Pediatrics *123*, e1052-8.

Oldreive, C.E., and Doherty, G.H. (2010). Effects of tumour necrosis factor-alpha on developing cerebellar granule and Purkinje neurons in vitro. J. Mol. Neurosci. *42*, 44–52.

Olmos, G., and Llado, J. (2014). Tumor necrosis factor alpha: A link between neuroinflammation and excitotoxicity. Mediators Inflamm.

Olusanya, B.O., Ogunlesi, T.A., and Slusher, T.M. (2014). Why is kernicterus still a major cause of death and disability in low-income and middle-income countries? Arch. Dis. Child.

Ossola, B., Lantto, T.A., Puttonen, K.A., Tuominen, R.K., Raasmaja, A., and Männistö, P.T. (2012). Minocycline protects SH-SY5Y cells from 6-hydroxydopamine by inhibiting both caspase-dependent and -independent programmed cell death. J. Neurosci. Res. *90*, 682–690.

Ostrow, J.D., Mukerjee, P., and Tiribelli, C. (1994). Structure and binding of unconjugated bilirubin: relevance for physiological and pathophysiological function. J. Lipid Res. *35*, 1715–1737.

Ostrow, J.D., Pascolo, L., Brites, D., and Tiribelli, C. (2004). Molecular basis of bilirubin-induced neurotoxicity. Trends Mol. Med. *10*, 65–70.

Owa, J.A., Ogunlesi, T.A., and Ogunlesi, T.A. (2009). Why we are still doing so many exchange blood transfusion for neonatal jaundice in Nigeria. World J. Pediatr. *5*, 51–55.

Palmela, I., Sasaki, H., Cardoso, F.L., Moutinho, M., Kim, K.S., Brites, D., and Brito, M. a (2012). Time-dependent dual effects of high levels of unconjugated bilirubin on the human blood-brain barrier lining. Front. Cell. Neurosci. *6*, 22.

Peter, M.E., Hadji, A., Murmann, A.E., Brockway, S., Putzbach, W., Pattanayak, A., Ceppi, P., and Mhc-i, T.C.R.A. (2015). The role of CD95 and CD95 ligand in cancer. *22*, 549–559.

Petzold, A., Tisdall, M.M., Girbes, A.R., Martinian, L., Thom, M., Kitchen, N., and Smith, M. (2011). In vivo monitoring of neuronal loss in traumatic brain injury : a microdialysis study. 464–483.

Pinkernelle, J., Fansa, H., Ebmeyer, U., and Keilhoff, G. (2013). Prolonged Minocycline Treatment Impairs Motor Neuronal Survival and Glial Function in Organotypic Rat Spinal Cord Cultures. PLoS One *8*, 1–22.

Pizzi, M., and Spano, P. (2006). Distinct roles of diverse nuclear factor-κB complexes in neuropathological mechanisms. Eur. J. Pharmacol. *545*, 22–28.

Plane, J.M., Shen, Y., Pleasure, D.E., and Deng, W. (2010). Prospects for minocycline neuroprotection. Arch. Neurol. *67*, 1442–1448.

Poland, R.L. (2002). Preventing kernicterus: almost there. J. Pediatr. *140*, 385–386.

Qaisiya, M., Coda Zabetta, C.D., Bellarosa, C., and Tiribelli, C. (2014). Bilirubin mediated oxidative stress involves antioxidant response activation via Nrf2 pathway. Cell. Signal. *26*, 512–520.

Reichman, N.E., Teitler, J.O., Moullin, S., Ostfeld, B.M., and Hegyi, T. (2015). Late-preterm birth and neonatal morbidities: Population-level and within-family estimates. Ann. Epidemiol. *25*, 126–132.

Rice, A.C., and Shapiro, S.M. (2008). A new animal model of hemolytic hyperbilirubinemia-induced bilirubin encephalopathy (kernicterus). Pediatr. Res. *64*, 265–269.

Rice, A.C., Chiou, V.L., Zuckoff, S.B., and Shapiro, S.M. (2011). Profile of minocycline neuroprotection in bilirubin-induced auditory system dysfunction. Brain Res. *1368*, 290–298.

Ritter, J.K., Chen, F., Sheen, Y.Y., Tran, H.M., Kimura, S., Yeatman, M.T., and Owens, I.S. (1992). A novel complex locus UGT1 encodes human bilirubin, phenol, and other UDP-glucuronosyltransferase isozymes with identical carboxyl termini. J. Biol. Chem. *267*, 3257–3261.

Rodkey, F.L. (1965). Direct spectrophotometric determination of albumin in human serum. Clin. Chem. *11*, 478–487.

Rodrigues, C.M., Solá, S., Silva, R., and Brites, D. (2000). Bilirubin and amyloid-beta peptide induce cytochrome c release through mitochondrial membrane permeabilization. Mol. Med. *6*, 936–946.

Rodrigues, C.M.P., Solá, S., and Brites, D. (2002). Bilirubin induces apoptosis via the mitochondrial pathway in developing rat brain neurons. Hepatology *35*, 1186–1195.

Rose, A.L., and Wisniewski, H. (1959). Acute bilirubin encephalopathy induced with sulfadimethoxinein gunn rats. J. Neuropathol. Exp. Neurol. 165–189.

Rubinsztein, D.C., Ravikumar, B., Acevedo-Arozena, A., Imarisio, S., O'Kane, C.J., and Brown, S.D.M. (2005). Dyneins, autophagy, aggregation and neurodegeneration. Autophagy *1*, 177–178.

Ryan, M.E., and Ashley, R.A. (1998). How do tetracyclines work? Adv. Dent. Res. *12*, 149–151.

Sarnat, H.B., Nochlin, D., and Born, D.E. (1998). Neuronal nuclear antigen (NeuN): A marker of neuronal maturation in the early human fetal nervous system. Brain Dev. *20*, 88–94.

Scheuer, T., Brockmöller, V., Blanco Knowlton, M., Weitkamp, J.-H., Ruhwedel, T., Mueller, S., Endesfelder, S., Bührer, C., and Schmitz, T. (2015). Oligodendroglial maldevelopment in the cerebellum after postnatal hyperoxia and its prevention by minocycline. Glia *63*, 1825–1839.

Schreuder, A.B., Vanikova, J., Vitek, L., Havinga, R., Ahlfors, C.E., Hulzebos, C. V, and Verkade, H.J. (2013a). Optimizing Exchange Transfusion for Severe Unconjugated Hyperbilirubinemia : Studies in the Gunn Rat. PLoS One *8*, 1–6.

Schreuder, A.B., Rice, A.C., Vanikova, J., Vitek, L., Shapiro, S.M., and Verkade, H.J. (2013b). Albumin administration protects against bilirubin-induced auditory brainstem dysfunction in Gunn rat pups. 1557–1565.

Schulz, S., Wong, R.J., Vreman, H.J., and Stevenson, D.K. (2012). Metalloporphyrins - An update. Front. Pharmacol. *3 APR*, 1–16.

Scott, R.C., Juh??sz, G., and Neufeld, T.P. (2007). Direct Induction of Autophagy

by Atg1 Inhibits Cell Growth and Induces Apoptotic Cell Death. Curr. Biol. *17*, 1–11.

Shah, Z., Chawla, A., Patkar, D., and Pungaonkar, S. (2003). MRI in kernicterus. Australas. Radiol. *47*, 55–57.

Shahian, M., and Moslehi, M.A. (2010). Effect of albumin administration prior to exchange transfusion in term neonates with hyperbilirubinemia--a randomized controlled trial. Indian Pediatr. *47*, 241–244.

Shapiro, S.M. (2003). Bilirubin toxicity in the developing nervous system. Pediatr. Neurol. *29*, 410–421.

Shapiro, S.M. (2010). Chronic bilirubin encephalopathy: diagnosis and outcome. Semin. Fetal Neonatal Med. *15*, 157–163.

Shapiro, S.M., and Nakamura, H. (2001). Bilirubin and the Auditory System. J. Perinatol. 852–855.

Silva, R.F., Rodrigues, C.M., and Brites, D. (2001). Bilirubin-induced apoptosis in cultured rat neural cells is aggravated by chenodeoxycholic acid but prevented by ursodeoxycholic acid. J. Hepatol. *34*, 402–408.

Silva, S.L., Vaz, A.R., Barateiro, A., Falcão, A.S., Fernandes, A., Brito, M. a., Silva, R.F.M., and Brites, D. (2010a). Features of bilirubin-induced reactive microglia: From phagocytosis to inflammation. Neurobiol. Dis. *40*, 663–675.

Silva, S.L., Vaz, A.R., Barateiro, A., Falcão, A.S., Fernandes, A., Brito, M.A., Silva, R.F.M., and Brites, D. (2010b). Neurobiology of Disease Features of bilirubin-induced reactive microglia : From phagocytosis to in fl ammation. Neurobiol. Dis. *40*, 663–675.

Smith, K., and Leyden, J.J. (2005). Safety of doxycycline and minocycline: A systematic review. Clin. Ther. *27*, 1329–1342.

Smitherman, H., Stark, A.R., and Bhutani, V.K. (2006). Early recognition of neonatal hyperbilirubinemia and its emergent management. Semin. Fetal Neonatal Med. *11*, 214–224.

Sofroniew, M. V., and Vinters, H. V. (2010). Astrocytes: Biology and pathology. Acta Neuropathol. *119*, 7–35.

Song, S., Hu, Y., Gu, X., Si, F., and Hua, Z. (2014). A novel newborn rat kernicterus model created by injecting a bilirubin solution into the cisterna magna. PLoS One *9*, e96171.

Van De Steeg, E., Stránecký, V., Hartmannová, H., Nosková, L., Wagenaar, E., Esch, A. Van, Waart, D.R. De, Martin, H., Elferink, R.P.J.O., Kenworthy, K.E., et al. (2012). Complete OATP1B1 and OATP1B3 deficiency causes human Rotor syndrome by interrupting conjugated bilirubin reuptake into the liver. J. Clin. Invest. *122*, 519–528.

Stevenson, D.K., Wong, R.J., Vreman, H.J., McDonagh, A.F., Maisels, M.J., and Lightner, D.A. (2004). NICHD Conference on Kernicterus: Research on Prevention of Bilirubin-Induced Brain Injury and Kernicterus: Bench-to-Bedside--Diagnostic

Methods and Prevention and Treatment Strategies. J. Perinatol. *24*, 521–525.

Stirling, D.P., Koochesfahani, K.M., Steeves, J.D., and Tetzlaff, W. (2005). Minocycline as a neuroprotective agent. Neuroscientist *11*, 308–322.

Stocker, R., Yamamoto, Y., Mcdonagh, A.F., Glazer, A.N., and Ames, B.N. (1987). Bilirubin is an Antioxidant of Possible Physiological Importance Published by : American Association for the Advancement of Science Stable URL : http://www.jstor.org/stable/1698769 Accessed : 07-06-2016 09 : 41 UTC. *235*, 1043–1046.

Stoeckius, M., Erat, A., Fujikawa, T., Hiromura, M., Koulova, A., Otterbein, L., Bianchi, C., Tobiasch, E., Dagon, Y., Sellke, F.W., et al. (2012). Essential roles of Raf/extracellular signal-regulated kinase/mitogen-activated protein kinase pathway, YY1, and Ca2+ influx in growth arrest of human vascular smooth muscle cells by bilirubin. J. Biol. Chem. *287*, 15418–15426.

Sumida, K., Kawana, M., Kouno, E., Itoh, T., Takano, S., Narawa, T., Tukey, R.H., and Fujiwara, R. (2013). Importance of UDP-glucuronosyltransferase 1A1 expression in skin and its induction by UVB in neonatal hyperbilirubinemia. Mol. Pharmacol. *84*, 679–686.

Suzuki, H., Sugimura, Y., Iwama, S., Suzuki, H., Nobuaki, O., Nagasaki, H., Arima, H., Sawada, M., and Oiso, Y. (2010). Minocycline prevents osmotic demyelination syndrome by inhibiting the activation of microglia. J. Am. Soc. Nephrol. *21*, 2090–2098.

Tanida, I., Ueno, T., and Kominami, E. (2008). LC3 and Autophagy. Methods Mol. Biol. *445*, 77–88.

Tell, G., and Gustincich, S. (2009). Redox state, oxidative stress, and molecular mechanisms of protective and toxic effects of bilirubin on cells. Curr. Pharm. Des. *15*, 2908–2914.

Tersey, S.A., Nishiki, Y., Templin, A.T., Cabrera, S.M., Stull, N.D., Colvin, S.C., Evans-Molina, C., Rickus, J.L., Maier, B., and Mirmira, R.G. (2012). Islet β-cell endoplasmic reticulum stress precedes the onset of type 1 diabetes in the nonobese diabetic mouse model. Diabetes *61*, 818–827.

Uttara, B., Singh, A. V, Zamboni, P., and Mahajan, R.T. (2009). Oxidative stress and neurodegenerative diseases: a review of upstream and downstream antioxidant therapeutic options. Curr. Neuropharmacol. *7*, 65–74.

Vaz, A.R., Delgado-Esteban, M., Brito, M.A., Bolaños, J.P., Brites, D., and Almeida, A. (2010). Bilirubin selectively inhibits cytochrome c oxidase activity and induces apoptosis in immature cortical neurons: assessment of the protective effects of glycoursodeoxycholic acid. J. Neurochem. *112*, 56–65.

Vincent, J.L., Wilkes, M.M., and Navickis, R.J. (2003). Safety of human albumin - Serious adverse events reported worldwide in 1998-2000. Br. J. Anaesth. *91*, 625–630.

Vítek, L., and Carey, M.C. (2003). Enterohepatic cycling of bilirubin as a cause of “black” pigment gallstones in adult life. Eur. J. Clin. Invest. *33*, 799–810.

Wang, X., Zhu, S., Drozda, M., Zhang, W., Stavrovskaya, I.G., Cattaneo, E., Ferrante, R.J., Kristal, B.S., and Friedlander, R.M. (2003). Minocycline inhibits caspase-independent and -dependent mitochondrial cell death pathways in models of Huntington's disease. Proc. Natl. Acad. Sci. U. S. A. *100*, 10483–10487.

Watchko, J.F. (2006). Kernicterus and the Molecular Mechanisms of Bilirubin-Induced CNS Injury in Newborns. *8*.

Watchko, J.F., and Tiribelli, C. (2013). Bilirubin-induced neurologic damage--mechanisms and management approaches. N. Engl. J. Med. *369*, 2021–2030.

Wen, Y., Zhai, R.G., and Kim, M.D. (2013). The Role of Autophagy in Nmnat-Mediated Protection Against Hypoxia-Induced Dendrite Degeneration. 140–151.

Wennberg, R.P., and Hance, A.J. (1986). Experimental bilirubin encephalopathy: importance of total bilirubin, protein binding, and blood-brain barrier. Pediatr. Res. *20*, 789–792.

Wennberg, R.P., Ahlfors, C.E., and Rasmussen, L.F. (1979). The pathochemistry of kernicterus. Early Hum. Dev. *3*, 353–372.

Wennberg, R.P., Ahlfors, C.E., Bhutani, V.K., Johnson, L.H., and Shapiro, S.M. (2006). Toward understanding kernicterus: a challenge to improve the management of jaundiced newborns. Pediatrics *117*, 474–485.

Whitney, E.R., Kemper, T.L., Rosene, D.L., Bauman, M.L., and Blatt, G.J. (2008). Calbindin-D28k is a more reliable marker of human Purkinje cells than standard Nissl stains: A stereological experiment. J. Neurosci. Methods *168*, 42–47.

Wood, B., Comley, A., and Sherwell, J. (1970). Effect of additional albumin administration during exchange transfusion on plasma albumin-binding capacity. Arch. Dis. Child. *45*, 59–62.

Wu, D.C., Jackson-Lewis, V., Vila, M., Tieu, K., Teismann, P., Vadseth, C., Choi, D.-K., Ischiropoulos, H., and Przedborski, S. (2002). Blockade of microglial activation is neuroprotective in the 1-methyl-4-phenyl-1,2,3,6-tetrahydropyridine mouse model of Parkinson disease. J. Neurosci. *22*, 1763–1771.

Xue, M., Mikliaeva, E.I., Casha, S., Zygun, D., Demchuk, A., and Yong, V.W. (2010). Improving outcomes of neuroprotection by minocycline: guides from cell culture and intracerebral hemorrhage in mice. Am. J. Pathol. *176*, 1193–1202.

Yokota, T., Morioka, I., Kodera, T., Morisawa, T., Sato, I., Kawano, S., Koda, T., Matsuo, K., Fujioka, K., Morikawa, S., et al. (2013). Novel treatment strategy for Japanese newborns with high serum unbound bilirubin. Pediatr. Int. *55*, 54–59.

Yong, V.W., Power, C., Forsyth, P., and Edwards, D.R. (2001). Metalloproteinases in biology and pathology of the nervous system. Nat. Rev. Neurosci. *2*, 502–511.

Yong, V.W., Wells, J., Giuliani, F., Casha, S., Power, C., and Metz, L.M. (2004). Minocycline and neurological diseases The promise of minocycline in neurology. *3*, 744–751.

Yrjänheikki, J., Tikka, T., Keinänen, R., Goldsteins, G., Chan, P.H., and Koistinaho, J. (1999). A tetracycline derivative, minocycline, reduces inflammation

and protects against focal cerebral ischemia with a wide therapeutic window. Proc. Natl. Acad. Sci. U. S. A. *96*, 13496–13500.

Yu, C., Wang, F., Jin, C., Wu, X., Chan, W., and Mckeehan, W.L. (2003). Increased Carbon Tetrachloride-Induced Liver Injury and Fibrosis in FGFR4-Deficient Mice. *161*, 2003–2010.

Yu, Z. Bin, Han, S.P., and Chen, C. (2014). Bilirubin nomograms for identification of neonatal hyperbilirubinemia in healthy term and late-preterm infants: a systematic review and meta-analysis. World J. Pediatr. *10*, 211–218.

Yueh, M.F., Chen, S., Nguyen, N., and Tukey, R.H. (2014). Developmental Onset of bilirubin-induced neurotoxicity involves toll-like receptor 2-dependent signaling in humanized UDP-glucuronosyltransferase1 mice. J. Biol. Chem. *289*, 4699–4709.

Yuste, J.E., Tarragon, E., Campuzano, C.M., and Ros-Bernal, F. (2015). Implications of glial nitric oxide in neurodegenerative diseases. Front. Cell. Neurosci. *9*, 322.

Zelenka, J., Lenícek, M., Muchová, L., Jirsa, M., Kudla, M., Balaz, P., Zadinová, M., Ostrow, J.D., Wong, R.J., and Vítek, L. (2008). Highly sensitive method for quantitative determination of bilirubin in biological fluids and tissues. J. Chromatogr. B. Analyt. Technol. Biomed. Life Sci. *867*, 37–42.

Zhang, T., Haws, P., and Wu, Q. (2004). Multiple Variable First Exons : A Mechanism for Cell- and Tissue-Specific Gene Regulation. Genome Res. 79–89.

Zhang, W., Narayanan, M., and Friedlander, R.M. (2003). Additive neuroprotective effects of minocycline with creatine in a mouse model of ALS. Ann. Neurol. *53*, 267–270.

Zhang, Y., Wu, Y., Cheng, Y., Zhao, Z., Tashiro, S. ichi, Onodera, S., and Ikejima, T. (2008). Fas-mediated autophagy requires JNK activation in HeLa cells. Biochem. Biophys. Res. Commun. *377*, 1205–1210.

Zhu, S., Stavrovskaya, I.G., Drozda, M., Kim, B.Y.S., Ona, V., Li, M., Sarang, S., Liu, A.S., Hartley, D.M., Wu, D.C., et al. (2002). Minocycline inhibits cytochrome c release and delays progression of amyotrophic lateral sclerosis in mice. Nature *417*, 74–78.

Appendix 1

Part of the Thesis was published as follows:

S. Vodret, G. Bortolussi, A. B. Schreuder, J. Jasprovà, L. Vitek, H. J. Verkade and A. F. Muro (2015). Albumin administration prevented neurological damage and death in a mouse model of severe neonatal hyperbilirubinemia. Scientific Reports, 5: 16203